Università degli Studi di Padova

Dipartimento di Biologia

SCUOLA DI DOTTORATO DI RICERCA IN: BIOSCIENZE E BIOTECNOLOGIE

INDIRIZZO: BIOCHIMICA E BIOFISICA

CICLO XXVIII

Identification and functional characterization of components of the OPA1 complexes targeted during apoptotic cristae remodeling

Direttore della Scuola: Ch.mo. Prof. Paolo Bernardi

Coordinatore d'indirizzo: Ch.mo. Prof. Fabio di Lisa

Supervisore: Ch.mo. Prof. Luca Scorrano

Dottoranda: Christina Glytsou

1 Feb 2016

Acknowledgements

I would first like to thank my primary supervisor, Prof. Luca Scorrano, for the opportunity to conduct research in his laboratory, for his mentorship, his motivation strategies and immense knowledge. Luca, thank you for making me think that nothing is impossible! I would like to further extend thanks to my associate supervisor, Prof. Mageni Soriano, for her guidance and significant contribution to this work. Mageni, thank you for being a great teacher and for all the help and words of encouragement throughout my doctorate.

I would like to express my gratitude to Prof. Jose Antonio Enriquez, Prof. Jesùs Vazquez, and Dr. Enrique Calvo in the Centro Nacional de Investigaciones Cardiovasculares Carlos III in Madrid for conducting all the mass spectrometry experiments and for a very fruitful collaboration. I am also grateful to Prof. Bernardi's lab for help with Seahorse experiments.

Moreover, I would like to thank every former and current member of the Scorrano group for their continuous assistance, the great work environment and the fun inside and outside the lab throughout these three years. Thank you to Sara Cogliati for sharing her biochemical expertise, Marta Giacomello and Sowmya Lakshminarayanan for confocal microscopy advice, Francesca Grespi for the assistance in qPCR experiments, Stephanie Herkenne for helpful suggestions and Lorenza Tsansizi for translating my thesis summary to Italian. Thank you to the bachelor students, Marta Medaglia and Nicolò Ilacqua, who helped with experiments during their three-month internship. Ruben Quintana, thank you for the inspiring scientific discussions, your continuous support and your jokes. A huge thank you to Charlotte Quirin, Claudia Savoia and Lena Pernas for being so supportive and helpful, and sharing all these moments in the lab and outside. Thank you to everyone for making me feel like home.

A big thank you to my friend and fellow graduate student, Eva Papachristou, for suggestions on data analysis.

I would like to acknowledge the Fondazione Santa Lucia and the Dulbecco-Telethon Institute for the financial support that made my PhD research possible.

I would also like to thank all my friends in Padova, Greece and all over the world for being close to me and supporting me all these years, even though most of them are far away. Special thanks to my best friend and flatmate, Eva Kakogiannou, for all the encouragement, understanding, endless discussions and fun during our parallel stay in Padova.

Finally, I would like to thank my family: my sisters, Katerina and Sophia, my brother-in-law and my parents for supporting me in my choice to leave home and follow my dream. Thank you for their valuable life-long advice and help, and for always being there for me. Last but not least, I want to dedicate my thesis to my little nephews, Gianni and Michael, as the least I can offer them in return for the happiness they have brought me. Ευχαριστώ!

Table of contents

Riassunto dell' attività svolta

I mitocondri sono organelli cellulari che partecipano attivamente alla produzione di energia, la trasduzione del segnale e l'apoptosi. Essi sono caratterizzati da una struttura sofisticata indispensabile per ospitare le molteplici funzioni mitocondriali. Una membrana esterna definisce il confine del organello e il citoplasma, mentre una membrana interna compartimentalizza lo spazio interno in spazio intermembrane, matrice e cristae. Le cristae sono i siti di fosforilazione ossidativa e sono separate dallo spazio intermembrana da strette giunzioni tubolari (Frey and Mannella, 2000; Vogel et al., 2006).

Durante la morte cellulare programmata la forma e l' ultrastruttura mitocondriale cambiano. Queste alterazioni morfologiche che comprendono l'ampliamento delle giunzioni strette delle cristae - il cosiddetto "rimodellamento di cristae" - contribuisce alla mobilitazione del citocromo c, e il suo rilascio completo dallo spazio intermembrana al citoplasma (Scorrano et al., 2002).

Ricerche genetiche e biochimiche sui meccanismi molecolari della modificazione mitocondriale durante l'apoptosi hanno svelato che la proteina della membrana mitocondriale interiore, optic atrophy (OPA1) è un regolatore chiave del rimodellamento delle cristae. OPA1 forma vari complessi che mantengono le giunzioni delle cristae regolando così la quantità del citocromo c che è disponibile nello spazio intermembrana per il suo rilascio nel citoplasma dopo la permeabilizzazione della membrana mitocondriale esterna. Su stimolo apoptotico, i complessi di alto peso molecolare (high molecular weight, HMW) contenenti OPA1 sono interrotti, con l'allargamento concomitante delle giunzioni e il rilascio del citocromo c (Frezza et al., 2006; Cogliati et al., 2013). È interessante notare che questi gruppi sono composti da forme transmembrana

(lunghe) e forme solubili (corte) di OPA1 e la loro dimensione è compresa tra i 500 e gli 800 KDa, come giudicato da elettroforesi su gel blu nativo e per dimensione cromatografia di esclusione. Questa dimensione suggerisce che essi contengono anche altre proteine oltre che OPA1, la cui identità e funzione deve essere esaminata.

Lo scopo della mia tesi di dottorato è di esplorare la composizione dei complessi-OPA1 contenenti, e di caratterizzare la funzione delle parti di OPA1 identificate nella fisiologia mitocondriale e nella morte cellulare.

Elettroforesi tridimensionale su gel di poliacrilammide blu nativo (*BN-PAGE*) (3D BN-BN-SDS PAGE) seguita da semi-quantitativa LC/MS analisi di mitocondri normali e apoptotici di fegato di topo, effettuata nel nostro laboratorio, ha rivelato una coorte di proteine putative presenti nei complessi OPA1–contenenti la cui distribuzione cambia durante la morte cellulare programmata. Per identificare meglio i partner putativi per OPA1 abbiamo inoltre eseguito un semi-quantitativa LC/MS analisi in su gel BlueNative dei mitocondri murini cardiaci. Inoltre, abbiamo impiegato etichettatura a isotopo stabile con aminoacidi (SILAC) (Ong and Mann, 2007) in fibroblasti di topo adulto (MAFS), in combinazione con 2D BN-BN PAGE e LC/MS. Per distinguere le proteine che sono regolate particolarmente durante il rimodellamento delle cristae, con questi due approcci abbiamo confrontato la popolazione mitocondriale normale con le popolazioni mitocondriali stimolate con BID, un fattore pro-apoptotico tagliato proteoliticamente dal caspasi 8, in forma wild type ($cBID^{wt}$) o con mutazione che compromette il rimodellamento delle cristae ($cBID^{KKAA}$) (Cogliati et al., 2013). I risultati ottenuti dalle tre strategie high throughput sono stati analizzati per ottenere gli elenchi definitivi dei potenziali interattori di OPA1 e il coorte delle proteine che sono ridotte o aumentate in modo significativo nei vari complessi multimerici di OPA1 durante il rimodellamento delle cristae. La scoperta degli stessi

interattori di OPA1 con le varie tecniche hanno dimostrato indipendenza dal tipo di tessuto, cosa che mostra che i nostri metodi hanno il livello di specificità necessario per l' ispezione dei complessi OPA1 nella vita e morte cellulare.

Tra le proteine identificate, la nostra attenzione è stata catturata da due componenti del complesso MICOS: Mic60 e Mic19. Il "Mitochondrial contact site and cristae organizing system" (MICOS) è una grande struttura proteica eterooligomerica, che regola la biogenesi delle giunzioni delle cristae. Tuttavia, il regolatore principale delle cristae OPA1 non fa parte del complesso MICOS e la sua esatta composizione, l'architettura e le funzioni nel lievito e nei mammiferi sono ancora sotto esame.

In tutti e tre gli approcci di proteomica e dopo immunoblotting con gel Blue Native, il componente principale di MICOS, Mic60, è stato individuato in complessi ad alto peso molecolare con simile mobilità elettroforetica a quelli di OPA1. Al fine di svelare il potenziale crosstalk tra OPA1 e Mic60, abbiamo effettuato analisi biochimiche e genetiche in situazione di ablazione di OPA1 o/e Mic60 e dimostrato che le due proteine interagiscono nelle membrane mitocondriali interne (inner mitochondrial membranes-IMM) e sono essenziali nella formazione dei complessi OPA1/Mic60. Esperimenti di microscopia elettronica hanno rivelato che questi complessi sono essenziali nella formazione della giunzione delle cristae, ma non per specificare la larghezza del loro lumen o la giunzione del loro foro.

Inoltre, abbiamo dimostrato che i complessi Mic60/OPA1 sono eliminati da $cBID^{wt}$ ma non dal suo mutante $cBID^{KKAA}$, indicando un nuovo ruolo di Mic60 che riguarda il rimodellamento apoptotico delle cristae. E' da notare che l'analisi bioinformatica ha mostrato una divergenza strutturale tra gli ortologi di Mic60 tra lievito e mammiferi, spiegando potenzialmente le ulteriori funzioni Mic60 sin dall'inizio dell'evoluzione. Allo

stesso modo, abbiamo anche dimostrato che Mic19 fa parte di complessi ad alto peso molecolare presenti durante la ristrutturazione delle cristae, aumentando la possibilità che il Mic19 dei mammiferi potrebbe anche regolare la biogenesi dei mitocondri attraverso il pathway di OPA1.

Oltre ai componenti di MICOS, abbiamo voluto, inoltre, indagare un'altra proteina trovata significativamente ridotta durante l' apoptosi. Questa proteina è chiamata ossido nitrico-associato 1 (nitric oxide-associated 1, NOA1). La coesistenza di NOA1 e OPA1 negli stessi complessi è stata confermata con metodi biochimici in BMH mitocondri crosslinked, così come dopo co-immunoprecipitazione. Questi dati iniziali, insieme al fatto che la funzione di questa proteina era all' oscuro sino ad ora, ci hanno spinto a studiare ulteriormente il suo ruolo nei mitocondri e la sua relazione con OPA1 nel controllo della morfologia mitocondriale e nel rimodellamento delle criste.

Per far luce al collegamento funzionale tra le due proteine di interesse, abbiamo utilizzato MEF carenti di NOA1 dove abbiamo sorprendentemente osservato un aumento di OPA1, sia a livello di proteine che a livello di trascrizione. Inoltre, mentre NOA1 era assente nelle *Opa1*$^{-/-}$ MEF, il suo livello è tornato alla normalità quando è stata reintrodotta OPA1, suggerendo un interazione genetica tra le due.

Successivamente, al fine di ottenere informazioni sul ruolo di NOA1 nei mitocondri, abbiamo analizzato *Noa1*$^{-/-}$ MEF mediante microscopia confocale ed elettronica. I mitocondri di cellule *Noa1*$^{-/-}$ sono frammentati e hanno alterazioni ultrastrutturali. È interessante notare che l' iperespressione di OPA1 ha corretto l' ultrastruttura mitocondriale aberrante in misura simile a quella di reintroduzione di NOA1, sostenendo ulteriormente l'ipotesi di una interazione funzionale OPA1-NOA1.

Dati i difetti strutturali mitocondriali, abbiamo ipotizzato che l' ablazione di NOA1 colpisca

anche funzioni mitocondriali. Infatti, analisi Seahorse ha mostrato una respirazione mitocondriale compromessa in cellule mancanti NOA1, coerente con quello che era già stato pubblicato. Analisi SDS e Blue Native hanno rivelato una notevole diminuzione nei livelli delle proteine delle varie subunità di OXPHOS e un difetto nel assemblaggio dei complessi respiratori mancanti NOA1. Sorprendentemente, il numero di copie di DNA mitocondriale (mtDNA) era inalterato, mentre la riduzione della proteina non era limitata alle proteine codificate da DNA mitocondriale. Di conseguenza, si suggerisce che l'instabilità generale delle proteine OXPHOS è probabilmente dovuta all' incapacità dei complessi della catena respiratoria ad essere assemblati correttamente, potenzialmente spiegando le disfunzioni bioenergetiche.

Funzionalmente, le cellule *Noa1*$^{-/-}$ crescevano più lentamente rispetto a quelle WT con medio contenente galattosio, e dopo 2 giorni non erano in grado di tollerare deprivazione di glucosio, suggerendo un ruolo potenziale di NOA1 nella crescita cellulare dipendente da mitocondri. A causa del fatto che OPA1 è una proteina antiapoptotica e i suoi complessi sono interrotti dopo stimoli apoptotici, abbiamo voluto studiare il suo partner, NOA1, nel corso dell' apoptosi. Come per OPA1, i complessi di NOA1 che hanno la stessa motilità elettroforetica dopo crosslink come quelli di OPA1 sono similmente interrotti su rimodellamento delle criste indotto da cBID. Oltre a ciò, durante l'apoptosi, è probabile una scissione proteolitica di NOA1, che potrebbe essere un potenziale meccanismo per l'eliminazione di complessi NOA1-OPA1 subito dopo la stimolazione della morte cellulare.

Summary

In conclusione, il nostro studio ha svelato la composizione dei complessi OPA1 che vengono eliminati durante l'apoptosi. Abbiamo scoperto un crosstalk tra i principali regolatori della biogenesi delle cristae, OPA1 e Mic60 e caratterizzato il ruolo di Mic60 durante il rimodellamento apoptotico delle cristae. Inoltre, abbiamo scoperto un nuovo giocatore nella manutenzione della forma delle cristae, nel loro rimodellamento e nella respirazione mitocondriale, NOA1, che agisce nello stesso pathway di OPA1.

Mitochondria are cellular organelles participating actively in energy production, signal transduction and apoptosis. They are characterized by a sophisticated structure essential for hosting the multiple mitochondrial functions. An outer membrane defines the border of the organelle and the cytoplasm, while an inner membrane compartmentalizes the internal space into intermembrane space, matrix and cristae. Cristae are the sites of oxidative phosphorylation and are separated from the intermembrane space by narrow tubular cristae junctions (Frey and Mannella, 2000; Vogel et al., 2006).

During programmed cell death mitochondrial shape and ultrastructure change. These morphological alterations that include the widening of the narrow cristae junctions – the so-called “cristae remodeling” – contribute to the mobilization of the cristae-endowed cytochrome c to the intermembrane space and its complete release to the cytosol (Scorrano et al., 2002).

Genetic and biochemical research on the molecular mechanisms of mitochondrial structure modifications during apoptosis unveiled that the inner mitochondrial membrane dynamin-related protein, Optic atrophy 1 (OPA1) is a key regulator of cristae remodeling. OPA1 forms multiple complexes that maintain the cristae junctions close;

thereby regulating how much cytochrome c is available in the intermembrane space for release in the cytosol upon permeabilization of the outer mitochondrial membrane. Upon apoptotic stimulus, the high molecular weight (H.M.W) OPA1-containing complexes are disrupted, with concomitant enlargement of the cristae junctions and cytochrome c release (Frezza et al., 2006; Cogliati et al., 2013). Interestingly, these assemblies are composed by the transmembrane (long) and soluble (short) OPA1 forms and their size ranges from 500 to 800 KDa, as judged by blue native gel electrophoresis and by size exclusion chromatography. This size suggests that they contain proteins other than OPA1, whose identity and function calls for investigation.

The aim of my PhD thesis is to explore the composition of the OPA1-containing complexes, as well as to characterize the function of identified OPA1 partners in mitochondrial physiology and cell death.

Three dimensional BlueNative-BlueNative-SDS PAGE (3D BN-BN-SDS PAGE) followed by semi-quantitative LC/MS analysis of normal and apoptotic mouse liver mitochondria, carried out in our lab, revealed a cohort of candidate proteins present in the OPA1-containing complexes whose distribution changes during programmed cell death. To further mark off the number of candidate OPA1 partners, we additionally performed a semi-quantitative LC/MS analysis in blue native PAGE of mouse heart mitochondria. Furthermore, we employed stable isotope labeling by amino acids (SILAC) (Ong and Mann, 2007) in mouse adult fibroblasts (MAFs), combined with blue native PAGE and LC-MS/MS. In order to distinguish the proteins that are regulated specifically during cristae remodeling, in the two latter approaches we compared a normal mitochondrial population with mitochondrial populations stimulated with the wild type pro-apoptotic caspase 8 cleaved BID ($cBID^{wt}$) or a cristae remodeling incompetent mutant of cBID

(cBID^{KKAA}) (Cogliati et al., 2013). The resulted hits of all the three high throughput strategies were analyzed collectively to obtain the final lists of potential OPA1 interactors and the subset of proteins that significantly decrease or increase in the various multimeric OPA1 complexes in the course of cristae remodeling. The discovery of the same OPA1 interactors between the techniques indicated a tissue-independency and that our methods had the level of definition required to inspect OPA1 complexes in cell life and death.

Among the identified proteins, our attention was firstly caught by two MICOS complex members: Mic60 and Mic19. “Mitochondrial contact site and cristae organizing system” (MICOS) is a large heterooligomeric protein structure, which regulates cristae junction biogenesis. Nevertheless, the master regulator of cristae shape OPA1 is not part of MICOS and its exact composition, architecture and functions in yeast and mammals are still under active investigation.

In all the three proteomic approaches and after immunoblotting of Blue Native PAGE the core component of MICOS, Mic60, was retrieved in high molecular weight complexes with similar electrophoretic mobility as those of OPA1. In order to unravel the potential crosstalk between OPA1 and Mic60, we performed biochemical and genetic analysis in OPA1 or/and Mic60 ablation and demonstrated that the two IMM proteins interact and are indispensable for the Mic60/OPA1 complexes formation. Functionally, electron microscopy revealed that these complexes are essential for cristae junction formation, but not for specifying the width of the cristae lumen or the cristae junction mouth.

Moreover, we showed that the Mic60/OPA1 complexes are eliminated by cBID^{wt} but not by its mutant cBID^{KKAA}, indicating a novel role of Mic60 that regards apoptotic cristae remodeling. Worth noting, bioinformatics analysis uncovered a structural divergence in

the transmembrane and middle domains between yeast and mammalian Mic60 orthologues, potentially explaining the additional Mic60 functions at the outset of evolution. Similarly, we also demonstrated that Mic19 is part of high molecular weight complexes, which are targeted during cristae remodeling, raising the possibility that mammalian Mic19 might also regulate mitochondria biogenesis through the OPA1 pathway.

Besides MICOS components, we, additionally, wished to investigate another identified protein that was significantly reduced in apoptosis. This protein is christened nitric oxide-associated 1 (NOA1). The co-existence of NOA1 and OPA1 in the same complexes was confirmed biochemically in BMH crosslinked mitochondria, as well as after co-immunoprecipitation. These initial data, along with the obscure exact function of this newly characterized protein, prompted us to further investigate its role in mitochondria and its relationship with OPA1 in the control of mitochondrial morphology and cristae remodeling.

To shed light on the functional link between the two proteins of interest, we used NOA1 deficient MEFs where we surprisingly observed an upregulation of OPA1, both at the protein and at the transcript level. In addition, NOA1 was absent in *Opa1*$^{-/-}$ MEFs, while its level went back to normal when OPA1 was re-introduced, suggesting a genetic interaction between the two.

Next, in order to gain an insight into the role of NOA1 in mitochondria, we analyzed NOA1 deficient MEFs by confocal and electron microscopy. Mitochondria of *Noa1*$^{-/-}$ cells were fragmented and displayed ultrastructural changes. Interestingly, overexpression of OPA1 corrected the aberrant mitochondrial ultrastructure at a similar extent as upon re-

introduction of NOA1, further supporting the hypothesis of an OPA1-NOA1 functional interplay.

Given the mitochondrial structural defects, we hypothesized that NOA1 ablation affected also mitochondrial functions. Indeed, Seahorse analysis showed impaired mitochondrial respiration in NOA1 lacking cells, consistent with previously published reports. SDS and blue native PAGE revealed a notable decrease of OXPHOS subunits protein levels and a defect on respiratory complexes assembly in NOA1 deficiency. Remarkably, mtDNA copy number was unaltered, while the protein reduction was not restricted to mtDNA encoded proteins. Consequently, we suggest that the general instability of OXPHOS proteins is probably due to the inability of the respiratory chain complexes to properly assemble, potentially explaining the bioenergetic dysfunction.

Functionally, *Noa1*$^{-/-}$ cells grew slower than WT in galactose-containing medium and after two days they were unable to tolerate glucose deprivation, suggesting a potential role of NOA1 in mitochondrial-dependent cell growth. Due to the fact that OPA1 is an anti-apoptotic protein whose complexes are disrupted after apoptotic stimulation, we aimed to study its partner, NOA1, in the course of apoptosis. Like OPA1, NOA1 complexes that have the same electrophoretic motility after crosslinking as those of OPA1 are similarly disrupted upon cBID induced cristae remodeling. On top of this, during apoptosis, NOA1 is likely proteolyticallly cleaved, which could be a potential mechanism for the elimination of NOA1/OPA1-contining complexes early in cell death stimulation.

In conclusion, our study unraveled the composition of OPA1 complexes that are eliminated during apoptosis. We uncovered a crosstalk between the core cristae biogenesis regulators, OPA1 and Mic60, and characterized the role of Mic60 during apoptotic cristae remodeling. Moreover, we discovered a novel player of cristae shape

maintenance, cristae remodeling and mitochondrial respiration, NOA1, that acts in the same pathway as OPA1.

Chapter I

Literature Review

1. General Introduction

Mitochondria are fundamental organelles in life and death of eukaryotic cells, participating in multiple cellular processes. They are the energy production “factories”, they are involved in apoptosis regulation, calcium homeostasis, signaling pathways, cell cycle and growth control and reactive oxygen species production. Dysfunctional mitochondria are implicated in ageing and several human pathologies, including cancer, neurodegenerative diseases, metabolic disorders, diabetes and inflammatory conditions. Mitochondrial shape is extremely complex and dynamic, constantly changing to support the various functions in response to the cellular demands. The organelles are bordered by two distinct membranes; the outer mitochondrial membrane (IMM), that separates them from the cytosol, and the inner mitochondrial membrane (IMM) that constitutes the site of oxidative phosphorylation (Palade, 1952). The latter can be further subdivided into two different compartments, the inner boundary membrane and the cristae. Electron tomography allowed the visualization of the 3D mitochondrial ultrastructure identifying the cristae as pleomorphic bag like structures connected by a bottleneck called cristae junction to the inner boundary membrane (Frey and Mannella, 2000). The respiratory complexes are accumulated in the membranes of these structures, as a consequence the vast majority of cytochrome c resides in the cristae space (Vogel et al., 2006).

During apoptosis, soluble mitochondrial components among which cytochrome c, are released to the cytosol, to amplify the apoptotic pathway. A dramatic cristae structure rearrangement occurs early upon apoptotic stimulation. These morphological alterations are described with the term “cristae remodeling” and include the widening of the cristae junctions as well as the individual cristae fusion (Scorrano et al., 2002). A key regulator of cristae remodeling is the mitochondrial shaping GTPase, Optic atrophy 1 (OPA1). OPA1 resides in multiple complexes, which keep the cristae junction close, whilst they are targeted and eliminated during cell death. In this thesis, we focus on the identification and characterization of OPA1 partners that collaborate to regulate the cristae shape before and after the apoptotic cristae remodeling.

1.1 Mitochondria, the multifunctional organelles

Mitochondria are double-membrane organelles where various vital cellular processes are carried out. They are the site of cellular respiration, where the majority of ATP is generated. According to the chemiosmotic theory, the enzymatic respiratory complexes sitting in the inner mitochondrial membrane (IMM), pump protons across the membrane during the transfer of electrons from NADH and FADH2 downhill their redox potentials to molecular O2, thus generating an electrochemical gradient. The free energy stored in this electrochemical gradient drives the F1F0-ATP-synthase to generate ATP. The whole process is named oxidative phosphorylation (OXPHOS), because oxygen is the final electron acceptor and the ultimate reaction is the phosphorylation of ADP to produce ATP (Mitchell and Moyle, 1967).

The OXPHOS system consists of five enzymatic complexes: NADH-Q oxidoreductase, succinate-Q reductase, Q-cytochrome c oxidoreductase, cytochrome c oxidase and ATP synthase, which are also called Complex I, II, III, IV and V, respectively. In 2000, the past understanding of the organization in discrete complexes was replaced unambiguously by the view of a higher order organization in supramolecular assemblies, thanks to analysis with Blue-Native gel electrophoresis (BN-PAGE) (Schagger and Pfeiffer, 2000). These structures, named "*respirosomes*" or "*respiratory supercomplexes*" (RSC) and composed by CI, CIII and CIV, enhance the efficiency of electron transfer rate, provide a kinetic advantage and limit reactive oxygen species (ROS) production from CI. More than that, the dynamic nature of the superassemblies provides an advantage for mitochondria to adapt to changing energy demands (Acin-Perez et al., 2008; Genova and Lenaz, 2014).

In addition to their role in cellular metabolism, mitochondria participate in the synchronization of Ca^{2+} waves inside the different intracellular compartments, thus regulating multiple calcium-dependent signaling pathways, such as apoptosis (Jouaville et al., 1995; Rizzuto et al., 2003; Rimessi et al., 2008). In particular, they can uptake, transiently store and release calcium, making them good "cytosolic buffers" for this ion type (Brighton and Hunt, 1974). Besides their indirect role in apoptosis through calcium regulation, mitochondria also actively take part in programmed cell death by receiving diverse cytosolic signals and, as a response, releasing back cofactors so as to amplify the apoptotic pathway (Wang, 2001). Aging and a plethora of human disorders, including

cancer, neurodegenerative diseases and neuropathy, are consequences of or aggravated by mitochondrial dysfunction, indicating the importance of proper mitochondrial functioning for the cell and the whole organism homeostasis (Schapira, 2006).

1.2 Mitochondrial DNA (mtDNA)

Mitochondria contain their own genome in multiple copies. Mitochondrial DNA (mtDNA) is circular, and according to the theory of endosymbiosis, originates evolutionary from the bacterial genome (Margulis, 1971). In humans, mtDNA encodes 13 polypeptides (subunits of respiratory complexes; seven subunits of complex I, one of complex III, three of complex IV and two subunits of ATP-synthase), as well as 22 transfer RNAs and two ribosomal RNAs (16S rRNA and 12S rRNA), which are required for mitochondrial translation (Fernandez-Silva et al., 2003). DNA in mammalian mitochondria is not naked; instead, it is organized with proteins in structural units named nucleoids (SOTELO and PORTER, 1959; Barat et al., 1985). Transcription factor A (TFAM) is the main packaging polypeptide and with one molecule of mtDNA, it composes the structural unit of nucleoid (Kukat et al., 2015; Kukat et al., 2011). Apart from TFAM, a number of proteins such as mitochondrial DNA replication, transcription and translation factors (mtSSB, EFTu, POLG1 and Twinkle), proteases (Lon), scaffold proteins (ATAD3, Prohibitin) and members of signaling pathways, have been proposed to interact with the nucleoids (Gilkerson et al., 2013).

Although the number of mitochondrial proteins encoded by the mitochondrial genome is small in relation to those encoded by the nuclear genome (around 1500 proteins), mtDNA integrity and its normal expression is essential for the assembly and function of respiratory chain. Any aberration of the mtDNA stability can be detrimental for the cellular function. Genetic defects affecting its integrity and expression are the cause of various human diseases (Szklarczyk et al., 2014).

1.3 Mitochondrial shape and ultrastructure

Mitochondria are bordered by two distinct phospholipids membranes – the outer mitochondrial membrane (OMM), which is permeable to small molecules, and the impermeable inner mitochondrial membrane (IMM) (Fig 1). The compartment between the two membranes is called intermembrane space (IMS) and the space enclosed by the IMM is called matrix. The IMM folds into a complex network of tubules and lamellae that protrude into the matrix, the so-called cristae; thus, the IMM is approximately 5 times larger than OMM. The area surrounded by the IMM of one crista is the cristae lumen, while the part of the IMM that is not invaginated to form cristae and lies parallel to the OMM is defined as inner boundary membrane (IBM) (Vogel et al., 2006). Cristae are connected to IBM by narrow tubular structures of varying length, the so-called cristae junctions (CJ). In steady-state the diameter of CJ ranges from approximately 20 to 30 nm, a size that is regulated to allow the flow of metabolites from the cristae invagination to the IMS and vice versa (Mannella et al., 1994; Scorrano et al., 2002).

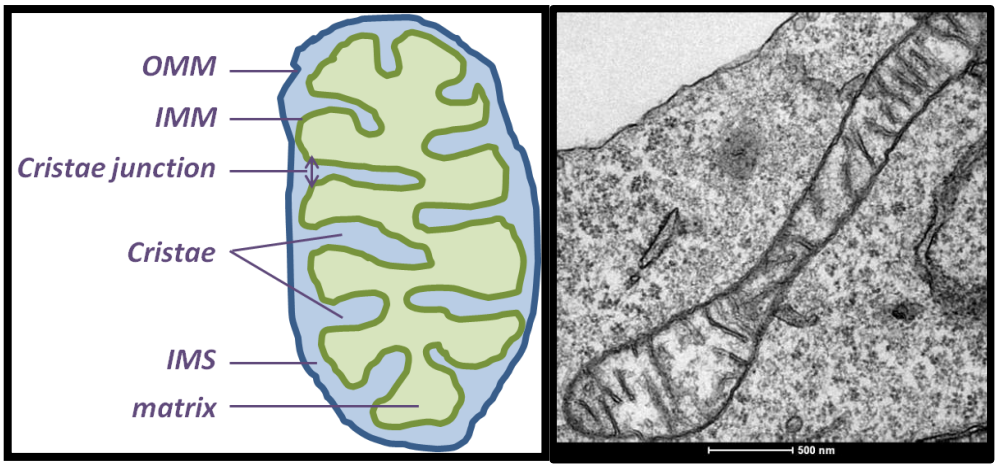

Figure 1. Mitochondrial structure. Schematic representation of mitochondrial structure (on the left). Electron microscopy image of a mitochondrion from mouse embryonic fibroblasts (on the right). OMM: outer mitochondrial membrane. IMM: inner mitochondrial membrane. IMS: intermembrane space.

1.4 The dynamic nature of mitochondrial shape

Mitochondrial diameter ranges from 0.5 to 1.0 μm and their shape varies from small spheres to interconnected tubules (Bereiter-Hahn and Voth, 1994). Because of this heterogeneous morphology, this organelle was christened “mitochondrion”, a term which originates from the Greek words “μίτος, mitos” (thread) and “χονδρίον, chondrion”

(grain). Although initially mitochondria were considered as static organelles - due to the limitation of conventional electron microscopy - confocal live-cell imaging with 3D reconstruction and electron tomography appeared to be promising visualization tools to unravel the plasticity of those organelles (Dimmer and Scorrano, 2006).

The dynamic nature of mitochondria derives from their ability to constantly undergo events of fusion and division, as well as to redistribute inside the cell along cytoskeleton tracks (van der Bliek et al., 2013). Occasionally, two mitochondria encounter each other and fuse, end to end or head to side. On the other hand, one tubule may undergo fission processes to give rise to two or more smaller mitochondria. Fusion and fission often occur in short time intervals within the same group of mitochondria. Additionally, movement of the organelles may occur upon their association with microtubules of the cytoskeleton or after intrinsic events by themselves. Given the complex structure and the fundamental roles of mitochondria, as well as the high frequency of the dynamic events, these processes should be tightly regulated by sophisticated machineries, in order to coordinate networks of organelles with double lipid bilayers (Fig 2).

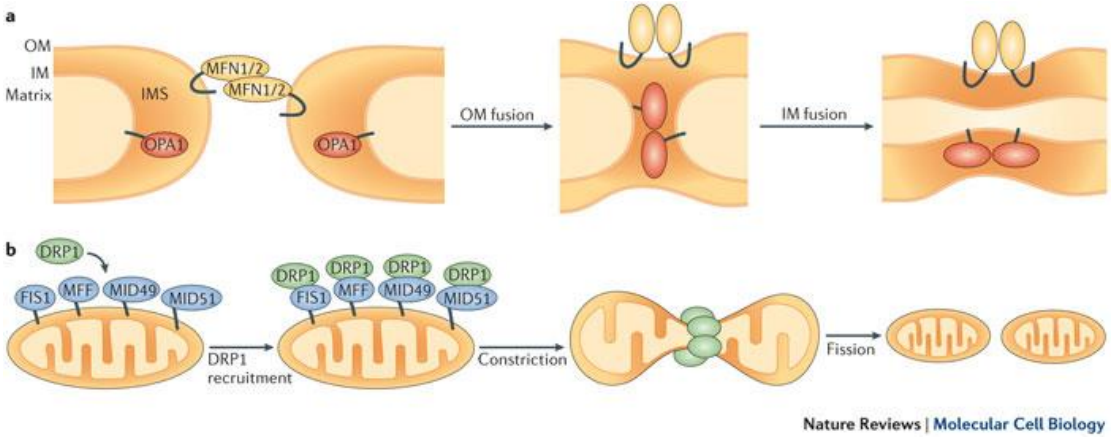

Figure 2. Mitochondrial fusion (a) and fission (b) in mammalian cells. Continual cycles of fusion and fission result in the intermixing of the mitochondrial population in the cell. OM fusion is mediated by mitofusin 1 (MFN1) and MFN2, which are dynamin-related GTPases at the OM. IM fusion is mediated by the dynamin-related protein optic atrophy 1 (OPA1). The opposing process of mitochondrial fission (see the figure, part b) requires the recruitment of dynamin-related protein 1 (DRP1) from the cytosol to the mitochondrial OM. Assembly of DRP1 on the mitochondrial surface causes constriction of the mitochondria and eventual division of the organelle into two separate entities. Four DRP1 receptors exist in mammals — mitochondrial fission 1 (FIS1), mitochondrial fission factor (MFF), Mitochondrial dynamics protein of 49 kDa (MID49) and MID51 — and these are located on the mitochondrial OM. Adapted from (Mishra and Chan, 2014).

1.4.1 Mechanisms of mitochondrial division

The control of mitochondria dynamics is mediated by a group of "mitochondria shaping proteins", whose number is growing in the last years. The majority of these proteins belong to the dynamin-superfamily, which consists of large GTPases capable to facilitate membrane tubulation and/or scission (Praefcke and McMahon, 2004).

1.4.1.1 Key player of fission machinery - DRP1

One of the proteins involved in mitochondrial fission is dynamin-like-protein (Dlp)1p DLP1/DRP1 and its specific function is conserved from yeast to mammals (Smirnova et al., 2001; Ingerman et al., 2005). Structurally, DRP1 possesses a. an N-terminal GTPase domain, which is considered to provide mechanical force, b. a dynamin-like middle domain, c. an Insert-B domain, which contains a motif essential for binding to adaptors and d. a C-terminal GTPase effector domain (Yoon et al., 2001; Okamoto and Shaw, 2005; Bui et al., 2012). DRP1 localizes predominately in the cytosol in the form of dimers or tetrameres, but it can be recruited to mitochondria upon dephosphorylation by calcineurin, in order to exert its function by GTP hydrolysis (Yoon et al., 2001; Cereghetti et al., 2008). There it self-assembles into large oligomeric structures forming spirals around the constriction OMM sites (Ingerman et al., 2005). It has been proposed that the fission sites are determined by the position of endoplasmic reticulum tubules around mitochondria (Friedman et al., 2011).

1.4.1.2 Coplayers of DRP1

DRP1 binds to several OMM anchored adaptors, including FIS1, MFF and MIEF1, however their roles and relevance for the initiation of mitochondrial division are not clear. Mitochondrial fission factor (MFF) is a protein anchored to the OMM via its C-tail and it interacts with DPR1 *in vitro* and *in vivo*. Overexpression of MFF correlates with increased DRP1 translocation to mitochondria along with extensive organelle division, while its downregulation leads to mitochondrial elongation, suggesting its essential DRP1-dependent role in fission (Otera et al., 2010).

FIS1 is another C-tail anchored OMM protein, which was initially considered as the only DRP1 adaptor in yeast and human cells, regulating mitochondrial morphology (Yoon et al.,

2003; Stojanovski et al., 2004). Nevertheless, its direct role in DRP1 recruitment to the OMM is questioned *in vivo* by other reports (Lee et al., 2004; Suzuki et al., 2003); hence, its exact function remains an enigma.

More recently two novel molecules influencing mitochondrial fission have been identified; the OMM proteins Mitochondrial dynamics 51 (MiD51, aka mitochondrial elongation factor 1, MIEF1) and Mitochondrial dynamics 49 (MiD49). Palmer *et al* proposed that MiD49/51 is able to recruit DRP1 on mitochondria, yet in a non-functional form, thereby inhibiting fission and shifting the balance towards mitochondrial elongation (Lee et al., 2004; Palmer et al., 2011). Zhao *et al* suggested that, besides recruiting and inhibiting DRP1 activity, MIEF1 promotes in parallel mitochondrial fusion in an active, Mfn2-independent manner (Zhao et al., 2011). Further studies are essential to clarify MIEF1 roles in mitochondrial dynamics.

The mitochondrial fission machinery contains other proteins, including GDAP1, endophilin B1, sascin and LRRK2, though their role is still not fully characterized. Ganglioside-induced differentiation-associated protein 1 (GDAP1) is located in the OMM, from where it induces mitochondrial fragmentation in cooperation with DRP1 (Lee et al., 2004; Niemann et al., 2005). Endophilins are fatty acyl transferases that participate in membrane scission, altering the membrane curvature possibly via a direct interaction with lipids (Schmidt et al., 1999; Gad et al., 2000). Endophilin B1 moves from cytosol to mitochondria during apoptosis, and changes in its protein levels result in morphological alterations. Experiments where DRP1 and endophilin B1 have been concomitantly downregulated indicate that the latter acts downstream of the former (Karbowski et al., 2004; Lee et al., 2004; Schmidt et al., 1999). Another candidate component of the mitochondrial scission machinery is a large multi-domain protein, named sascin. A study on a mouse model where sascin is knocked-out shed light on its role in mitochondrial dynamics; cells lacking sascin displayed a similar abnormal mitochondrial phenotype to the one observed in DRP1 deficiency. The two proteins colocalize in the fission foci, while a direct interaction was validated with immunoprecipitation. All the data of this report revealed a regulation of DRP1 by sascin (Girard et al., 2012). A similar role to the one of sascin has been attributed to the large kinase, leucine-rich repeat kinase 2 (LRRK2). LRRK2 mediates DRP1 recruitment to mitochondria by a direct interaction, resulting in the induction of mitochondrial fragmentation (Wang et al., 2012).

Although several reports have identified regulators of OMM fission, less attention has been given to the division of the inner mitochondrial membrane. One could think that the scission of both membranes is coordinated by the same proteins. On the other hand, distinct mitochondrial shaping proteins residing in the IMM could potentially control its fission, like the yeast protein MDM33 (Messerschmitt et al., 2003).

1.4.1.3 Regulation of DRP1

Apart from the multiple and dynamic proposed protein interactions, mitochondrial division is also regulated by a variety of post-translational modifications of the key player DRP1. Among these modifications we find the already mentioned (de)phosphorylation, as well as SUMOylation, S-nitrosylation, ubiquitination and O-GlcNAcylation.

Phosphorylation of DRP1 is mediated by PKA at its residues Ser637 and Ser656, to inhibit its GTPase activity and block fission, while a third residue Ser585 can be phosphorylated by Cdk1 during mitosis in order to promote mitochondrial fragmentation. Dephosphorylation at Ser637 is carried out by the Ca^{2+}-dependent phosphatase calcineurin, which normally interacts with DRP1. This is a consequence of increased cytosolic Ca^{2+} concentration (such as in case of mitochondrial depolarization) and results in DRP1 translocation to mitochondria with subsequent fission events (Jahani-Asl and Slack, 2007; Taguchi et al., 2007; Chang and Blackstone, 2007; Cereghetti et al., 2008; Jahani-Asl and Slack, 2007; Lee et al., 2004; Schmidt et al., 1999). Very recently, the phosphorylation of DRP1 was shown to be controlled by DAP3 - a protein that resides in the mitochondrial matrix, raising the question of whether this effect is direct (Xiao et al., 2015). Overall, the phosphorylation status of Drp1 can determine the shape of mitochondria during the changing cellular conditions.

Moreover, DRP1 activity is controlled by SUMOylation, during which a small SUMO protein binds to its substrate through the mitochondrial-anchored SUMO E3 ligase (MAPL); thus DRP1 is protected by ubiquitination, stabilized, associated to mitochondria, favoring mitochondrial division (Braschi et al., 2009; Wasiak et al., 2007). In contrast, ubiquitination targets DRP1 for degradation by the proteasome. March5 is a mitochondrial-associated RING-finger E3 ubiquitin ligase, which ubiquitinates DRP1 at the OMM. However, the effect of this regulation on mitochondrial morphology is still

controversial (Karbowski et al., 2007). Finally yet importantly, two more modifications occur in the polypeptidic sequence of DRP1. First, the GED domain residue Cys644 can be S-nitrosylated upon nitric oxide production in neuronal injury, enhancing its GTPase activity and subsequently its fission capacity (Cho et al., 2009). Second, O-Glc-NAcylation of Thr-585 and Thr-586 in the insert B-domain significantly decreases Ser637 DRP1 phosphorylation in cardiac myocytes, driving DRP1 translocation and mitochondrial fragmentation. All these multi-site posttranslational modifications on the key regulator of fission suggest a tight control of mitochondrial morphology (Gawlowski et al., 2012; Wasiak et al., 2007). The exact mechanisms by which these modulations are orchestrated remain still obscure.

1.4.2 Mechanisms of mitochondrial fusion

Similar to mitochondrial fission, fusion of the outer and inner mitochondrial membranes is mediated by dynamin-like GTPases, which are analyzed in the next paragraphs.

1.4.2.1 Key players of fusion machinery

1.4.2.1.1 Fzo1/Mitofusins

The first identified protein to be implicated in fusion was the D. *melanogaster* Fuzzy onions 1 protein (Fzo1), a large GTPase whose activity is required for the elongation of mitochondria during spermatogenesis (Hales and Fuller, 1997). Further studies demonstrated a genetic and functional conservation of this mitochondrial-shaping protein across the species. The yeast orthologue Fzo1p contains an N-terminal GTPase, exposed to the cytosol, four coiled-coil domains and two adjacent transmembrane domains that span the OMM. Lack of Fzo1 leads to mitochondrial fragmentation, mtDNA loss and absence of IMM. Anton *et al* proposed that, in order to execute its fusogenic activities, Fzo1 assembles into homo-dimers upon formation of mitochondrial contacts facilitating the tethering of the juxtaposed membranes (Fritz et al., 2001; Anton et al., 2011).

In mammals, the two broadly, but differentially expressed homologues of Fzo1, Mitofusin 1 and 2 (Mfn1 and Mfn2) are required for OMM fusion. Mfn1 resides in the OMM and

promotes membrane fusion, while Mfn2 localizes to both endoplasmic reticulum and mitochondria and is able to tether the two different organelles in trans. Similar to their yeast homologues, Mitofusins possess a GTPase domain and a coiled-coil domain (heptad repeat domain, HR1) at the N-terminus, protruding towards the cytosol. Mfns are anchored to the OMM via two transmembrane domains, which form a U-shape, while their C-terminal coiled-coil domain (heptad repeat domain, HR2) faces the cytosol and is responsible for the oligomerization (Santel and Fuller, 2001; Santel et al., 2003; Rojo et al., 2002). Thanks to their cytoplasmic coiled-coil domains, mitofusins can form homotypic (Mfn1-Mfn1, Mfn2-Mfn2) or heterotypic (Mfn2-Mfn1) dimers or complexes, and in that way dock two mitochondria to facilitate their fusion. Cells lacking one or both mitofusins display a fragmented mitochondrial phenotype, and the Mfn1-null, Mfn2-null or Mfn1/2-null mice are not viable (Chen et al., 2003; Chen et al., 2005).

Despite their high degree of structural and functional similarities, mitofusins play distinguishable specific roles, with Mfn1 being the core fusion component, exerting the higher GTPase activity (Ishihara et al., 2004). Loss of Mfn1 leads to more pronounced fusion defects than loss of Mfn2. Accordingly, while Mfn1 is able to rescue completely the phenotype of Mfn1 or Mfn2 loss, Mfn2 can only partially correct the mitochondrial shaping defects in a *Mfn1*$^{-/-}$ background, further supporting the central role of Mfn1 (Chen et al., 2005).

The differential functional partners of each protein could further explain differences in the function of mitofusins. For instance, only Mfn1 requires adequate levels of OPA1 to promote fusion and, conversely, only Mfn1 is implicated in OPA1-driven mitochondrial tubulation (Cipolat et al., 2004). Besides OPA1, Mfn1 interacts directly with mitofusin binding protein (MIB), controlling mitochondrial morphology by inhibiting mitofusin function. Although also Mfn2 coimmunoprecipitates with MIB, it is not yet clear whether this interaction is direct or through Mfn1 (Eura et al., 2006). On the other hand, Mfn2 interacts specifically with Stomatin-like protein 2 (SLP2) – though without any determined role in mitochondrial fusion – and the Bcl-2 family members Bcl-2 and Bclx. Bak has been shown to interact with both mitofusins, but its relative association with each one of them is altered during apoptosis (Hajek et al., 2007; Delivani et al., 2006). Finally, Mfn2 associates with the mitochondrial ubiquitin-ligase membrane-associated ring CH (MARCH-V), without being ubiquitinated by this. MARCH-V ubiquitinates the key player of

fission machinery, DRP1, indicating that it provides a common regulator of fusion and scission yet in a diverse manner (Nakamura et al., 2006).

1.4.2.1.2 Mgm1/OPA1

Mgm1 is a dynamin-related GTPase that fuses the IMM in yeast. Initially, *Mgm1* was characterized as a gene important for the maintenance of mitochondrial genome (Jones and Fangman, 1992). The protein contains an N-terminal mitochondrial targeting sequence (MTS), which is cleaved by matrix-processing peptidase (MPP) after its insertion into the organelle. An N-terminal transmembrane serves as a protein anchor to the IMM. The other part of Mgm1 consisted of a GTPase domain, a middle domain and two hydrophobic segments, is exposed in the IMS (Sesaki et al., 2003; Shepard and Yaffe, 1999; Wong et al., 2000). Mgm1 is processed by the rhomboid-related membrane protease Pcp1p at steady state; as a result, it appears in two forms: a long form integrated into the IMM and a short form lacking the transmembrane domain, located in the IMS. Both Mgm1 forms are necessary for mitochondrial fusion (Herlan et al., 2003). In addition, Mgm1p participates in a complex together with other fusion-promoting proteins - Fzo1p and Ugo1p - which as a multimeric unit contributes to the coordination of the simultaneous fusion of four mitochondrial membranes in yeast (Wong et al., 2003).

The orthologue of Mgm1 in mammals was discovered as a product of a gene which is mutated in patients with autosomal dominant optic atrophy, hence it was christened Optic Atrophy 1 (Opa1) (Alexander et al., 2000). *OPA1* gene in humans is built from 30 exons (Fig. 3), three of which (4, 4b and 5b) are alternatively spliced giving rise to 8 mRNAs and polypeptidic variants (Delettre et al., 2001). In spite of the ubiquitous expression, patterns vary across tissues, being highly abundant in retina, brain, heart and pancreas. Moreover, the relative expression of each isoform also shows tissue specificity (Akepati et al., 2008; Delettre et al., 2001).

At the protein level, although Mgm1 and OPA1 display just 20% amino-acid sequence identity, they share highly conserved secondary features (Fig. 3). Specifically, like Mgm1, OPA1 possesses an MTS (or MIS) responsible for its targeting to the mitochondria that is cleaved upon its import. After MTS, OPA1 contains a putative transmembrane domain (exon 1 and 2), which spans the IMM (Delettre et al., 2000; Olichon et al., 2002), a central

GTPase and a middle domain. The GTPase domain is crucial for the fusion-promoting activity of OPA1 (Cipolat et al., 2004), while the role of OPA1 middle domain is still undefined. Considering that in dynamins the middle domain is implicated in higher order self-assembly, also OPA1 might form complexes through this domain (Olichon et al., 2007; Ramachandran et al., 2007). Additionally, OPA1 has two coiled-coil domains (CC), one close to the N-terminus and one in the C-terminus; the latter is considered to function as a GTPase effector domain (GED) (Akepati et al., 2008). Both the coiled-coil domains are possibly responsible for homotypic or heterotypic protein-protein interactions, and the GED domain is also essential for OPA1 fusogenic function (Cipolat et al., 2004). Two additional hydrophobic domains (TM2a and TM2b) are present exclusively in the spliced exons 4b and 5b.

Apart from the post-transcriptional regulation, OPA1 is also subject to post-translations modifications, mainly due to proteolytic cleavage (Fig. 3). Mitochondrial processing peptidase (MPP) acts on the precursor protein to remove MTS upon its targeting into the organelle (Ishihara et al., 2006). The result of OPA1 processing at the cleavage site S2 is the formation of long and short forms, like in yeast, which can be detected by western blotting as five distinct bands ranging from 100 to 80 kDa. The two higher bands are considered to be the long forms of the all the splicing isoforms 1, 2, 4 and 7, while the three lower molecular weight bands derive from the translation of isoforms 3, 5, 6, 7 and 8. The long forms are reported to be anchored into the IMM, while the short forms, lacking the TM1, are peripherally associated with the membrane facing the IMS (Olichon et al., 2002; Satoh et al., 2003). Ban and coworkers suggested that the short forms are able to associate with cardiolipin *in vitro* and show an enhanced GTPase activity (Ban et al., 2010). The proteases involved in OPA1 cleavage are the rhomboid-related protease presenilin-associated rhomboid-like (PARL), the inner membrane metalloendopeptidase (OMA1), the IMS AAA (i-AAA) protease Yme1L, as well as the matrix AAA (m-AAA) protease subunits paraplegin, AFG3L1 and AFG3L2 (Cipolat et al., 2006; Ehses et al., 2009; Griparic et al., 2007; Song et al., 2007). OPA1 cleavage is either constitutive or inducible. PARL, Yme1l and OMA1 cleave OPA1 constitutively to form fusion competent isoforms (long and low abundant short). PARL activity on OPA1 is dependent on the phosphorylation status of the substrate's cleavage site, pointing out another layer of OPA1 regulation (Pellegrini and Scorrano, 2007), while Yme1l processes exclusively a subset of OPA1 isoforms (Griparic et

al., 2007). Besides the cleavage in physiological conditions, OPA1 further processed in sites other than S2 in response to apoptotic stimuli or dissipation of membrane potential, indicating a dynamic post-translational regulation. The extensive formation of short OPA1 forms under these conditions is accompanied by mitochondrial fragmentation, suggesting that the long forms are essential for fusion promotion (Ishihara et al., 2006). Inducible cleavage in vitro was shown to be mediated by OMA1 (Head et al., 2009). Recently, OMA1 cleavage of OPA1 was reported also *in vivo*, under ischemic brain and kidney injury, underlining the importance of this regulation as a quality control in pathological conditions (Xiao et al., 2014; Baburamani et al., 2015). Moreover, mAAA-protease paraplegin has been proposed to cleave OPA1 at the site S1 upon dissipation of membrane potential (Ishihara et al., 2006). At last, a novel OPA1 cleavage was identified in postprandial liver, that is mediated by an unknown cysteine protease in a Mfn2-dependent manner, suggesting a more complicated proteolytic mechanism in response to metabolic shifts (Sood et al., 2014).

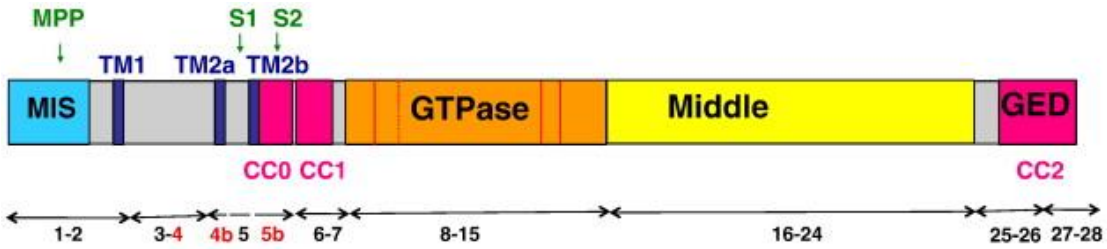

Figure 3. Schematic illustration of OPA1 structure. OPA1 displays a mitochondrial import sequence (MIS) followed by a predicted transmembrane region (TM1), hydrophobic segments (TM2a and TM2b), as well as coiled coil domains (CC), a GTPase domain and a middle domain. TM2a, TM2b and CC0 are found only in spliced exons 4b and 5b. OPA1 exons are depicted by double arrows. Inta-mitochondrial proteolytic cleavage sites for mitochondrial peptidase (MPP), paraplegin (S1) and YME1L (S2) are indicated above the schema. Adapted from (Belenguer and Pellegrini, 2013).

The pro-fusion activity of OPA1 was evident from gene knockout or downregulation. More specifically, OPA1 promotes fusion of the IMM, while it does not affect mitochondrial docking. Surprisingly, in other reports overexpression of OPA1 led to mitochondrial fragmentation, suggesting an opposite function, i.e. fission induction. This observation was made only in already elongated mitochondria. However, in such cells mitochondria retain their capability to fuse, excluding the possibility that OPA1 additionally mediates

fission. Contrary to Mgm1p and mitofusins, OPA1 is not required to be present simultaneously in adjacent mitochondria, in order for them to be fused. However, OPA1 requires MFN1 in order to induce fusion, while Mfn2 is dispensable (Cipolat et al., 2004; Griparic et al., 2004; Song et al., 2009). Furthermore, despite some contradictions (Anand et al., 2014), it is more likely that both long and short OPA1 forms are essential for the accomplishment of its action (Song et al., 2007). Contrary to steady state, stress induced mitochondrial hyperfusion relies only on long OPA1 forms (Tondera et al., 2009). Additionally, OPA1 regulates mitochondrial ultrastucture maintenance and cristae remodeling, independently of its profusion role.

Recent evidence supports the notion that OPA1 interacts with other proteins, which contribute to its fusogenic function, making the picture more complicated. Apart from Mfn1, An *et al* demonstrated that OPA1 cleavage is controlled by its association with Higd-1a, which is crucial for proper mitochondrial fusion (An et al., 2013). Moreover, a proteomic approach in anti-OPA1 immunoprecipitated mitochondrial extracts from Drosophila revealed that dMitofilin (Mic60 orthologue), Hsc70-5 (Mortalin orthologue), as well as Marf (Mitofusin orthologue) act as OPA1-like partners, influencing mitochondrial morphology (Banerjee and Chinthapalli, 2014). However, the mechanism by which they take part in the control of mitochondrial dynamics is not yet clarified. A recent study provided evidence that the mitochondrial nucleoside diphosphase kinase (NM23-H4), which catalyzes the synthesis of GTP through ATP-driven conversion of GDP, provides the fuel for Opa1, enhancing its GTPase activity and thus membrane remodeling (Boissan et al., 2014). A few more proteins, specified in the following pages, have been proposed to interact with OPA1, regulating though its function on cristae shape. Generally, it is obvious that the function of this shaping protein is tightly regulated in various levels (transcriptionally, post-transcriptionally, prost-translationally and in a protein-protein interaction level), underscoring the significance of its role in the organelle.

1.4.2.1.3 Ugo1

Ugo1 is another fusion-promoting protein identified in yeast. It is an integral outer mitochondrial membrane protein. Its N-terminus is exposed to the cytosol, interacting with Fzo1, while its C-terminal faces the IMS and associates with Mgm1. Ugo1p functions

as a bridge between Fzo1 and Mgm1, essential for both OMM and IMM fusion (Sesaki and Jensen, 2001; Sesaki and Jensen, 2004). Abrams *et al* characterized a solute carrier Slc25a46 as an Ugo1-like protein and showed that it plays a role in mitochondrial dynamics. Mutations in *Slc25a46* gene are the cause of a spectrum of optic atrophy disorders, which have been already associated with OPA1 mutations as well (Abrams et al., 2015).

1.4.2.2 Other regulators of fusion

Fzo1/Mitofusins, Mgm1/OPA1 and Ugo1 are the hitherto well-established fusogenic proteins. In the past few years, other proteins have been proposed to participate in the control of mitochondrial morphology by promoting fusion. ROMO1 is one of those: its silencing leads to mitochondrial fragmentation, loss of cristae, deficient OXPHOS and sensitivity to cell death. Norton et al proposed that it acts in the same pathway as OPA1 and that ROMO1 oligomerization is differentially regulated according to the redox state (Norton et al., 2014). Additionally, LETM1 loss results in striking abnormalities in mitochondrial morphology, indicating that is a member of the group of mitochondrial dynamics regulators (Dimmer et al., 2008). Prohibitin 2 is another protein that has been associated with mitochondrial elongation, as well as in ultrastructure integrity (Kasashima et al., 2006). Its exact function is discussed in the following sections.

1.4.2.3 Lipids

Besides the mitochondrial shaping proteins, recent studies ascribe to non–bilayer-forming lipids a role in mitochondrial fusion. In particular, cardiolipin (CL) and phosphatidylethanolamine (PE) are required for proper mitochondrial morphology. These lipids generate a negative membrane curvature, which facilitates mitochondrial fusion. Interestingly, loss of CL and PE in yeast led to mitochondrial fragmentation, along with a reduction of the fusion protein Mgm1, interpreting probably the fusion defect. Chan and McQuibban proposed that PE influences mitochondrial fusion by regulating biophysical properties of the membranes, as well as contributing to the biogenesis of short forms of Mgm1. Although the exact mechanisms of action are not fully exploited yet, it is obvious

that the delicate functional coordination of lipids and polypeptidic molecules is essential for balanced mitochondrial dynamics (Joshi et al., 2012; Chan and McQuibban, 2012).

1.5 The physiological role of mitochondrial dynamics

Changes in the morphology of mitochondria affect organelle functions, having an impact on a wide range of cellular biological processes. In general, mitochondrial dynamics provides a mechanism for mitochondrial quality control, keeping the organelles in "good shape". In particular, mitochondrial fusion favors the continuous exchange of mitochondrial content, such as mtDNA and metabolites, between different organelle units. In that way, a damage in one mitochondrion can be attenuated by its fusion with a functional one (Yoneda et al., 1994).

The link between mitochondrial shaping proteins and mtDNA maintenance was originally reported in studies using yeast, showing that functional Fzo1 and Mgm1p are essential for the integrity of mitochondrial genome (Guan et al., 1993; Hermann et al., 1998; Rapaport et al., 1998). Accordingly, Chen and co-workers observed a lack of mtDNA nucleoids in *Opa1* null and double *Mfn1/2* null cells, suggesting that the mammalian fusion machinery is required for the maintenance of the mtDNA organization units (Chen et al., 2007; Chen et al., 2010). However, these experiments were conducted in cells with chronic ablation of fusogenic proteins and, in contrast, mtDNA copy number is unaltered when OPA1 is deleted acutely; hence, the effects on mtDNA stability might be indirect consequences of fusion impairment (Cogliati et al., 2013). On the other hand, prevention of mitochondrial fission (DRP1 loss of function) is linked to mtDNA loss (Parone et al., 2008). Although there are several lines of evidence correlating mitochondrial dynamics to genome stability, this link is more likely due to the importance of the balance between fusion and fission events, rather than to a selective role of one mitochondrial shaping protein on mtDNA.

Apart from mtDNA maintenance, several studies have associated the loss of mitochondrial shaping proteins to mitochondrial respiration defects. The laboratories of Zorzano and Chan, analyzing the effects of *Mfn2* mutations or *Mfn2* or *Opa1* knockdown, observed reduced membrane potential and decreased oxygen consumption in these cells (Bach et al., 2003; Chen et al., 2005). As far as mitochondrial fission is concerned, its inhibition by DRP1 or Fis1 silencing leads to similar bioenergetic defects to those appearing after

blockage of fusion regulators, including reduction of respiration rates (Benard et al., 2007; Twig et al., 2008). On the other hand, mitochondria overexpressing Mfn2 aggregate in the periphery of the nucleus and display an increased membrane potential, while the whole cell show an enhanced glucose oxidation. To clarify whether the effects of the overexpression were due to increased fusion rates, the researchers performed the same analysis with a truncated form of Mfn2 that has no longer the ability to induce fusion. Their results suggested that mitochondrial metabolism alterations are not depending on the imbalance of mitochondrial dynamics (Pich et al., 2005). In sum, mitochondrial fusion-fission events might influence the OXPHOS efficiency *per se* or in indirect manners through distinct roles of the mitochondrial shaping proteins (i.e. Mfn2 via regulating the tethering of mitochondria to the endoplasmic reticulum, thus controlling calcium influx, Opa1 via the regulation of cristae shape, as described in the next chapters).

Moreover, elongation of healthy mitochondria protects them from clearance by autophagy (Gomes et al., 2011). On the other hand, mitochondrial division facilitates the mitochondrial biogenesis and the segregation of damaged and dysfunctional mitochondria by autophagy (Knott et al., 2008; Twig et al., 2008). Moreover, under stress conditions, mitochondrial network is fragmented with parallel changes in the individual organelle's ultrastructure that contribute to the apoptotic pathway, leading to cell death (Youle and van der Bliek, 2012). These structural changes upon apoptotic stimulation are further described in the following chapters.

1.6 Macromolecular complexes and lipids involved in cristae shape integrity

The cristae are the principal site of oxidative phosphorylation, since its membranes host all the complexes implicated in mitochondrial respiration, while the only soluble OXPHOS member, cytochrome c, mainly localizes in the area engulfed by cristae (Scorrano et al., 2002; Gilkerson et al., 2003). Such a highly defined compartmentalization suggests that the IMM is organized into cristae to ensure optimal conditions for ATP production minimizing the diffusion of metabolites, such as protons and ADP during respiration (Demongeot et al., 2007). The shape of cristae changes in response to different mitochondrial respiratory states in order to enhance OXPHOS efficiency (Hackenbrock,

1966; Mannella et al., 2001; Hackenbrock et al., 1980; Cogliati et al., 2013). Moreover, given the fact that factors residing within the folds of IMM, such as cytochrome c, are involved in mitochondrial apoptotic pathways (Scorrano et al., 2002), the maintenance of an intact ultrastructure is instrumental to protect cells from apoptosis.

The active modulation of cristae spatial organization is a consequence of spontaneous forces, including intrinsic lipid curvature, combined with complex protein interactions and binding to other membranes. Regarding the first, the OMM likely serves as a border to limit the extension of cristae structures, while the protein-rich matrix determines the minimum volume of the inner compartments of the organelles. As far as the lipids and protein interactions are concerned, below we describe all the so far identified macromolecular factors that affect cristae shape integrity.

1.6.1 MICOS complex

"Mitochondrial contact site and cristae organizing system" (MICOS) is a large heterooligomeric protein structure of the IMM composed by Mic10 (MINOS1), Mic12, Mic19 (CHCHD3), Mic25 (CHCHD6), Mic26 (APOO), Mic27 (MOMA1, APOOL) and Mic60 (Mitofilin) (Fig. 4). Very recently, this complex was described as two independent protein assemblies – Mic27/Mic10/Mic12 and Mic60/Mic19 – which are linked via Mic19 (Fig. 5) (Friedman et al., 2015a). Moreover, a novel essential MICOS member was identified: the protein QIL1 (C19orf70) (Guarani et al., 2015); thus its exact composition and architecture are still under active investigation. A comprehensive evolutionary study revealed a widespread conservation of MICOS complex among eukaryotes, but also an origin from α-protobacteria – the ancestors of mitochondria. Interestingly, its components are found exclusively in organisms with cristae-containing mitochondria (Munoz-Gomez et al., 2015).

This whole protein assembly organizes the mitochondrial membranes in terms of inner membrane architecture, cristae junction maintenance and IMM-OMM contact sites formation (Fig. 4). Genetic ablation of individual MICOS subunits leads to mitochondrial fragmentation, cristae junction loss and concentric IMM structures formation. Recently, a proposed model in yeast suggested that specifically Mic19 might determine the number of cristae junction through its action as a connector of the two independent MICOS

subcomplexes found predominantly in different cristae junction. Besides the mitochondrial morphology and ultrastructural defects, MICOS disassembly leads to reduced respiration, due to faulty OXPHOS complexes distribution and activity. Additionally, MICOS dysfunction is correlated to apoptosis impairment and nucleoids aggregation (Xie et al., 2007; von der et al., 2011; Alkhaja et al., 2012; Yang et al., 2012; Weber et al., 2013; Itoh et al., 2013; Darshi et al., 2011; Friedman et al., 2015b; John et al., 2005). Notably, MICOS members have non-redundant functions in yeast since the absence of both MICOS subcomplexes leads to more severe morphological and respiratory growth defects than deletion of single MICOS subunits or subcomplexes (Friedman et al., 2015a).

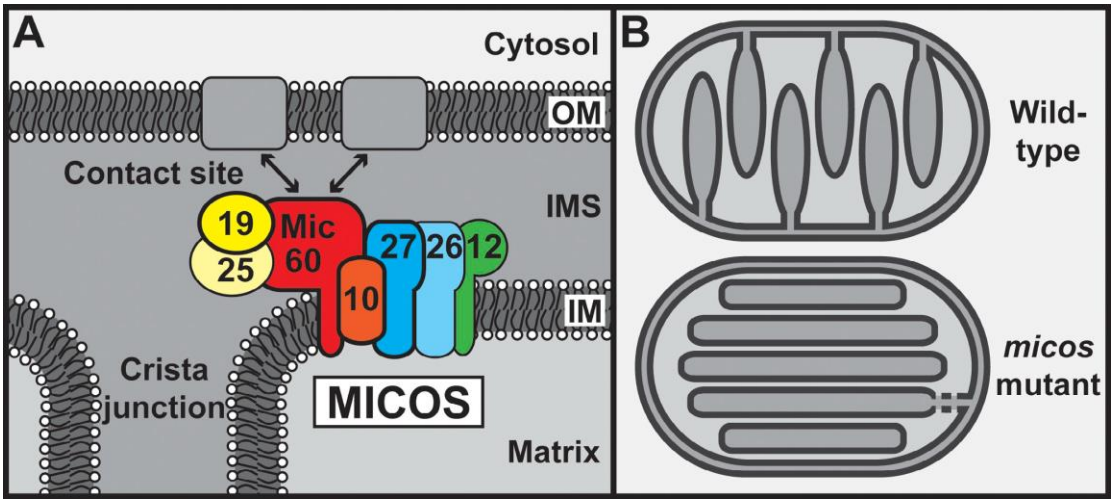

Figure 4. A. MICOS complex (Hypothetical model). MICOS complex is required for maintenance of the characteristic architecture of inner mitochondrial membrane (IM) and forms contact sites with the outer membrane (OM). In budding yeast, six subunits of MICOS have been identified. All subunits are exposed to the intermembrane space (IMS), five are integral inner membrane proteins (Mic10, Mic12, Mic26, Mic27, and Mic60), and one is a peripheral inner membrane protein (Mic19). The MICOS complex of metazoa additionally contains Mic25, which is related to Mic19, yet subunits corresponding to Mic12 and Mic26 have not been identified so far. Bold boundary lines indicate MICOS subunits that have been conserved in most organisms analyzed. **B.** Top. Wild-type architecture of the mitochondrial inner membrane with crista junctions and cristae. Bottom. This architecture is considerably altered in micos mutant mitochondria: most cristae membranes are detached from the inner boundary membrane and form internal membrane stacks. Adapted from (Pfanner et al., 2014).

Furthermore, MICOS complex connects the IMM with the OMM through its association with the mitochondrial import machinery (SAM and TOM complexes) (Xie et al., 2007),

thus displaying an additional, distinct role on mitochondrial protein biogenesis (von der et al., 2011). Looking at a higher hierarchical membrane organization, MICOS complex has been proposed to consist of a multimeric structure that spans three membranes – the endoplasmic reticulum membrane, the OMM and IMM (van der Laan et al., 2012). Apart from MICOS, also SAM complex and the endoplasmic reticulum (ER)-mitochondria encounter structure (ERMES) participate in this protein machinery - via proposed physical and genetic interactions (Hoppins et al., 2011a; Meisinger et al., 2004) -, which likely coordinates the inter-organellar organization and communication.

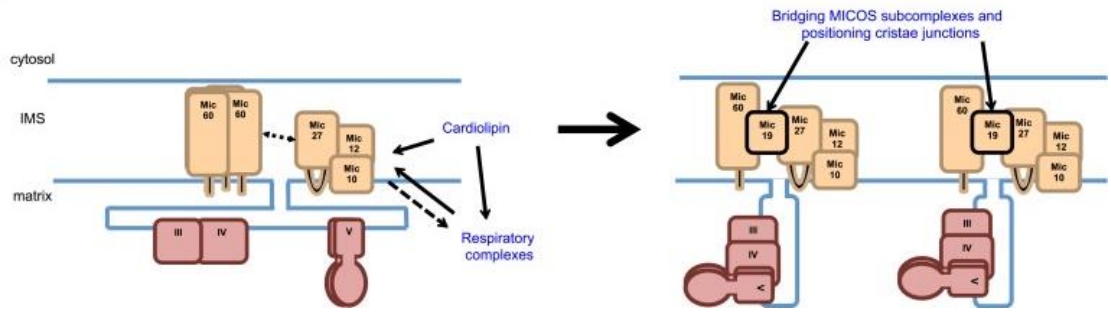

Figure 5. The proposed model by Friedman and colleagues. The schematic representation depicts the organization and roles of MICOS subcomplexes in budding yeast. Additionally, it indicates the interrelationship between MICOS, cardiolipin and respiratory supercomplexes. Adapted by (Friedman et al., 2015a).

In this Thesis we focus specifically on the major component of MICOS complex, consequently a detailed description of its structure and function follows.

Mic60/Mitofilin

Mic60, also known as Mitofilin/IMMT, Formation of Cristae Junctions (Fcj1) or Heart Muscle Protein (HMP) is the largest and one of the core components of MICOS complex. Mic60 is a 90kDa protein possessing an N-terminal mitochondrial targeting sequence, a transmembrane helix and a C-terminal domain exposed into the IMS; the latter consists of a coiled-coil domain and a conserved C-terminal domain (Rabl et al., 2009; Zerbes et al., 2012). The same secondary structural sequence is shared between species from yeast to human (Rabl et al., 2009; Zerbes et al., 2012).

Downregulation of Mic60 results in instability of other MICOS subunits and consequently of the whole multiprotein assembly (Li et al., 2015). Mic60-deficient mitochondria of yeast and human cells form abnormal interconnected membrane network and cristae structures disconnected from the inner boundary membrane, pointing to a conserved function of Mic60 on cristae formation and/or maintenance of cristae junctions (Rabl et al., 2009; Zerbes et al., 2012; John et al., 2005; Rabl et al., 2009; Zerbes et al., 2012). Additionally, downregulation of Mic60 results in OXPHOS defects, abnormal nucleoids distribution and impaired mitochondrial translation. The latter link has been explained by its interaction with the core nucleoid proteins TFAM and TFB2M (Itoh et al., 2013; Yang et al., 2015). Another hypothesis relating Mic60 to mtDNA integrity is its assumed interaction with PARP-1 - a nuclear enzyme that translocates in unidentified way inside mitochondria, possibly to regulate mtDNA stability (Rossi et al., 2009). Moreover, Mic60 interacts with Mic19/Chchd3 – a scaffold protein for MICOS complex, important for Mic60 stability – as well as with OPA1, in order to ensure the correct mitochondrial ultrastructure and the proper bioenergetic capacity of mitochondria (Darshi et al., 2011). Interestingly, Mic60 homeostasis is controlled by proteolytic cleavage by the mitochondrial i-AAA protease Yme1L (Li et al., 2015).

Mic60 is reduced by approximately 50% in fetal Down syndrome brain (Myung et al., 2003) and is a target antigen in melanoma-associated retinopathy (Pfohler et al., 2007). On top of this, Mic60 alterations correlate to various diseases in studies on animal models, including cardiomyopathies and neurodegeneration (Van Laar et al., 2008; Omori et al., 2002; Baseler et al., 2011); thus emphasizing the relevance of cristae network stability for cell physiology.

1.6.2 Cardiolipin

Besides polypeptidic molecules and complexes, also cardiolipin has been associated with the modulation of mitochondrial membranes shape, along with mitochondrial fusion, as described before. Cardiolipin is a four-tailed phospholipid located predominately in the inner mitochondrial membrane, where it is also biosynthesized. This phospholipid has been shown to interact non covalently with various proteins, such as the substrate carrier proteins (Pebay-Peyroula et al., 2003), cytochrome c (Tyurin et al., 2007) and the

respiratory chain complexes (Fry and Green, 1981; Lange et al., 2001; Robinson, 1993), playing, therefore, an important role in the complexes activity. On top of this, cardiolipin is essential for the respiratory supercomplexes assembly, thus contributing to OXPHOS efficiency (Pfeiffer et al., 2003; Zhang et al., 2002). Importantly, cardiolipin is required for yeast Mic27/Mic10/Mic12 assembly, suggesting the coordination between lipids and proteins for the correct topology of the IMM (Friedman et al., 2015a). Furthermore, cardiolipin is needed for the assembly of the different Mgm1 isoforms in *Saccharomyces cerevisiae*, further supporting the role of this lipid in the modulation of cristae architecture (DeVay et al., 2009). Besides mitochondrial respiration, cardiolipin is involved in the apoptotic pathway, by providing the platform for action of the proapoptotic proteins BID and caspase-8 (Lutter et al., 2000; Gonzalvez et al., 2008).

From a mechanical point of view, cardiolipin exerts a high-intrinsic-curvature and a tendency to form homogeneous clusters that spontaneously localize to curved membrane regions of prokaryotic cells in order to stabilize their geometry (Huang et al., 2006). In a cell-free, minimal membrane system, cardiolipin is sufficient to form dynamic invaginations, similar to cristae, in response to a local pH gradient (Khalifat et al., 2011; Khalifat et al., 2008).

Cardiolipin is post-synthetically modified to produce its mature form. Disturbances in cardiolipin maturation are associated with human pathologies, including Barth syndrome (Schlame and Ren, 2006), diabetes (Han et al., 2007), heart failure (Sparagna et al., 2007) and Parkinson's disease (Ellis et al., 2005), underlying the important functions of the lipid. Barth syndrome is caused by mutations in the gene encoding for the enzyme tafazzin, which catalyzes cardiolipin maturation. Mitochondria of Barth syndrome patients display aberrant ultrastructure and disassembled respiratory supercomplexes (Schlame and Ren, 2006; McKenzie et al., 2006), further supporting the potential function of cardiolipin on cristae organization.

1.6.3 ATP-synthase

Mitochondrial F1F0-ATP-synthase is organized in dimers in the cristae edge, which in turn assemble to form oligomers. These long double rows composed by the enzyme dimers along the cristae ridges are conserved across species. They were firstly observed by

freeze-fracture electron microscopy in *Paramecium multimicronucleatum* (Allen et al., 1989) and 3D reconstruction of cryo-electrotomograms confirmed their existence in various species, including algae, yeast, plants and mammals (Davies et al., 2012; Strauss et al., 2008; Davies et al., 2011). Davies and colleagues suggested that ATP-synthase dimers are crucial for cristae morphology, since their formation is the driving force for the lipid bilayer bending. This subsequently results to their association into rows due to the elastic membrane conformation. Accordingly, the dimer rows favor the positive curvature in the cristae tips (Fig. 6). In line with this idea, knocking out either ATP-synthase dimer-specific subunits e or g, impairing ATP synthase dimerization, leads to onion-like cristae structures (Davies et al., 2012; Paumard et al., 2002). In addition, electron cryotomography revealed cristae collapse in aging mitochondria, which was accompanied by disassembly of ATP-synthase dimers (Daum et al., 2013).

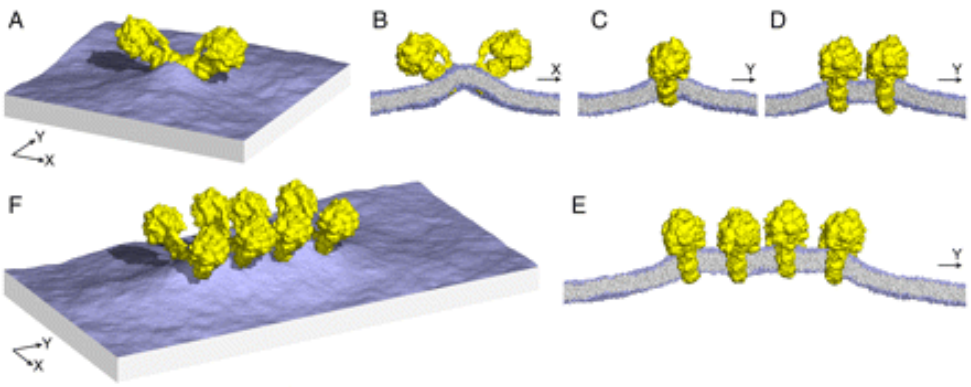

Figure 6. Membrane curvature induced by ATP synthase dimers (A**)** perspective view of a simulated membrane patch with an ATP synthase dimer distorting the planar lipid bilayer. **(**B**,** C**)** cross sections through the membrane patch in (**A**) showing the curvature profile of the lipid bilayer in ***x*** and ***y*** direction. **(**D**)** and **(**E**),** curvature profiles as in (**C**) for membranes with two or four ATP synthase dimers, side by side. **(**F**)** perspective view of the row of four dimers shown in (**E**). Adapted from (Davies et al., 2012).

Apart from the structure and organization of ATP-synthase, also F1F0-ATPase inhibitor factor (IF1) has been suggested to determine the cristae shape. When mitochondrial respiration is compromised, IF1 negatively regulates the reversed function of ATP-synthase and, hence, conserves ATP at the expense of Delta(psi). Changes in its levels result in alterations in cristae density and oligomerization status of ATP-synthase during physiological and pathological conditions (Campanella et al., 2008).

Conversely, a study by Bornhövd and colleagues does not prove any direct consequence of the destabilization of ATP-synthase rows to cristae morphology. Instead, they proposed that mutations in the subunits g and e lead to a reduction of membrane potential due to altered inner mitochondrial membrane dynamics, disruption of lipid microdomains and subsequent impaired overall flux through the respiratory chain complexes (Bornhovd et al., 2006). Consequently, whether the 3D status of ATP-synthase assemblies impact directly on cristae curvature is still under debate.

1.6.4 OPA1 complex

Mgm1p/OPA1 is another protein that regulates cristae shape independently of its profusion role (Frezza et al., 2006; Griparic et al., 2004). In both yeast and human cells, ablation or mutation of this protein has been associated with cristae disorganization, characterized by irregular shape and large cristae junctions, indicating a role in the formation and maintenance of cristae. Interestingly, Amutha et al. demonstrated that Mgm1p deficiency additionally correlates to the inability of ATP-synthase to oligomerize. Yet, whether this is a cause or the consequence of cristae structure aberrations was not clarified (Amutha et al., 2004; Sesaki et al., 2003; Griparic et al., 2004).

Studies in our laboratory pointed out that mammalian OPA1 controls cristae shape by being organized in high molecular weight complexes, which are eliminated upon apoptotic stimulation. In particular, OPA1 complexes reside in the cristae junctions determining the CJ diameter, as well as cristae lumen width (CLW). Overexpression of OPA1 tightens cristae (decreased CLW) whereas, *Opa1* depleted cells are more prone to cytochrome c release from the cristae into the IMS and eventually to the cytosol, leading to increased apoptosis sensitivity. It is worth mentioning that for the formation of OPA1 complexes both the transmembrane and the soluble form of the dynamin-like protein are needed, underlining the importance of OPA1 processing also in cristae biogenesis (Cogliati et al., 2013; Frezza et al., 2006; Varanita et al., 2015).

A similar model has been proposed for yeast Mgm1p by the group of Nunnari Mgm1p is required in trans on mitochondria to maintain their ultrastructure intact, while mutations in its GED domain are linked to abnormal cristae structure, suggesting that intermolecular

Mgm1 interactions are mechanistically crucial for cristae formation (Meeusen et al., 2006).

In spite of the suggested homotypic OPA1 interactions, we cannot exclude the possibility that also proteins other than OPA1 are part of these assemblies regulating cristae shape. These proteins could act either as OPA1 coplayers to directly function on cristae biogenesis or by assisting the complexes formation or even by stabilizing OPA1. Very recently, a few lines of evidence supported this hypothesis. Patten et al identified among the OPA1 interactors certain mitochondrial solute carriers (SLC25A) , whose ablation or inhibition led to loss of the mitochondrial architecture integrity, along with blockage of OPA1 oligomerization and function (Patten et al., 2014a). Moreover, Mitofilin (Mic60) and Chchd3 (Mic19) have been shown to interact with OPA1 (Darshi et al., 2011).

1.6.5 Prohibitins

The Prohibitin (PHB) complex is another macromolecular polypeptide assembly in the inner mitochondrial membrane, composed by two evolutionary conserved and highly homologous proteins, PHB1 and PHB2. Both prohibitins are indispensable for the complex formation, which is anchored to the IMM (Artal-Sanz et al., 2003; Tatsuta et al., 2005).

The ring shape of prohibitins complex could suggest a scaffolding function for proteins or lipids (Back et al., 2002; Nijtmans et al., 2000; Browman et al., 2007), essential for the modulation of the inner, outer membrane as well as cristae junction organization. Indeed, deficiency of PHB2 led to cristae network disorganization and mitochondrial fragmentation. These morphological aberrations coincided with excessive OPA1-cleavage, increased sensitivity to apoptotic stimulation and impaired cell proliferation, defects that were corrected by the reintroduction of a long form of OPA1. Therefore, PHB2 exerts its functions on mitochondria via the regulation of OPA1-processing (Merkwirth et al., 2008). Another line of evidence supporting this regulation is that PHB1 interacts with SPG7, a member of mAAA-protease complex, which is involved in OPA1 proteolytic cleavage (Steglich et al., 1999; Duvezin-Caubet et al., 2007).

Prohibitins are involved also in the biogenesis and assembly of respiratory complexes, via their interaction with the protease complex or by a scaffolding action (Steglich et al., 1999; Nijtmans et al., 2002). The hypothesis of a scaffold function of prohibitins derives from

their similarity with a large family of distantly related membrane proteins, the SPFH family. Members of this family have been observed in lipid rafts, indicating their scaffold action (Tavernarakis et al., 1999; Browman et al., 2007). More specifically, prohibitins interact with stomatin-like protein 2, which in turn binds cardiolipin and hence organize the respiratory complexes and supercomplexes in an optimal and efficient assembly (Da et al., 2008; Christie et al., 2011; Mitsopoulos et al., 2015). Furthermore, a systematic study in yeast revealed a genetic interaction between prohibitins and enzymes participating in phosphatidylethanolamine (PE) and cardiolipin (CL) biosynthesis. Indeed, downregulation of prohibitins in cells with low PE resulted in severe inner membrane abnormalities followed by dissipation of membrane potential and cell death (Osman et al., 2009). Recently, prohibitin was proposed to interact with DNAJC19 forming a large complex to control cardiolipin remodeling. Ablation of any of the components of this assembly leads to accumulation of immature cardiolipin, defective cell growth and impaired mitochondrial ultrastructure, defects similar to cells from Barth syndrome patients (Richter-Dennerlein et al., 2014). All the above data point to a function of prohibitins in phospholipid metabolism, which is consistent with its role as a scaffold complex. Moreover, prohibitins complex participates in mtDNA maintenance (Bogenhagen et al., 2008). Whether this role is due to a direct interaction with mtDNA or proteins of the nucleoid structure, like TFAM (Kasashima et al., 2008), or indirect via the modulation of the inner membrane structure or lipid composition is still unanswered.

1.6.6 MICS1/GHITM

Mitochondrial morphology and cristae structure 1 (MICS1), aka TMBIM5 or growth hormone-inducible transmembrane protein (GHITM) is a member of Bax inhibitory protein-like family. It is ubiquitously expressed in mammalian tissues, and it is overexpressed in breast cancers (Reimers et al., 2007; Lisak et al., 2015). MICS1 has seven transmembrane domains, which span to the inner mitochondrial membrane, while its carboxy-terminal region faces the IMS. As its name points, MICS1 is essential for the proper cristae organization, since its downregulation has been associated with less cristae and ring-like IMM structures. Similarly to the other members of this family (Bax Inhibitor 1, Lifeguard and h-GAAP), MICS1 exerts a cytoprotective role through the regulation of

cytochrome c release, independently of the modulation of mitochondrial morphology maintenance (Oka et al., 2008). Recently, a collective study on Bax inhibitory-like protein family revealed a novel function shared between all the members in Ca^{2+} homeostasis (Lisak et al., 2015). However, the precise mechanism of MICS1 action is not clear.

1.6.7 NOA1

Nitric Oxide-Associated 1 (NOA1) is a protein highly conserved across bacteria and eukaryotes. Although the very first studies on NOA1 orthologues in *Helix pomatia* and *Arapidopsis thaliana* proposed a catalytic role of NOA1 in NO production, leading the authors to christen it as "Nitric Oxide Synthase" (NOS) (Huang et al., 1997; Guo et al., 2003), this was challenged early after its characterization (Zemojtel et al., 2006a; Moreau et al., 2008). Instead, NOA1 is a functional GTPase (Moreau et al., 2008), belonging to the circularly permutated GTPase family (Sudhamsu et al., 2008), whose exact function in eukaryotes is still obscure. The bacterial homolog of NOA1, YqeH, catalyzes the hydrolysis of GTP to GDP in a potassium dependent manner and is essential for *Bacilus subtilis* growth (Anand et al., 2010; Zemojtel et al., 2006b). Its crystal structure, apart from a circularly permutated GTPase domain, revealed additionally a peculiar C-terminal β-domain probably responsible for nucleic acid and peptide recognition (Sudhamsu et al., 2008). YqeH along with other members of its protein superfamily appeared to be required for proper ribosome biogenesis and assembly (Loh et al., 2007; Uicker et al., 2007; Anand et al., 2009).

In eukaryotes, NOA1 contains a classical mitochondrial targeting sequence (MTS) (Zemojtel et al., 2006b), but also, according to a recent report, a classical bipartite nuclear localization signal (Fig. 7) (Al-Furoukh et al., 2014). In yeast, YOR205C (alternative names: mitochondrial GTPase MTG3, AIM40, GEP3, FMP38) was shown to be important for the correct assembly of the small mitoribosomal subunit, efficient respiration, as well as mtDNA stability (Paul et al., 2012). Two genetic interactome studies in yeast – one in the whole mitochondrial genome held in the laboratory of Nunnari J. (Hoppins et al., 2011b) and another focused on prohibitins performed by the group of Langer T. (Osman et al., 2009) – identified YOR205C as a genetic interactor of prohibitins (GEP3), necessary for cell survival in the absence of prohibitins. Mutation in its gene correlates to decreased

cardiolipin and PE levels. Moreover, GEP3 was associated with mitochondrial genome maintenance.

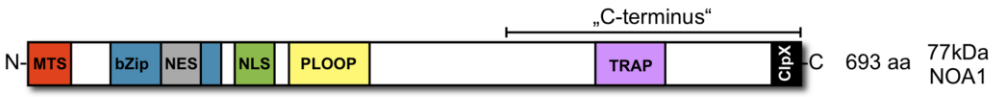

Figure 7. Schematic representation of functional mammalian NOA1 domains. MTS: mitochondrial targeting sequence, bZip: basic Leucine zipper domain, NES: nuclear export signal, NLS: nuclear localization signal, PLOOP: circularly permutated GTPase domain, TRAP: RNA binding domain, ClpX: ClpX recognition motif. Adapted from (Al-Furoukh et al., 2014).

Mammalian NOA1 localizes predominately to mitochondria, being associated with the IMM and facing the matrix. The GTPase domain contains a 100-aa insert absent from YeqH, which could possibly suggest diversity in its function along evolution. NOA1 is ubiquitously expressed in mammalian tissues, being present in a slightly higher level in heart, kidney and lung (Tang et al., 2009).

The significance of this protein's role for cell survival is underlined by the fact that NOA1 deficient mice are lethal at midgestation. Interestingly, cells lacking NOA1 exhibit an aberrant mitochondrial morphology and cristae structure (Tang et al., 2009; Kolanczyk et al., 2011). Like its bacterial homologue, the mammalian NOA1 is essential for the proper mitochondrial translation, but also mtDNA maintenance (Kolanczyk et al., 2011; He et al., 2012). Various lines of evidence from three different groups converge to the role of NOA1 in mitochondrial metabolism. Tang *et al* showed reduced mitochondrial oxygen consumption when the substrate is only glutamate/malate, as well as an interaction between NOA1 and complex I subunits (Tang et al., 2009). On the other hand, Heidler *et al* suggested that NOA1 regulates OXPHOS through its interaction with complex IV and RSC facilitating their assembly (Heidler et al., 2011). In the study of Kolanczyk, where the knockout NOA1 fibroblasts were generated, a global respiration defect was reported. The only complex excluded from the OXPHOS defects was CII, the only one containing exclusively nuclear-encoded subunits. Thus, Kolanczyk et al correlated OXPHOS deficiency to mitochondrial translation insufficiency (Kolanczyk et al., 2011). Last but not least, loss

of NOA1 was associated with extensive ROS production and oxidative stress, but also increased staurosporine-induced apoptosis (Heidler et al., 2011; Kolanczyk et al., 2011).
Immunoprecipitation followed by stable isotopic labeling by amino acids (SILAC) analysis unveiled prohibitin as a potential interactor of mammalian NOA1, a result that is in line with the interactome studies on yeast (Heidler et al., 2011; Osman et al., 2009). However, the interaction was not confirmed biochemically in mammalian cells. Among the suggested candidate interactors of NOA1 is the pro-apoptotic protein death-associated protein 3 (DAP3), which is supposed to be a regulator of not only programmed cell death, but also mitochondrial dynamics and mitochondrial protein synthesis (Xiao et al., 2015). Although it is conceivable that NOA1 plays vital roles for mitochondrial physiology and architecture, further investigation is required to unravel its precise function.

1.7 Physiological role of mitochondrial ultrastructure

The topology of the inner membrane has an impact on specific mitochondrial functions, namely metabolism, ROS production and apoptotic signaling. Recently, our laboratory provided experimental evidence supporting that the cristae shape influences the respiration rate through the regulation of the assembly of the respiratory supercomplexes (RCS). More specifically, a mild overexpression of OPA1 caused the tightening of the cristae resulting in a higher RCS assembly and hence in an enhanced oxidative phosphorylation. These events had a further impact on the cell, since it favored the mitochondrial-dependent cell growth (Cogliati et al., 2013). Considering that the cells have to respond in the constantly changing metabolic demands of the tissue, it is reasonable to hypothesize that, in order to adapt to these, their mitochondria could dynamically alter their organization. Indeed, upon starvation or energy substrate deprivation, OPA1 oligomerization is rapidly increased to regulate cristae shape and improve the bioenergetic status of mitochondria. In this modulation, the OPA1 interactor SLC25A is implicated (Patten et al., 2014b).
Furthermore, oxidative stress causes a reorganization of the IMM of mitochondria of protozoans that survive in extreme environments. Under normal conditions, the mitochondrial cristae of the amoeba *Chaos carolinensis* have a tubular shape. This is altered remarkably after fasting, leading to the formations of a paracrystalline IMM

network with cubic symmetry (Deng et al., 1999). This structural transition coincides with increased ROS production, along with breakdown of internal carbon stores. Therefore, it was suggested that rearrangement of cristae upon starvation might protect the organelles from oxidative damage and, in particular, provide a shelter of RNA while enhancing their translation (Deng and Almsherqi, 2015; Deng et al., 2002).

Last but not least, another example of the correlation between inner membrane dynamics and mitochondrial function is the so-called cristae remodeling during apoptosis. Scorrano and co-workers demonstrated that stimulation by a truncated form of a pro-apoptotic protein, Bid, led to a rapid mitochondrial ultrastructural rearrangement, which was characterized by increased interconnectivity of the intracristal spaces and a notable widening of the cristae junctions. This dramatic change in the cristae shape is accompanied by an enhanced mobilization of the cristae endowed cytochrome c, which subsequently amplifies the cytosolic caspase –dependent apoptotic pathway (Scorrano et al., 2002). Since my thesis focuses on cristae remodeling during programmed cell death, we are dedicating a separate chapter for the detailed analysis of this process.

Taking into account all the above, interventions of the inner membrane organization might serve as a beneficial way to regulate metabolism in pathological situations. Interestingly, our lab crossing two animal models characterized by respiratory deficiency with mice mildly overexpressing OPA1, demonstrated that amelioration of cristae shape can per se counteract mitochondrial dysfunction (Civiletto et al., 2015).

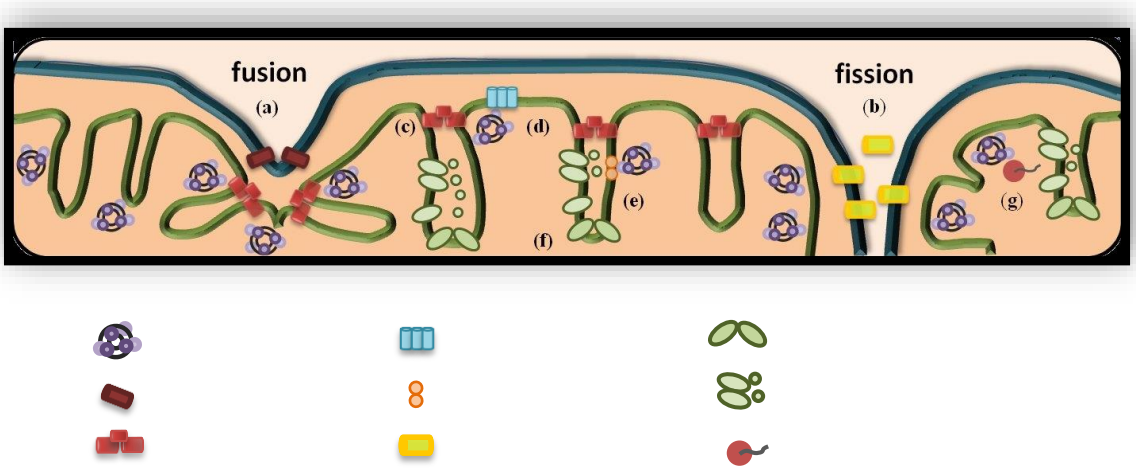

Figure 8. Core regulators of mitochondrial morphology and ultrastructure. (a-b) Mitochondrial fusion is facilitated by mitofusins and OPA1, and fission by DRP1. (c) OPA1 form complexes determining the shape of cristae junctions. (d)

MICOS complex organizes the cristae. (e) Prohibitins participating in the formation of proper mitochondrial architecture. (f) ATP synthase dimers stabilize cristae structure by forming the positive membrane curvature. (g) Nucleoids associated with ribosomes compose the mitochondrial genome expression machinery, whose optimal function is affected by the correct mitochondrial internal organization. The outer mitochondrial membrane is indicating in blue, while the inner membrane in green.

1.8 Diseases associated with aberrant mitochondrial dynamics

Deregulation of mitochondria-shaping proteins has been associated with a number of human pathologies, underscoring the relevance of mitochondrial dynamics in cellular functions and tissue homeostasis. Targeting mitochondrial dynamics regulators or downstream mitochondrial factors could ameliorate the symptoms or even treat the diseases. The broad spectrum of diseases linked to imbalanced fusion and fission or aberrant mitochondrial architecture include neuronal and neurodegenerative disorders, cancer and diabetes.

1.8.1 Neurodegeneration

The precise mechanisms underlying neuronal cell loss in neurodegenerative disorders remain elusive. Nevertheless, various hints suggest that imbalanced mitochondrial dynamics, excessive fission and apoptosis may be liable for some kinds of neurodegeneration.

ADOA

In 2000, two different research groups identified OPA1 mutations as the cause of autosomal dominant optic atrophy (ADOA), which is the most common form of inherited optic neuropathy (Alexander et al., 2000; Delettre et al., 2000). ADOA is a clinically heterogeneous disease mainly characterized by visual impairment with moderate to severe loss of visual acuity, temporal optic disc pallor, blue-yellow dyschromatopsia and central scotoma. The penetrance in family members sharing the same mutation and the onset of the disease symptoms can vary remarkably (Ferre et al., 2005; Votruba et al., 1998). From a histopathological point of view, the fundamental pathology shared in all the ADOA patients is the degeneration of retinal ganglion cells (RGCs) accompanied by optic nerve atrophy (Kjer et al., 1983; Kline and Glaser, 1979). RGCs are the only affected cells among the 60 different neuronal cell types found in the retina. Although Opa1 protein level in the retina are particular high (Alexander et al., 2000) they are not higher

in RGCs than in any other retinal cells (Kamei et al., 2005); thus the reason for ADOA specificity is still unidentified.

The hundreds of the different Opa1 mutations published so far – collected in the eOPA1 database – consist of substitutions, as well as deletions and insertions. They have been detected to locate in various regions of the protein, including the GTPase domain, but also other functional OPA1 regions (N-terminus, coiled coil domains, middle and GED domain) (Ferre et al., 2005). The majority of the mutations lead to a truncated product, which probably causes loss of function, suggesting that haploinsufficiency causes the pathogenesis of the disease (Marchbank et al., 2002; Pesch et al., 2001). Besides haploinsufficiency, some data indicate that the mutated OPA1 might act in a dominant negative way by binding to wild-type protein, impairing the mechanoenzymatic activity of the protein complex. Alternatively, the missense mutations might ablate the oligomerization capacity of OPA1 and hence, affect its functions in membrane fusion and/or cristae junction maintenance (Pesch et al., 2001).

The molecular mechanism explaining ADOA pathogenesis in the presence of *Opa1* mutations is not clear yet. A study in fibroblasts from ADOA patients revealed a remarkable sensitivity of these cells to death stimulation, suggesting that possible the antiapoptotic function of OPA1 is defective in these pathological cases (Olichon et al., 2003). Although several studies in human patients point out the common feature of mitochondrial fragmentation, contradictory results have been reported in regards to mitochondrial respiration dysfunction (Lodi et al., 2004; Spinazzi et al., 2008; Zanna et al., 2008; Mayorov et al., 2008). Interestingly, a detailed survey in ADOA patients with poor or normal vision revealed that mitochondria of the former display abnormalities in OXPHOS, while those of the latter show increased respiration, which might act as compensation to preserve vision (Van Bergen et al., 2011).

For further investigation, two ADOA mouse models of the disease have been developed in which the animals carry Opa1 mutations in the GTPase domain (missense or nonsense). The heterozygous mutant mice display a progressive loss of RGC, abnormalities in the number, shape and myelinization of axons, along with visual impairment. RGC of these mice show increased autophagy rates, the reason of which is not determined yet (Alavi et al., 2007; Davies et al., 2007; White et al., 2009).

Charcot-Marie-Tooth Disease Type 2A (CMT2A)

Charcot-Marie-Tooth neuropathy Type 2A (CMT2A) is another example of a hereditary disorder in which mutations on a mitochondrial shaping protein, Mfn2, have been identified as the causative factors (Zuchner et al., 2004). Charcot-Marie-Tooth neuropathies are inherited in an autosomal dominant way and manifest with clinical symptoms like weakness and distal muscle atrophy, as well as sensory loss. Additional signs of CMT are decreased reflexes, foot deformities, cranial nerve involvement, scoliosis and glaucoma. The pathophysiological basis of type 2 CMT include the chronic axonal degeneration and regeneration leading to the loss of sensory and motor axons (Dyck et al., 1998; Dyck et al., 2000).

The detected mutations in the gene of Mfn2 are several and cluster mainly in the region that encodes the GTPase domain, without though being limited only in this region (Kijima et al., 2005; Lawson et al., 2005; Zuchner et al., 2004). The genetic and clinical heterogeneity complicate the investigation of the link between genotype and phenotype, and indeed the molecular pathogenesis of CMT2A with Mfn2 mutations is still unclear. Mfn2 ablation in a mouse model correlated the lack of mitochondrial fusion with the impairment of dendrite outgrowth, spine formation and cell survival. Based on these observations, the authors suggested that fusion is crucial for the mitochondrial content exchange and the proper organelle distribution in the neurons (Chen et al., 2007). Given the distinct role of Mfn2 in tethering ER to mitochondria modulating calcium flux, (de Brito and Scorrano, 2008b), an alternative probable pathway implicated in CMT2A pathogenesis could be calcium signaling, which is very important for neuronal cells. Further studies are required to address the open questions regarding the etiology of this neurodegenerative disorder.

Charcot-Marie-Tooth Disease Type 4A (CMT4A)

Another type of Charcot-Marie-Tooth neuropathy (CMT4A) has been correlated to mutations in a member of the fission machinery, GDAP, further supporting the notion that a balance between fission and fusion is detrimental for neurons functions (Baxter et al., 2002; Cuesta et al., 2002). Analyses in a mouse model indicated that loss of functional GDAP leads to abnormalities in calcium homeostasis; a probable reason for the

pathogenesis of the disease, due to aberration in mitochondrial network (Barneo-Munoz et al., 2015).

Abnormal brain development

In 2007 a mutation in the DRP1 gene was found to be responsible for microcephaly, abnormal brain development, optic atrophy and death of a newborn female patient (Waterham et al., 2007). Further biochemical investigation on the case revealed that the mutation localized in the middle domain of the fission protein and unraveled that this domain is crucial for the formation of DRP1 high-assemblies and the subsequent induction of mitochondrial division (Chang et al., 2010).

Other neurodegenerative disorders

Mitochondrial dynamics deregulation has been additionally linked to the most common neurodegenerative disorders (Alzheimer's, Huntington's and Parkinson's diseases). Cho and colleagues demonstrated that amyloid-β, which is associated with Alzheimer's disease (AD), induces S-nitrosylation of DRP1. Consequently, the mitochondria are fragmented and dysfunctional, contributing to the pathogenesis of AD (Cho et al., 2009).
Our laboratory has demonstrated that mitochondrial fragmentation and cristae alterations are two important traits of Huntington's disease (HD). Increased activity of the phosphatase calcineurin dephosphorylates DRP1, leading to its excessive translocation to mitochondria followed by fission of the organelles in HD cells. The fragmented mitochondria display hypersensitivity to cristae remodeling and apoptosis (Costa et al., 2010). In a slightly different model, the causative factor of Huntington's disease, mutated Huntingtin has been shown to trigger mitochondrial scission, via its abnormal binding to DRP1, stimulating its enzymatic activity. Impairment in mitochondrial dynamics leads likewise to defects in the organelles intracellular transport and eventually to cell death in an HD rat model and in fibroblast of HD patients (Wang et al., 2009; Song et al., 2011).
Finally yet importantly, familiar Parkinson's disease has been linked to mitochondrial morphology and function, since two of the basic proteins involved in its pathogenesis, Parkin and PINK1, influence the fusion machinery in a Mfn2-dependent manner, as well as the degradation of the organelles through mitophagy (Knott and Bossy-Wetzel, 2008). On top of this, missense mutations of OPA1 have been found in sporadic Parkinsonism,

which were associated with impaired fusion, respiration and increased autophagy and mitophagy (Carelli et al., 2015). In line with this discovery, sporadic Parkinson's disease has been correlated to fragmented mitochondrial network, due to abnormal processing of OPA1 or to excessive DRP1 translocated in the OMM. Although overexpression of OPA1 could not correct the mitochondrial dysfunctions, DRP1 knockdown was sufficient to rescue the phenotype (Santos et al., 2015). Intriguingly, according to a study in a Parkinson's disease mouse model concluded that inhibition of DRP1 could serve as a promising therapeutic strategy for the neuronal disease (Rappold et al., 2014).

Collectively, disruption of mitochondrial dynamics seems to be a common trait in a variety of neurodegenerative disorders and inhibitors of mitochondrial fission/fusion could serve as promising therapeutic strategies for them.

1.8.2 Cancer

Increasing amount of data indicate that mitochondrial dynamics is altered in various types of cancer. Clinical studies in lung adenocarcinoma unraveled an overexpression of DRP1 along with its peculiar localization in the nucleus preventing its translocation to mitochondria, rendering resistance of the tumor to cisplatin (Chiang et al., 2009). Upregulation of DRP1 expression as well as downregulation of Mfn1 expression has been observed in invasive breast malignancies in comparison with non-metastatic tumors. Therefore, deregulation of mitochondrial dynamics appears to be implicated in the migration of breast tumors (Zhao et al., 2013a). Furthermore, DRP1 upregulation has been associated with malignant oncocytic thyroid tumors (Ferreira-da-Silva et al., 2015). In addition, another protein of the fission machinery FIS1 is upregulated in some malignant subtypes of malignant melanoma (Su et al., 2009). Besides players of fusion and fission, also proteins that influence mitochondrial ultrastructure, such as prohibitins, have been involved in carcinogenesis (Czarnecka et al., 2006). One could hypothesize that prohibitins are implicated in tumorigenesis through their role in regulating the functional processing of the anti-apoptotic protein OPA1. However, the topic is not explored yet. Nevertheless, there are some lines of evidence indicating that OPA1-dependend cytochrome c release and cell death could contribute to malignancies and possibly serve as a target to sensitize cancer cells (Zhao et al., 2013b). Given the extremely complex biology of cancers and the

multiplicity in the functions of mitochondrial shaping proteins, investigation is needed to shed light on the mechanism how mitochondrial dynamics are involved in cell transformation and metastasis.

1.8.3 Type I Diabetes

Type I diabetes is an autoimmune disorder which results from the autoimmune destruction of the insulin-producing β cells in the pancreas. Accumulation of glucose in blood and urine is a common feature in diabetes and can cause various complications, including cardiac dysfunction. Coronary endothelial cells from diabetic mice, as well as high-glucose treated neonatal cardiac myocytes possess fragmented mitochondria, displaying a downregulation of OPA1 and an upregulation of DRP1 (Makino et al., 2011; Makino et al., 2010). On the other hand prohibitin has been shown to have a protective role in pancreatic β cells, possibly due to its control of OPA1 processing (Lee et al., 2010).

1.9 Mitochondria as cell death executioners

Apoptosis is a process crucial for the embryonic development in metazoan, adult tissue turnover, as well as for host defense pathways and the protection from cancer. Insufficiency or acceleration of apoptosis, is associated with diseases, including cancer, autoimmunity or neurodegenerative disorders (Danial and Korsmeyer, 2004). All the pathways of apoptosis converge on the activation of caspases, proteases that orchestrate the efficient and non-inflammatory demolition of cells.

The two main pathways leading to caspase activation include: a) the extrinsic route initiated by cell surface death receptors leading directly to caspase 8 activation, and b) the intrinsic pathway that is regulated by mitochondria. The intrinsic pathway is activated after an internal damage, such as DNA damage, lack of nutrients or oxygen (Scaffidi et al., 1998; Scaffidi et al., 1999). In certain cell types, like hepatocytes, the extrinsic branch is not sufficient to directly activate caspases-8; therefore, they require, additionally, a mitochondrial amplification loop.

The discovery by the group of Korsmeyer that the antiapoptotic oncogene *Bcl-2* targets its product to mitochondria (Hockenbery et al., 1990) strongly suggested that they were actively involved in the control of programmed cell death. A few years later, cytochrome

c, the only soluble component of the respiratory chain inside the cristae, was proved to be required in the cytosol to instigate apoptosis, while presumably, disabling energy production from mitochondria (Liu et al., 1996). Indeed, after the activation of both pathways, mitochondria release cytochrome c in the cytosol that in complex with APAF-1 activate caspase 9 by processing, which in turn activates the effector caspase 3, thus triggering cell death (Cain et al., 2002; Garrido et al., 2006). Furthermore, several soluble factors of mitochondria, other than cytochrome c, have been shown to participate in the apoptotic machinery, among which Smac/DIABLO. Nevertheless, whether SMAC acts as proapoptotic or antiapoptotic protein is still under debate (Verhagen et al., 2000; Du et al., 2000; Martins et al., 2004). Apoptosis-inducing factor (AIF), endonuclease G (EndoG) and Omi stress-regulated endoprotease are three other mitochondrial proteins released to the cytosol upon apoptosis stimulation, yet they function in a caspase-independent manner (Li et al., 2001; Susin et al., 1999; Verhagen et al., 2002).

The mitochondrial pathway of cell death is finely regulated by the BCL2-family members, which comprise a functionally diverse set of proteins with sequence and structural similarity. They possess α-helices with sequence conservation in BCL-2 homology (BH) domains. These proteins are categorized as pro-survival and pro-apoptotic proteins, according to the BH domains they possess. The pro-survival proteins, like BCL-2, BCL-XL and BCL-W, exhibit the homology in all BH1 to 4 regions. The pro-apoptotic polypeptides lack stringent sequence conservation of the first α-helical BH4 domain and can be further subdivided into ‘‘multidomain’’ and ‘‘BH3-only’’ proteins. Multidomain pro-apoptotic members, such as BAX and BAK, display sequence conservation in BH1, BH2 and BH3 domains, while BH3-only members (BIM, BID, BAD, BIK, NOXA, PUMA, Hrk, Bmf) display sequence conservation exclusively in the amphipathic α-helical of the BH3 region (Adams and Cory, 2001). The multidomain pro-apoptotic members BAX and BAK are required for apoptosis execution in response to diverse stimuli, including intrinsic and extrinsic death signals, since cells deficient of both proteins show resistance to cell death (Lindsten et al., 2000; Wei et al., 2001).

As the anti-apoptotic BCL-2 family members closely resemble the pro-apoptotic members in structure, it is proposed that they function as dominant negative inhibitors by binding to BAX and BAK and hampering programmed cell death. In agreement with this notion, Nouraini and coworkers demonstrated that BAX associates with the anti-apoptotic

protein BCL-XL, inserting the BH3 domain in the hydrophobic grove of the latter (Nouraini et al., 2000).

The BH3-only proteins, such as Bid, reside upstream in the pathway and they can directly or indirectly activate BAX and BAK (Wei et al., 2000). Death signals trigger their activation by transcriptional regulation or post-translational modification to connect proximal signals with the cytochrome c release. For example, after activation of CD95 (Fas) or TNFR1 death receptors, BID is cleaved and to p15 tBID by caspase 8, thus it is activated. The efficiency of the translocation process at the OMM surface can be enhanced by modifications such as the N-terminal myristoylation of tBID that follows its cleavage by caspase-8 (Luo et al., 1998; Zha et al., 2000; Gross et al., 1999).

The mechanisms by which activated BH3-only proteins interact with the pro-survival members are summarized in two models (Adams and Cory, 2007).

A. The direct activation mode: certain BH3-only proteins, termed *activators*, namely Bim and tBid, can directly bind to BAX and BAK and promote their activation (Letai et al., 2002; Walensky, 2013; Walensky et al., 2004). According to this model, the remaining BH3-only proteins, termed sensitizers, bind only to the pro-survival proteins and act by displacing any bound BIM or tBID, allowing them to directly activate BAX and BAK.
B. The indirect activation model: all the BH3-only proteins bind solely their pro-survival relatives; thereby they act by preventing them from countering BAX or BAK activation (Willis et al., 2007). In this model, BIM and tBID are potent inducers of apoptosis simply because they can engage all the pro-survival proteins.

1.9.1 OMM permeabilization

Until very recently, it was believed that in healthy cells BAX was exclusively residing into the cytosol, while it was actively translocated to mitochondria upon apoptotic stimulation (Hsu et al., 1997; Wolter et al., 1997). However, elegant studies using FLIP (fluorescence loss in photobleaching) and FRAP (fluorescence recovery after photobleaching) challenged this and proposed that BAX localizes predominantly to mitochondria, but is actively retro-translocated by pro-survival proteins to the cytosol (Todt et al., 2013; Schellenberg et al., 2013). In such a model, inhibition of retro-translocation causes BAX to

accumulate at mitochondria, thereby sensitizing cells to apoptosis. In contrast to BAX, BAK was thought to be constitutively anchored into the OMM (Ferrer et al., 2012). A very recent study suggests that also BAK shuttles from mitochondria to the cytosol, though with a slow pace, resulting in its predominant localization on the organelles membrane (Todt et al., 2015). Why these proteins move back and forward in the cellular compartments is still an open question. One would speculate that in this way BAX and BAK are "ready to attack" after a swift in the balance of kinetics. Alternatively, BAX and BAK might have additional functions on different fields of action. Interestingly, BAX is involved in mitochondrial fusion and in calcium dynamics on the ER-mitochondria interface (Hoppins et al., 2011c; Scorrano et al., 2003). Therefore, the retro-translocation might serve as a mechanism to integrate diverse roles of a multifaceted molecule.

Nevertheless, under physiological conditions, both multidomain pro-apoptotic members are found in "harmless" monomers. Upon receipt of death signal BAX and BAK undergo major conformational changes, triggered by BH3-only proteins, leading to their activation (Dewson et al., 2008; Gavathiotis et al., 2010). Once activated, BAX and BAK have exposed hydrophobic regions that need to be buried in a membrane or a protein interface, leading to the formation of membrane-spanning high-molecular weight oligomers. Recently, Subburaj et al showed that BAX forms dimers in the OMM that further self-assemble into multimeres (Subburaj et al., 2015). BAX/BAK oligomerization in the OMM is responsible for the membrane permeabilization, which is a crucial step for cytochrome c release to the cytosol (Newmeyer and Ferguson-Miller, 2003).

The exact mechanism by which BAX/BAK mediates the egress of cytochrome c is still obscure. A probable scenario is that the BAX/BAK-mediated apoptotic pores in the OMM are permeable to cytochrome c and possibly to other IMS pro-apoptotic proteins. Alternatively, BAX and BAK cooperate with resident mitochondrial proteins, such as the channel VDAC or ANT, triggering permeability transition and subsequently cytochrome c release (Marzo et al., 1998; Shimizu et al., 1999). A different model suggests that the BAX/BAK-induced permeabilization of OMM is enhanced by various factors, including lipids that lead to a disruption of bilayer (Kluck et al., 1999; Kuwana et al., 2002). In any case, BAX/BAK permeabilization appears to be an important step for cytochrome c release; nonetheless, it is not sufficient for the completion of the process.

1.9.2 Alterations in mitochondrial morphology during apoptosis

One of the major criteria to distinguish apoptosis from necrosis was the morphological derangement of mitochondria in the latter, but not in the former. Accordingly, the notion that mitochondrial shape changes during programmed cell death was unexplored for many years, despite the understanding that soluble components are released from mitochondria during apoptosis. Nevertheless, research of the two last decades revealed that mitochondrial organization is altered in apoptotic cells. These rearrangements include a) the fragmentation of mitochondrial network and b) changes mitochondrial membrane topology.

1.9.2.1 Mitochondrial fragmentation

The first links between mitochondrial fragmentation to apoptosis were provided by studies of Martinou *et al* and Frank *et al*. DRP1, the key fission regulator, plays a central role in this process, since a dominant negative mutant of DRP1 inhibits cell death (Frank et al., 2001; Martinou et al., 2000). The importance of apoptotic fission was substantiated in the nematode *Caenorhabditis elegans*, where the homologue of DRP1 is required for programmed cell death during development (Jagasia et al., 2005). Upon apoptosis induction, DRP1 translocates to mitochondria and forms polypeptidic assemblies in the constriction sites, together with the proapoptotic protein BAX and the fusogenic protein Mfn2 (Karbowski et al., 2002). The function of this protein association is not fully understood. Yuan and coworkers proposed that DRP1 foci formation into neuronal mitochondria precedes BAX translocation and it provides a platform for recruitment of apoptosis executors and fusion/fission regulators (Yuan et al., 2007). Conversely, the DRP1 dominant negative mutant does not block BAX translocation to mitochondria, indicating that the former acts downstream of BAX (Karbowski et al., 2002). However, loss of DRP1 prevents cytochrome c release, even though BAX has moved to the mitochondria (Lee et al., 2004). Furthermore, BAX activation enhances the stability of DRP1 on mitochondria by controlling its SUMOylation (Wasiak et al., 2007). All the above suggest that fission and cytochrome c release are subject of regulation of the same protein very close in time, but likely as two distinct events. Moreover, FIS1 has been demonstrated to act as a pro-apoptotic protein, independently of DRP1, possibly by recruiting proteins in

mitochondria (Lee et al., 2004) or by engaging the calcium dependent function of BAX and BAK at the endoplasmic reticulum (Alirol et al., 2006).

Besides the components of fission machinery, also Mfn2 participates in mitochondrial related apoptotic events. Mfn2 co-localizes in the foci of DRP1 and BAX in a GTPase dependent manner. Overexpression of Mfn2, residing in this foci, induce apoptosis. Conversely, when Mfn2 is restricted outside the foci, BAX translocation is inhibited (Karbowski et al., 2002; Neuspiel et al., 2005; Huang et al., 2007). Therefore, this protein seems to be important for BAX-mediated initiation of cell death, but most likely independently of its effects on mitochondrial dynamics. A possible explanation could be that there is an increased tethering between ER and mitochondria in the Mfn2-containing puncta (de Brito and Scorrano, 2008a), favoring the enrichment of lipids required for BAX-BAK permeabilization of the OMM in these sites (Kuwana et al., 2002).

1.9.2.2 Cristae remodeling

Kinetic studies of cytochrome c release in response to any apoptotic stimulation indicated that the release is a rapid and single step procedure whose extent is remarkably complete (Goldstein et al., 2000). Noteworthy, the narrow IMS contains only 15%-20% of total cytochrome c, while the majority of it resides inside the cristae (Frey and Mannella, 2000; Bernardi and Azzone, 1981). Accordingly, besides BAX/BAK action and OMM permeabilization, another process should occur for the substantial release of cristae-endowed cytochrome c, prior to any mitochondrial swelling. This pathway involves a striking reorganization of the IMM - the so-called cristae remodeling - and contributes to the inversion of cristae curvature with a simultaneous mobilization of the cytochrome c stored inside the cristae. More specifically, 3D electron tomographic analysis and physiological measurements revealed a notable widening of the narrow cristae junctions and fusion of independent cristae in isolated mitochondria or intact cells treated with tBID (Fig. 9). These morphological alterations in response to death stimulus are time- and stimulus concentration-dependent. Remarkably, this process can be inhibited by cyclosporine A, which blocks the permeability transition pore, suggesting a correlation between cristae remodeling and the opening of the IMM channel. Moreover, cristae reorganization early during apoptosis is independent of BH3 domain and of BAX/BAK-

mediated OMM permeabilization, suggesting that tBID has two distinct targets: a. BAX/BAK to mediate the cytochrome c across the OMM and b. an alternative factor that facilitates cristae remodeling (Scorrano et al., 2002; Yamaguchi et al., 2008). Apart from tBID, also other death stimuli, like BIK, BIM and Fas activation, lead to apoptotic IMM remodeling (Germain et al., 2005; Mootha et al., 2001; Yamaguchi et al., 2008).

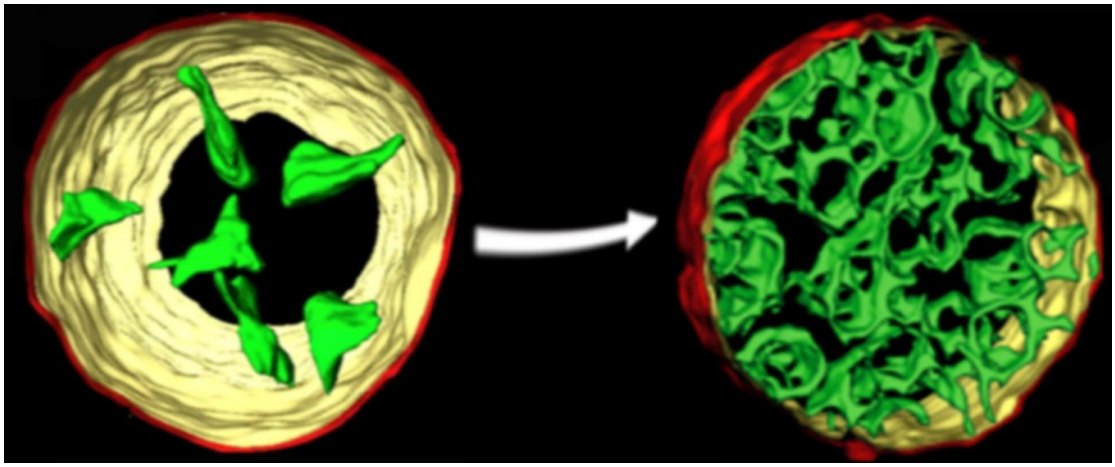

Figure 9. Cristae remodeling during apoptosis. Upon tBID, BIM or BIK stimulation, the narrow cristae junctions widen and the independent cristae fuse.

OPA1, as cristae shape and diameter regulator, plays a crucial role during apoptotic cristae remodeling. OPA1 resides in high molecular weight complexes, which act as a molecular staple between the adjacent cristae membranes and, hence, maintain the cristae junctions close. Early after stimulation by tBID, BIM and BNIP3, these complexes are targeted, since they rapidly disassemble with a concomitant opening of the cristae junctions and the complete cytochrome c release (Fig. 10). Accordingly, high levels of OPA1 stabilize the protein assemblies and prevent the mobilization of cytochrome c, while silencing of its gene results in an increased cristae junction diameter (Frezza et al., 2006; Landes et al., 2010; Yamaguchi et al., 2008).

OPA1 complexes targeted during apoptosis consist of both the long membrane integral forms and the short soluble forms of the protein. Among the proteases involved in the processing of OPA1 is the presenilin-associated rhomboid-like (PARL), which specifically participates in the control of cristae remodeling, via the balanced generation of OPA1 soluble forms. Cells lacking PARL display reduced levels of short OPA1 form, along with

faster apoptotic cristae rearrangements and cytochrome c mobilization towards the cytosol, as well as sensitivity to intrinsic apoptotic stimuli (Cipolat et al., 2006).

An outstanding question is how OPA1 complexes are disassembled during programmed cell death. Yamaguchi *et al* demonstrated that the elimination of the complexes requires the presence of BAK, without its activation, further supporting the notion that cristae remodeling is not a direct consequence of OMM permeabilization (Yamaguchi et al., 2008). Recently, Jiang and coworkers proposed that OPA1 is cleaved by OMA1 upon apoptotic stimulation, leading to the disassembly of the complexes and cytochrome c release. The authors linked OMA1 activation to the upstream event of BAX and BAK oligomerization, thus placing the two distinct pathways into one (Jiang et al., 2014). Nevertheless, studies in our lab succeeded in genetically dissecting outer mitochondrial membrane permeabilization from cristae remodeling (Cogliati et al., 2013). Cogliati and colleagues took advantage of two mutants of the prototypical inducer of cristae remodeling, BID:

a) The already known BID^{G94E}, which carries a mutation at the BH3 domain and, thus, it is unable to induce opening of the permeability transition pore and cytochrome c mobilization (Wei et al., 2000).
b) BID^{KKAA} that carries two mutations in the highly conserved lysines of its α6 helix. This domain shares high homology not only with the transmembrane domains of Bnip3 and BimS, that also remodel cristae, but also with mastoparan (a peptide of wasp venom, which perturbs mitochondrial inner membrane) (Pfeiffer et al., 1995; Landes et al., 2010; Yamaguchi et al., 2008; Cogliati et al., 2013). While BID^{G94E} induces no cytochrome c release, BID^{KKAA} is able to release 20%-30% more cytochrome c than the baseline, which corresponds to the IMS cytochrome c stores. In general, BID^{KKAA} is sufficient to induce BAX and BAK oligomerization, but it is incapable to disrupt OPA1 complexes and trigger cristae remodeling (Fig. 10). Consequently, BID exerts two distinct functions in mitochondria via two different protein domains (Cogliati et al., 2013).

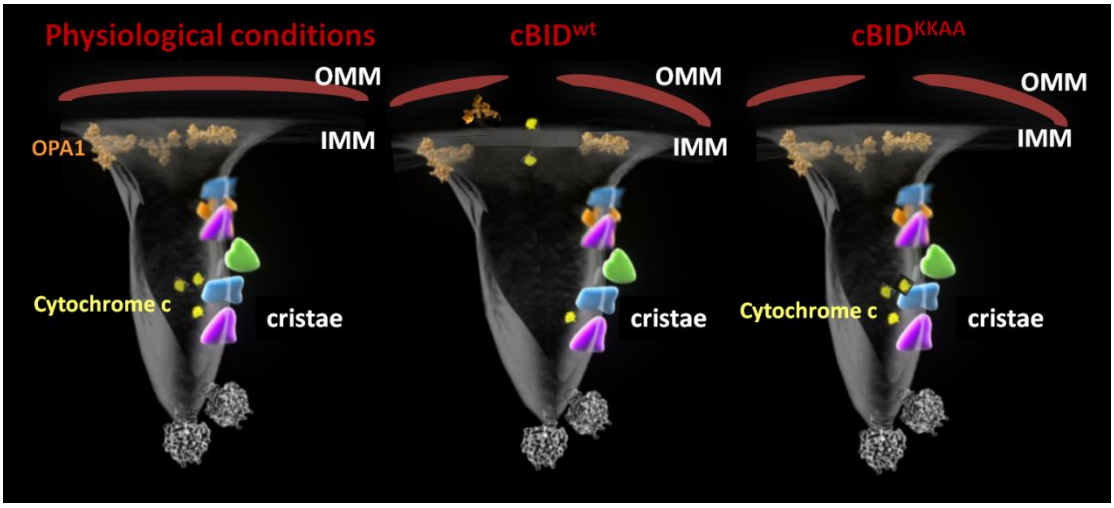

Figure 10. OPA1 complexes disruption, cristae remodeling and outer membrane permeabilization upon cBID^{wt} stimulation. The mutant cBID^{KKAA} is sufficient to induce OMM permeabilization, while is it unable to dissociate OPA1 complexes and induce cristae remodeling. OMM: outer mitochondrial membrane, IMM: inner mitochondrial membrane.

A possible mechanism by which tBID causes cristae remodeling is through its capacity to bind selected lipids, i.e. cardiolipin of IMM (Esposti et al., 2001; Gonzalvez et al., 2005). According to this hypothesis, cardiolipin per se as well as its oxidation is essential for BID induced apoptosis (Lutter et al., 2000; Ott et al., 2002). Recently, another BH3-only protein inducer of apoptotic cristae remodeling Bnip3 has been proposed to interact OPA1, and hence destabilizing its high molecular weight complexes (Landes et al., 2010). This line of evidence supports the notion that also BID potentially interacts directly with OPA1 or other protein that incorporates in the complexes targeted during apoptosis, exerting its action.

As judged by blue native PAGE, multiple OPA1 containing complexes exist (Cogliati et al., 2013), suggesting that other proteins participate in their assembly and elimination upon apoptotic stimulation. Moreover, considering that OPA1 is a multifunctional protein, it is conceivable that the candidate partners of this protein participate in the regulation of the various functions, an hypothesis that calls for investigation.

1.9.2.3 Impact of cristae remodeling on physiology

In addition to its role in cytochrome c release, cristae remodeling also impairs mitochondrial function by the disassembly of respiratory supercomplexes (Cogliati et al.,

2013). A very recent study of our laboratory shed light into the relevance of apoptotic cristae remodeling in vivo using OPA1 transgenic mice as a genetic tool. OPA^{tg} cells showed resistance to cristae remodeling and cytochrome c release, as expected. Furthermore, $OPA1^{tg}$ mice displayed a protection from cell death upon activation of FAS pathway. Experimental evidence from these mice indicated that OPA1-dependent cristae remodeling plays a fundamental role in cell death following tissue damage, including acute or chronic muscular atrophy, brain and heart ischemia and apoptotic liver damage (Varanita et al., 2015). As a result, it has been proposed that cristae remodeling could serve as a promising target for pathologies in which cell death due to tissue damage occurs.

2. Hypothesis and aims of the thesis

Given the relevance of cristae integrity and remodeling during apoptosis in cell physiology and pathology, we aimed to provide further insight into their regulation by OPA1. OPA1 is retrieved in multiple complexes. The size of the OPA1-containing complexes that are targeted during apoptosis range from 500 to 800 KDa, as judged by blue native gel electrophoresis and by size exclusion chromatography. Therefore, we hypothesized that OPA1 is not the only component of the complexes, but instead cooperates with other proteins to control cristae remodeling.

In this thesis, we specifically aimed to identify and characterize biochemically and functionally the components of OPA1 complexes targeted during apoptosis. We took advantage of three-dimensional Blue Native – Blue Native – SDS electrophoreses that we adapted to proteomic strategies, in order to retrieve all the proteins that compose the native complexes of interest. Two identified candidate OPA1 interactors were further analyzed biochemically in order to explore their role in cristae biogenesis, cristae remodeling, mitochondrial morphology and physiology.

Chapter II

Results

2.1. A molecular atlas of the Optic atrophy 1 (Opa1) high molecular weight complexes targeted during apoptotic cristae remodeling

A molecular atlas of the Optic atrophy 1 (Opa1) high molecular weight complexes targeted during apoptotic cristae remodeling

Maria Eugenia Soriano[1*], Christina Glytsou[1,2*], Enrique Calvo[3], Jesùs Vazquez[3], Jose Antonio Enriquez[3], and Luca Scorrano[1,2]

[1] Department of Biology, University of Padova, Padova, Italy

[2] Dulbecco-Telethon Institute, Venetian Institute of Molecular Medicine, Padova, Italy

[3] Centro Nacional de Investigaciones Cardiovasculares Carlos III, Madrid, Spain

* these authors contributed equally

Address correspondence to Luca Scorrano: luca.scorrano@unipd.it or Maria Eugenia Soriano mariaeugenia.soriano@unipd.it

ABSTRACT

Optic Atrophy 1 (OPA1) is a dynamin-like protein of the inner mitochondrial membrane that controls cristae shape and remodeling required for complete cytochrome c release. The composition of the OPA1 high molecular weight (HMW) complexes disrupted upon apoptotic stimulation is unknown. Here we inspected by quantitative and semi-quantitative proteomic approaches native OPA1-containing complexes of three different tissues to create a compendium of the proteins whose distribution is altered during apoptotic cristae remodeling. This approach identified members of MICOS complexes, the mitochondrial calcium uniporter and its regulators, and proteins with undefined biological function, like GHITM. Biochemical analysis of these candidates validated our proteomic methods and served as a proof of principle to investigate OPA1 interactors. Our results illustrate the dynamicity of individual proteins association and of mitochondrial functions during apoptotic cristae remodeling.

INTRODUCTION

Mitochondria are fundamental organelles in life and death of eukaryotic cells, participating in multiple cellular processes, including energy production, calcium homeostasis, signaling pathways and apoptosis regulation. Their multifunctional properties are accompanied by dynamic changes in their complex shape (Vogel et al., 2006). Continuous cycles of fusion and fission provide a quality control for the organelle homeostasis, by controlling their biogenesis and clearance, favoring the exchange of mitochondrial content and influencing the efficiency of oxidative phosphorylation (Yoneda et al., 1994; Chen and Chan, 2005; Pernas and Scorrano, 2015). During apoptosis mitochondrial network fragments, the outer mitochondrial membrane is permeabilized and the topology of the inner mitochondrial membrane (IMM) drastically changes (Martinou and Green, 2001; Frank et al., 2001; Scorrano et al., 2002). This striking reorganization of the IMM, named cristae remodeling, includes the inversion of cristae curvature with a simultaneous mobilization of the cytochrome c stored inside the cristae; eventually contributing to the amplification of the apoptotic pathway (Scorrano et al., 2002).

Optic Atrophy 1 (OPA1), the only pro-fusion dynamin-related protein of the IMM known so far, is, additionally, a regulator of cristae shape and diameter, playing a crucial role in apoptotic cristae remodeling. OPA1 resides in high molecular weight (HMW) complexes that maintain the cristae junctions tight. Early after stimulation by tBID, BIM or BNIP3, these complexes disassemble with a concomitant opening of the cristae junctions and complete cytochrome c release (Frezza et al., 2006). Notably, separate domains of the same stimulus, BID, are responsible for distinct functions: the α6 helix for OPA1 complexes disruption and the BH3 domain for the OMM pore formation (Cogliati et al., 2013),

indicating that OPA1-dependent cristae remodeling and OMM permeabilization are molecularly distinguishable events.

OPA1 complexes targeted during apoptosis contain both the long membrane integral forms and the soluble short forms of the protein (Frezza et al., 2006). On top of this, as judged by blue native PAGE, multiple OPA1 containing complexes exist with sizes ranging from 500 to 800 kDa (Cogliati et al., 2013), suggesting that other proteins participate in their assembly and elimination upon apoptotic stimulation. Moreover, considering that OPA1 is a multifunctional protein, it is conceivable that the candidate partners of this protein participate in the regulation of its various functions. However, our knowledge on OPA1 interacting proteins is limited to pull down experiments (Banerjee and Chinthapalli, 2014; Patten et al., 2014; Darshi et al., 2011a) that do not take into account endogenous interactions or the dynamic behavior of these complexes that are targeted during cristae shape changes.

With this in mind, we decided to explore the components of OPA1-containing HMW complexes. Using a three-dimensional Blue Native (BN)–BN–SDS electrophoresis approach that we adapted to quantitative and semi-quantitative proteomic strategies, we restricted our analysis to the proteins that compose the native complexes of interest across multiple tissues. We capitalized on a cristae remodeling incompetent mutant cBID ($cBID^{KKAA}$) to identify proteins that leave the OPA1 complexes only during cristae shape changes. Further analysis of four of our candidates confirmed that the proteomic approaches applied here are powerful tools to investigate the dynamic OPA1 interactions.

RESULTS

Three dimensional Blue Native – Blue Native – SDS – PAGE allows to investigate OPA1 complexes

Blue native electrophoresis (BN-PAGE) of 1.2% digitonin solubilized mitochondrial extracts allowed us to identify multiple macromolecular assemblies containing OPA1, which span from approximately 250 kDa up to 1000 kDa (Fig. 1A and 1B). Upon treatment of isolated mitochondria with the recombinant pro-apoptotic caspase 8-cleaved BID (cBID), OPA1 levels in higher molecular weight complexes, i.e. from 480 kDa to 1000 kDa significantly decreased (Fig. 1B), indicating that these are particularly targeted during programmed cell death. Their size and multiplicity prompted us to hypothesize that proteins other than OPA1 whose identity is not known yet participate in the assembly of these complexes.

In order to identify the proteins in a strong association with OPA1 and minimize the false positive interactors, we continued with a second dimension blue native electrophoresis (2D BN-PAGE). Specifically, we excised the lane of the first dimension BN-PAGE and loaded it directly onto a single-well native gel using an electrophoresis buffer which contained 0.002% of the detergent n-Dodecyl-β-D-maltopyranoside (DDM). The stable native complexes ran along a diagonal, while the weak interactors of the protein assemblies dissociated and ran faster below the diagonal (Fig. 1A). After immunoblotting we were able to detect the more stable OPA1-containing assemblies, indicating that OPA1 associates strongly with a number of proteins. Notably, these stable complexes were diminished in apoptotic (cBID treated) mitochondria (Fig. 1C).

To separate the individual components of the complexes of interest and further confirm the existence of OPA1 in those, we then proceeded to a third dimension denaturating

electrophoresis (3rd D SDS-PAGE). Each resulted diagonal of the 2nd D gels was cut in thickness of 1 cm and subsequently loaded onto another single-well polyacrylamide gel under denaturating conditions (Fig. 1A). Immunodetection allowed us to verify the reduction of OPA1 in the stable, higher molecular weight complexes in response to an apoptotic stimulus (Fig. 1D). In conclusion, this 3D BN-BN-SDS-PAGE appears to be a useful tool to investigate the dynamic nature of OPA1-containing complexes.

3D BN-BN-SDS-PAGE followed by LC/MS explores OPA1-containing complexes composition

In order to identify the more stable components of the OPA1-containing assemblies, we coupled 3D BN-BN-SDS-PAGE to mass spectrometry analysis (Fig. 1A). To this end, we isolated mouse liver mitochondria and extracted the membrane complexes with digitonin 1.2%. The samples were subsequently separated by 3D-BN-BN-SDS-PAGE. The obtained gels were stained with Coomassie to visualize the protein complexes (Fig. 1E, 1F and 1G). The diagonals of the 2nd D-BN-PAGE were cut into 7 spots (Fig. 1F) and each one of those run in an independent SDS electrophoresis. The lane of each 3rd D-SDS PAGE was subdivided into small spots, trypsinized and subjected to mass spectrometry (Fig. 1G). The identified peptides of each spot were analyzed statistically with Scaffold Software (Version 4.0) using the Mouse MitoCarta dataset (Pagliarini et al., 2008) to obtain a cohort of 576 different mitochondrial proteins that reside in the multiple spots of the diagonal, corresponding to the various molecular weight OPA1-containing complexes (Suppl. Table 1). Bioinformatics analysis revealed that the candidate partners of OPA1 belong to 13 biological function categories that include metabolic process, cellular process, localization, cellular component organization or biogenesis, biological regulation,

developmental process, response to stimulus, immune system process, multicellular organismal process, apoptotic process, reproduction, biological adhesion, locomotion (Fig. 2A) (http://pantherdb.org/) (Thomas et al., 2003). Intuitive enrichment analysis of the cellular component of our hits validated that the vast majority of the proteins reside in the mitochondrial inner membrane or matrix (Fig. 2B) (http://amp.pharm.mssm.edu/Enrichr) (Chen et al., 2013), enhancing the reliability of our results. STRING 10 (http://string-db.org/) (Jensen et al., 2009) analysis provided information about the evident and predicted functional interactions of the total of our identified proteins (Fig. S1).

In addition, given the multiple functions of OPA1, we aimed to distinguish the candidate OPA1 interactors that are specifically regulated during apoptosis. To this end, we performed the same proteomic approach in parallel in normal (untreated) and apoptotic (cBID treated) mitochondria. The electrophoreses were performed simultaneously for the two samples and the obtained diagonals of the 2nd D BN-PAGE were cut into spots of the same molecular weight, which were subsequently loaded onto the same SDS gels. This strategy provided us with semi-quantitative stoichiometric results of the identified proteins whose levels increase or decrease in each spot/complex compared to control after cBID treatment (Suppl. Tables 2-8); thus obtaining a measurement of the potential changes in the distribution across the different OPA1-containing complexes of each candidate interactor during apoptosis. Enrichment analysis on the functional pathways revealed that our hits which decrease during apoptosis are mainly involved in TCA cycle, mitochondrial translation and organelle biogenesis and maintenance (Fig. 2C), also organized in a network of predicted interactions (Figure S2).

BN-PAGE-LQ/MS of mouse heart mitochondria identifies OPA1-containing complexes targeted during apoptosis

We next asked whether the composition of the complexes was similar in a tissue where OPA1-controlled mitochondria dependent cell death plays a crucial role and we therefore turned our attention to heart, protected from ischemia reperfusion damage by moderate Opa1 overexpression (Varanita et al., 2015). In this approach, in order to distinguish the proteins that are regulated specifically during cristae remodeling, mitochondria were treated with the wild type pro-apoptotic caspase 8 cleaved BID ($cBID^{wt}$) or a mutant cBID, which is unable to widen cristae junctions and to disrupt OPA1 complexes ($cBID^{KKAA}$) (Cogliati et al., 2013). Immunoblotting verified that also in the heart OPA1 leaves high molecular weights complexes upon $cBID^{wt}$, but not cristae remodeling incompetent mutant $cBID^{KKAA}$ (Fig 3A).

The resulting gel lanes were cut into 26 successive slices starting from the higher molecular weights; each slice was trypsinized and subjected to mass spectrometry (Fig. 3B). We graphically depicted the MS results as a migration pattern of each identified protein, which derived from its values along the whole electrophoretic run. The peaks of OPA1 pattern correspond to the molecular weights of the highly immunodetected protein in western blotting, strengthening the reliability of this proteomic approach (Fig. 3C). The similarity between the migration profiles of each identified protein and OPA1 was measured using Pearson correlation coefficient (r), in order to acquire the list of candidate hits that are retrieved in the same spots with OPA1 in untreated mitochondria ($r \geq +0.1$). Filtering our list using the mitochondrial proteomics database Mitominer (http://mitominer.mrc-mbu.cam.ac.uk) (Smith and Robinson, 2016), we ended up with 643 identified proteins that were assigned to mitochondria, a number that corresponded

to the 74% of the total of our hits, confirming the high purity of the sample. Our catalog included 213 mitochondrial proteins which are likely associated with the various OPA1-containing complexes in heart (Fig. 4A, Suppl. Table 9). These proteins reside mainly in the mitochondrial inner membrane (Fig. 4B) and are classified into 12 categories according to their biological function, including metabolic process, cellular process, localization, cellular component organization or biogenesis, biological regulation, developmental process, response to stimulus, immune system process, multicellular organismal process, apoptotic process, reproduction, biological adhesion, locomotion (Fig 4C). Among these target proteins, 189 of them had a smaller total score value along the blue native lane than in control after cBIDwt treatment, indicating that they were decreased upon apoptosis stimulation (Fig. 4D, Suppl. Table 10). Hence, overall the high molecular weight complexes were quantitatively reduced. The majority of these polypeptides are involved in mitochondrial respiration, mitochondrial translation as well as organelle biogenesis and maintenance (Fig. 4E). Interestingly, 128 mitochondrial proteins were reduced only after treatment with $cBID^{wt}$, but not $cBID^{KKAA}$; thus these candidates dissociate from the complexes of interest because of apoptotic cristae remodeling and not of OMM permeabilization (Fig. 4F, Suppl. Table 11).

OPA1 interactions are largely tissue independent

The two different high-throughput approaches allowed us to come up with a subgroup of OPA1 interactors which are detected by both strategies deployed so far (142 mitochondrial proteins, Fig. 5A and C). The presence of common hits in mouse heart and liver mitochondria suggested a tissue-independency of OPA1 associations. According to their biological function, these proteins are annotated to the following categories: metabolic process, cellular process, localization, cellular component organization or

biogenesis, biological regulation, developmental process, response to stimulus, immune system process, apoptotic process and biological adhesion (Fig. 5B). Among the candidate partners of OPA1 common in heart and liver, 43 proteins were reduced from the OPA1-containing complexes after $cBID^{wt}$ treatment (Fig. 5D and E).

SILAC allows quantification of proteins leaving OPA1 complexes during apoptosis

In order to give a quantitative aspect to our analysis, we took advantage of stable isotope labeling by amino acids (SILAC) (Ong et al., 2002) which we applied to our experimental setting (Fig. 6). We grew two different populations of mouse adult fibroblasts (MAFs) with light (containing normal amino acids) or heavy medium (containing ^{15}C labeled Arg and Lys). After six cellular doublings, all the proteome incorporated metabolically the corresponding amino acids. Isolated mitochondria from one cellular population were treated with $cBID^{wt}$ or $cBID^{KKAA}$, whereas mitochondria of the other served as a control-untreated. Next, the organelles were solubilized using digitonin and equal amounts of *heavy* and *light* (treated and untreated) mitochondrial extracts were mixed. The samples were then separated by BN-PAGE and the higher molecular weights, corresponding to the complexes targeted during apoptosis (500-1000 kDa), were cut into seven successive gel bands to be trypsinized and analyzed by MS. This strategy allowed us to distinguish simultaneously the proteomes of each population (normal or apoptotic) and determine their relative abundance by measuring the ratio in peak heights between two forms of the same protein in the two cell states.

This analysis revealed a list of 90 mitochondrial proteins whose levels are significantly altered ($Z>1.2$) after $cBID^{wt}$ stimulation in respect to the untreated mitochondrial population (Fig. 7A). These polypeptides are located mainly in mitochondrial inner

membrane (Fig. 7B) and belong to 9 gene ontology entries regarding their biological function; metabolic process, cellular process, localization, cellular component organization or biogenesis, biological regulation, developmental process, response to stimulus, multicellular organismal process, immune system process (Fig. 7C). Among those, 49 unique hits were decreased upon apoptosis in the various gel bands (Fig. 7D, E and Suppl. Table 12), while 47 were specifically decreased following apoptotic cristae remodeling (Fig. 7F and Suppl. Table 13).

Immunodetection after blue native analysis confirms mass spectrometry results

To validate biochemically the results of the high-throughput approaches, we performed blue native electrophoresis in solubilized mitochondria deriving from liver and heart and proceeded with western blotting against four identified hits. First, the major member of the MICOS complex Mic60 (Mitofilin), being identified by all the three proteomic techniques, was selected for further investigation. BN-PAGE and western blotting revealed that Mic60 participates in the formation of high molecular weight complexes, some of which share similar electrophoretic mobility with OPA1-containing assemblies in native conditions (Fig. 8A). In line with our proteomics data (Suppl. Table 11 and 13), the OPA1/Mic60 complexes were disassembled after $cBID^{wt}$ but not after $cBID^{KKAA}$ treatment, as judged by western blotting. In order to further verify our result, we performed 3D BN-BN-SDS PAGE followed by western blotting and we confirmed that Mic60 is part of the HMW OPA1-containing complexes, since their electrophoretic runs overlap. After cBID stimulation, the proteins of interest disappear from the high molecular weights (Fig. 8B), suggesting their dissociation from the HMW complexes upon apoptosis.

Besides MICOS complex, also members of the calcium uniporter of the inner membrane, MCU and MICU1, were detected in heart mitochondria (Suppl. Table 9), and specifically in the bands 10-13 in the complexes which correspond approximately to the molecular weights 500-720 kDa. Biochemical analysis confirmed the existence of these two proteins in various independent assemblies with a size range between 300 and 720 kDa (Fig. 8C).

Last but not least, a protein named Mitochondrial morphology and cristae structure 1 (MICS1), aka GHITM and retrieved in our complexome approaches (Suppl. Table 9), caught our attention, because, although it has been previously correlated to mitochondrial ultrastructural maintenance, its exact function is still obscure. Blue native PAGE validated the co-existence of GHITM with OPA1 in 600 kDa HMW assemblies, and its slight decrease of it specifically after $cBID^{wt}$ stimulation (Fig. 8C).

DISCUSSION

The comprehensive proteomic study described here yielded insight into the nature and composition of the HMW complexes containing the mitochondrial shaping protein, OPA1. Taking advantage of the high resolution of blue native electrophoresis (Schagger et al., 1994), we were able to separate and detect the multiple intact macromolecular assemblies in which OPA1 is present. Applying this technique in digitonin-solubilized mouse liver and heart mitochondria and coupling it to mass spectrometry unveiled that OPA1 resides in these complexes together with a variety of interactors, whose nature is independent of the tissue. Overall, identification of the same interactors in the three different approaches used in this study indicated that our methods had the level of definition required to inspect OPA1 complexes in cell life and death.

The higher molecular weight complexes of OPA1 are targeted early during apoptosis, contributing to cristae remodeling and cytochrome c mobilization (Cogliati et al., 2013). Our data from all the high throughput approaches confirmed the elimination of these complexes and indicated a general remarkable alteration in their composition and organization upon apoptosis. The comparison of the identity and the abundance of the OPA1 complexes components in normal and cBID treated mitochondria provided us with valuable information about their differential distribution in the presence of an apoptotic stimulus. On top of this, our study allowed us to identify the proteins that are specifically redistributed during cristae remodeling, suggesting that they play a role mitochondrial ultrastructure alterations during programmed cell death. These proteins could possibly act either as OPA1 co-players to directly control cristae biogenesis and stability or by assisting the complexes formation or even by stabilizing OPA1 under steady state conditions. Alternatively, candidate OPA1 partners could probably be direct targets of

cBID, thus facilitating the elimination of the protein complexes in order to trigger cristae remodeling.

The power of our high-throughput analyses was validated by blue native PAGE followed by western blotting against identified OPA1 complexes constituents. We confirmed that Mic60 share common HMW complexes with OPA1, which are significantly eliminated upon apoptotic cristae remodeling. Mic60 is the major component of "Mitochondrial contact site and cristae organizing system" (MICOS), a machinery that participates in cristae biogenesis and maintenance (Harner et al., 2011). Although a possible interaction between the MICOS member and OPA1 has been suggested before (Darshi et al., 2011b; Banerjee and Chinthapalli, 2014), we indicate that Mic60 can possibly play a role in cristae remodeling. An intriguing aspect to be investigated is the mechanism by which the main regulators of cristae shape collaborate for the fulfillment of their action.

Moreover, among the identified proteins that are reduced during cell death, we found members of mitochondrial intermembrane space bridging (MIB) complex, namely Metaxin-1, Samm50 and Dnajc11. This is another heteromeric protein assembly crucial for the preservation of cristae and assembly of respiratory complexes. MIB associates with MICOS members (Mic60 and Mic19) (Ott et al., 2012; Huynen et al., 2016); thus, it is conceivable that all the multiprotein machineries responsible for cristae organization (OPA1 multimers, MICOS and SAM) might crosstalk to achieve a higher hierarchical membrane organization under physiological and apoptotic conditions.

Additionally, various previously characterized OPA1 modulators were retrieved in our proteomics analysis and, hence, served as a proof of principle for studying OPA1 co-players. Particularly, we found that the inner mitochondrial membrane protein important for mitochondrial morphology, Letm1 (Dimmer et al., 2008), is specifically eliminated from

OPA1-containing complexes in cBID induced cristae remodeling. Letm1 was previously described as a regulator of OPA1-mediated fusion as well as apoptosis (Piao et al., 2009). Moreover, the mitochondrial nucleoside diphosphase kinase (Nme) that provides the fuel for Opa1, enhancing its GTPase activity (Boissan et al., 2014) was found to be dissociated from OPA1-complexes only after $cBID^{wt}$ treatment, indicating an active OPA1 regulation by NME in order to promote membrane remodeling. Furthermore, prohibitins, which exert their functions on mitochondria via the regulation of OPA1-processing (Merkwirth et al., 2008) were detected in the HMW assemblies containing OPA1. Additional proteins discovered at our proteomics methods were the proteases OMA1 and Ymel1, which cleave the mitochondrial shaping protein, as well as its partner OPA3, whose exact function is still elusive. Importantly, Mfn1, the well-characterized partner of OPA1 for its profusion action, was retrieved in the OPA1-containing complexes. Nevertheless, apoptotic stimulation did not alter its identification levels; hence Mfn1 is not required for the anti-apoptotic role of OPA1, which is indeed distinct from its fusogenic function (Frezza et al., 2006).

Patten and coworkers identified certain mitochondrial solute carriers (SLC25A) as OPA1 interactors, whose ablation or inhibition led to loss of the mitochondrial architecture integrity, along with blockage of OPA1 oligomerization and function (Patten et al., 2014). In agreement with this study, we detected calcium-binding mitochondrial carriers (SLC25A12 and SLC25A13) in the HMW OPA1-containing complexes, which dissociated from them in apoptotic cristae remodeling; overall suggesting a direct interplay between the solute carriers and OPA1 under apoptotic conditions to mediate membrane rearrangements. Besides the calcium carriers, we demonstrated that also the multiprotein channel of mitochondrial calcium uniporter (MCU), as well as its regulators

MICU1 and Ccdc90a (De Stefani et al., 2011; Raffaello et al., 2013; Vais et al., 2015) resides in common complexes with OPA1 and are redistributed during apoptosis. Thus, our data indicate a link between mitochondrial calcium homeostasis and cristae morphology in steady state and cell death, an interesting correlation that calls for further investigation.

As evident from clustering analysis and STRING networks in all our approaches, a large part of the proteins targeted during apoptosis was represented by oxidative phosphorylation (OXPHOS) complexes subunits. Although their direct interaction with OPA1 is not proven or expected, their reduction during cristae remodeling is conceivable. The OXPHOS members are assembled into complexes and further organized in a higher order forming metabolically active supramolecular assemblies, the respiratory supercomplexes (Acin-Perez et al., 2008) that are disassembled during cristae remodeling (Cogliati et al., 2013), possibly explaining the changes in the distribution of the individual components demonstrated by our proteomic approaches. Similarly, we found several subunits of ATP synthase (ATP5H, ATP5L, ATP5F1, mtATP8), as well as integral membrane proteins loosely associated with complex V (MP68, DAPIT) to leave the HMW complexes in cBID stimulated mitochondria. Given the crucial role of ATP-synthase dimerization in cristae morphology (Davies et al., 2012), it is likely that complex V disassembles during cristae remodeling. An open question is how OPA1-mediated definition of cristae junctions and the adjustment of the cristae tips positive curvature by ATP-synthase dimers are coordinated. Our study provides hints for understanding the interplay between OPA1 complexes and ATP-synthase and suggested some candidate mediators for this crosstalk. Several members of the mitochondrial translational machinery (ribosome or nucleoid subunits, such as Atad3, Mrpl12, Mrpl23, Lonp1) were shown to be regulated upon apoptotic cristae remodeling. One can expect a disassembly of the nucleoids after

dramatic architectural rearrangements, considering that the translational units are associated with the inner mitochondrial membrane. However, we cannot exclude the possibility of an indirect link between OPA1 and components of the protein synthesis "factory".

More interestingly, our lists contained also novel candidate OPA1 partners whose precise biological function in mitochondria is still obscure. Among these proteins we distinguished Nitric oxide-associated 1 (NOA1), Growth hormone-inducible transmembrane protein (GHITM), Death-associated protein 3 (DAP3) and NLR family member X1 (NLRX1); all of which are dissociating from the HMW complexes upon cBID treatment. Previous studies have correlated these four proteins to apoptosis and mitochondrial morphology and architecture (Oka et al., 2008; Tang et al., 2009; Kolanczyk et al., 2011; Xiao et al., 2015; Soares et al., 2014; Imbeault et al., 2014). Our study provides evidence that these proteins interact with OPA1 and are implicated in the cristae remodeling pathway. Further biochemical experiments will shed light on their exact function on mitochondrial remodeling modulation and their interplay with OPA1.

In conclusion, our mass spectrometry based on blue native PAGE appeared to be an optimal technique to identify OPA1 partners and unravel the changes in composition and distribution of mitochondrial heteromeric complexes during cristae remodeling. Furthermore, we provided hints into the cooperation between the major cristae shape determinants (OPA1, MICOS, MIB and ATP-synthase), but also discovered novel candidate OPA1-coplayers in cristae shaping in life and death of the cell.

EXPERIMENTAL PROCEDURES

Recombinant Protein Expression

p7/p15 recombinant BID was produced, purified and cleaved with caspase-8 as previously described (Frezza et al., 2006).

Mitochondria isolation, apoptosis stimulation and membrane complexes extraction

Mitochondria from mouse liver and mouse adult fibroblasts (MAFs) were purified by standard differential centrifugation as described in (Frezza et al., 2007). Mouse heart mitochondria were isolated from two CD1 wild type mice as described in (Fernandez-Vizarra et al., 2010).

Isolated mitochondria from liver (250 µg), heart (250 µg) or MAFs (150 µg) were treated with cBID and $cBID^{KKAA}$. The treatment was performed at 25°C in Experimental Buffer (EBc, 150 mM KCl, 1 mM Pi, 5 mM glutamate, 2.5 mM malate, 10 µM EGTA-Tris and 10 mM Tris-MOPS pH 7.4) at a final mitochondrial concentration of 0.5 mg/ml. The treatment was terminated by a 10 min centrifugation at 10000 x g at 4°C. The pellet was suspended in 50 µl of native buffer (Native Sample Buffer, Invitrogen) containing 1.2% digitonin (Invitrogen) and 1:100 protease inhibitors cocktail (PIC, Sigma). After 10 min incubation on ice, mitochondria were centrifuged at maximal speed in a table bench centrifuge for 20min, at 4°C, to extract the soluble membrane complexes. Supernatants were transferred into a new tube and 2 µl of Native PAGE Sample additive G250 5% (Invitrogen) was added before loading onto a native gel.

BN-PAGE and 3D BN-BN-SDS gel electrophoresis (BN-BN-SDS-PAGE)

To detect OPA1 complexes, equal volumes of the native samples were loaded onto a precast Native 3-12% Bis-Tris gel (Invitrogen). Electrophoresis was performed in the presence of cathode (dark blue cathode: 45min; light blue cathode: 90min) and anode buffers prepared following manufacturer's instructions (Invitrogen). When indicated, protein complexes were blotted onto a PVDF membrane, which was probed for the indicated antibodies, or stained with Coomassie blue. Coomassie stain was composed of 40% methanol, 10% acetic acid, 0.25 gr Coomassie Brilliant Blue R-250 (Biorad).

Second BN-PAGE was performed by excising and casting the lane obtained from the first BN-PAGE on a single-well native gel (NuPAGE Novex 4-12% Bis-Tris ZOOM gel, Invitrogen). In the cathode buffers used 0.02% n-Dodecyl-D-maltoside (DDM, SIGMA) was added. Electrophoresis was performed at 125 V for 1 hr 30 min using dark cathode buffer and at 150 V, overnight using with light cathode buffer. During 2D BN-BN-PAGE, complexes resistant to detergent are aligned in a diagonal easily identified by Coomassie contained into the running samples. When indicated, the native gel was subjected to western blotting to detect OPA1 complexes or stained with homemade Coomassie blue.

The third dimension SDS-PAGE was performed after excising the diagonal and incubating it with reducing solutions RSa for 10 min, RSb for 7 min and RSc for 12 min, in order to facilitate the complexes dissociation during the 3D SDS (RSa=1x LDS sample buffer (Invitrogen), 4% β-mercaptoethanol, RSb=1x LDS sample buffer (Invitrogen), 1% N N-dimethylacrylamide (DMA, SIGMA) and RSc=1x LDS sample buffer (Invitrogen), 20% ethanol and 0.1% β-mercaptoethanol). After the treatment, the diagonal was loaded onto a gel (NuPAGE Novex 4-12% Bis-Tris ZOOM gel, Invitrogen) and run under denaturating conditions to separate the individual proteins that were then transferred onto

polyvinylidene fluoride (PVDF) membranes and immunodetected for the indicated antibodies.

3D BN-BN-SDS gel electrophoresis for semi-quantitative proteomic analysis

Untreated and cBID treated mitochondria (10 mg/ml) were suspended in buffer D (1 M 6-aminohexanoic acid, 1.2% V/V digitonin, 50 mM Bis-Tris-HCl, pH 7) and centrifuged. The supernatants containing the extracted membrane complexes were collected and 5% Serva Blue G dye in 1 M6-aminohexanoic acid was added to 1/3 of the final sample volume. Equal amounts (100 mg) of mitochondrial proteins were separated in a homemade gradient gel of 3%–13% acrylamide gradient. The lanes of Untreated and cBID samples of the first dimension BN-PAGE were excised, casted on top of a native single-well 3%–14% gradient gel and run in the presence of 0.002% Dodecyl D Maltoside (DDM, Sigma). The resulted diagonals were divided into the same seven spots (“1”, “2”, “4”, “5”, “7”, “10” and “11”), cut and treated with 1% SDS and 1% β-mercaptoethanol for 1 hr. Spots of the same molecular weight from untreated and cBID treated samples were loaded onto an SDS-PAGE and each lane was subdivided into small spots to be analyzed by LC/MS. Gel pieces were then digested with modified porcine trypsin (Promega) at a final ratio 1:20 (trypsin-protein). Digestion proceeded overnight at 37ºC in 100 mM ammonium bicarbonate, pH 8.8. The resulting tryptic peptide mixtures were subjected to nano-liquid chromatography coupled to mass spectrometry (LC-MS) for protein identification. Peptides were injected onto a C-18 reversed phase (RP) nano-column (75 µm I.D. and 50 cm, Acclaim PepMap100, Thermo Scientific) and analyzed in a continuous acetonitrile gradient consisting of 0-30% B in 240 min, 50-90% B in 3 min (B=90% acetonitrile, 0.5% acetic acid). A flow rate of ca. 200 nL/min was used to elute peptides from the RP nano-

column to an emitter nanospray needle for real time ionization and peptide fragmentation on an Orbitrap Fusion mass spectrometer (Thermo Fisher, San José, CA, USA). For protein identification, tandem mass spectra were extracted and charge state deconvoluted by Proteome Discoverer 1.4.0.288 (Thermo Fisher Scientific). All MS/MS samples were analyzed using SEQUESTTM (Thermo Fisher Scientific).

For data analysis the results were processed using the proteome software of Scaffold (Version 4.0) using the Mouse MitoCarta dataset (Pagliarini et al., 2008). The protein threshold was set at 99%, the minimum number of peptides (to determine if a protein is present) at 2 and the peptide threshold at 95%. The results of its sub-spot retrieved in 3rd D-PAGE were consolidated for each spot of the 2nd D-PAGE. The fold change was quantified to report how much the protein's level was altered, by calculating the ratio of the number of identified peptides in treated over the number of identified peptides in untreated. Fold change less than 0.8 was considered significant for the proteins that decrease after treatment.

BN-PAGE based semi-quantitative proteomic analysis

Mitochondrial proteins (250 µg) from two mouse hearts were treated and solubilized as described above. Blue Native Electrophoresis (BN-PAGE) was used to separate the native membrane complexes in a homemade gradient gel from 4% to 13% acrylamide, 20 x 20 cm, for control samples and for samples treated with cBID or cBID^{KKAA} (1 mg of protein per sample). The electrophoresis was performed as described for the 1st dimension BN-PAGE. Subsequently, gels were stained using GelCode Blue Stain Reagent (Thermo Scientific). Each lane was divided and excised in 26 bands covering the whole electrophoretic run.

Gel pieces were then digested trypsinized and subjected to mass spectrometry as described above.

Each identified protein displayed a score value for every spot analyzed; thus we resulted with a pattern of identification along the whole electrophoretic run for every hit. The strength of relation between the patterns of identification of each protein and the one of OPA1 was measured using Pearson correlation coefficiency (r). Positive association was considered when $r \geq +0.1$. The results were filtered for the mitochondrial predicted proteins using the proteomics database MitoMiner (http://mitominer.mrc-mbu.cam.ac.uk) (Smith and Robinson, 2016). The quantification between treated and untreated was performed after calculating their fold change by dividing the sum of their score values. Proteins that decrease after $cBID^{wt}$ but increase, remain unaltered, or the decrease is less after $cBID^{KKAA}$ are considered to be reduced only upon cristae remodelling.

SILAC labelling and quantitative proteomic analysis

Mouse adult fibroblasts (MAFs) were grown separately in DMEM-Flex medium containing 4.5 g/L glucose, 2 mM glutamine, 10% fetal bovine serum (FBS), 50 U/ml Penicillin, 50 mg/ml Streptomycin, 50 mg/ml Uridine and Phenol Red supplemented with either *light* L-Lysine and L-Arginine or *heavy* [U-$^{13}C_6$]-L-Lysine HCl and [U-$^{13}C_6$]-L-Arginine (100 mg/L of each amino acid) (SILAC Protein Identification and Quantification Media Kit, Invitrogen). After 6 doublings cell subpopulations, *light* and *heavy*, were harvested and mitochondria were isolated separately. In experiment "a" *light* mitochondria were treated with 20 pmol/mg cBID for 30 min in EB, and *heavy* mitochondria were untreated. After centrifugation at 10000 *x g*, 10 min, 4°C, the pellets from both samples were mixed and resuspended together in NB indicated above. In experiment "b", *light* mitochondria were

untreated while *heavy* mitochondria were treated with 20 pmol/mg cBID^{KKAA} for 30 min, 25°C. After centrifugation the samples were mixed and processed as in experiment "a" before proceeding with the BN-PAGE. Protein complexes (500 µg) from experiments "a" and "b" were loaded in parallel lanes and complexes were separated by BN-PAGE electrophoresis. Three lanes from experiment "a" and "b" were stained with Coomassie and bands between 600 and 1000kDa (Spot A1-2, A3-4, A5-6 and A7) were excised with a scalpel and digested with trypsin. Digestion proceeded overnight at 37ºC in 100 mM ammonium bicarbonate, pH 8.8. The resulting tryptic peptide mixtures were subjected to nano-liquid chromatography coupled to mass spectrometry (LC-MS) for protein identification. Peptides were injected onto a C-18 reversed phase (RP) nano-column (75 mm I.D. and 50 cm, Acclaim PepMap100, Thermo Scientific) and analyzed in a continuous acetonitrile gradient consisting of 0-30% B in 240 min, 50-90% B in 3 min (B=90% acetonitrile, 0.5% acetic acid). A flow rate of ca. 200 nL/min was used to elute peptides from the RP nano-column to an emitter nanospray needle for real time ionization and peptide fragmentation on a Q Exactive mass spectrometer (Thermo Fisher, San José, CA, USA). For protein identification, tandem mass spectra were extracted and charge state deconvoluted by Proteome Discoverer 1.4.0.288 (Thermo Fisher Scientific). All MS/MS samples were analyzed using SEQUESTTM (Thermo Fisher Scientific).

Change in peptide abundance in the studied complexes was considered when FDRq < 0.05 and Zq was > 1.2 or < -1.2 after treatment. To calculate the fold change of each protein we measured the median of fold change of all the peptides detected corresponding to one protein and fold change > 1.2 or < -1.2 was considered significant. Hits that decrease with cBID^{wt}, while no difference or less folds of decrease was observed in the treatment

with the mutant cBID^{KKAA}, were considered as candidate proteins which are reduced specifically during apoptotic cristae remodelling.

Bioinformatics Analysis

For classification according to Gene Ontology and enrichment analysis, our data were clustered using the databases Panther (http://pantherdb.org/) (Thomas et al., 2003) and Enrichr (http://amp.pharm.mssm.edu/Enrichr) (Chen et al., 2013). For pathway analysis the curated database of Reactome was used, which was implemented in Enrichr. To construct the interaction networks we used the meta-server STRING 10 (http://string-db.org/) (Jensen et al., 2009) and the confidence view was selected. Each network node represents a protein and the thickness of the edges represents the confidence of a predicted functional association. The prediction methods used were: co-occurrence, co-expression, experiments, databases and text mining.

Antibodies

For the immunoblots of the Blue Native gels, PVDF membranes were probed with the following antibodies: mouse monoclonal anti-OPA1 (1:1000 BD Biosciences), anti-MICU1 (1:1000 SIGMA), anti-MCU (1:1000 SIGMA), GHITM/MICS1 (1:200, kind gift from Toshihiko Oka). The incubation was overnight at 4°C. Isotype matched, horseradish peroxidase-conjugated secondary antibodies (GE Healthcare Life Sciences) were employed for chemiluminescence detection.

Acknowledgments

We thank Toshihiko Oka for kindly providing us with anti-GHITM.

Reference List

Acin-Perez,R., Fernandez-Silva,P., Peleato,M.L., Perez-Martos,A., and Enriquez,J.A. (2008). Respiratory active mitochondrial supercomplexes. Mol Cell *32*, 529-539.

Banerjee,S. and Chinthapalli,B. (2014). A proteomic screen with Drosophila Opa1-like identifies Hsc70-5/Mortalin as a regulator of mitochondrial morphology and cellular homeostasis. Int. J. Biochem. Cell Biol. *54*, 36-48.

Boissan,M., Montagnac,G., Shen,Q., Griparic,L., Guitton,J.+., Romao,M., Sauvonnet,N., Lagache,T., Lascu,I., Raposo,G., Desbourdes,C.+., Schlattner,U., Lacombe,M.L., Polo,S., van der Bliek,A.M., Roux,A.l., and Chavrier,P. (2014). Nucleoside diphosphate kinases fuel dynamin superfamily proteins with GTP for membrane remodeling. Science *344*, 1510-1515.

Chen,E.Y., Tan,C.M., Kou,Y., Duan,Q., Wang,Z., Meirelles,G.V., Clark,N.R., and Ma'ayan,A. (2013). Enrichr: interactive and collaborative HTML5 gene list enrichment analysis tool. BMC. Bioinformatics. *14*, 128.

Chen,H. and Chan,D.C. (2005). Emerging functions of mammalian mitochondrial fusion and fission. Hum Mol Genet *14 Spec No. 2*.

Cogliati,S., Frezza,C., Soriano,M.E., Varanita,T., Quintana-Cabrera,R., Corrado,M., Cipolat,S., Costa,V., Casarin,A., Gomes,L.C., Perales-Clemente,E., Salviati,L., Fernandez-Silva,P., Enriquez,J.A., and Scorrano,L. (2013). Mitochondrial cristae shape determines respiratory chain supercomplexes assembly and respiratory efficiency. Cell *155*, 160-171.

Darshi,M., Mendiola,V.L., Mackey,M.R., Murphy,A.N., Koller,A., Perkins,G.A., Ellisman,M.H., and Taylor,S.S. (2011a). ChChd3, an inner mitochondrial membrane protein, is essential for maintaining crista integrity and mitochondrial function. J. Biol. Chem. *286*, 2918-2932.

Darshi,M., Mendiola,V.L., Mackey,M.R., Murphy,A.N., Koller,A., Perkins,G.A., Ellisman,M.H., and Taylor,S.S. (2011b). ChChd3, an inner mitochondrial membrane protein, is essential for maintaining crista integrity and mitochondrial function. J Biol Chem. *286*, 2918-2932.

Davies,K.M., Anselmi,C., Wittig,I., Faraldo-Gomez,J.D., and Kuhlbrandt,W. (2012). Structure of the yeast F1Fo-ATP synthase dimer and its role in shaping the mitochondrial cristae. Proc. Natl. Acad. Sci. U. S. A *109*, 13602-13607.

De Stefani,D., Raffaello,A., Teardo,E., SzabГ²,I., and Rizzuto,R. (2011). A forty-kilodalton protein of the inner membrane is the mitochondrial calcium uniporter. Nature.

Dimmer,K.S., Navoni,F., Casarin,A., Trevisson,E., Endele,S., Winterpacht,A., Salviati,L., and Scorrano,L. (2008). LETM1, deleted in Wolf Hirschhorn syndrome is required for normal mitochondrial morphology and cellular viability. Hum Mol Genet *17*, 201-214.

Fernandez-Vizarra,E., Ferrin,G., Perez-Martos,A., Fernandez-Silva,P., Zeviani,M., and Enriquez,J.A. (2010). Isolation of mitochondria for biogenetical studies: An update. Mitochondrion. *10*, 253-262.

Frank,S., Gaume,B., Bergmann-Leitner,E.S., Leitner,W.W., Robert,E.G., Catez,F., Smith,C.L., and Youle,R.J. (2001). The role of dynamin-related protein 1, a mediator of mitochondrial fission, in apoptosis. Dev. Cell *1*, 515-525.

Frezza,C., Cipolat,S., Martins,d.B., Micaroni,M., Beznoussenko,G.V., Rudka,T., Bartoli,D., Polishuck,R.S., Danial,N.N., De Strooper,B., and Scorrano,L. (2006). OPA1 Controls Apoptotic Cristae Remodeling Independently from Mitochondrial Fusion. Cell *126*, 177-189.

Frezza,C., Cipolat,S., and Scorrano,L. (2007). Organelle isolation: functional mitochondria from mouse liver, muscle and cultured fibroblasts. Nat. Protoc. *2*, 287-295.

Harner,M., Korner,C., Walther,D., Mokranjac,D., Kaesmacher,J., Welsch,U., Griffith,J., Mann,M., Reggiori,F., and Neupert,W. (2011). The mitochondrial contact site complex, a determinant of mitochondrial architecture. EMBO J. *30*, 4356-4370.

Huynen,M.A., Muhlmeister,M., Gotthardt,K., Guerrero-Castillo,S., and Brandt,U. (2016). Evolution and structural organization of the mitochondrial contact site (MICOS) complex and the mitochondrial intermembrane space bridging (MIB) complex. Biochim. Biophys. Acta *1863*, 91-101.

Imbeault,E., Mahvelati,T.M., Braun,R., Gris,P., and Gris,D. (2014). Nlrx1 regulates neuronal cell death. Mol. Brain *7*, 90.

Jensen,L.J., Kuhn,M., Stark,M., Chaffron,S., Creevey,C., Muller,J., Doerks,T., Julien,P., Roth,A., Simonovic,M., Bork,P., and von,M.C. (2009). STRING 8--a global view on proteins and their functional interactions in 630 organisms. Nucleic Acids Res. *37*, D412-D416.

Kolanczyk,M., Pech,M., Zemojtel,T., Yamamoto,H., Mikula,I., Calvaruso,M.A., van den Brand,M., Richter,R., Fischer,B., Ritz,A., Kossler,N., Thurisch,B., Spoerle,R., Smeitink,J., Kornak,U., Chan,D., Vingron,M., Martasek,P., Lightowlers,R.N., Nijtmans,L., Schuelke,M., Nierhaus,K.H., and Mundlos,S. (2011). NOA1 is an essential GTPase required for mitochondrial protein synthesis. Mol. Biol. Cell *22*, 1-11.

Martinou,J.C. and Green,D.R. (2001). Breaking the mitochondrial barrier. Nat. Rev. Mol. Cell Biol. *2*, 63-67.

Merkwirth,C., Dargazanli,S., Tatsuta,T., Geimer,S., Lower,B., Wunderlich,F.T., von Kleist-Retzow,J.C., Waisman,A., Westermann,B., and Langer,T. (2008). Prohibitins control cell proliferation and apoptosis by regulating OPA1-dependent cristae morphogenesis in mitochondria. Genes Dev. *22*, 476-488.

Oka,T., Sayano,T., Tamai,S., Yokota,S., Kato,H., Fujii,G., and Mihara,K. (2008). Identification of a novel protein MICS1 that is involved in maintenance of mitochondrial morphology and apoptotic release of cytochrome c. Mol. Biol. Cell *19*, 2597-2608.

Ong,S.E., Blagoev,B., Kratchmarova,I., Kristensen,D.B., Steen,H., Pandey,A., and Mann,M. (2002). Stable Isotope Labeling by Amino Acids in Cell Culture, SILAC, as a Simple and Accurate Approach to Expression Proteomics. Molecular & Cellular Proteomics *1*, 376-386.

Ott,C., Ross,K., Straub,S., Thiede,B., Gotz,M., Goosmann,C., Krischke,M., Mueller,M.J., Krohne,G., Rudel,T., and Kozjak-Pavlovic,V. (2012). Sam50 functions in mitochondrial intermembrane space bridging and biogenesis of respiratory complexes. Mol. Cell Biol. *32*, 1173-1188.

Pagliarini,D.J., Calvo,S.E., Chang,B., Sheth,S.A., Vafai,S.B., Ong,S.E., Walford,G.A., Sugiana,C., Boneh,A., Chen,W.K., Hill,D.E., Vidal,M., Evans,J.G., Thorburn,D.R., Carr,S.A., and Mootha,V.K. (2008). A mitochondrial protein compendium elucidates complex I disease biology. Cell *134*, 112-123.

Patten,D.A., Wong,J., Khacho,M., Soubannier,V., Mailloux,R.J., Pilon-Larose,K., MacLaurin,J.G., Park,D.S., McBride,H.M., Trinkle-Mulcahy,L., Harper,M.E., Germain,M., and Slack,R.S. (2014). OPA1-dependent cristae modulation is essential for cellular adaptation to metabolic demand. EMBO J *33*, 2676-2691.

Pernas,L. and Scorrano,L. (2015). Mito-Morphosis: Mitochondrial Fusion, Fission, and Cristae Remodeling as Key Mediators of Cellular Function. Annu. Rev. Physiol.

Piao,L., Li,Y., Kim,S.J., Sohn,K.C., Yang,K.J., Park,K.A., Byun,H.S., Won,M., Hong,J., Hur,G.M., Seok,J.H., Shong,M., Sack,R., Brazil,D.P., Hemmings,B.A., and Park,J. (2009). Regulation of OPA1-mediated mitochondrial fusion by leucine zipper/EF-hand-containing transmembrane protein-1 plays a role in apoptosis. Cell Signal. *21*, 767-777.

Raffaello,A., De,S.D., Sabbadin,D., Teardo,E., Merli,G., Picard,A., Checchetto,V., Moro,S., Szabo,I., and Rizzuto,R. (2013). The mitochondrial calcium uniporter is a multimer that can include a dominant-negative pore-forming subunit. EMBO J. *32*, 2362-2376.

Schagger,H., Cramer,W.A., and von Jagow,G. (1994). Analysis of molecular masses and oligomeric states of protein complexes by blue native electrophoresis and isolation of membrane protein complexes by two-dimensional native electrophoresis. Anal. Biochem. *217*, 220-230.

Scorrano,L., Ashiya,M., Buttle,K., Weiler,S., Oakes,S.A., Mannella,C.A., and Korsmeyer,S.J. (2002). A distinct pathway remodels mitochondrial cristae and mobilizes cytochrome c during apoptosis. Dev. Cell *2*, 55-67.

Smith,A.C. and Robinson,A.J. (2016). MitoMiner v3.1, an update on the mitochondrial proteomics database. Nucleic Acids Res. *44*, D1258-D1261.

Soares,F., Tattoli,I., Rahman,M.A., Robertson,S.J., Belcheva,A., Liu,D., Streutker,C., Winer,S., Winer,D.A., Martin,A., Philpott,D.J., Arnoult,D., and Girardin,S.E. (2014). The mitochondrial protein NLRX1 controls the balance between extrinsic and intrinsic apoptosis. J. Biol. Chem. *289*, 19317-19330.

Tang,T., Zheng,B., Chen,S.H., Murphy,A.N., Kudlicka,K., Zhou,H., and Farquhar,M.G. (2009). hNOA1 interacts with complex I and DAP3 and regulates mitochondrial respiration and apoptosis. J. Biol. Chem. *284*, 5414-5424.

Thomas,P.D., Kejariwal,A., Campbell,M.J., Mi,H., Diemer,K., Guo,N., Ladunga,I., Ulitsky-Lazareva,B., Muruganujan,A., Rabkin,S., Vandergriff,J.A., and Doremieux,O. (2003). PANTHER: a browsable database of gene products organized by biological function, using curated protein family and subfamily classification. Nucleic Acids Res. *31*, 334-341.

Vais,H., Tanis,J.E., Muller,M., Payne,R., Mallilankaraman,K., and Foskett,J.K. (2015). MCUR1, CCDC90A, Is a Regulator of the Mitochondrial Calcium Uniporter. Cell Metab *22*, 533-535.

Varanita,T., Soriano,M.E., Romanello,V., Zaglia,T., Quintana-Cabrera,R., Semenzato,M., Menabç,R., Costa,V., Civiletto,G., Pesce,P., Viscomi,C., Zeviani,M., Di Lisa,F., Mongillo,M., Sandri,M., and Scorrano,L. (2015). The Opa1-Dependent Mitochondrial Cristae Remodeling Pathway Controls Atrophic, Apoptotic, and Ischemic Tissue Damage. Cell Metabolism *21*.

Vogel,F., Bornhovd,C., Neupert,W., and Reichert,A.S. (2006). Dynamic subcompartmentalization of the mitochondrial inner membrane. J. Cell Biol. *175*, 237-247.

Xiao,L., Xian,H., Lee,K.Y., Xiao,B., Wang,H., Yu,F., Shen,H.M., and Liou,Y.C. (2015). Death-associated Protein 3 Regulates Mitochondrial-encoded Protein Synthesis and Mitochondrial Dynamics. J. Biol. Chem. *290*, 24961-24974.

Yoneda,M., Miyatake,T., and Attardi,G. (1994). Complementation of mutant and wild-type human mitochondrial DNAs coexisting since the mutation event and lack of complementation of DNAs introduced separately into a cell within distinct organelles. Mol. Cell Biol. *14*, 2699-2712.

FIGURE LEGENDS

Figure 1. Three dimensional BlueNative-BlueNative-SDS PAGE is a useful tool to investigate OPA1 complexes

A. Schematic representation of the method. Mitochondria were isolated from mouse liver and mitochondrial membrane complexes were extracted by solubilization with 10 min incubation in 1.2% digitonin. The samples were then subjected to 3D-BN-BN-SDS-PAGE following LC-MS/MS for protein identification in the complexes of interest.
B. 1st Dimension BN-PAGE and western blotting against OPA1 of untreated (Untr) and cBid treated (cBID) mitochondrial membrane extracts. The higher molecular weight OPA1 complexes decrease after cBid treatment. Molecular weight markers are indicated on the left.
C. 2nd Dimension BN-PAGE and western blotting against OPA1 of untreated (Untr, left) and cBid treated (cBID, right) mitochondrial membrane extracts. Molecular weight markers are indicated on the top of the blots.
D. 3rd Dimension SDS-PAGE and western blotting against OPA1 of untreated (Untr, top) and cBid treated samples (cBID, bottom). Molecular weight markers are indicated on the left and on the top.
E. Coomassie staining of 1st Dimension BN-PAGE of untreated (Untr) and cBid treated (cBID) mitochondrial membrane extracts. Molecular weight markers are indicated on the left.
F. Coomassie staining of 2nd Dimension BN-PAGE of untreated (Untr, left) and cBid treated (cBID, right) mitochondrial membrane extracts. The resulted parallel diagonals

were divided into the same seven spots and processed for SDS-PAGE. Molecular weight markers are indicated on the top.

G. Coomassie staining of the 3rd Dimension SDS PAGE. The complexes of a representative spot of the 2nd-D BN-PAGE, from both untreated (Untr) and cBid treated samples, were separated in their components by SDS PAGE. The gel was subdivided into various spots were subsequently analysed by LC/MS. The resulting identified peptides were analyzed with Scaffold Software and Mitocarta Database was used.

Figure 2. Clustering of candidate OPA1 partners in mouse liver mitochondria

A. Pie showing protein classification of the identified OPA1 partners based on protein biological function.
B. Enrichment bar graph depicting the identified OPA1 partners in its complexes classified based on the cellular component.
C. Enrichment bar graph of the reactome of the identified OPA1 partners in its complexes that decrease after $cBID^{wt}$ treatment.

Figure 3. BN-PAGE - LQ/MS of mouse heart mitochondria identifies OPA1 containing complexes targeted during apoptosis

A. BN-PAGE and western blotting against OPA1 of untreated (Untr), $cBid^{wt}$ and $cBID^{KKAA}$ treated mitochondrial membrane extracts. As a loading control, GRP75 was used.
B. Coomassie staining of a Blue Native gel lane. The numbers of the spots in which each lane was cut are indicated on the left.

C. Graphs depicting the score value of the identified OPA1 peptides to each spot of the lane in untreated (Untr), cBid^{wt} and cBID^{KKAA} treated mitochondrial samples. On top of each graph the corresponding BN lanes of figure 1A are depicted horizontally in analogy to the molecular weights. The smaller the spot number is the higher the molecular weight represents.

Figure 4. Clustering of candidate OPA1 partners in mouse heart mitochondria

A. STRING network of all the identified proteins present in OPA1-containing complexes in heart mitochondria. Each network node represents a protein and the thickness of the edges represents the confidence of a predicted functional association.
B. Enrichment bar graph depicting the identified OPA1 partners in its complexes according to the cellular component.
C. Pie showing the gene ontology of all the identified OPA1 partners in its complexes according to their biological function.
D. STRING network of the identified proteins present in OPA1-containing complexes in heart mitochondria which decrease after cBID^{wt} treatment.
E. Enrichment bar graph of the reactome of the identified OPA1 partners that decrease after cBID^{wt} treatment.
F. STRING network of the candidate proteins present in OPA1-containing complexes in heart mitochondria which are reduced during cristae remodeling.

Figure 5. Intersection between candidate OPA1 interactors in liver and heart

A. Intersection between liver and heart OPA1 interactions.

B. Pie depicting the classification of the candidate OPA1-containing complexes components identified in both heart and liver based on their biological function.
C. STRING network of the candidate components of OPA1-containing complexes found in both liver and heart mitochondria. Each network node represents a protein and the thickness of the edges represents the confidence of a predicted functional association.
D. Enrichment bar graph of the reactome of the identified OPA1 interactors that decrease after $cBID^{wt}$ treatment.
E. STRING network of the candidate components of OPA1-containing complexes that are reduced upon apoptosis in both liver and heart mitochondria.

Figure 6. SILAC allows quantification of proteins leaving Opa1 complexes during apoptosis

Schematic representation of Stable Isotopic Labeling using Amino Acids (SILAC) in $OPA1^{fl/fl}$ MAFs followed by blue native PAGE. Gel bands between 600 kDa and 1000 kDa were excised and subjected to LC-MS/MS.

Figure 7. Clustering of candidate OPA1 partners in MAFs after SILAC analysis

A. STRING network of all the candidate components of OPA1-containing complexes, regulated upon apoptosis. Each network node represents a protein and the thickness of the edges represents the confidence of a predicted functional association.
B. Enrichment bar graph depicting the identified OPA1 partners in its complexes, regulated upon apoptosis, according to the cellular component.

C. Pie showing protein classification of the identified OPA1 partners regulated upon apoptosis based on protein biological function.

D. STRING network of the candidate components of OPA1-containing complexes, which are reduced upon apoptosis.

E. Enrichment bar graph of the reactome of the identified OPA1 interactors that decrease after cBID^{wt} treatment.

F. STRING network of the candidate components of OPA1-containing complexes that are reduced upon apoptotic cristae remodeling.

Figure 8. Biochemical validation of components of OPA1-containing complexes

A. BN-PAGE and western blotting against OPA1 and Mic60 of untreated (-), cBID^{wt} and cBID^{KKAA} treated mitochondrial membrane extracts deriving from liver. Molecular weight markers are indicated on the left.

B. 3rd Dimension SDS-PAGE and western blotting against OPA1 and Mic60 of untreated (Untr) and cBID treated samples (cBID^{wt}). Molecular weight markers are indicated on the top.

C. BN-PAGE and western blotting against OPA1, MICU1 and MCU in untreated liver mitochondria. Molecular weight markers are indicated on the left.

D. BN-PAGE and western blotting against OPA1 and GHITM of untreated (-), cBID^{wt} and cBID^{KKAA} treated mitochondrial membrane extracts deriving from heart. Molecular weight markers are indicated on the left.

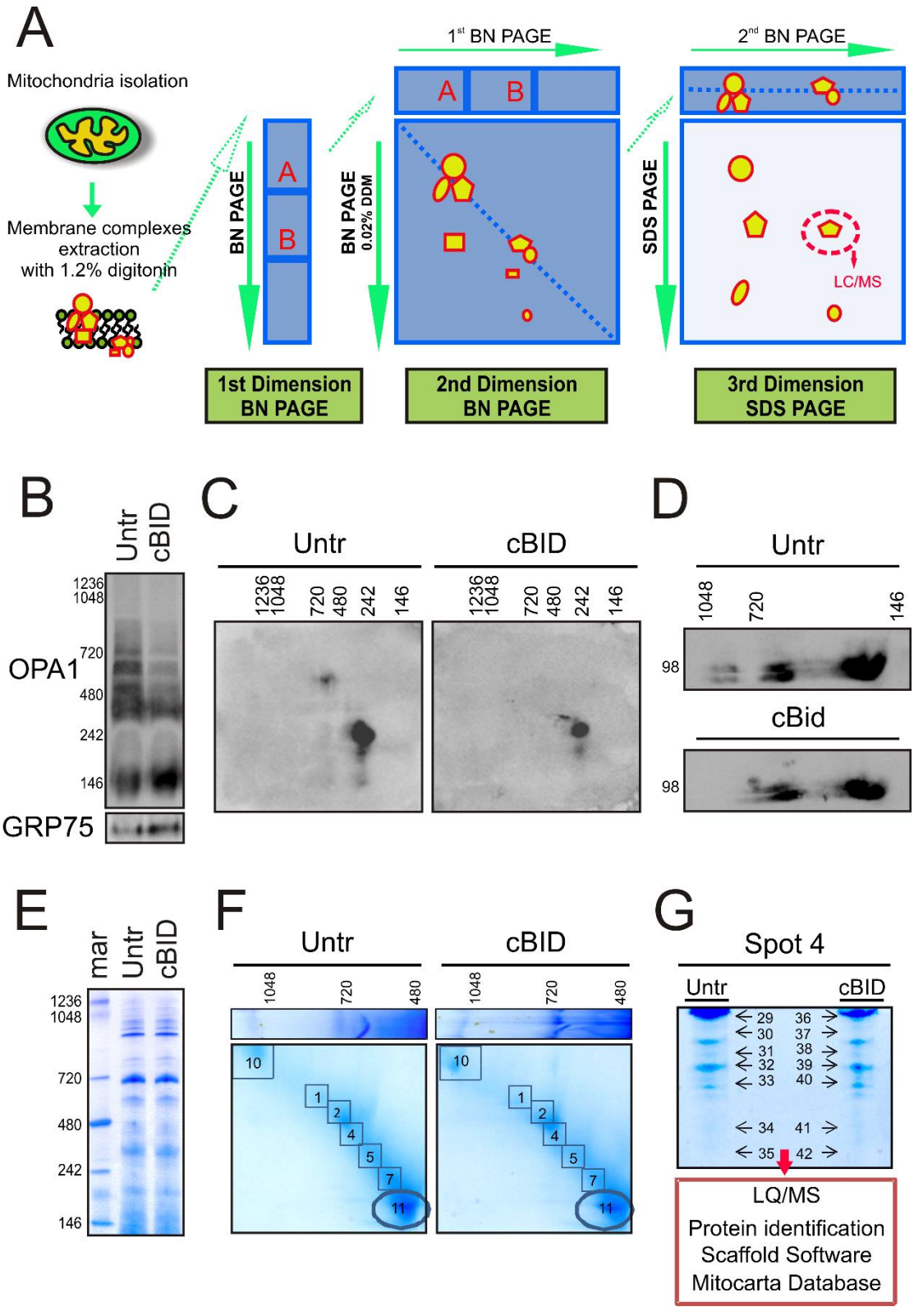
A
Mitochondria isolation
Membrane complexes extraction with 1.2% digitonin
1st BN PAGE
2nd BN PAGE
BN PAGE
BN PAGE 0.02% DDM
SDS PAGE
LC/MS
1st Dimension BN PAGE
2nd Dimension BN PAGE
3rd Dimension SDS PAGE
B
Untr
cBID
OPA1
GRP75
C
Untr
cBID
D
Untr
cBid
E
mar
Untr
cBID
F
Untr
cBID
G
Spot 4
Untr
cBID
LQ/MS
Protein identification
Scaffold Software
Mitocarta Database

Figure 1

A

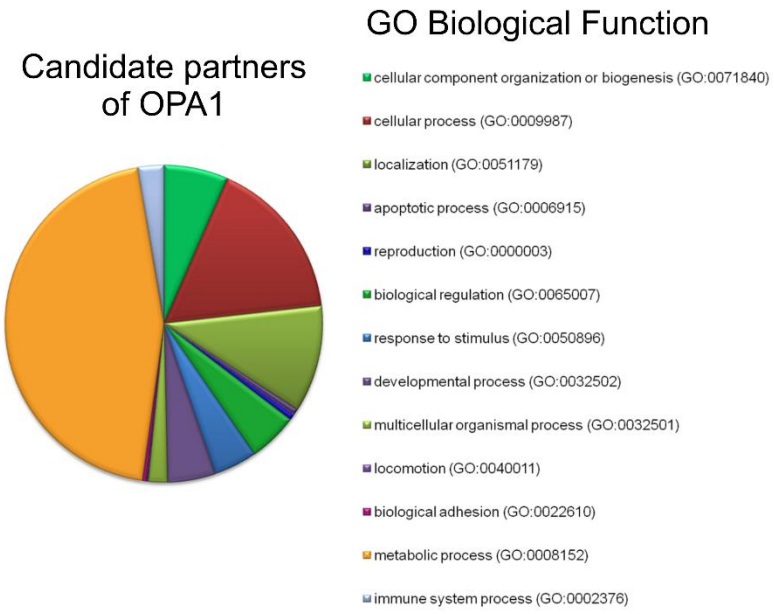
Candidate partners of OPA1
GO Biological Function
cellular component organization or biogenesis (GO:0071840)
cellular process (GO:0009987)
localization (GO:0051179)
apoptotic process (GO:0006915)
reproduction (GO:0000003)
biological regulation (GO:0065007)
response to stimulus (GO:0050896)
developmental process (GO:0032502)
multicellular organismal process (GO:0032501)
locomotion (GO:0040011)
biological adhesion (GO:0022610)
metabolic process (GO:0008152)
immune system process (GO:0002376)

B

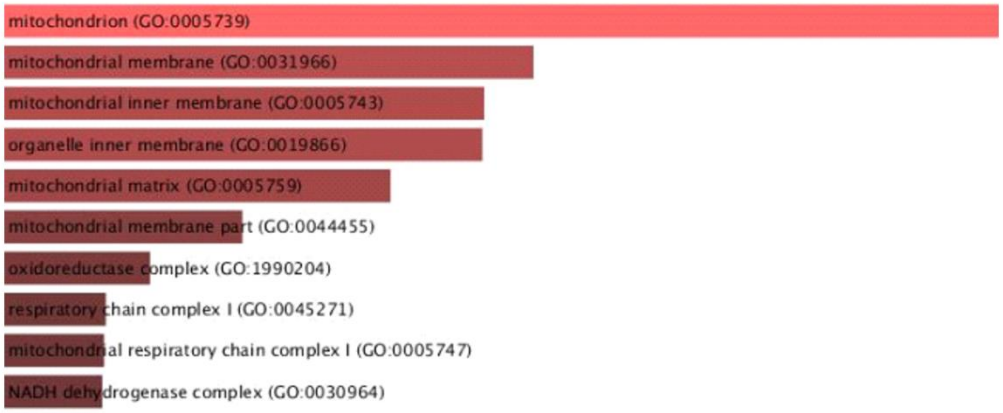
GO Cellular Component
mitochondrion (GO:0005739)
mitochondrial membrane (GO:0031966)
mitochondrial inner membrane (GO:0005743)
organelle inner membrane (GO:0019866)
mitochondrial matrix (GO:0005759)
mitochondrial membrane part (GO:0044455)
oxidoreductase complex (GO:1990204)
respiratory chain complex I (GO:0045271)
mitochondrial respiratory chain complex I (GO:0005747)
NADH dehydrogenase complex (GO:0030964)

C

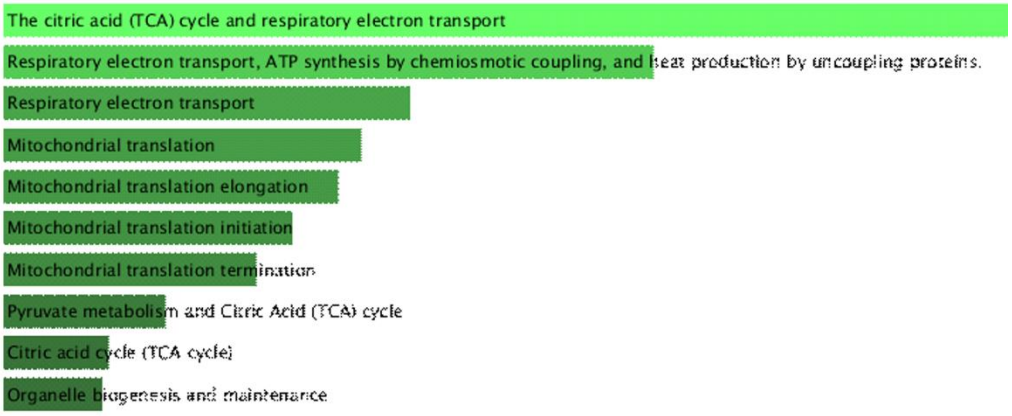
Reactome
The citric acid (TCA) cycle and respiratory electron transport
Respiratory electron transport, ATP synthesis by chemiosmotic coupling, and heat production by uncoupling proteins.
Respiratory electron transport
Mitochondrial translation
Mitochondrial translation elongation
Mitochondrial translation initiation
Mitochondrial translation termination
Pyruvate metabolism and Citric Acid (TCA) cycle
Citric acid cycle (TCA cycle)
Organelle biogenesis and maintenance

Figure 2

Figure 3

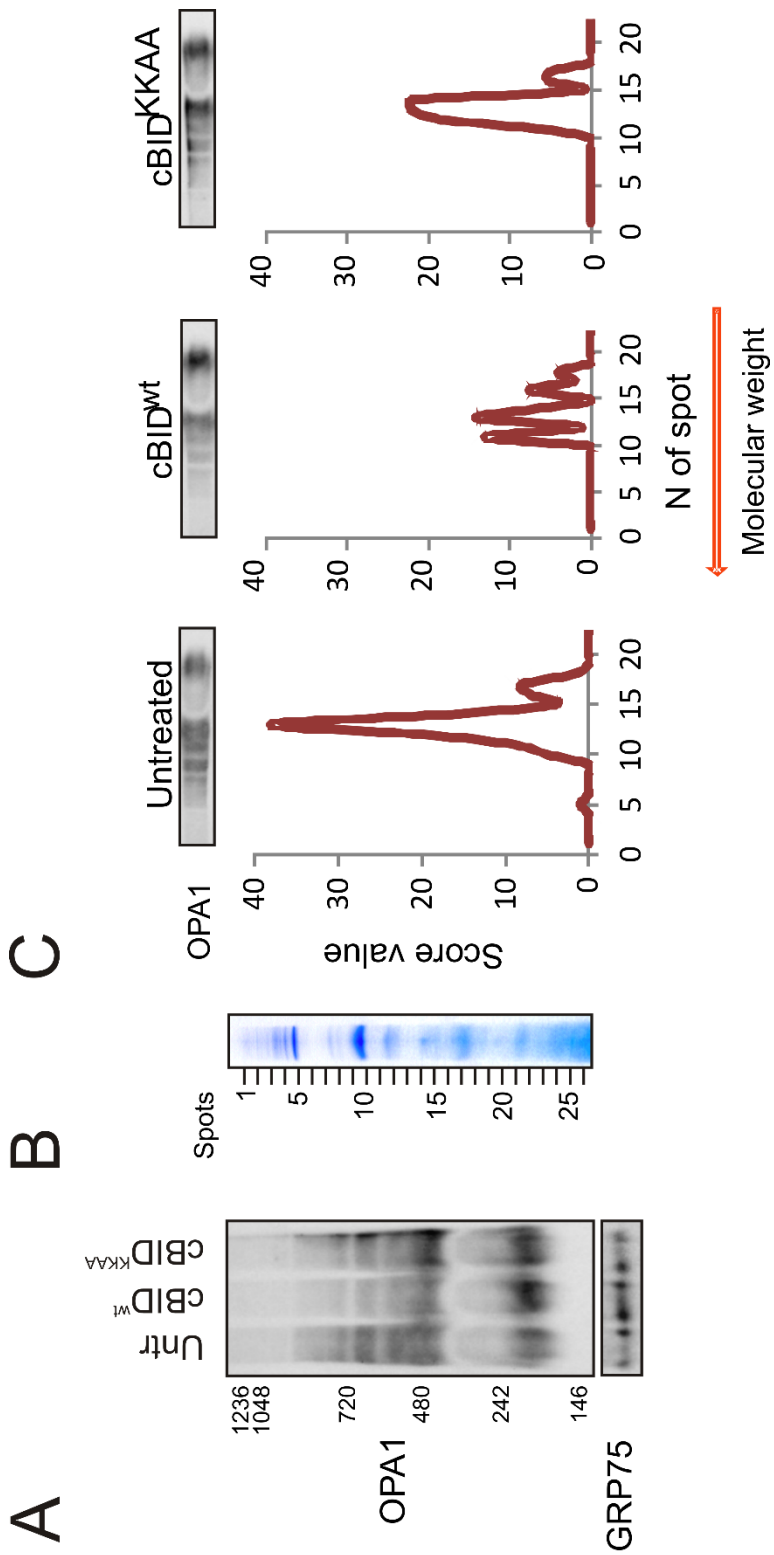
A
B
C
Untr
cBID^wt
cBID^KKAA
1236
1048
720
480
242
146
OPA1
GRP75
Spots
1
5
10
15
20
25
OPA1
Untreated
cBID^wt
cBID^KKAA
Score value
0
10
20
30
40
0 5 10 15 20
N of spot
Molecular weight

Figure 4

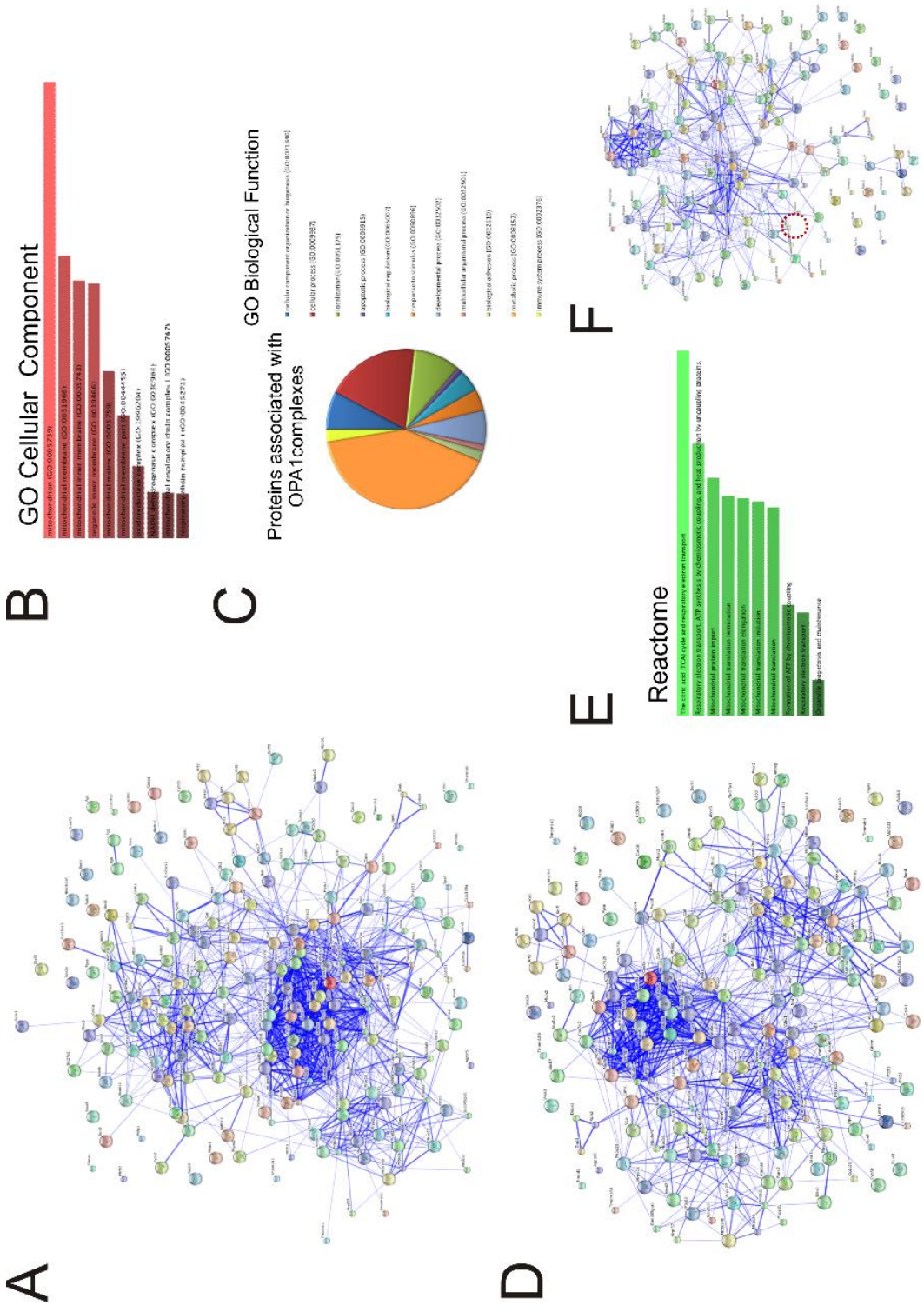
A
B
GO Cellular Component
C
GO Biological Function
Proteins associated with OPA1complexes
D
E
Reactome
F

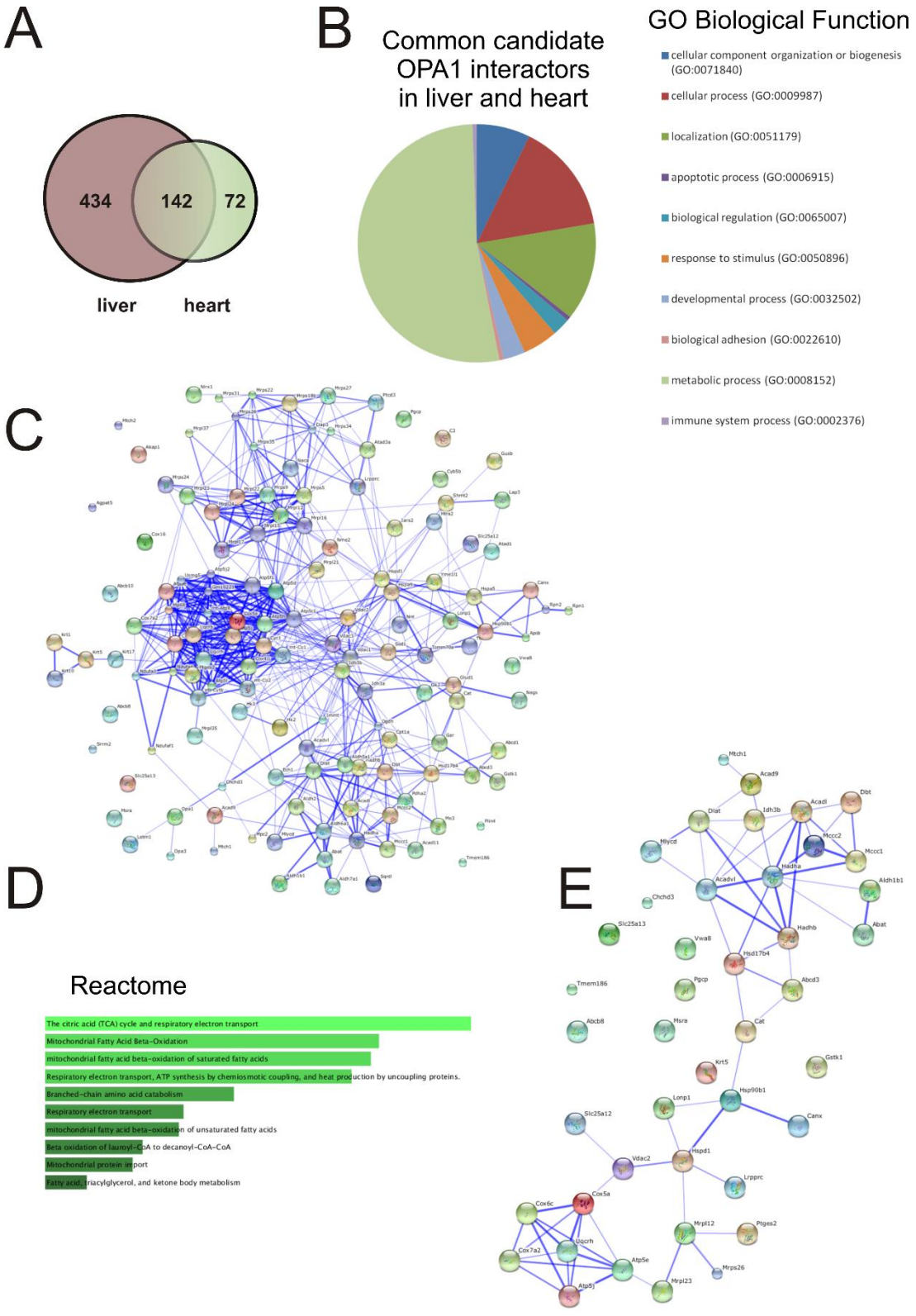
A
434
142
72
liver
heart
B
Common candidate OPA1 interactors in liver and heart
GO Biological Function
cellular component organization or biogenesis (GO:0071840)
cellular process (GO:0009987)
localization (GO:0051179)
apoptotic process (GO:0006915)
biological regulation (GO:0065007)
response to stimulus (GO:0050896)
developmental process (GO:0032502)
biological adhesion (GO:0022610)
metabolic process (GO:0008152)
immune system process (GO:0002376)
C
D
Reactome
The citric acid (TCA) cycle and respiratory electron transport
Mitochondrial Fatty Acid Beta-Oxidation
mitochondrial fatty acid beta-oxidation of saturated fatty acids
Respiratory electron transport, ATP synthesis by chemiosmotic coupling, and heat production by uncoupling proteins.
Branched-chain amino acid catabolism
Respiratory electron transport
mitochondrial fatty acid beta-oxidation of unsaturated fatty acids
Beta oxidation of lauroyl-CoA to decanoyl-CoA-CoA
Mitochondrial protein import
Fatty acid, triacylglycerol, and ketone body metabolism
E

Figure 5

Experimental Workflow

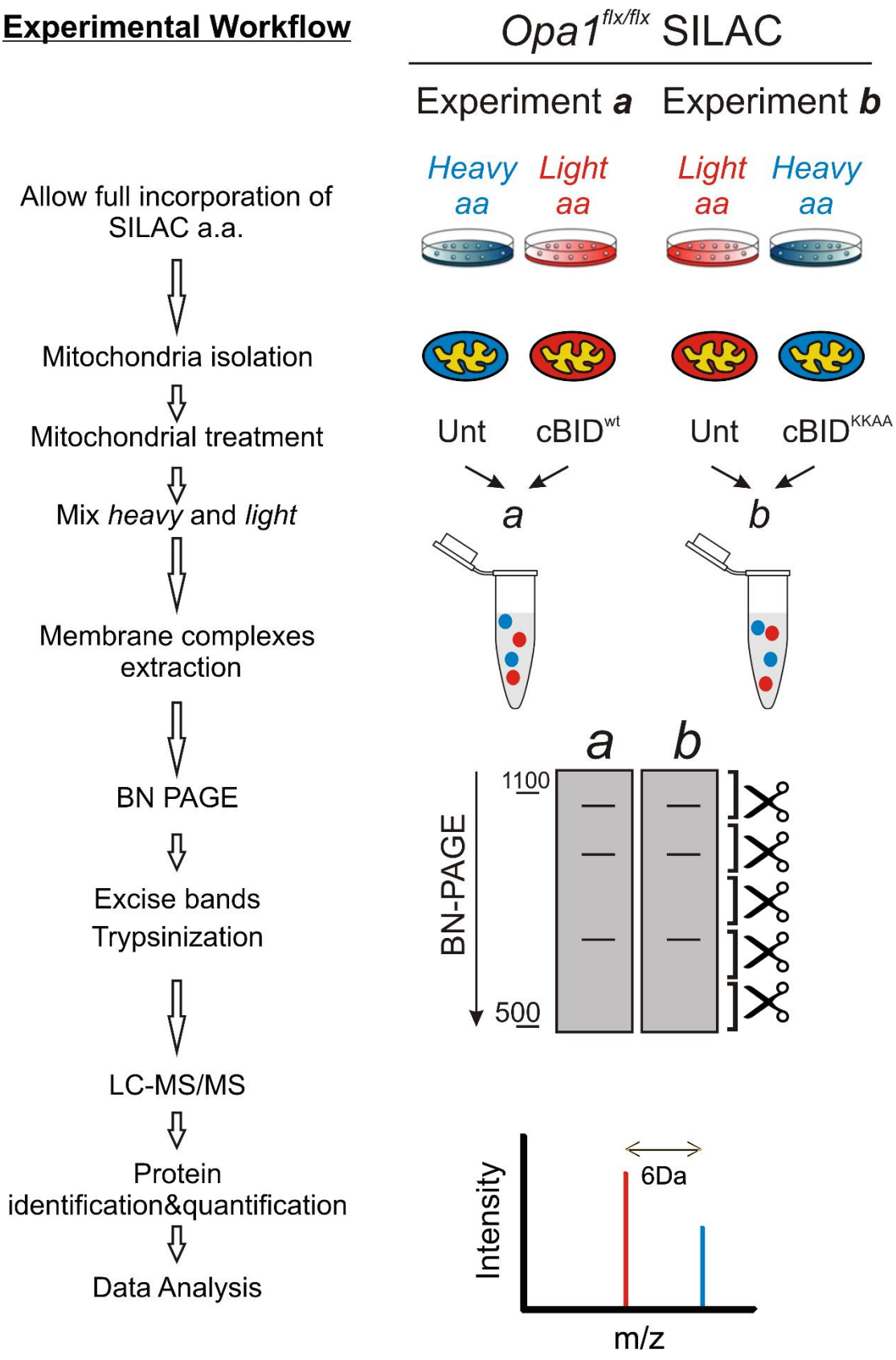

Figure 6

Figure 7

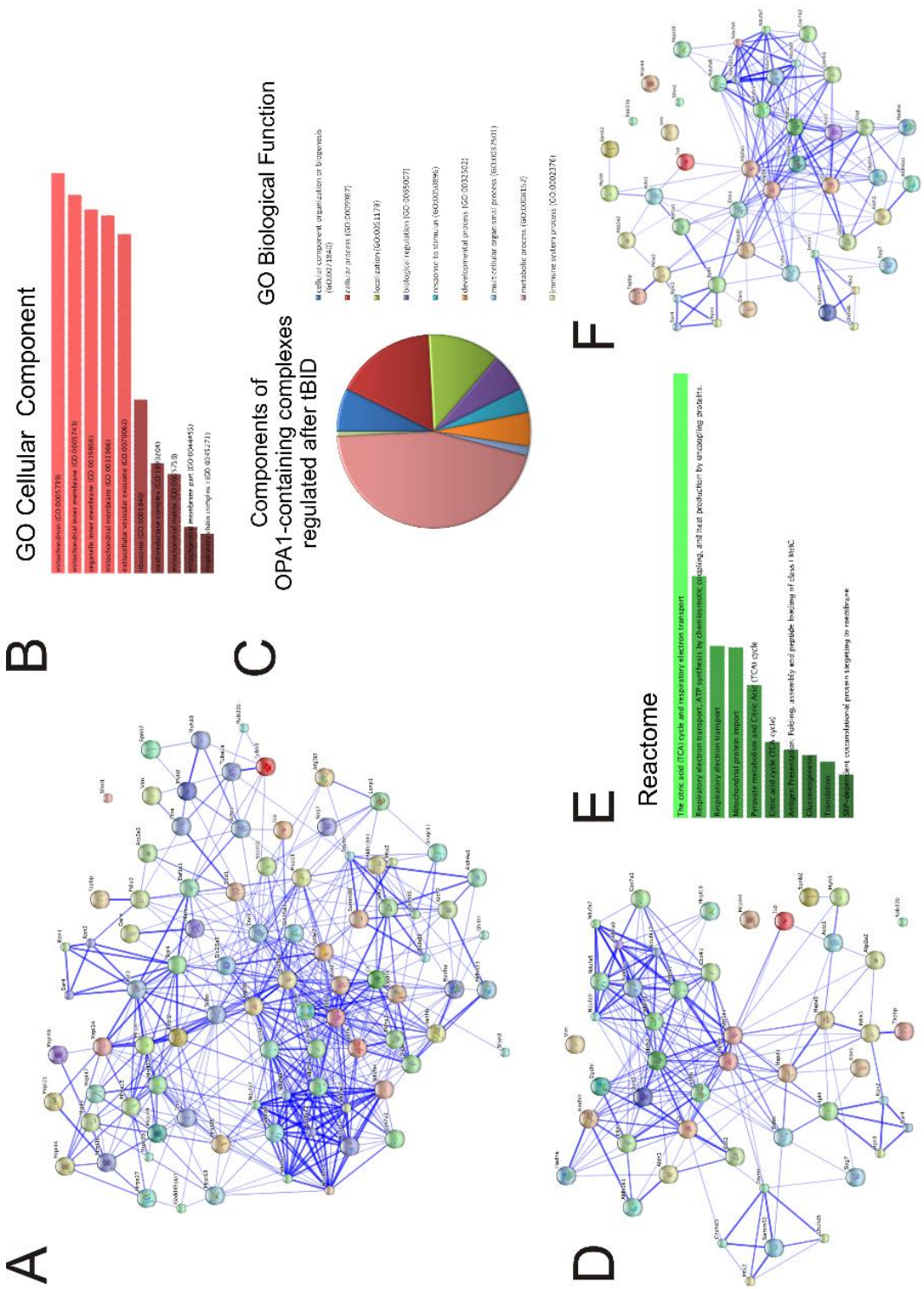
A
B
GO Cellular Component
C
Components of OPA1-containing complexes regulated after tBID
GO Biological Function
D
E
Reactome
F

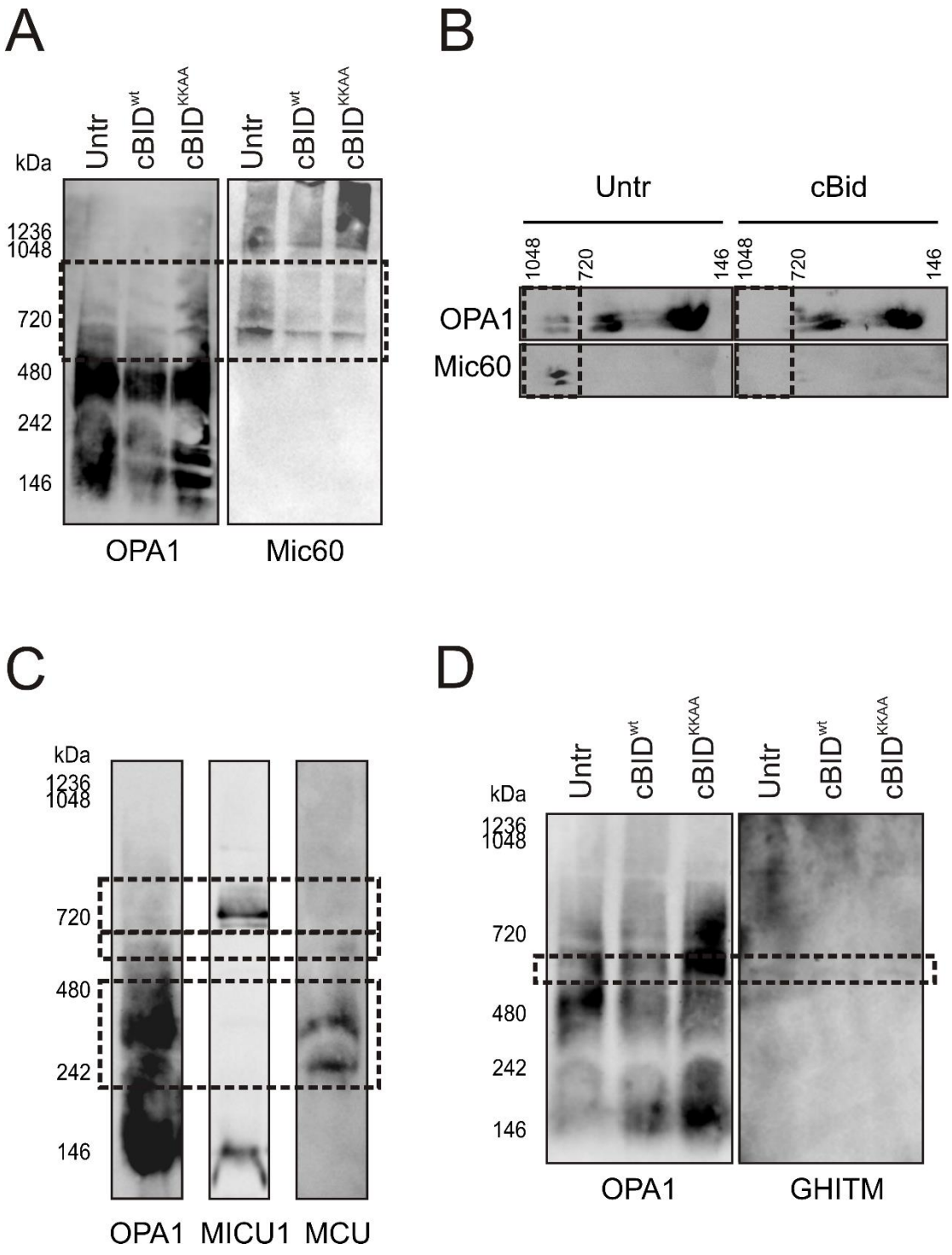
A
Untr
cBID^wt
cBID^KKAA
Untr
cBID^wt
cBID^KKAA
kDa
1236
1048
720
480
242
146
OPA1
Mic60
B
Untr
cBid
1048
720
146
1048
720
146
OPA1
Mic60
C
kDa
1236
1048
720
480
242
146
OPA1
MICU1
MCU
D
Untr
cBID^wt
cBID^KKAA
Untr
cBID^wt
cBID^KKAA
kDa
1236
1048
720
480
242
146
OPA1
GHITM

Figure 8

A molecular atlas of the Optic atrophy 1 (Opa1) high molecular weight complexes targeted during apoptotic cristae remodeling

Maria Eugenia Soriano[1*], Christina Glytsou[1,2*], Enrique Calvo[3], Jesùs Vazquez[3], Jose Antonio Enriquez[3], and Luca Scorrano[1,2]

Supplemental online material

Legends of Supplementary figures

Supplementary Figure S1. Functional network of candidate OPA1 partners in mouse liver mitochondria

STRING network of all the identified proteins retrieved in OPA1-containing complexes in liver mitochondria. Each network node represents a protein and the thickness of the edges represents the confidence of a predicted functional association.

Supplementary Figure S2. Functional network of candidate OPA1 partners in mouse liver mitochondria that are reduced upon apoptosis stimulation

STRING network of the identified proteins present in OPA1-containing complexes in liver mitochondria, which decrease after $cBID^{wt}$ treatment. Each network node represents a protein and the thickness of the edges represents the confidence of a predicted functional association.

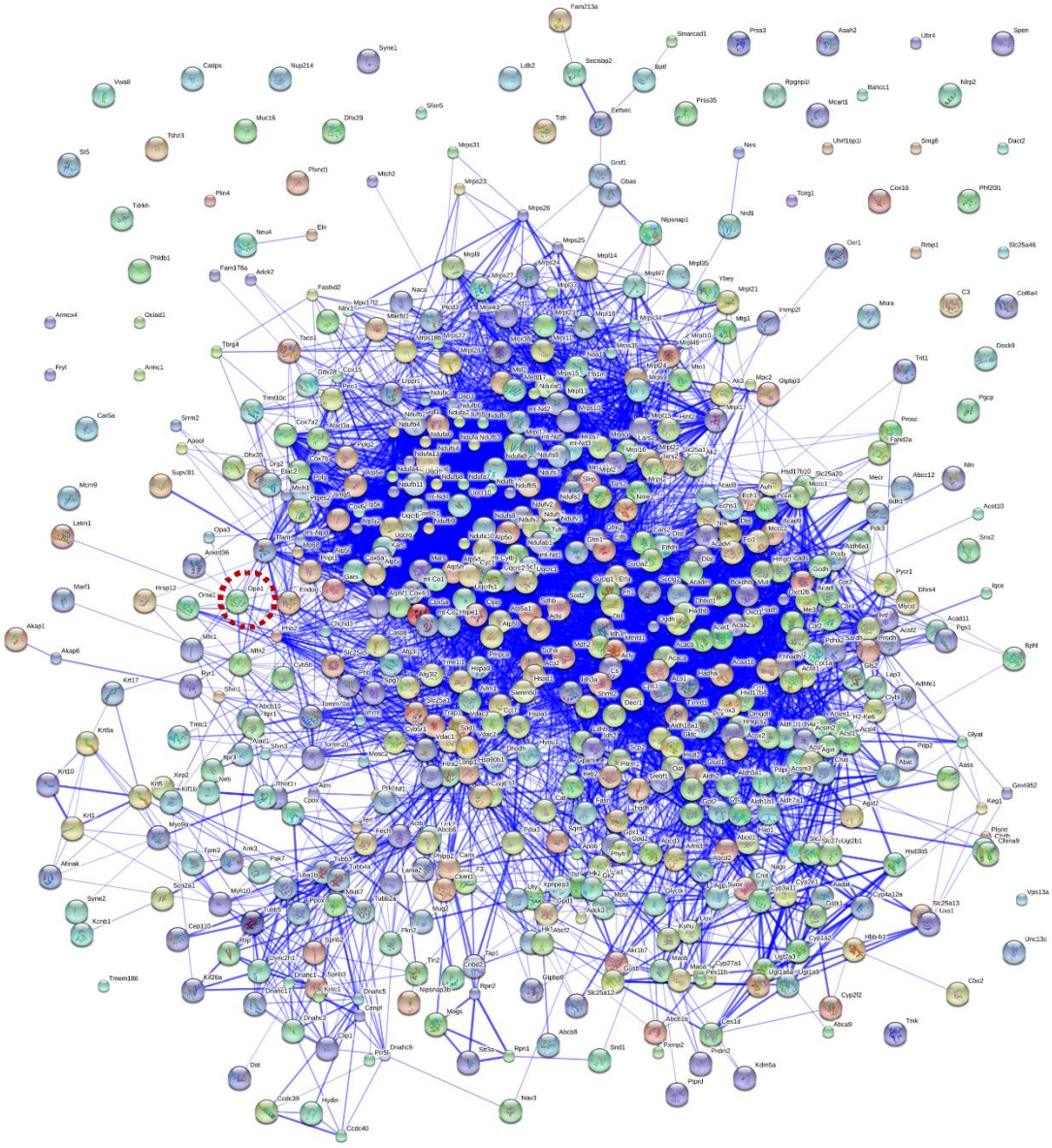

Suppl. Figure S1

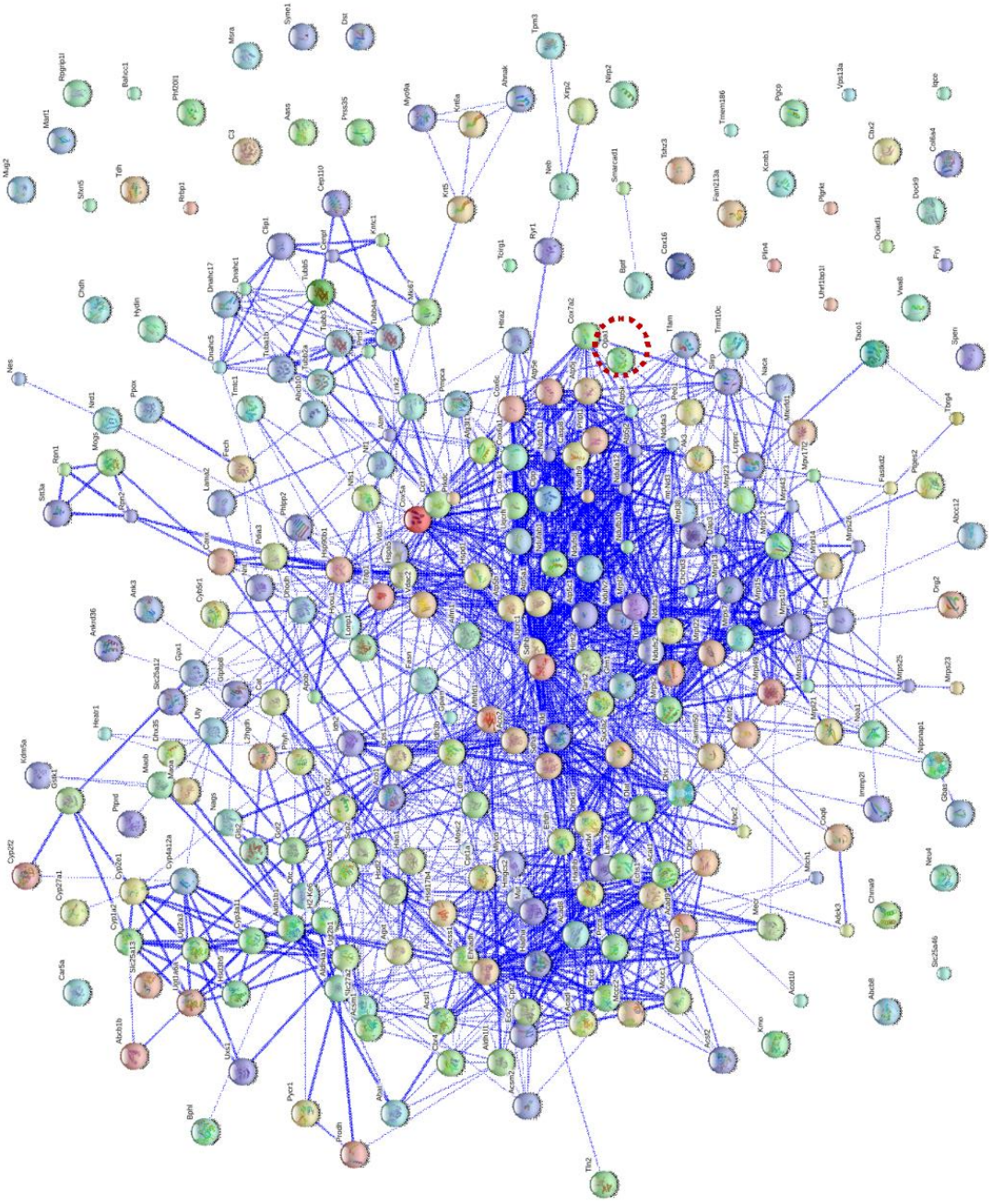

Suppl. Figure S2

Legends of Supplementary tables

Supplemental table 1 (Related to Fig. 4). List of all the OPA1 interaction partners identified in liver.

Supplemental table 2 (Related to Fig. 4). List of OPA1 interaction partners that decrease after cBID^{wt} treatment in Spot 1.

Supplemental table 3 (Related to Fig. 4). List of OPA1 interaction partners that decrease after cBID^{wt} treatment in Spot 2.

Supplemental table 4 (Related to Fig. 4). List of OPA1 interaction partners that decrease after cBID^{wt} treatment in Spot 4.

Supplemental table 5 (Related to Fig. 4). List of OPA1 interaction partners that decrease after cBID^{wt} treatment in Spot 5.

Supplemental table 6 (Related to Fig. 4). List of OPA1 interaction partners that decrease after cBID^{wt} treatment in Spot 7.

Supplemental table 7 (Related to Fig. 4). List of OPA1 interaction partners that decrease after cBID^{wt} treatment in Spot 10.

Supplemental table 8 (Related to Fig. 4). List of OPA1 interaction partners that decrease after cBID^{wt} treatment in Spot 11.

Supplemental table 9 (Related to Fig. 7). List of OPA1 interaction partners in heart. Pearson: Pearson correlation coefficiency (r). High Pearson correlation coefficiency indicates high confidence of association with OPA1.

Supplemental table 10 (Related to Fig. 7). List of OPA1 interaction partners in heart that decrease after cBID^{wt} treatment. Only fold change < 0.8 is considered to be significant.

Supplemental table 11 (Related to Fig. 7). List of OPA1 interaction partners in heart that decrease during cristae remodeling.

Supplemental table 12 (Related to Fig. 8). List of OPA1 interaction partners in MAFs that decrease after cBID^{wt} treatment (identified by SILAC). Only fold change > 1.2 is considered to be significant.

Supplemental table 13 (Related to Fig. 8). List of OPA1 interaction partners in MAFs that decrease in the various spots during cristae remodeling (identified by SILAC). Only fold change > 1.2 is considered to be significant.

Suppl. Table 1. Consolidate list of all the unique proteins identified in the different spots (581 proteins)			
A/A	**ACCESSION NUMBER**	**PROTEIN NAME**	**GENE**
1	Q9WVM8	Kynurenine/alpha-aminoadipate aminotransferase, mitochondrial	Aadat
2	Q99K67	Alpha-aminoadipic semialdehyde synthase, mitochondrial	Aass
3	P61922	4-aminobutyrate aminotransferase, mitochondrial	Abat
4	P41233	ATP-binding cassette sub-family A member 1	Abca1
5	Q8K449	ATP-binding cassette sub-family A member 9	Abca9
6	Q9JI39	ATP-binding cassette sub-family B member 10, mitochondrial	Abcb10
7	P06795	Multidrug resistance protein 1B	Abcb1b
8	Q9DC29	ATP-binding cassette sub-family B member 6, mitochondrial	Abcb6
9	Q9CXJ4	ATP-binding cassette sub-family B member 8, mitochondrial	Abcb8
10	Q80WJ6	Multidrug resistance-associated protein 9 (ATP-binding cassette sub-family C member 12)	Abcc12
11	P48410	ATP-binding cassette sub-family D member 1 (Adrenoleukodystrophy protein) (ALDP)	Abcd1
12	Q61285	ATP-binding cassette sub-family D member 2 (Adrenoleukodystrophy-related protein)	Abcd2
13	P55096	ATP-binding cassette sub-family D member 3 (68 kDa peroxisomal membrane protein) (PMP68)	Abcd3
14	Q99LE6	ATP-binding cassette sub-family F member 2	Abcf2
15	Q8VCH0	3-ketoacyl-CoA thiolase B, peroxisomal	Acaa1b
16	Q8BWT1	3-ketoacyl-CoA thiolase, mitochondrial	Acaa2
17	Q5SWU9	Acetyl-CoA carboxylase 1 (ACC1)	Acaca
18	E9Q4Z2	Acetyl-CoA carboxylase 2	Acacb
19	Q80XL6	Acyl-CoA dehydrogenase family member 11 (ACAD-11)	Acad11
20	Q9D7B6	Isobutyryl-CoA dehydrogenase, mitochondrial	Acad8
21	Q8JZN5	Acyl-CoA dehydrogenase family member 9, mitochondrial (ACAD-9)	Acad9
22	P51174	Long-chain specific acyl-CoA dehydrogenase, mitochondrial (LCAD)	Acadl
23	P45952	Medium-chain specific acyl-CoA dehydrogenase, mitochondrial (MCAD)	Acadm
24	Q07417	Short-chain specific acyl-CoA dehydrogenase, mitochondrial (SCAD)	Acads
25	P50544	Very long-chain specific acyl-CoA dehydrogenase, mitochondrial	Acadvl
26	Q8QZT1	Acetyl-CoA acetyltransferase, mitochondrial	Acat1
27	Q91V92	ATP-citrate synthase	Acly
28	P28271	Cytoplasmic aconitate hydratase (Aconitase)	Aco1
29	Q99KI0	Aconitate hydratase, mitochondrial (Aconitase)	Aco2
30	Q32MW3	Acyl-coenzyme A thioesterase 10, mitochondrial (Acyl-CoA thioesterase 10)	Acot10
31	Q9QXD1	Peroxisomal acyl-coenzyme A oxidase 2	Acox2
32	Q9EPL9	Peroxisomal acyl-coenzyme A oxidase 3	Acox3
33	Q8VCW8	Acyl-CoA synthetase family member 2, mitochondrial	Acsf2
34	P41216	Long-chain-fatty-acid--CoA ligase 1	Acsl1
35	Q9QUJ7	Long-chain-fatty-acid--CoA ligase 4	Acsl4
36	Q8JZR0	Long-chain-fatty-acid--CoA ligase 5	Acsl5
37	Q91VA0	Acyl-coenzyme A synthetase ACSM1, mitochondrial	Acsm1
38	Q8K0L3	Acyl-coenzyme A synthetase ACSM2, mitochondrial	Acsm2

39	Q3UNX5	Acyl-coenzyme A synthetase ACSM3, mitochondrial	Acsm3
40	Q99NB1	acetyl-CoA synthetase 2-like	Acss1
41	Q99NB1	Acetyl-coenzyme A synthetase 2-like, mitochondrial	Acss1
42	P60710	Actin, cytoplasmic 1 (Beta-actin)	Actb
43	Q6NSR3	Uncharacterized aarF domain-containing protein kinase 2	Adck2
44	Q60936	Atypical kinase ADCK3, mitochondrial	Adck3
45	Q8R0N6	Hydroxyacid-oxoacid transhydrogenase, mitochondrial (HOT)	Adhfe1
46	P54822	Adenylosuccinate lyase (ASL)	Adsl
47	Q920A7	AFG3-like protein 1	Afg3l1
48	Q8JZQ2	AFG3-like protein 2	Afg3l2
49	Q9D1E8	1-acyl-sn-glycerol-3-phosphate acyltransferase epsilon	Agpat5
50	O35423	Serine--pyruvate aminotransferase, mitochondrial (SPT)	Agxt
51	H7BWY3	Alanine--glyoxylate aminotransferase 2, mitochondrial	Agxt2
52	A0JLR7	Ahnak protein (Fragment)	Ahnak
53	B1AU25	Apoptosis-inducing factor 1, mitochondrial	Aifm1
54	Q3TY86	Apoptosis-inducing factor 3	Aifm3
55	Q9WTP6	Adenylate kinase 2, mitochondrial (AK 2)	Ak2
56	Q9WTP7	GTP:AMP phosphotransferase AK3, mitochondrial	Ak3
57	O08715	A-kinase anchor protein 1, mitochondrial	Akap1
58	Q2VEB3	A-kinase anchoring protein beta	Akap6
59	P21300	Aldose reductase-related protein 1	Akr1b7
60	Q9Z110	Delta-1-pyrroline-5-carboxylate synthase (P5CS)	Aldh18a1
61	Q9CZS1	Aldehyde dehydrogenase X, mitochondrial	Aldh1b1
62	Q8R0Y6	Cytosolic 10-formyltetrahydrofolate dehydrogenase (10-FTHFDH) (FDH)	Aldh1l1
63	Q544B1	Aldehyde dehydrogenase 2, mitochondrial, isoform CRA_b (Aldehyde dehydrogenase, mitochondrial)	Aldh2
64	P47738	Aldehyde dehydrogenase, mitochondrial	Aldh2
65	Q8CHT0	Delta-1-pyrroline-5-carboxylate dehydrogenase, mitochondrial (P5C dehydrogenase)	Aldh4a1
66	Q8BWF0	Succinate-semialdehyde dehydrogenase, mitochondrial	Aldh5a1
67	Q9EQ20	Methylmalonate-semialdehyde dehydrogenase [acylating], mitochondrial (MMSDH)	Aldh6a1
68	Q9DBF1	Alpha-aminoadipic semialdehyde dehydrogenase (Alpha-AASA dehydrogenase)	Aldh7a1
69	Q9WUD7	Brain-specific ankyrin-G (Fragment)	ANK3
70	Q5QNR3	Protein Ankrd36 (Fragment)	Ankrd36
71	E9Q414	Apolipoprotein B-100 (Apo B-100) [Cleaved into: Apolipoprotein B-48 (Apo B-48)]	Apob
72	Q78IK4	MICOS complex subunit Mic27 (Apolipoprotein O-like) (Protein FAM121A)	Apool
73	Q9D7A8	Armadillo repeat-containing protein 1	Armc1
74	A2VCS7	Armcx4 protein (Fragment)	Armcx4
75	Q9JHE3	Neutral ceramidase (N-CDase) (NCDase)	Asah2
76	Q9D5T0	ATPase family AAA domain-containing protein 1	Atad1
77	Q925I1	ATPase family AAA domain-containing protein 3 (AAA-ATPase TOB3)	Atad3
78	Q62388	Serine-protein kinase ATM (	Atm
79	Q03265	ATP synthase subunit alpha, mitochondrial	Atp5a1
80	P56480	ATP synthase subunit beta, mitochondrial	Atp5b

81	Q91VR2	ATP synthase subunit gamma, mitochondrial (F-ATPase gamma subunit)	Atp5c1
82	Q9D3D9	ATP synthase subunit delta, mitochondrial (F-ATPase delta subunit)	Atp5d
83	P56382	ATP synthase subunit epsilon, mitochondrial (ATPase subunit epsilon)	Atp5e
84	Q5I0W0	ATP synthase F(0) complex subunit B1, mitochondrial	Atp5f1
85	Q9CQQ7	ATP synthase F(0) complex subunit B1, mitochondrial (ATP synthase subunit b)	Atp5f1
86	Q9DCX2	ATP synthase subunit d, mitochondrial (ATPase subunit d)	Atp5h
87	Q06185	ATP synthase subunit e, mitochondrial (ATPase subunit e)	Atp5i
88	P97450	ATP synthase-coupling factor 6, mitochondrial (ATPase subunit F6)	Atp5j
89	P56135	ATP synthase subunit f, mitochondrial	Atp5j2
90	Q9CPQ8	ATP synthase subunit g, mitochondrial (ATPase subunit g)	Atp5l
91	Q9DB20	ATP synthase subunit O, mitochondrial (Oligomycin sensitivity conferral protein) (OSCP)	Atp5o
92	Q9JLZ3	Methylglutaconyl-CoA hydratase, mitochondrial	Auh
93	Q3UHR0	BAH and coiled-coil domain-containing protein 1	Bahcc1
94	Q6P3A8	2-oxoisovalerate dehydrogenase subunit beta, mitochondrial	Bckdhb
95	Q80XN0	D-beta-hydroxybutyrate dehydrogenase, mitochondrial (BDH)	Bdh1
96	Q8R164	Valacyclovir hydrolase (VACVase) (Valacyclovirase)	Bphl
97	A2A655	Protein Bptf	Bptf
98	P01027	Complement C3 (HSE-MSF)	C3
99	P23589	Carbonic anhydrase 5A, mitochondrial	Ca5a
100	Q80TJ1	Calcium-dependent secretion activator 1 (Calcium-dependent activator protein for secretion 1)	Cadps
101	P35564	Calnexin	Canx
102	O89110	Caspase-8 (CASP-8)	Casp8
103	P24270	Catalase	Cat
104	Q91VT4	Carbonyl reductase family member 4	Cbr4
105	Q9D5Y1	Coiled-coil domain-containing protein 39	Ccdc39
106	Q8BI79	Coiled-coil domain-containing protein 40 (Protein links)	Ccdc40
107	P80313	T-complex protein 1 subunit eta (TCP-1-eta) (CCT-eta)	Cct7
108	Q155P7	LEK1	Cenpf
109	Q8VCT4	Carboxylesterase 1D (Carboxylesterase 3)	Ces1d
110	Q8C6S9	Cilia- and flagella-associated protein 54	Cfap54
111	Q8BQV2	Choline O-acetyltransferase (Choline acetyltransferase)	Chat
112	Q9CRB9	MICOS complex subunit Mic19 (Coiled-coil-helix-coiled-coil-helix domain-containing protein 3)	Chchd3
113	Q8BJ64	Choline dehydrogenase, mitochondrial (CDH)	Chdh
114	Q8K3J4	Nicotinic acetylcholine receptor alpha 9 subunit (Fragment)	Chrna9
115	P30275	Creatine kinase U-type, mitochondrial	Ckmt1
116	Q922J3	CAP-Gly domain-containing linker protein 1	Clip1
117	O88696	ATP-dependent Clp protease proteolytic subunit, mitochondrial	Clpp
118	Q8R4N0	Citrate lyase subunit beta-like protein, mitochondrial (Citrate lyase beta-like) (Beta-methylmalate synthase)	Clybl
119	Q9D5U8	Cyclic nucleotide-binding domain-containing protein 2	Cnbd2
120	A2AL36	Centriolin (Centrosomal protein 1)	Cntrl
121	A2AX52	Collagen alpha-4(VI) chain	Col6a4
122	Q8R1S0	Ubiquinone biosynthesis monooxygenase COQ6, mitochondrial	Coq6

123	Q8BJ03	Cytochrome c oxidase assembly protein COX15 homolog	Cox15
124	Q9CR63	Cytochrome c oxidase assembly protein COX16 homolog, mitochondrial	Cox16
125	P19783	Cytochrome c oxidase subunit 4 isoform 1, mitochondrial (Cytochrome c oxidase polypeptide IV)	Cox4i1
126	P12787	Cytochrome c oxidase subunit 5A, mitochondrial (Cytochrome c oxidase polypeptide Va)	Cox5a
127	P43024	Cytochrome c oxidase subunit 6A1, mitochondrial (Cytochrome c oxidase polypeptide VIa-liver)	Cox6a1
128	P56391	Cytochrome c oxidase subunit 6B1 (Cytochrome c oxidase subunit VIb isoform 1)	Cox6b1
129	Q9CPQ1	Cytochrome c oxidase subunit 6C (Cytochrome c oxidase polypeptide VIc)	Cox6c
130	P48771	Cytochrome c oxidase subunit 7A2, mitochondrial	Cox7a2
131	P56393	Cytochrome c oxidase subunit 7B, mitochondrial (Cytochrome c oxidase polypeptide VIIb)	Cox7b
132	P36552	Oxygen-dependent coproporphyrinogen-III oxidase, mitochondrial (COX) (Coprogen oxidase)	Cpox
133	Q9WVJ3	Carboxypeptidase Q	Cpq
134	Q8C196	Carbamoyl-phosphate synthase [ammonia], mitochondrial	Cps1
135	P97742	Carnitine O-palmitoyltransferase 1, liver isoform (CPT1-L)	Cpt1a
136	P52825	Carnitine O-palmitoyltransferase 2, mitochondrial	Cpt2
137	Q9DC50	Peroxisomal carnitine O-octanoyltransferase (COT)	Crot
138	Q9CZU6	Citrate synthase, mitochondrial	Cs
139	Q9CQX2	Cytochrome b5 type B (Cytochrome b5 outer mitochondrial membrane isoform)	Cyb5b
140	Q9DB73	NADH-cytochrome b5 reductase 1 (b5R.1)	Cyb5r1
141	Q9D0M3	Cytochrome c1, heme protein, mitochondrial	Cyc1
142	P00186	Cytochrome P450 1A2	Cyp1a2
143	Q9DBG1	Sterol 26-hydroxylase, mitochondrial	Cyp27a1
144	Q05421	Cytochrome P450 2E1	Cyp2e1
145	P33267	Cytochrome P450 2F2	Cyp2f2
146	Q64459	Cytochrome P450 3A11	Cyp3a11
147	Q91WL5	Cytochrome P450 4A12A	Cyp4a12a
148	Q7TN08	Dapper homolog 2 (mDpr2)	Dact2
149	Q9ER88	28S ribosomal protein S29, mitochondrial (Death-associated protein 3) (DAP-3)	Dap3
150	P53395	Lipoamide acyltransferase component of branched-chain alpha-keto acid dehydrogenase complex, mitochondrial	Dbt
151	Q9CWT6	Probable ATP-dependent RNA helicase DDX28	Ddx28
152	Q9CQ62	2,4-dienoyl-CoA reductase, mitochondrial	Decr1
153	O35435	Dihydroorotate dehydrogenase (quinone), mitochondrial (DHOdehase)	Dhodh
154	Q99LB2	Dehydrogenase/reductase SDR family member 4)	Dhrs4
155	A2ATU0	Probable 2-oxoglutarate dehydrogenase E1 component DHKTD1, mitochondrial	Dhtkd1
156	Q6PGC1	ATP-dependent RNA helicase Dhx29	Dhx29
157	Q8K1G9	DEAH (Asp-Glu-Ala-His) box polypeptide 35	Dhx35
158	Q8BMF4	Dihydrolipoyllysine-residue acetyltransferase component of pyruvate dehydrogenase complex, mitochondrial	Dlat
159	O08749	Dihydrolipoyl dehydrogenase, mitochondrial	Dld
160	Q9D2G2	Dihydrolipoyllysine-residue succinyltransferase component of 2-oxoglutarate dehydrogenase complex, mitochondrial	Dlst

161	Q9DBT9	Dimethylglycine dehydrogenase, mitochondrial	Dmgdh
162	O08828	Axonemal dynein heavy chain (Fragment)	Dnah1
163	O08825	Dynein heavy chain (Fragment)	Dnah10
164	Q69Z23	Dynein heavy chain 17, axonemal	Dnah17
165	Q8BW94	Dynein heavy chain 3, axonemal	Dnah3
166	Q8VHE6	Dynein heavy chain 5, axonemal	Dnah5
167	Q5SX07	Protein Dnah9	Dnah9
168	Q8BIK4	Dedicator of cytokinesis protein 9 (Cdc42 guanine nucleotide exchange factor zizimin-1)	Dock9
169	Q9QXB9	Developmentally-regulated GTP-binding protein 2 (DRG-2)	Drg2
170	Q91ZU6	Dystonin (Bullous pemphigoid antigen 1)	Dst
171	Q45VK7	Cytoplasmic dynein 2 heavy chain 1	Dync2h1
172	Q9CXJ1	Probable glutamate--tRNA ligase, mitochondrial	Ears2
173	O35459	Delta(3,5)-Delta(2,4)-dienoyl-CoA isomerase, mitochondrial	Ech1
174	Q8BH95	Enoyl-CoA hydratase, mitochondrial	Echs1
175	P42125	Enoyl-CoA delta isomerase 1, mitochondrial	Eci1
176	Q9WUR2	Enoyl-CoA delta isomerase 2, mitochondrial	Eci2
177	Q9JHW4	Selenocysteine-specific elongation factor (Elongation factor sec)	Eefsec
178	Q9DBM2	Peroxisomal bifunctional enzyme (PBE)	Ehhadh
179	Q80Y81	Zinc phosphodiesterase ELAC protein 2	Elac2
180	P54320	Elastin (Tropoelastin)	Eln
181	O08600	Endonuclease G, mitochondrial (Endo G)	Endog
182	Q8R0W0	Epiplakin	Eppk1
183	Q99LC5	Electron transfer flavoprotein subunit alpha, mitochondrial (Alpha-ETF)	Etfa
184	Q9DCW4	Electron transfer flavoprotein subunit beta (Beta-ETF)	Etfb
185	Q921G7	Electron transfer flavoprotein-ubiquinone oxidoreductase, mitochondrial (ETF-QO) (ETF-ubiquinone oxidoreductase)	Etfdh
186	Q3TC72	Fumarylacetoacetate hydrolase domain-containing protein 2A	Fahd2
187	Q6P9P0	Protein FAM178A	Fam178a
188	Q9CYH2	Redox-regulatory protein FAM213A	Fam213a
189	P19096	Fatty acid synthase	Fasn
190	Q922E6	FAST kinase domain-containing protein 2	Fastkd2
191	Q544X6	ferrochelatase	Fech
192	P97807	Fumarate hydratase, mitochondrial (Fumarase)	Fh
193	Q8CHD0	MKIAA0826 protein (Fragment)	Fryl
194	Q9CZD3	Glycine--tRNA ligase	Gars
195	Q99JT1	Glutamyl-tRNA(Gln) amidotransferase subunit B, mitochondrial (Glu-AdT subunit B)	Gatb
196	Q7TMG8	Glioblastoma amplified sequence	Gbas
197	Q60759	Glutaryl-CoA dehydrogenase, mitochondrial (GCD)	Gcdh
198	Q8K0D5	Elongation factor G, mitochondrial (EF-Gmt)	Gfm1
199	Q8R2Q4	Ribosome-releasing factor 2, mitochondrial (RRF2mt)	Gfm2
200	Q9WU65	Glycerol kinase 2 (GK 2) (Glycerokinase 2)	Gk2
201	Q91W43	Glycine dehydrogenase (decarboxylating), mitochondrial	Gldc
202	Q571F8	Glutaminase liver isoform, mitochondrial (GLS)	Gls2
203	P26443	Glutamate dehydrogenase 1, mitochondrial (GDH 1)	Glud1
204	Q91XE0	Glycine N-acyltransferase (EC 2.3.1.13)	Glyat

205	Q8QZY2	Glycerate kinase	Glyctk
206	Q3TNU4	Putative uncharacterized protein ENSP00000382790 homolog	Gm3414
207	Q5FW57	Glycine N-acyltransferase-like protein	Gm4952
208	P05202	Aspartate aminotransferase, mitochondrial (mAspAT)	Got2
209	Q61586	Glycerol-3-phosphate acyltransferase 1, mitochondrial (GPAT-1)	Gpam
210	P13707	Glycerol-3-phosphate dehydrogenase [NAD(+)], cytoplasmic (GPD-C)	Gpd1
211	A2AQR0	Glycerol-3-phosphate dehydrogenase	Gpd2
212	Q64521	Glycerol-3-phosphate dehydrogenase, mitochondrial (GPD-M)	Gpd2
213	Q8BGT5	Alanine aminotransferase 2 (ALT2)	Gpt2
214	P11352	Glutathione peroxidase 1 (GPx-1)	Gpx1
215	Q8C5Q4	G-rich sequence factor 1 (GRSF-1)	Grsf1
216	P47791	Glutathione reductase, mitochondrial (GR)	Gsr
217	Q9DCM2	Glutathione S-transferase kappa 1	Gstk1
218	Q923K4	tRNA modification GTPase GTPBP3, mitochondrial (GTP-binding protein 3)	Gtpbp3
219	Q9CY28	GTP-binding protein 8	Gtpbp8
220	Q8C3X4	Translation factor Guf1, mitochondrial	Guf1
221	P12265	Beta-glucuronidase	Gusb
222	Q61425	Hydroxyacyl-coenzyme A dehydrogenase, mitochondrial (HCDH)	Hadh
223	Q8BMS1	Trifunctional enzyme subunit alpha, mitochondrial (TP-alpha)	Hadha
224	Q99JY0	Trifunctional enzyme subunit beta, mitochondrial (TP-beta)	Hadhb
225	Q9WU19	Hydroxyacid oxidase 1 (HAOX1)	Hao1
226	A8DUK7	Beta-globin	Hbbt1
227	Q9D0S9	Histidine triad nucleotide-binding protein 2, mitochondrial (HINT-2)	Hint2
228	Q6GQU1	Hexokinase	Hk1
229	O08528	Hexokinase-2	Hk2
230	P38060	Hydroxymethylglutaryl-CoA lyase, mitochondrial (HL) (HMG-CoA lyase)	Hmgcl
231	P54869	Hydroxymethylglutaryl-CoA synthase, mitochondrial (HMG-CoA synthase)	Hmgcs2
232	P52760	Ribonuclease UK114	Hrsp12
233	Q99N15	17beta-hydroxysteroid dehydrogenase type 10/short chain L-3-hydroxyacyl-CoA dehydrogenase	Hsd17b10
234	P51660	Peroxisomal multifunctional enzyme type 2 (MFE-2)	Hsd17b4
235	P50171	Estradiol 17-beta-dehydrogenase 8	Hsd17b8
236	Q61694	3 beta-hydroxysteroid dehydrogenase type 5	Hsd3b5
237	Q2TPA8	Hydroxysteroid dehydrogenase-like protein 2	Hsdl2
238	P08113	Endoplasmin (94 kDa glucose-regulated protein) (GRP-94)	Hsp90b1
239	P20029	78 kDa glucose-regulated protein (GRP-78)	Hspa5
240	P38647	Stress-70 protein, mitochondrial (75 kDa glucose-regulated protein)	Hspa9
241	P63038	60 kDa heat shock protein, mitochondrial (60 kDa chaperonin)	Hspd1
242	Q64433	10 kDa heat shock protein, mitochondrial (Hsp10)	Hspe1
243	Q9JIY5	Serine protease HTRA2, mitochondrial	Htra2
244	Q80W93	Hydrocephalus-inducing protein (Protein Hy-3)	Hydin
245	Q9JKR6	Hypoxia up-regulated protein 1 (GRP-170)	Hyou1
246	Q8BIJ6	Isoleucine--tRNA ligase, mitochondrial	Iars2
247	Q8R035	Peptidyl-tRNA hydrolase ICT1, mitochondrial	Ict1
248	P54071	Isocitrate dehydrogenase [NADP], mitochondrial (IDH)	Idh2

249	Q9D6R2	Isocitrate dehydrogenase [NAD] subunit alpha, mitochondrial	Idh3a
250	Q91VA7	Isocitrate dehydrogenase [NAD] subunit, mitochondrial	Idh3b
251	Q91VA7	Isocitrate dehydrogenase [NAD] subunit, mitochondrial	Idh3b
252	Q8BPT6	Mitochondrial inner membrane protease subunit 2	Immp2l
253	Q8CAQ8	MICOS complex subunit Mic60 (Mitochondrial inner membrane protein) (Mitofilin)	Immt
254	Q6PCQ0	IQ domain-containing protein E	Iqce
255	Q811J3	Iron-responsive element-binding protein 2 (IRE-BP 2)	Ireb2
256	P11881	Inositol 1,4,5-trisphosphate receptor type 1 (IP3 receptor isoform 1)	Itpr1
257	P70227	Inositol 1,4,5-trisphosphate receptor type 3 (IP3 receptor isoform 3)	Itpr3
258	Q9JHI5	Isovaleryl-CoA dehydrogenase, mitochondrial (IVD)	Ivd
259	Q99MN1	Lysine--tRNA ligase	Kars
260	Q03717	Potassium voltage-gated channel subfamily B member 1 (Voltage-gated potassium channel subunit Kv2.1)	Kcnb1
261	Q3UXZ9	Lysine-specific demethylase 5A	Kdm5a
262	Q9DCY0	Glycine N-acyltransferase-like protein Keg1	Keg1
263	Q60575	Kinesin-like protein KIF1B	Kif1b
264	Q52KG5	Kinesin-like protein KIF26A	Kif26a
265	Q91WN4	Kynurenine 3-monooxygenase	Kmo
266	Q8C3Y4	Kinetochore-associated protein 1	Kntc1
267	P04104	Keratin, type II cytoskeletal 1 (67 kDa cytokeratin)	Krt1
268	P02535	Keratin, type I cytoskeletal 10 (56 kDa cytokeratin)	Krt10
269	Q9QWL7	Keratin, type I cytoskeletal 17 (Cytokeratin-17)	Krt17
270	Q922U2	Keratin, type II cytoskeletal 5 (Cytokeratin-5)	Krt5
271	P50446	Keratin, type II cytoskeletal 6A (Cytokeratin-6A)	Krt6a
272	Q9CXF0	Kynureninase (EC 3.7.1.3) (L-kynurenine hydrolase)	Kynu
273	Q91YP0	L-2-hydroxyglutarate dehydrogenase, mitochondrial	L2hgdh
274	Q60675	Laminin subunit alpha-2 (Laminin M chain)	Lama2
275	Q9CPY7	Cytosol aminopeptidase	Lap3
276	Q8VDC0	Probable leucine--tRNA ligase, mitochondrial	Lars2
277	O55203	LIM domain-binding protein 2 (LDB-2) (Carboxyl-terminal LIM domain-binding protein 1)	Ldb2
278	P16125	L-lactate dehydrogenase B chain (LDH-B)	Ldhb
279	Q9Z2I0	LETM1 and EF-hand domain-containing protein 1, mitochondrial	Letm1
280	Q8CGK3	Lon protease homolog, mitochondrial	Lonp1
281	Q6PB66	Leucine-rich PPR motif-containing protein, mitochondrial	Lrpprc
282	Q5S006	Leucine-rich repeat serine/threonine-protein kinase 2	Lrrk2
283	Q64133	Amine oxidase [flavin-containing] A	Maoa
284	Q8BW75	Amine oxidase [flavin-containing] B	Maob
285	Q922Q1	Mitochondrial amidoxime reducing component 2 (mARC2)	Marc2
286	Q8BJ34	Meiosis arrest female protein 1 (Limkain-b1)	Marf1
287	Q68FL6	Methionine--tRNA ligase, cytoplasmic	Mars
288	Q99MR8	Methylcrotonoyl-CoA carboxylase subunit alpha, mitochondrial (MCCase subunit alpha)	Mccc1
289	Q3ULD5	Methylcrotonoyl-CoA carboxylase beta chain, mitochondrial (MCCase subunit beta)	Mccc2
290	Q8VI13	MCG117370, isoform CRA_b (MCG5438)	mCG_117370

291	Q2KHI9	DNA helicase MCM9	Mcm9
292	P08249	Malate dehydrogenase, mitochondrial	Mdh2
293	Q8BMF3	NADP-dependent malic enzyme, mitochondrial (NADP-ME)	Me3
294	Q9DCS3	Trans-2-enoyl-CoA reductase, mitochondrial	Mecr
295	Q3U2U7	Methyltransferase-like protein 17, mitochondrial	Mettl17
296	Q811U4	Mitofusin-1	Mfn1
297	Q80U63	Mitofusin-2	Mfn2
298	Q61769	Ki-67 protein	Mki67
299	Q99J39	Malonyl-CoA decarboxylase, mitochondrial (MCD)	Mlycd
300	Q80UM7	Mannosyl-oligosaccharide glucosidase	Mogs
301	P56379	6.8 kDa mitochondrial proteolipid	Mp68
302	Q9D023	Mitochondrial pyruvate carrier 2 (Brain protein 44)	Mpc2
303	Q3UW66	Sulfurtransferase	Mpst
304	Q8VIK2	Mpv17-like protein 2	Mpv17l2
305	Q3TBW2	39S ribosomal protein L10, mitochondrial (L10mt) (MRP-L10)	Mrpl10
306	Q9CQF0	39S ribosomal protein L11, mitochondrial (L11mt) (MRP-L11)	Mrpl11
307	Q9DB15	39S ribosomal protein L12, mitochondrial (L12mt) (MRP-L12)	Mrpl12
308	Q9D1P0	39S ribosomal protein L13, mitochondrial (L13mt) (MRP-L13)	Mrpl13
309	Q9D1I6	39S ribosomal protein L14, mitochondrial (L14mt) (MRP-L14)	Mrpl14
310	Q9CPR5	39S ribosomal protein L15, mitochondrial (L15mt) (MRP-L15)	Mrpl15
311	Q99N93	39S ribosomal protein L16, mitochondrial (L16mt) (MRP-L16)	Mrpl16
312	Q9D8P4	39S ribosomal protein L17, mitochondrial (L17mt) (MRP-L17)	Mrpl17
313	Q9CQL5	39S ribosomal protein L18, mitochondrial (L18mt) (MRP-L18)	Mrpl18
314	Q9D773	39S ribosomal protein L2, mitochondrial (L2mt) (MRP-L2)	Mrpl2
315	Q9D1N9	39S ribosomal protein L21, mitochondrial (L21mt) (MRP-L21)	Mrpl21
316	Q8BU88	39S ribosomal protein L22, mitochondrial (L22mt) (MRP-L22)	Mrpl22
317	O35972	39S ribosomal protein L23, mitochondrial (L23mt) (MRP-L23)	Mrpl23
318	Q9CQ06	39S ribosomal protein L24, mitochondrial (L24mt) (MRP-L24)	Mrpl24
319	Q9D1B9	39S ribosomal protein L28, mitochondrial (L28mt) (MRP-L28)	Mrpl28
320	Q9CQL6	39S ribosomal protein L35, mitochondrial (L35mt) (MRP-L35)	Mrpl35
321	Q921S7	39S ribosomal protein L37, mitochondrial (L37mt) (MRP-L37)	Mrpl37
322	Q8K2M0	39S ribosomal protein L38, mitochondrial (L38mt) (MRP-L38)	Mrpl38
323	Q9JKF7	39S ribosomal protein L39, mitochondrial (L39mt) (MRP-L39)	Mrpl39
324	Q5RL20	39S ribosomal protein L43, mitochondrial	Mrpl43
325	Q8K2Y7	39S ribosomal protein L47, mitochondrial (L47mt) (MRP-L47)	Mrpl47
326	Q9CQ40	39S ribosomal protein L49, mitochondrial (L49mt) (MRP-L49)	Mrpl49
327	Q99N94	39S ribosomal protein L9, mitochondrial (L9mt) (MRP-L9)	Mrpl9
328	E9QJS0	28S ribosomal protein S10, mitochondrial	Mrps10
329	Q9DC71	28S ribosomal protein S15, mitochondrial (MRP-S15) (S15mt)	Mrps15
330	Q99N84	28S ribosomal protein S18b, mitochondrial (MRP-S18-b)	Mrps18b
331	Q924T2	28S ribosomal protein S2, mitochondrial (MRP-S2) (S2mt)	Mrps2
332	Q9CXW2	28S ribosomal protein S22, mitochondrial (MRP-S22) (S22mt)	Mrps22
333	Q8VE22	28S ribosomal protein S23, mitochondrial (MRP-S23) (S23mt)	Mrps23
334	Q9CQV5	28S ribosomal protein S24, mitochondrial (MRP-S24) (S24mt)	Mrps24
335	Q9D125	28S ribosomal protein S25, mitochondrial (MRP-S25) (S25mt)	Mrps25
336	Q80ZS3	28S ribosomal protein S26, mitochondrial (MRP-S26) (S26mt)	Mrps26

337	Q8BK72	28S ribosomal protein S27, mitochondrial (MRP-S27) (S27mt)	Mrps27
338	Q61733	28S ribosomal protein S31, mitochondrial (MRP-S31) (S31mt)	Mrps31
339	Q9JIK9	28S ribosomal protein S34, mitochondrial (MRP-S34) (S34mt)	Mrps34
340	Q8BJZ4	28S ribosomal protein S35, mitochondrial (MRP-S35) (S35mt)	Mrps35
341	Q99N87	28S ribosomal protein S5, mitochondrial (MRP-S5) (S5mt)	Mrps5
342	Q80X85	28S ribosomal protein S7, mitochondrial (MRP-S7) (S7mt)	Mrps7
343	Q9D7N3	28S ribosomal protein S9, mitochondrial (MRP-S9) (S9mt)	Mrps9
344	Q9D6Y7	Mitochondrial peptide methionine sulfoxide reductase	Msra
345	P00848	ATP synthase subunit a (F-ATPase protein 6)	Mtatp6
346	P03930	ATP synthase protein 8 (A6L) (F-ATPase subunit 8)	Mtatp8
347	Q791T5	Mitochondrial carrier homolog 1 (Mitochondrial carrier-like protein 1)	Mtch1
348	Q791V5	Mitochondrial carrier homolog 2	Mtch2
349	P00397	Cytochrome c oxidase subunit 1	Mtco1
350	P00405	Cytochrome c oxidase subunit 2 (Cytochrome c oxidase polypeptide II)	Mtco2
351	P00158	Cytochrome b (Complex III subunit 3) (Complex III subunit III)	Mt-Cyb
352	Q8R3J4	Transcription termination factor 3, mitochondrial (Mitochondrial transcription termination factor 3) (	Mterf3
353	Q8R2R6	Mitochondrial ribosome-associated GTPase 1 (GTP-binding protein 7) (Mitochondrial GTPase 1)	Mtg1
354	Q922D8	C-1-tetrahydrofolate synthase, cytoplasmic (C1-THF synthase)	Mthfd1
355	Q91YJ5	Translation initiation factor IF-2, mitochondrial (IF-2(Mt))	Mtif2
356	P03888	NADH-ubiquinone oxidoreductase chain 1	Mtnd1
357	P03893	NADH-ubiquinone oxidoreductase chain 2	Mtnd2
358	P03899	NADH-ubiquinone oxidoreductase chain 3	Mtnd3
359	P03911	NADH-ubiquinone oxidoreductase chain 4	Mtnd4
360	Q9MD82	NADH-ubiquinone oxidoreductase chain 5	mt-Nd5
361	Q923Z3	Protein MTO1 homolog, mitochondrial	Mto1
362	Q9D1H1	MCG4778 (Protein Muc16)	Muc16
363	P28666	Murinoglobulin-2 (MuG2)	Mug2
364	P16332	Methylmalonyl-CoA mutase, mitochondrial (MCM)	Mut
365	Q5SV64	Myosin-10	Myh10
366	Q8C170	Unconventional myosin-IXa (Unconventional myosin-9a)	Myo9a
367	P70670	Nascent polypeptide-associated complex subunit alpha, muscle-specific form	Naca
368	Q8R4H7	N-acetylglutamate synthase, mitochondrial	Nags
369	Q80TN7	Neuron navigator 3 (Pore membrane and/or filament-interacting-like protein 1)	Nav3
370	Q99LC3	NADH dehydrogenase [ubiquinone] 1 alpha subcomplex subunit 10, mitochondrial (Complex I-42kD)	Ndufa10
371	Q7TMF3	NADH dehydrogenase [ubiquinone] 1 alpha subcomplex subunit 12 (Complex I-B17.2)	Ndufa12
372	Q9ERS2	NADH dehydrogenase [ubiquinone] 1 alpha subcomplex subunit 13 (Cell death regulatory protein GRIM-19) (Complex I-B16.6)	Ndufa13
373	Q9CQ75	NADH dehydrogenase [ubiquinone] 1 alpha subcomplex subunit 2 (Complex I-B8)	Ndufa2
374	Q9CQ91	NADH dehydrogenase [ubiquinone] 1 alpha subcomplex subunit 3 (Complex I-B9)	Ndufa3
375	Q62425	Cytochrome c oxidase subunit NDUFA4	Ndufa4
376	Q9CQZ5	NADH dehydrogenase [ubiquinone] 1 alpha subcomplex subunit 6 (Complex I-B14) (	Ndufa6

377	Q9Z1P6	NADH dehydrogenase [ubiquinone] 1 alpha subcomplex subunit 7 (Complex I-B14.5a)	Ndufa7
378	Q9DCJ5	NADH dehydrogenase [ubiquinone] 1 alpha subcomplex subunit 8 (Complex I-19kD)	Ndufa8
379	Q9DC69	NADH dehydrogenase [ubiquinone] 1 alpha subcomplex subunit 9, mitochondrial (Complex I-39kD)	Ndufa9
380	Q9CR21	Acyl carrier protein, mitochondrial (ACP) (CI-SDAP) (NADH-ubiquinone oxidoreductase 9.6 kDa subunit)	Ndufab1
381	Q9CWX2	Complex I intermediate-associated protein 30, mitochondrial (NADH dehydrogenase [ubiquinone] 1 alpha subcomplex assembly factor 1)	Ndufaf1
382	Q9DCS9	NADH dehydrogenase [ubiquinone] 1 beta subcomplex subunit 10 (Complex I-PDSW)	Ndufb10
383	O09111	NADH dehydrogenase [ubiquinone] 1 beta subcomplex subunit 11, mitochondrial (Complex I-ESSS)	Ndufb11
384	Q9CPU2	NADH dehydrogenase [ubiquinone] 1 beta subcomplex subunit 2, mitochondrial (Complex I-AGGG)	Ndufb2
385	Q9CQZ6	NADH dehydrogenase [ubiquinone] 1 beta subcomplex subunit 3 (Complex I-B12)	Ndufb3
386	Q9CQC7	NADH dehydrogenase [ubiquinone] 1 beta subcomplex subunit 4 (Complex I-B15)	Ndufb4
387	Q9CQH3	NADH dehydrogenase [ubiquinone] 1 beta subcomplex subunit 5, mitochondrial (Complex I-SGDH)	Ndufb5
388	Q3UIU2	NADH dehydrogenase [ubiquinone] 1 beta subcomplex subunit 6 (Complex I-B17)	Ndufb6
389	Q9CR61	NADH dehydrogenase [ubiquinone] 1 beta subcomplex subunit 7 (Complex I-B18)	Ndufb7
390	Q9D6J5	NADH dehydrogenase [ubiquinone] 1 beta subcomplex subunit 8, mitochondrial (Complex I-ASHI)	Ndufb8
391	Q9CQJ8	NADH dehydrogenase [ubiquinone] 1 beta subcomplex subunit 9 (Complex I-B22)	Ndufb9
392	Q91VD9	NADH-ubiquinone oxidoreductase 75 kDa subunit, mitochondrial	Ndufs1
393	Q91WD5	NADH dehydrogenase [ubiquinone] iron-sulfur protein 2, mitochondrial	Ndufs2
394	Q9DCT2	NADH dehydrogenase [ubiquinone] iron-sulfur protein 3, mitochondrial	Ndufs3
395	Q9CXZ1	NADH dehydrogenase [ubiquinone] iron-sulfur protein 4, mitochondrial (Complex I-18 kDa)	Ndufs4
396	Q99LY9	NADH dehydrogenase [ubiquinone] iron-sulfur protein 5 (Complex I-15 kDa)	Ndufs5
397	Q9DC70	NADH dehydrogenase [ubiquinone] iron-sulfur protein 7, mitochondrial	Ndufs7
398	Q8K3J1	NADH dehydrogenase [ubiquinone] iron-sulfur protein 8, mitochondrial	Ndufs8
399	Q91YT0	NADH dehydrogenase [ubiquinone] flavoprotein 1, mitochondrial	Ndufv1
400	Q9D6J6	NADH dehydrogenase [ubiquinone] flavoprotein 2, mitochondrial	Ndufv2
401	A2AQA9	Protein Neb	Neb
402	Q6P5H2	Nestin	Nes
403	Q8BZL1	Sialidase-4 (EC 3.2.1.18) (N-acetyl-alpha-neuraminidase 4) (Neuraminidase 4)	Neu4
404	Q04690	Neurofibromin (Neurofibromatosis-related protein NF-1)	Nf1
405	Q9Z1J3	Cysteine desulfurase, mitochondrial (m-Nfs1)	Nfs1
406	O55125	Protein NipSnap homolog 1 (NipSnap1)	Nipsnap1
407	Q9CQE1	Protein NipSnap homolog 3B (NipSnap3B)	Nipsnap3b
408	Q91YP2	Neurolysin, mitochondrial	Nln
409	Q4PLS0	NACHT (Protein Nlrp2)	Nlrp2
410	Q3TL44	NLR family member X1	Nlrx1
411	Q01768	Nucleoside diphosphate kinase B (NDK B)	Nme2
412	Q8C1W8	nicotinamide nucleotide transhydrogenase	Nnt

413	Q9JJG9	Nitric oxide-associated protein 1	Noa1
414	Q8BHG1	Nardilysin	Nrd1
415	Q80U93	Nuclear pore complex protein Nup214	Nup214
416	P29758	Ornithine aminotransferase, mitochondrial	Oat
417	Q9CRD0	OCIA domain-containing protein 1	Ociad1
418	Q60597	2-oxoglutarate dehydrogenase, mitochondrial	Ogdh
419	Q9D8H7	Metalloendopeptidase OMA1, mitochondrial	Oma1
420	P58281	Dynamin-like 120 kDa protein, mitochondrial	Opa1
421	Q505D7	Optic atrophy 3 protein homolog	Opa3
422	P11725	Ornithine carbamoyltransferase, mitochondrial	Otc
423	Q9D0K2	Succinyl-CoA:3-ketoacid coenzyme A transferase 1, mitochondrial	Oxct1
424	Q9ESL0	Succinyl-CoA:3-ketoacid coenzyme A transferase 2B, mitochondrial	Oxct2b
425	Q4KMM3	Oxidation resistance protein 1 (Protein C7)	Oxr1
426	Q8C015	Serine/threonine-protein kinase PAK 7	Pak7
427	Q05920	Pyruvate carboxylase, mitochondrial	Pc
428	Q91ZA3	Propionyl-CoA carboxylase alpha chain, mitochondrial (PCCase subunit alpha)	Pcca
429	Q99MN9	Propionyl-CoA carboxylase beta chain, mitochondrial (PCCase subunit beta)	Pccb
430	Q8BP54	Putative uncharacterized protein (Fragment)	Pcx
431	P35487	Pyruvate dehydrogenase E1 component subunit alpha, testis-specific form, mitochondrial	Pdha2
432	P27773	Protein disulfide-isomerase A3 (	Pdia3
433	Q4FJR4	Pdk3 protein (Pyruvate dehydrogenase kinase, isoenzyme 3, isoform CRA_b)	Pdk3
434	Q504M2	MCG53395 (Protein Pdp2) (Uncharacterized protein)	Pdp2
435	Q7TSQ8	Pyruvate dehydrogenase phosphatase regulatory subunit, mitochondrial (PDPr)	Pdpr
436	Q8CIW5	Twinkle protein, mitochondrial	Peo1
437	Q9Z210	Peroxisomal membrane protein 11B (Peroxin-11B)	Pex11b
438	Q8BHF7	CDP-diacylglycerol--glycerol-3-phosphate 3-phosphatidyltransferase, mitochondrial	Pgs1
439	P67778	Prohibitin (B-cell receptor-associated protein 32)	Phb
440	O35129	Prohibitin-2 (B-cell receptor-associated protein BAP37)	Phb2
441	Q8CCJ9	PHD finger protein 20-like protein 1	Phf20l1
442	Q6PDH0	Pleckstrin homology-like domain family B member 1 (Protein LL5-alpha)	Phldb1
443	Q8BXA7	PH domain leucine-rich repeat-containing protein phosphatase 2	Phlpp2
444	O35386	Phytanoyl-CoA dioxygenase, peroxisomal	Phyh
445	Q8K411	Presequence protease, mitochondrial	Pitrm1
446	Q8BWW9	Serine/threonine-protein kinase N2	Pkn2
447	Q9D3P8	Plasminogen receptor (KT) (Plg-R(KT))	Plgrkt
448	O88492	Perilipin-4 (Adipocyte protein S3-12)	Plin4
449	Q3UH93	Plexin-D1	Plxnd1
450	Q9DC61	Mitochondrial-processing peptidase subunit alpha	Pmpca
451	Q8K1R3	Polyribonucleotide nucleotidyltransferase 1, mitochondrial	Pnpt1
452	Q75WC0	DNA polymerase subunit gamma-1 (Polymerase (DNA directed), gamma)	Polg
453	Q9QZM2	DNA polymerase subunit gamma-2, mitochondrial	Polg2
454	P51175	Protoporphyrinogen oxidase (PPO)	Ppox

455	A2A7B5	Protein Prdm2	Prdm2
456	P97313	DNA-dependent protein kinase catalytic subunit (DNA-PK catalytic subunit)	Prkdc
457	Q9WU79	Proline dehydrogenase 1, mitochondrial	Prodh
458	Q9Z2Y8	Proline synthase co-transcribed bacterial homolog protein	Prosc
459	A2AVJ5	Proline-rich protein 5-like (Protein observed with Rictor-2) (Protor-2)	Prr5l
460	B9EJ35	Protease, serine, 3	Prss3
461	Q8C0F9	Inactive serine protease 35	Prss35
462	Q14C51	Pentatricopeptide repeat domain-containing protein 3, mitochondrial (28S ribosomal protein S39, mitochondrial)	Ptcd3
463	Q8BWM0	Prostaglandin E synthase 2	Ptges2
464	B9EJA3	Protein tyrosine phosphatase, receptor type, D (Receptor-type tyrosine-protein phosphatase delta)	Ptprd
465	P42925	Peroxisomal membrane protein 2 (22 kDa peroxisomal membrane protein)	Pxmp2
466	Q922W5	Pyrroline-5-carboxylate reductase 1, mitochondrial	Pycr1
467	Q8BG51	Mitochondrial Rho GTPase 1 (MIRO-1)	Rhot1
468	Q5ND29	Rab-interacting lysosomal protein	Rilp
469	Q8CG73	Protein fantom (Nephrocystin-8) (RPGR-interacting protein 1-like protein)	Rpgrip1l
470	Q91YQ5	Dolichyl-diphosphooligosaccharide--protein glycosyltransferase subunit 1	Rpn1
471	Q9DBG6	Dolichyl-diphosphooligosaccharide--protein glycosyltransferase subunit 2	Rpn2
472	Q99PL5	Ribosome-binding protein 1 (Ribosome receptor protein) (RRp) (mRRp)	Rrbp1
473	P70272	Skeletal muscle ryanodine receptor (Fragment)	ryr1
474	Q8BGH2	Sorting and assembly machinery component 50 homolog	Samm50
475	Q99LB7	Sarcosine dehydrogenase, mitochondrial (SarDH)	Sardh
476	A9JQD3	Protein Scn2a1 (Sodium channel Nav1.2) (Fragment)	Scn2a1
477	P32020	Non-specific lipid-transfer protein (NSL-TP)	Scp2
478	Q8K2B3	Succinate dehydrogenase [ubiquinone] flavoprotein subunit, mitochondrial	Sdha
479	Q9CQA3	Succinate dehydrogenase [ubiquinone] iron-sulfur subunit, mitochondrial	Sdhb
480	Q3TGQ4	Putative uncharacterized protein	Secisbp2
481	Q99JR1	Sideroflexin-1	Sfxn1
482	Q91V61	Sideroflexin-3	Sfxn3
483	Q925N0	Sideroflexin-5	Sfxn5
484	Q9CZN7	Serine hydroxymethyltransferase	Shmt2
485	Q8JZU2	Tricarboxylate transport protein, mitochondrial (Citrate transport protein)	Slc25a1
486	Q9CR62	Mitochondrial 2-oxoglutarate/malate carrier protein (OGCP)	Slc25a11
487	Q8BH59	Calcium-binding mitochondrial carrier protein Aralar1 (Mitochondrial aspartate glutamate carrier 1)	Slc25a12
488	Q9QXX4	Calcium-binding mitochondrial carrier protein Aralar2 (Citrin) (Mitochondrial aspartate glutamate carrier 2)	Slc25a13
489	Q9Z2Z6	Mitochondrial carnitine/acylcarnitine carrier protein (Carnitine/acylcarnitine translocase) (CAC)	Slc25a20
490	Q9CQS4	Solute carrier family 25 member 46	Slc25a46
491	P51881	ADP/ATP translocase 2 (ADP,ATP carrier protein 2)	Slc25a5
492	Q5HZI9	Solute carrier family 25 member 51 (Mitochondrial carrier triple repeat protein 1)	Slc25a51

493	O35488	Very long-chain acyl-CoA synthetase (VLACS) (VLCS)	Slc27a2
494	Q4LDG0	Bile acyl-CoA synthetase (BACS)	Slc27a5
495	Q9D8T7	SRA stem-loop-interacting RNA-binding protein, mitochondrial	Slirp
496	Q04692	SWI/SNF-related matrix-associated actin-dependent regulator of chromatin subfamily A containing DEAD/H box 1	Smarcad1
497	Q8VE18	Protein SMG8 (Protein smg-8 homolog)	Smg8
498	Q78PY7	Staphylococcal nuclease domain-containing protein 1 (100 kDa coactivator) (p100 co-activator)	Snd1
499	Q9CWK8	Sorting nexin-2	Snx2
500	P08228	Superoxide dismutase [Cu-Zn]	Sod1
501	P09671	Superoxide dismutase [Mn], mitochondrial	Sod2
502	Q62504	Msx2-interacting protein (SMART/HDAC1-associated repressor protein)	Spen
503	Q3ULF4	Paraplegin	Spg7
504	Q62261	Spectrin beta chain, non-erythrocytic 1 (Beta-II spectrin)	Sptbn1
505	O35411	Beta III spectrin (Fragment)	Sptbn2
506	Q9R112	Sulfide:quinone oxidoreductase, mitochondrial (SQOR)	Sqrdl
507	Q9WTN3	Sterol regulatory element-binding protein 1 (SREBP-1)	Srebf1
508	Q8BTI8	Serine/arginine repetitive matrix protein 2	Srrm2
509	Q924W7	Suppression of tumorigenicity 5 protein (DENN domain-containing protein 2B)	St5
510	P46978	Dolichyl-diphosphooligosaccharide--protein glycosyltransferase subunit STT3A (Oligosaccharyl transferase subunit STT3A)	Stt3a
511	Q9Z2I9	Succinyl-CoA ligase [ADP-forming] subunit beta, mitochondrial	Sucla2
512	Q9WUM5	Succinyl-CoA ligase [ADP/GDP-forming] subunit alpha, mitochondrial	Suclg1
513	Q9Z2I8	Succinyl-CoA ligase [GDP-forming] subunit beta, mitochondrial	Suclg2
514	Q8R086	Sulfite oxidase, mitochondrial	Suox
515	Q80YD1	ATP-dependent RNA helicase SUPV3L1, mitochondrial	Supv3l1
516	Q7TQH5	Synaptic nuclear envelope 1	Syne1
517	Q6ZWQ0	Nesprin-2 (Nuclear envelope spectrin repeat protein 2)	Syne2
518	Q8K0Z7	Translational activator of cytochrome c oxidase 1 (Coiled-coil domain-containing protein 44)	Taco1
519	P21958	Antigen peptide transporter 1 (APT1)	Tap1
520	Q3UQ84	Threonine--tRNA ligase, mitochondrial	Tars2
521	Q91YM4	Protein TBRG4 (Transforming growth factor beta regulator 4)	Tbrg4
522	Q9JHF5	V-type proton ATPase subunit a	Tcirg1
523	Q8K3F7	L-threonine 3-dehydrogenase, mitochondrial	Tdh
524	Q80VL1	Tudor and KH domain-containing protein (Tudor domain-containing protein 2)	Tdrkh
525	O70372	Telomerase reverse transcriptase	Tert
526	Q921I1	Serotransferrin (Transferrin)	Tf
527	P40630	Transcription factor A, mitochondrial (mtTFA)	Tfam
528	Q8JZM0	Dimethyladenosine transferase 1, mitochondrial	Tfb1m
529	B2RY15	Tln2 protein	Tln2
530	Q9CR76	Transmembrane protein 186	Tmem186
531	Q3UV71	Transmembrane and TPR repeat-containing protein 1	Tmtc1
532	P83510	Traf2 and NCK-interacting protein kinase	Tnik
533	Q9DCC8	Mitochondrial import receptor subunit TOM20 homolog	Tomm20
534	Q9CZW5	Mitochondrial import receptor subunit TOM70	Tomm70a

535	P21107	Tropomyosin alpha-3 chain	Tpm3
536	Q9CQN1	Heat shock protein 75 kDa, mitochondrial (HSP 75)	Trap1
537	Q80UN9	tRNA dimethylallyltransferase, mitochondrial	Trit1
538	Q3UFY8	Mitochondrial ribonuclease P protein 1 (Mitochondrial RNase P protein 1)	Trmt10c
539	Q8CGV9	Teashirt homolog 3 (Zinc finger protein 537)	Tshz3
540	P52196	Thiosulfate sulfurtransferase (Rhodanese)	Tst
541	A2ASS6	Titin (Connectin)	Ttn
542	P05213	Tubulin alpha-1B chain (Alpha-tubulin 2)	Tuba1b
543	Q7TMM9	Tubulin beta-2A chain	Tubb2a
544	Q9ERD7	Tubulin beta-3 chain	Tubb3
545	Q9D6F9	Tubulin beta-4A chain (Tubulin beta-4 chain)	Tubb4a
546	P99024	Tubulin beta-5 chain	Tubb5
547	Q8BFR5	Elongation factor Tu, mitochondrial	Tufm
548	Q9JMH6	Thioredoxin reductase 1, cytoplasmic (TR)	Txnrd1
549	A2AN08	E3 ubiquitin-protein ligase UBR4	Ubr4
550	Q64435	UDP-glucuronosyltransferase 1-6 (UDPGT 1-6)	Ugt1a6
551	Q62452	UDP-glucuronosyltransferase 1-9 (UDPGT 1-9)	Ugt1a9
552	Q8BWQ1	UDP-glucuronosyltransferase 2A3 (UDPGT 2A3)	Ugt2a3
553	Q8R084	UDP-glucuronosyltransferase	Ugt2b1
554	A2RSJ4	UHRF1-binding protein 1-like	Uhrf1bp1l
555	Q8K0T7	Protein unc-13 homolog C (Munc13-3)	Unc13c
556	P25688	Uricase	Uox
557	Q8R1I1	Cytochrome b-c1 complex subunit 9 (Complex III subunit 9)	Uqcr10
558	Q9CQB4	Cytochrome b-c1 complex subunit 7	Uqcrb
559	Q9CZ13	Cytochrome b-c1 complex subunit 1, mitochondrial (Complex III subunit 1)	Uqcrc1
560	Q9DB77	Cytochrome b-c1 complex subunit 2, mitochondrial (Complex III subunit 2)	Uqcrc2
561	Q9CR68	Cytochrome b-c1 complex subunit Rieske, mitochondrial	Uqcrfs1
562	P99028	Cytochrome b-c1 complex subunit 6, mitochondrial (Complex III subunit 6)	Uqcrh
563	Q9CQ69	Cytochrome b-c1 complex subunit 8 (Complex III subunit 8)	Uqcrq
564	Q78IK2	Up-regulated during skeletal muscle growth protein 5 (Diabetes-associated protein in insulin-sensitive tissues)	Usmg5
565	P79457	Histone demethylase UTY	Uty
566	Q91XL3	UDP-glucuronic acid decarboxylase 1	Uxs1
567	Q60932	Voltage-dependent anion-selective channel protein 1 (VDAC-1)	Vdac1
568	Q60930	Voltage-dependent anion-selective channel protein 2 (VDAC-2)	Vdac2
569	Q60931	Voltage-dependent anion-selective channel protein 3 (VDAC-3)	Vdac3
570	Q5H8C4	Vacuolar protein sorting-associated protein 13A	Vps13a
571	Q8CC88	von Willebrand factor A domain-containing protein 8	Vwa8
572	Q4U4S6	Xin actin-binding repeat-containing protein 2 (Beta-xin)	Xirp2
573	B7ZMP1	Probable Xaa-Pro aminopeptidase 3 (X-Pro aminopeptidase 3)	Xpnpep3
574	Q8CAV0	Putative ribonuclease	Ybey
575	O88967	ATP-dependent zinc metalloprotease YME1L1	Yme1l1
576	Q3V2K0	MCG48927 (Uncharacterized protein)	1700071K01Rik

Suppl. Table 2. Mitochondrial proteins that decrease after cBID treatment – Spot 1				
A/A	**ACCESSION NUMBER**	**PROTEIN NAME**	**GENE**	**FOLD CHANGE**
1	Q9ER88	28S ribosomal protein S29, mitochondrial (MRP-S29)	Dap3	0
2	Q91WD5	NADH dehydrogenase [ubiquinone] iron-sulfur protein 2, mitochondrial	Ndufs2	0
3	Q921G7	Electron transfer flavoprotein-ubiquinone oxidoreductase, mitochondrial (ETF-QO)	Etfdh	0
4	Q8K1R3	Polyribonucleotide nucleotidyltransferase 1, mitochondrial	Pnpt1	0
5	Q91YP0	L-2-hydroxyglutarate dehydrogenase, mitochondrial	L2hgdh	0
6	Q8C1W8	nicotinamide nucleotide transhydrogenase	Nnt	0
7	P16125	L-lactate dehydrogenase B chain (LDH-B)	Ldhb	0
8	P97450	ATP synthase-coupling factor 6, mitochondrial (ATPase subunit F6)	Atp5j	0
9	P06795	Multidrug resistance protein 1B	Abcb1b	0
10	Q920A7	AFG3-like protein 1	Afg3l1	0
11	Q9D773	39S ribosomal protein L2, mitochondrial (L2mt) (MRP-L2)	Mrpl2	0
12	Q64133	Amine oxidase [flavin-containing] A	Maoa	0
13	Q544X6	ferrochelatase	Fech	0
14	Q9DBG1	Sterol 26-hydroxylase, mitochondrial	Cyp27a1	0
15	Q8VCW8	Acyl-CoA synthetase family member 2, mitochondrial	Acsf2	0
16	Q3UFY8	Mitochondrial ribonuclease P protein 1	Trmt10c	0
17	Q60936	Atypical kinase ADCK3, mitochondrial	Adck3	0
18	P50544	Very long-chain specific acyl-CoA dehydrogenase, mitochondrial	Acadvl	0.27
19	Q9DBM2	Peroxisomal bifunctional enzyme (PBE)	Ehhadh	0.33
20	Q8CHT0	Delta-1-pyrroline-5-carboxylate dehydrogenase, mitochondrial	Aldh4a1	0.42
22	Q6PB66	Leucine-rich PPR motif-containing protein, mitochondrial	Lrpprc	0.60
23	Q9QXX4	Calcium-binding mitochondrial carrier protein Aralar2 (Citrin)	Slc25a13	0.63
24	Q03265	ATP synthase subunit alpha, mitochondrial	Atp5a1	0.66
25	Q99KI0	Aconitate hydratase, mitochondrial (Aconitase)	Aco2	0.67
26	Q9Z2I9	Succinyl-CoA ligase [ADP-forming] subunit beta, mitochondrial	Sucla2	0.67
27	P55096	ATP-binding cassette sub-family D member 3	Abcd3	0.67
28	Q61694	3 beta-hydroxysteroid dehydrogenase type 5	Hsd3b5	0.67
29	Q922U2	Keratin, type II cytoskeletal 5	Krt5	0.71
30	Q8CGK3	Lon protease homolog, mitochondrial	Lonp1	0.71
31	P63038	60 kDa heat shock protein, mitochondrial	Hspd1	0.73
32	P51660	Peroxisomal multifunctional enzyme type 2	Hsd17b4	0.75
33	Q8QZT1	Acetyl-CoA acetyltransferase, mitochondrial	Acat1	0.78

Suppl. Table 3. Mitochondrial proteins that decrease after cBID treatment – Spot 2				
A/A	**ACCESSION NUMBER**	**PROTEIN NAME**	**GENE**	**FOLD CHANGE**
1	Q8VCH0	3-ketoacyl-CoA thiolase B, peroxisomal	Acaa1b	0
2	P61922	4-aminobutyrate aminotransferase, mitochondrial	Abat	0
3	Q6NSR3	Uncharacterized aarF domain-containing protein kinase 2	Adck2	0
4	Q07417	Short-chain specific acyl-CoA dehydrogenase, mitochondrial (SCAD)	Acads	0
5	P41216	Long-chain-fatty-acid--CoA ligase 1	Acsl1	0
6	P54822	Adenylosuccinate lyase (ASL)	Adsl	0
7	Q9D5T0	ATPase family AAA domain-containing protein 1	Atad1	0
8	Q8CHT0	Delta-1-pyrroline-5-carboxylate dehydrogenase, mitochondrial	Aldh4a1	0
9	Q9D5T0	ATPase family AAA domain-containing protein 1	Atad1	0
10	Q8K449	ATP-binding cassette sub-family A member 9	Abca9	0
11	P48410	ATP-binding cassette sub-family D member 1	Abcd1	0
12	Q9Z2Z6	Mitochondrial carnitine/acylcarnitine carrier protein	Slc25a20	0
13	P30275	Creatine kinase U-type, mitochondrial	Ckmt1	0
14	P56393	Cytochrome c oxidase subunit 7B, mitochondrial	Cox7b	0
15	Q3U2U7	Methyltransferase-like protein 17, mitochondrial	Mettl17	0
16	O08600	Endonuclease G, mitochondrial (Endo G)	Endog	0
17	P97807	Fumarate hydratase, mitochondrial (Fumarase)	Fh	0
18	Q8R2Q4	Ribosome-releasing factor 2, mitochondrial (RRF2mt)	Gfm2	0
19	Q8BGT5	Alanine aminotransferase 2 (ALT2)	Gpt2	0
20	Q9WU65	Glycerol kinase 2 (GK 2) (Glycerokinase 2)	Gk2	0
21	P38647	Stress-70 protein, mitochondrial (75 kDa glucose-regulated protein)	Hspa9	0
22	Q8CEW7	Putative uncharacterized protein	Zbed5	0
23	Q8BIJ6	Isoleucine--tRNA ligase, mitochondrial	Iars2	0
24	Q61425	Hydroxyacyl-coenzyme A dehydrogenase, mitochondrial (HCDH)	Hadh	0
25	Q9CQ69	Cytochrome b-c1 complex subunit 8 (Complex III subunit 8)	Uqcrq	0
26	Q8BMF3	NADP-dependent malic enzyme, mitochondrial (NADP-ME)	Me3	0
27	Q99JY0	Trifunctional enzyme subunit beta, mitochondrial (TP-beta)	Hadhb	0
28	Q5HZI9	Solute carrier family 25 member 51 (Mitochondrial carrier triple repeat protein 1)	Slc25a51	0
29	Q99N84	28S ribosomal protein S18b, mitochondrial	Mrps18b	0
30	Q9D7N3	28S ribosomal protein S9, mitochondrial (MRP-S9)	Mrps9	0
31	Q923Z3	Protein MTO1 homolog, mitochondrial	Mto1	0
32	Q505D7	Optic atrophy 3 protein homolog	Opa3	0
33	Q9WUR2	Enoyl-CoA delta isomerase 2, mitochondrial	Eci2	0
34	Q9Z0X1	Apoptosis-inducing factor 1, mitochondrial	Aifm1	0
35	Q9JIY5	Serine protease HTRA2, mitochondrial	Htra2	0
36	Q7TSQ8	Pyruvate dehydrogenase phosphatase regulatory subunit, mitochondrial	Pdpr	0

37	Q9CR62	Mitochondrial 2-oxoglutarate/malate carrier protein (OGCP)	Slc25a11	0
38	Q9QXX4	Calcium-binding mitochondrial carrier protein Aralar2 (Citrin)	Slc25a13	0
39	P52196	Thiosulfate sulfurtransferase	Tst	0
40	Q8JZM0	Dimethyladenosine transferase 1, mitochondrial	Tfb1m	0
41	B7ZMP1	Probable Xaa-Pro aminopeptidase 3 (X-Pro aminopeptidase 3)	Xpnpep3	0
42	Q91ZA3	Propionyl-CoA carboxylase alpha chain, mitochondrial (PCCase subunit alpha)	Pcca	0.21
43	P51660	Peroxisomal multifunctional enzyme type 2	Hsd17b4	0.33
44	Q9Z2I0	LETM1 and EF-hand domain-containing protein 1, mitochondrial	Letm1	0.33
45	Q91XE0	Glycine N-acyltransferase	Glyat	0.38
46	P54869	Hydroxymethylglutaryl-CoA synthase, mitochondrial	Hmgcs2	0.43
47	Q9DBM2	Peroxisomal bifunctional enzyme (PBE) (PBFE)	Ehhadh	0.43
48	Q8JZU2	Tricarboxylate transport protein, mitochondrial	Slc25a1	0.43
49	Q61694	3 beta-hydroxysteroid dehydrogenase type 5	Hsd3b5	0.50
50	Q6PB66	Leucine-rich PPR motif-containing protein, mitochondrial	Lrpprc	0.50
51	Q9CWX2	Complex I intermediate-associated protein 30, mitochondrial	Ndufaf1	0.50
52	Q99JR1	Sideroflexin-1	Sfxn1	0.50
53	Q60931	Voltage-dependent anion-selective channel protein 3 (VDAC-3)	Vdac3	0.50
54	Q9DCY0	Glycine N-acyltransferase-like protein Keg1	Keg1	0.57
55	Q80XN0	D-beta-hydroxybutyrate dehydrogenase, mitochondrial (BDH)	Bdh1	0.63
56	Q922Q1	Mitochondrial amidoxime reducing component 2 (mARC2)	Mosc2	0.63
57	Q3V2K0	MCG48927 (Uncharacterized protein)	1700071K01 Rik	0.67
58	P11725	Ornithine carbamoyltransferase, mitochondrial	Otc	0.67
59	Q99MN9	Propionyl-CoA carboxylase beta chain, mitochondrial	Pccb	0.67
60	Q9Z2I8	Succinyl-CoA ligase [GDP-forming] subunit beta, mitochondrial	Suclg2	0.67
61	Q8R1I1	Cytochrome b-c1 complex subunit 9 (Complex III subunit 9)	Uqcr10	0.67
62	Q9CR68	Cytochrome b-c1 complex subunit Rieske, mitochondrial	Uqcrfs1	0.67
63	O55125	Protein NipSnap homolog 1 (NipSnap1)	Nipsnap1	0.70
64	Q78IK2	Up-regulated during skeletal muscle growth protein 5 (Diabetes-associated protein in insulin-sensitive tissues)	Usmg5	0.75
65	Q5I0W0	ATP synthase F(0) complex subunit B1, mitochondrial	Atp5f1	0.77

Suppl. Table 4. Mitochondrial protein that decrease after cBID treatment - Spot 4

A/A	ACCESSION NUMBER	PROTEIN NAME	GENE	FOLD CHANGE
1	Q9D1I6	39S ribosomal protein L14, mitochondrial	Mrpl14	0
2	P54822	Adenylosuccinate lyase (ASL)	Adsl	0
3	Q9CXJ4	ATP-binding cassette sub-family B member 8, mitochondrial	Abcb8	0
4	Q922D8	C-1-tetrahydrofolate synthase, cytoplasmic (C1-THF synthase)	Mthfd1	0

5	Q8BWM0	Prostaglandin E synthase 2	Ptges2	0
6	Q7TSQ8	Pyruvate dehydrogenase phosphatase regulatory subunit, mitochondrial (PDPr)	Pdpr	0
7	P80313	T-complex protein 1 subunit eta (TCP-1-eta)	Cct7	0
8	Q8BH59	Calcium-binding mitochondrial carrier protein Aralar1	Slc25a12	0.20
9	Q61694	3 beta-hydroxysteroid dehydrogenase type 5	Hsd3b5	0.25
10	Q8R3J4	Transcription termination factor 3, mitochondrial (Mitochondrial transcription termination factor 3)	Mterf3	0.25
11	Q6PB66	Leucine-rich PPR motif-containing protein, mitochondrial	Lrpprc	0.29
12	Q8BJZ4	28S ribosomal protein S35, mitochondrial	Mrps35	0.33
13	Q8CIW5	Twinkle protein, mitochondrial	Peo1	0.33
14	P19783	Cytochrome c oxidase subunit 4 isoform 1, mitochondrial	Cox4i1	0.40
15	Q8BFR5	Elongation factor Tu, mitochondrial	Tufm	0.43
16	Q3TGQ4	Putative uncharacterized protein	Secisbp2	0.43
17	P05202	Aspartate aminotransferase, mitochondrial (mAspAT)	Got2	0.45
18	Q9D1N9	39S ribosomal protein L21, mitochondrial (L21mt)	Mrpl21	0.50
19	Q8JZN5	Acyl-CoA dehydrogenase family member 9, mitochondrial (ACAD-9)	Acad9	0.50
20	Q91VA0	Acyl-coenzyme A synthetase ACSM1, mitochondrial	Acsm1	0.50
21	Q80XN0	D-beta-hydroxybutyrate dehydrogenase, mitochondrial (BDH)	Bdh1	0.50
22	P97807	Fumarate hydratase, mitochondrial (Fumarase)	Fh	0.50
23	Q9D7B6	Isobutyryl-CoA dehydrogenase, mitochondrial	Acad8	0.50
24	Q922Q1	Mitochondrial amidoxime reducing component 2 (mARC2)	Mosc2	0.50
25	Q3UFY8	Mitochondrial ribonuclease P protein 1	Trmt10c	0.50
26	Q8VIK2	Mpv17-like protein 2	Mpv17l2	0.50
27	Q80WJ6	Multidrug resistance-associated protein 9 (ATP-binding cassette sub-family C member 12)	Abcc12	0.50
28	Q8R4H7	N-acetylglutamate synthase, mitochondrial	Nags	0.50
29	Q9CRD0	OCIA domain-containing protein 1	Ociad1	0.50
30	Q8VDC0	Probable leucine--tRNA ligase, mitochondrial	Lars2	0.50
31	Q91YM4	Protein TBRG4 (Transforming growth factor beta regulator 4)	Tbrg4	0.50
32	Q8BZL1	Sialidase-4	Neu4	0.50
33	Q9CR76	Transmembrane protein 186	Tmem186	0.50
34	Q9JI39	ATP-binding cassette sub-family B member 10, mitochondrial	Abcb10	0.60
35	Q9CQN1	Heat shock protein 75 kDa, mitochondrial (HSP 75)	Trap1	0.60
36	P08249	Malate dehydrogenase, mitochondrial	Mdh2	0.60
37	Q8VCW8	Acyl-CoA synthetase family member 2, mitochondrial	Acsf2	0.62
38	Q9WUM5	Succinyl-CoA ligase [ADP/GDP-forming] subunit alpha, mitochondrial	Suclg1	0.64
39	Q9D3D9	ATP synthase subunit delta, mitochondrial (F-ATPase delta subunit)	Atp5d	0.67
40	Q9DB73	NADH-cytochrome b5 reductase 1 (b5R.1)	Cyb5r1	0.67
41	Q91VD9	NADH-ubiquinone oxidoreductase 75 kDa subunit, mitochondrial	Ndufs1	0.67
42	A2AVJ5	Proline-rich protein 5-like	Prr5l	0.67
43	Q925N0	Sideroflexin-5	Sfxn5	0.67
44	Q9CQS4	Solute carrier family 25 member 46	Slc25a46	0.67
45	Q8CGV9	Teashirt homolog 3 (Zinc finger protein 537)	Tshz3	0.67

46	Q3ULD5	Methylcrotonoyl-CoA carboxylase beta chain, mitochondrial	Mccc2	0.70
47	Q60932	Voltage-dependent anion-selective channel protein 1	Vdac1	0.71
48	P50544	Very long-chain specific acyl-CoA dehydrogenase, mitochondrial	Acadvl	0.73
49	Q9CZS1	Aldehyde dehydrogenase X, mitochondrial	Aldh1b1	0.75
50	P19096	Fatty acid synthase	Fasn	0.75
51	P54869	Hydroxymethylglutaryl-CoA synthase, mitochondrial	Hmgcs2	0.75
52	Q9JHI5	Isovaleryl-CoA dehydrogenase, mitochondrial (IVD)	Ivd	0.75
53	Q9R112	Sulfide:quinone oxidoreductase, mitochondrial (SQOR)	Sqrdl	0.75
54	Q91XL3	UDP-glucuronic acid decarboxylase 1	Uxs1	0.75
55	P26443	Glutamate dehydrogenase 1, mitochondrial (GDH 1)	Glud1	0.77
56	Q9QXX4	Calcium-binding mitochondrial carrier protein Aralar2 (Citrin)	Slc25a13	0.78
57	Q8CHT0	Delta-1-pyrroline-5-carboxylate dehydrogenase, mitochondrial	Aldh4a1	0.78
58	Q9CWT6	Probable ATP-dependent RNA helicase DDX28	Ddx28	0.78
59	Q99JY0	Trifunctional enzyme subunit beta, mitochondrial (TP-beta)	Hadhb	0.79

Suppl. Table 5. Mitochondrial proteins that decrease after cBID treatment - Spot 5

A/A	ACCESSION NUMBER	PROTEIN NAME	GENE	FOLD CHANGE
1	Q9DCW5	Caspase-8 (CASP-8)	Casp8	0
2	Q9D5T0	Choline dehydrogenase, mitochondrial	Chdh	0
3	Q32MW3	Cytochrome b-c1 complex subunit 6, mitochondrial	Uqcrh	0
4	P43024	Cytochrome c oxidase subunit 6A1, mitochondrial	Cox6a1	0
5	O89110	Cytochrome c oxidase subunit NDUFA4	Ndufa4	0
6	P99028	Dihydrolipoyllysine-residue acetyltransferase component of pyruvate dehydrogenase complex, mitochondrial	Dlat	0
7	Q921G7	Electron transfer flavoprotein-ubiquinone oxidoreductase, mitochondrial	Etfdh	0
8	Q9JJG9	Mitochondrial carrier homolog 2	Mtch2	0
9	Q8BJ64	Prostaglandin E synthase 2	Ptges2	0
10	P51175	Protoporphyrinogen oxidase (PPO)	Ppox	0
11	Q8K0D5	Putative ribonuclease	Ybey	0
12	Q62425	Sorting and assembly machinery component 50 homolog	Samm50	0
13	Q8R1S0	Ubiquinone biosynthesis monooxygenase COQ6, mitochondrial	Coq6	0
14	Q8C0F9	Inactive serine protease 35	Prss35	0.08
15	Q8BW75	Amine oxidase	Maob	0.20
16	Q8K0D5	Elongation factor G, mitochondrial (EF-Gmt)	Gfm1	0.20
17	Q8BW75	ATPase family AAA domain-containing protein 1	Atad1	0.25
18	Q8BU88	39S ribosomal protein L22, mitochondrial	Mrpl22	0.33
19	O35386	Cytochrome c oxidase assembly protein COX16 homolog, mitochondrial	Cox16	0.33
20	Q8R1S0	Dihydrolipoyllysine-residue succinyltransferase component of 2-oxoglutarate dehydrogenase complex, mitochondrial	Dlst	0.33
21	Q99J39	Malonyl-CoA decarboxylase, mitochondrial (MCD)	Mlycd	0.33

22	Q9JHF5	V-type proton ATPase subunit a	Tcirg1	0.38
23	Q8C3X4	Translation factor Guf1, mitochondrial	Guf1	0.40
24	Q922E6	FAST kinase domain-containing protein 2	Fastkd2	0.44
25	Q60932	Voltage-dependent anion-selective channel protein 1	Vdac1	0.47
26	Q99NB1	Acetyl-coenzyme A synthetase 2-like, mitochondrial	Acss1	0.50
27	Q791V5	Acyl-CoA dehydrogenase family member 11	Acad11	0.50
28	Q9D2G2	Acyl-coenzyme A thioesterase 10, mitochondrial	Acot10	0.50
29	P56391	Cytochrome c oxidase subunit 6B1	Cox6b1	0.50
30	P28271	Cytoplasmic aconitate hydratase (Aconitase)	Aco1	0.50
31	Q8CHT0	Delta-1-pyrroline-5-carboxylate dehydrogenase, mitochondrial (P5C dehydrogenase)	Aldh4a1	0.50
32	Q80XL6	Glycine N-acyltransferase	Glyat	0.50
33	Q9CY28	GTP-binding protein 8	Gtpbp8	0.50
34	Q9CY28	GTP-binding protein 8	Gtpbp8	0.50
35	Q99MR8	Methylcrotonoyl-CoA carboxylase subunit alpha, mitochondrial	Mccc1	0.50
36	Q8BHG1	Nardilysin	Nrd1	0.50
37	Q9JJG9	Nitric oxide-associated protein 1	Noa1	0.50
38	Q922W5	Phytanoyl-CoA dioxygenase, peroxisomal	Phyh	0.50
39	Q922W5	Pyrroline-5-carboxylate reductase 1, mitochondrial	Pycr1	0.50
40	P21958	Antigen peptide transporter 1 (APT1)	Tap1	0.55
41	Q61586	Glycerol-3-phosphate acyltransferase 1, mitochondrial	Gpam	0.55
42	P12787	Cytochrome c oxidase subunit 5A, mitochondrial	Cox5a	0.57
43	Q3U1C4	MCG1271 (Protein Secisbp2)	Secisbp2	0.57
44	P55096	ATP-binding cassette sub-family D member 3	Abcd3	0.59
45	Q9DB77	Cytochrome b-c1 complex subunit 2, mitochondrial	Uqcrc2	0.59
46	Q8BHF7	CDP-diacylglycerol--glycerol-3-phosphate 3-phosphatidyltransferase, mitochondrial	Pgs1	0.60
47	P97742	Carnitine O-palmitoyltransferase 1, liver isoform (CPT1-L)	Cpt1a	0.62
48	P52825	Carnitine O-palmitoyltransferase 2, mitochondrial	Cpt2	0.62
49	P19783	Cytochrome c oxidase subunit 4 isoform 1, mitochondrial	Cox4i1	0.63
50	P40630	Transcription factor A, mitochondrial (mtTFA)	Tfam	0.63
51	Q9CZS1	Aldehyde dehydrogenase X, mitochondrial	Aldh1b1	0.64
52	Q6PB66	Leucine-rich PPR motif-containing protein, mitochondrial	Lrpprc	0.65
53	Q9CZ13	Cytochrome b-c1 complex subunit 1, mitochondrial	Uqcrc1	0.65
54	E9QJS0	28S ribosomal protein S10, mitochondrial	Mrps10	0.67
55	Q9CXF0	ATPase family AAA domain-containing protein 3	Atad3	0.67
56	Q8K449	ATP-binding cassette sub-family A member 9	Abca9	0.67
57	Q91V92	ATP-citrate synthase	Acly	0.67
58	Q925I1	Elongation factor G, mitochondrial	Gfm1	0.67
59	Q91XE0	Kynureninase	Kynu	0.67
60	Q3UQ84	Threonine--tRNA ligase, mitochondrial	Tars2	0.67
61	P50544	Very long-chain specific acyl-CoA dehydrogenase, mitochondrial	Acadvl	0.67
62	Q9Z2I0	LETM1 and EF-hand domain-containing protein 1, mitochondrial	Letm1	0.70
63	Q9DBM2	Peroxisomal bifunctional enzyme	Ehhadh	0.74

64	Q9WUM5	Succinyl-CoA ligase [ADP/GDP-forming] subunit alpha, mitochondrial	Suclg1	0.75
65	P26443	Glutamate dehydrogenase 1, mitochondrial (GDH 1)	Glud1	0.77
66	Q99K67	Alpha-aminoadipic semialdehyde synthase, mitochondrial (LKR/SDH)	Aass	0.78
67	O35423	Serine--pyruvate aminotransferase, mitochondrial	Agxt	0.78

Suppl. Table 6. Mitochondrial proteins that decrease after cBID treatment - Spot 7

A/A	ACCESSION NUMBER	PROTEIN NAME	GENE	FOLD CHANGE
1	E9Q414	Apolipoprotein B-100	Apob	0
2	Q62388	Serine-protein kinase ATM	Atm	0
3	A2A655	Protein Bptf	Bptf	0
4	A2AX52	Collagen alpha-4(VI) chain	Col6a4	0
5	P00186	Cytochrome P450 1A2	Cyp1a2	0
6	Q8K1G9	DEAH (Asp-Glu-Ala-His) box polypeptide 35	Dhx35	0
7	Q9WUR2	Enoyl-CoA delta isomerase 2, mitochondrial	Eci2	0
8	Q80W93	Hydrocephalus-inducing protein	Hydin	0
9	Q03717	Potassium voltage-gated channel subfamily B member 1	Kcnb1	0
10	Q3UXZ9	Lysine-specific demethylase 5A	Kdm5a	0
11	Q8BJ34	Meiosis arrest female protein 1	Marf1	0
12	Q791T5	Mitochondrial carrier homolog 1	Mtch1	0
13	P28666	Murinoglobulin-2 (MuG2)	Mug2	0
14	Q8C170	Unconventional myosin-Ixa	Myo9a	0
15	Q6P5H2	Nestin	Nes	0
16	Q4PLS0	NACHT (Protein Nlrp2)	Nlrp2	0
17	Q8BXA7	PH domain leucine-rich repeat-containing protein phosphatase 2	Phlpp2	0
18	O88492	Perilipin-4 (Adipocyte protein S3-12)	Plin4	0
19	P70670	Nascent polypeptide-associated complex subunit alpha, muscle-specific form	Prkdc	0
20	B9EJA3	Protein tyrosine phosphatase, receptor type, D	Ptprd	0
21	Q8CG73	Protein fantom (Nephrocystin-8)	Rpgrip1l	0
22	Q8K2B3	Succinate dehydrogenase [ubiquinone] flavoprotein subunit, mitochondrial	Sdha	0
23	Q04692	SWI/SNF-related matrix-associated actin-dependent regulator of chromatin subfamily A containing DEAD/H box 1	Smarcad1	0
24	A2RSJ4	UHRF1-binding protein 1-like	Uhrf1bp1l	0
25	Q4U4S6	Xin actin-binding repeat-containing protein 2	Xirp2	0
26	Q91VA0	Acyl-coenzyme A synthetase ACSM1, mitochondrial	Acsm1	0.17
27	Q7TQH5	Synaptic nuclear envelope 1	Syne1	0.17

28	Q8CGK3	Lon protease homolog, mitochondrial	Lonp1	0.18
29	Q571F8	Glutaminase liver isoform, mitochondrial (GLS)	Gls2	0.20
30	P46978	Dolichyl-diphosphooligosaccharide--protein glycosyltransferase subunit STT3A	Stt3a	0.20
31	Q922Q1	Mitochondrial amidoxime reducing component 2 (mARC2)	Mosc2	0.22
32	Q9WU19	Hydroxyacid oxidase 1 (HAOX1)	Hao1	0.25
33	Q9JIY5	Serine protease HTRA2, mitochondrial (EC 3.4.21.108) (High temperature requirement protein A2) (HtrA2) (Omi stress-regulated endoprotease) (Serine protease 25) (Serine proteinase OMI)	Htra2	0.25
34	P70272	Skeletal muscle ryanodine receptor (Fragment)	Naca	0.25
35	P21107	Tropomyosin alpha-3 chain (Gamma-tropomyosin)	Tpm3	0.25
36	Q69Z23	Dynein heavy chain 17, axonemal		0.25
37	Q99MR8	Methylcrotonoyl-CoA carboxylase subunit alpha, mitochondrial	Mccc1	0.31
38	Q5QNR3	Protein Ankrd36 (Fragment)	Ankrd36	0.33
39	P33267	Cytochrome P450 2F2	Cyp2f2	0.33
40	Q64459	Cytochrome P450 3A11	Cyp3a11	0.33
41	Q8VHE6	Dynein heavy chain 5, axonemal	Dnah5	0.33
42	Q8C3Y4	Kinetochore-associated protein 1	Kntc1	0.33
43	O55125	Protein NipSnap homolog 1 (NipSnap1)	Nipsnap1	0.33
44	P58281	Dynamin-like 120 kDa protein, mitochondrial	Opa1	0.33
45	P27773	Protein disulfide-isomerase A3	Pdia3	0.33
46	Q8CC88	von Willebrand factor A domain-containing protein 8	Vwa8	0.33
47	P79457	Histone demethylase UTY		0.33
48	P51660	Peroxisomal multifunctional enzyme type 2	Hsd17b4	0.38
49	Q3UHR0	BAH and coiled-coil domain-containing protein 1	Bahcc1	0.40
50	O08828	Axonemal dynein heavy chain (Fragment)		0.40
51	O54850	Endonuclease/reverse transcriptase		0.40
52	Q8BIK4	Dedicator of cytokinesis protein 9 (Cdc42 guanine nucleotide exchange factor zizimin-1)		0.40
53	Q8K3J4	Nicotinic acetylcholine receptor alpha 9 subunit (Fragment)		0.40
54	Q9DBG1	Sterol 26-hydroxylase, mitochondrial	Cyp27a1	0.42
55	Q99K67	Alpha-aminoadipic semialdehyde synthase, mitochondrial (LKR/SDH)	Aass	0.43
56	P08113	Endoplasmin (94 kDa glucose-regulated protein) (GRP-94)	Hsp90b1	0.44
57	Q91YQ5	Dolichyl-diphosphooligosaccharide--protein glycosyltransferase subunit 1	Rpn1	0.45
58	B2RY15	Tln2 protein	Tln2	0.50

59	Q8CHT0	Delta-1-pyrroline-5-carboxylate dehydrogenase, mitochondrial (P5C dehydrogenase)	Aldh4a1	0.50
60	A2AQR0	Glycerol-3-phosphate dehydrogenase	Gpd2	0.50
61	Q60675	Laminin subunit alpha-2 (Laminin M chain) (Laminin-12 subunit alpha)	Lama2	0.50
62	Q04690	Neurofibromin (Neurofibromatosis-related protein NF-1)	Nf1	0.50
63	Q99PL5	Ribosome-binding protein 1 (Ribosome receptor protein)	Rrbp1	0.50
64	Q9QXX4	Calcium-binding mitochondrial carrier protein Aralar2	Slc25a13	0.50
65	O35488	Very long-chain acyl-CoA synthetase (VLACS)	Slc27a2	0.50
66	Q64435	UDP-glucuronosyltransferase 1-6 (UDPGT 1-6)	Ugt1a6a	0.50
67	Q5H8C4	Vacuolar protein sorting-associated protein 13A	Vps13a	0.50
68	A2A8E9	Carnitine O-palmitoyltransferase 2, mitochondrial (Fragment)	Cpt2	0.55
69	A2ATU0	Probable 2-oxoglutarate dehydrogenase E1 component DHKTD1, mitochondrial	Dhtkd1	0.56
70	B1AU25	Apoptosis-inducing factor 1, mitochondrial	Aifm1	0.57
71	Q61586	Glycerol-3-phosphate acyltransferase 1, mitochondrial (GPAT-1)	Gpam	0.57
72	P61922	4-aminobutyrate aminotransferase, mitochondrial	Abat	0.58
73	Q03265	ATP synthase subunit alpha, mitochondrial	Atp5a1	0.60
74	P01027	Complement C3 (HSE-MSF)	C3	0.60
75	Q91VA7	Isocitrate dehydrogenase [NAD] subunit, mitochondrial	Idh3b	0.60
76	Q91WN4	Kynurenine 3-monooxygenase	Kmo	0.60
77	P50446	Keratin, type II cytoskeletal 6A (Cytokeratin-6A)	Krt6a	0.60
78	Q9WU79	Proline dehydrogenase 1, mitochondrial	Prodh	0.60
79	P97313	DNA-dependent protein kinase catalytic subunit		0.60
80	Q62504	Msx2-interacting protein		0.60
81	O35423	Serine--pyruvate aminotransferase, mitochondrial (SPT)	Agxt	0.63
82	P32020	Non-specific lipid-transfer protein (NSL-TP)	Scp2	0.63
83	Q6PB66	Leucine-rich PPR motif-containing protein, mitochondrial	Lrpprc	0.63
84	Q9D6F9	Tubulin beta-4A chain (Tubulin beta-4 chain)	Tubb4a	0.65
85	Q9CZS1	Aldehyde dehydrogenase X, mitochondrial	Aldh1b1	0.67
86	Q922J3	CAP-Gly domain-containing linker protein 1	Clip1	0.67
87	Q05421	Cytochrome P450 2E1	Cyp2e1	0.67
88	Q9DBM2	Peroxisomal bifunctional enzyme	Ehhadh	0.67
89	Q61769	Ki-67 protein	Ki67	0.67
90	Q5S006	Leucine-rich repeat serine/threonine-protein kinase 2	Lrrk2	0.67
91	Q80UM7	Mannosyl-oligosaccharide glucosidase	Mogs	0.67

92	A2AQA9	Protein Neb	Neb	0.67
93	Q8CCJ9	PHD finger protein 20-like protein 1	Phf20l1	0.67
94	Q9DBG6	Dolichyl-diphosphooligosaccharide--protein glycosyltransferase subunit 2	Rpn2	0.67
95	P99024	Tubulin beta-5 chain	Tubb5	0.67
96	Q8BWQ1	UDP-glucuronosyltransferase 2A3 (UDPGT 2A3)	Ugt2a3	0.67
97	Q8R084	UDP-glucuronosyltransferase	Ugt2b1	0.67
98	Q99KI0	Aconitate hydratase, mitochondrial (Aconitase)	Aco2	0.70
99	Q91WL5	Cytochrome P450 4A12A	Cyp4a12a	0.71
100	Q05920	Pyruvate carboxylase, mitochondrial		0.73
101	P05213	Tubulin alpha-1B chain	Tuba1b	0.74
102	P35564	Calnexin	Canx	0.75
103	Q9WVJ3	Carboxypeptidase Q	Cpq	0.75
104	Q91ZU6	Dystonin	Dst	0.75
105	Q3ULD5	Methylcrotonoyl-CoA carboxylase beta chain, mitochondrial	Mccc2	0.75
106	P16332	Methylmalonyl-CoA mutase, mitochondrial	Mut	0.75
107	P11725	Ornithine carbamoyltransferase, mitochondrial	Otc	0.75
108	Q9CQN1	Heat shock protein 75 kDa, mitochondrial	Trap1	0.75
109	Q7TMM9	Tubulin beta-2A chain	Tubb2a	0.75
110	P20029	78 kDa glucose-regulated protein	Hspa5	0.78
111	Q60932	Voltage-dependent anion-selective channel protein 1	Vdac1	0.78

Suppl. Table 7. Mitochondrial proteins that decrease after cBID treatment - Spot 10

A/A	ACCESSION NUMBER	PROTEIN NAME	GENE	FOLD CHANGE
1	P55096	ATP-binding cassette sub-family D member 3	Abcd3	0
2	O35435	Dihydroorotate dehydrogenase (quinone), mitochondrial (DHOdehase)	Dhodh	0
3	P50544	Very long-chain specific acyl-CoA dehydrogenase, mitochondrial	Acadvl	0
4	Q5RL20	39S ribosomal protein L43, mitochondrial	Mrpl43	0
5	Q62425	Cytochrome c oxidase subunit NDUFA4	Ndufa4	0
6	Q9Z2Z6	Mitochondrial carnitine/acylcarnitine carrier protein	Slc25a20	0
7	Q60930	Voltage-dependent anion-selective channel protein 2	Vdac2	0
8	P26443	Glutamate dehydrogenase 1, mitochondrial (GDH 1)	Glud1	0
9	Q9D1P0	39S ribosomal protein L13, mitochondrial (L13mt) (MRP-L13)	Mrpl13	0
10	Q9D125	28S ribosomal protein S25, mitochondrial (MRP-S25)	Mrps25	0
11	Q8R4H7	N-acetylglutamate synthase, mitochondrial	Nags	0
12	Q9DC61	Mitochondrial-processing peptidase subunit alpha	Pmpca	0
13	Q99MN9	Propionyl-CoA carboxylase beta chain, mitochondrial (PCCase subunit beta)	Pccb	0.09

14	P19783	Cytochrome c oxidase subunit 4 isoform 1, mitochondrial	Cox4i1	0.14
15	Q99JT1	Glutamyl-tRNA(Gln) amidotransferase subunit B, mitochondrial	Gatb	0.20
16	P54071	Isocitrate dehydrogenase [NADP], mitochondrial	Idh2	0.20
17	Q99JY0	Trifunctional enzyme subunit beta, mitochondrial	Hadhb	0.21
18	Q9Z2I8	Succinyl-CoA ligase [GDP-forming] subunit beta, mitochondrial	Suclg2	0.25
19	Q9Z110	Delta-1-pyrroline-5-carboxylate synthase (P5CS)	Aldh18a1	0.25
20	P38647	Stress-70 protein, mitochondrial (75 kDa glucose-regulated protein)	Hspa9	0.25
21	Q91YJ5	Translation initiation factor IF-2, mitochondrial	Mtif2	0.25
22	P00405	Cytochrome c oxidase subunit 2 (Cytochrome c oxidase polypeptide II)	Mtco2	0.29
23	O88967	ATP-dependent zinc metalloprotease YME1L1	Yme1l1	0.33
24	Q60597	2-oxoglutarate dehydrogenase, mitochondrial	Ogdh	0.33
25	Q61694	3 beta-hydroxysteroid dehydrogenase type 5	Hsd3b5	0.33
26	Q8JZU2	Tricarboxylate transport protein, mitochondrial	Slc25a1	0.33
27	Q9CQ91	NADH dehydrogenase	Ndufa3	0.33
28	Q8BPT6	Mitochondrial inner membrane protease subunit 2	Immp2l	0.33
29	Q925I1	ATPase family AAA domain-containing protein 3	Atad3	0.33
30	Q924T2	28S ribosomal protein S2, mitochondrial	Mrps2	0.33
31	Q9DB15	39S ribosomal protein L12, mitochondrial	Mrpl12	0.33
32	Q9CQE1	Protein NipSnap homolog 3B	Nipsnap3b	0.33
33	P47738	Aldehyde dehydrogenase, mitochondrial	Aldh2	0.33
34	O35972	39S ribosomal protein L23, mitochondrial	Mrpl23	0.33
35	Q80X85	28S ribosomal protein S7, mitochondrial (MRP-S7)	Mrps7	0.40
36	Q3UV71	Transmembrane and TPR repeat-containing protein 1	Tmtc1	0.40
37	Q6PB66	Leucine-rich PPR motif-containing protein, mitochondrial	Lrpprc	0.43
38	Q8CHT0	Delta-1-pyrroline-5-carboxylate dehydrogenase, mitochondrial	Aldh4a1	0.43
39	Q8VE22	28S ribosomal protein S23, mitochondrial (MRP-S23)	Mrps23	0.43
40	Q9ER88	28S ribosomal protein S29, mitochondrial	Dap3	0.43
41	Q9D3D9	ATP synthase subunit delta, mitochondrial	Atp5d	0.44
42	Q9D3P8	Plasminogen receptor (KT)	Plgrkt	0.50
43	P51881	ADP/ATP translocase 2 (ADP,ATP carrier protein 2)	Slc25a5	0.50
44	Q925N0	Sideroflexin-5	Sfxn5	0.50
45	Q61586	Glycerol-3-phosphate acyltransferase 1, mitochondrial	Gpam	0.50
46	Q8JZN5	Acyl-CoA dehydrogenase family member 9, mitochondrial (ACAD-9)	Acad9	0.50
47	Q9D7N3	28S ribosomal protein S9, mitochondrial	Mrps9	0.50
48	Q9CRB9	MICOS complex subunit Mic19	Chchd3	0.50
49	P21300	Aldose reductase-related protein 1	Akr1b7	0.50
50	Q9CR21	Acyl carrier protein, mitochondrial	Ndufab1	0.50
51	P30275	Creatine kinase U-type, mitochondrial	Ckmt1	0.50

52	P11725	Ornithine carbamoyltransferase, mitochondrial	Otc	0.50
53	Q60932	Voltage-dependent anion-selective channel protein 1	Vdac1	0.50
54	P48771	Cytochrome c oxidase subunit 7A2, mitochondrial	Cox7a2	0.50
55	Q99N84	28S ribosomal protein S18b, mitochondrial	Mrps18b	0.50
56	Q9CQ40	39S ribosomal protein L49, mitochondrial (L49mt)	Mrpl49	0.50
57	P56379	6.8 kDa mitochondrial proteolipid	Mp68	0.50
58	P41216	Long-chain-fatty-acid--CoA ligase 1	Acsl1	0.55
59	Q9DBM2	Peroxisomal bifunctional enzyme (PBE)	Ehhadh	0.56
60	P00848	ATP synthase subunit a (F-ATPase protein 6)	Mtatp6	0.57
61	Q9CPQ8	ATP synthase subunit g, mitochondrial (ATPase subunit g)	Atp5l	0.57
62	P54869	Hydroxymethylglutaryl-CoA synthase, mitochondrial	Hmgcs2	0.57
63	P97742	Carnitine O-palmitoyltransferase 1, liver isoform	Cpt1a	0.57
64	Q9QXX4	Calcium-binding mitochondrial carrier protein Aralar2	Slc25a13	0.60
65	Q06185	ATP synthase subunit e, mitochondrial	Atp5i	0.60
66	P56135	ATP synthase subunit f, mitochondrial	Atp5j2	0.60
67	P53395	Lipoamide acyltransferase component of branched-chain alpha-keto acid dehydrogenase complex, mitochondrial	Dbt	0.60
68	Q9CXJ4	ATP-binding cassette sub-family B member 8, mitochondrial	Abcb8	0.60
69	P63038	60 kDa heat shock protein, mitochondrial	Hspd1	0.60
70	Q9DC71	28S ribosomal protein S15, mitochondrial	Mrps15	0.60
71	Q91VR2	ATP synthase subunit gamma, mitochondrial	Atp5c1	0.62
72	G5E8R3	Pyruvate carboxylase	Pcx	0.63
73	Q9CQQ7	ATP synthase F(0) complex subunit B1, mitochondrial	Atp5f1	0.63
74	Q91XL3	UDP-glucuronic acid decarboxylase 1	Uxs1	0.67
75	Q8K3J1	NADH dehydrogenase [ubiquinone] iron-sulfur protein 8, mitochondrial (EC 1.6.5.3)	Ndufs8	0.67
76	Q7TMF3	NADH dehydrogenase [ubiquinone] 1 alpha subcomplex subunit 12	Ndufa12	0.67
77	P03899	NADH-ubiquinone oxidoreductase chain 3	Mtnd3	0.67
78	Q8BHF7	CDP-diacylglycerol--glycerol-3-phosphate 3-phosphatidyltransferase, mitochondrial	Pgs1	0.67
79	Q80XN0	D-beta-hydroxybutyrate dehydrogenase, mitochondrial	Bdh1	0.67
80	Q99KI0	Aconitate hydratase, mitochondrial (Aconitase)	Aco2	0.67
81	Q99JR1	Sideroflexin-1	Sfxn1	0.67
82	Q9CQV5	28S ribosomal protein S24, mitochondrial	Mrps24	0.67
83	Q8K2M0	39S ribosomal protein L38, mitochondrial	Mrpl38	0.67
84	Q99N87	28S ribosomal protein S5, mitochondrial	Mrps5	0.67
85	Q9DCM2	Glutathione S-transferase kappa 1	Gstk1	0.67
86	Q8BMS1	Trifunctional enzyme subunit alpha, mitochondrial	Hadha	0.68
87	Q91ZA3	Propionyl-CoA carboxylase alpha chain, mitochondrial	Pcca	0.68
88	Q8BJZ4	28S ribosomal protein S35, mitochondrial	Mrps35	0.70
89	Q9CXW2	28S ribosomal protein S22, mitochondrial	Mrps22	0.70
90	Q9D8H7	Metalloendopeptidase OMA1, mitochondrial	Oma1	0.71

91	Q80Y81	Zinc phosphodiesterase ELAC protein 2	Elac2	0.71
92	P51660	Peroxisomal multifunctional enzyme type 2	Hsd17b4	0.71
93	Q9DBG1	Sterol 26-hydroxylase, mitochondrial	Cyp27a1	0.75
94	O09111	NADH dehydrogenase [ubiquinone] 1 beta subcomplex subunit 11, mitochondrial	Ndufb11	0.75
95	P42925	Peroxisomal membrane protein 2	Pxmp2	0.75
96	P09671	Superoxide dismutase [Mn], mitochondrial	Sod2	0.75
97	Q8R035	Peptidyl-tRNA hydrolase ICT1, mitochondrial	Ict1	0.75
98	Q9CPR5	39S ribosomal protein L15, mitochondrial	Mrpl15	0.75
99	Q9JIK9	28S ribosomal protein S34, mitochondrial	Mrps34	0.78

Suppl. Table 8. Mitochondrial proteins that decrease after cBID treatment - Spot 11

A/A	ACCESSION NUMBER	PROTEIN NAME	GENE	FOLD CHANGE
1	P00397	Cytochrome c oxidase subunit 1	Mtco1	0
2	Q9CZW5	Mitochondrial import receptor subunit TOM70	Tomm70a	0
3	Q9D6Y7	Mitochondrial peptide methionine sulfoxide reductase	Msra	0
4	P43024	Cytochrome c oxidase subunit 6A1, mitochondrial	Cox6a1	0
5	Q9WU79	Proline dehydrogenase 1, mitochondrial	Prodh	0
6	Q8K0Z7	Translational activator of cytochrome c oxidase 1	Taco1	0
7	Q9WVM8	Kynurenine/alpha-aminoadipate aminotransferase, mitochondrial (KAT/AadAT)	Aadat	0.17
8	P52825	Carnitine O-palmitoyltransferase 2, mitochondrial	Cpt2	0.25
9	Q925N0	Sideroflexin-5	Sfxn5	0.25
10	Q9CQN1	Heat shock protein 75 kDa, mitochondrial	Trap1	0.25
11	Q9EQ20	Methylmalonate-semialdehyde dehydrogenase	Aldh6a1	0.31
12	Q9D0S9	Histidine triad nucleotide-binding protein 2, mitochondrial	Hint2	0.33
13	Q9Z0X1	Apoptosis-inducing factor 1, mitochondrial	Aifm1	0.38
14	Q5FW57	Glycine N-acyltransferase-like protein	Gm4952	0.40
15	Q99LB2	Dehydrogenase/reductase SDR family member 4	Dhrs4	0.42
16	P42925	Peroxisomal membrane protein 2	Pxmp2	0.43
17	Q8BFR5	Elongation factor Tu, mitochondrial	Tufm	0.45
18	Q9CPY7	Cytosol aminopeptidase	Lap3	0.50
19	Q2TPA8	Hydroxysteroid dehydrogenase-like protein 2	Hsdl2	0.50
20	Q571F8	Glutaminase liver isoform, mitochondrial (GLS)	Gls2	0.50
21	Q9CZU6	Citrate synthase, mitochondrial	Cs	0.50
22	Q60930	Voltage-dependent anion-selective channel protein 2	Vdac2	0.50
23	Q9WTP7	GTP:AMP phosphotransferase AK3, mitochondrial	Ak3	0.50
24	Q99J39	Malonyl-CoA decarboxylase, mitochondrial	Mlycd	0.50
25	Q9CQQ7	ATP synthase F(0) complex subunit B1, mitochondrial	Atp5f1	0.50
26	Q7TMG8	Glioblastoma amplified sequence	Gbas	0.50
27	Q3UW66	Sulfurtransferase	Mpst	0.50
28	Q8BWT1	3-ketoacyl-CoA thiolase, mitochondrial	Acaa2	0.50

29	Q9D6Y7	Mitochondrial peptide methionine sulfoxide reductase	Msra	0.50
30	P23589	Carbonic anhydrase 5A, mitochondrial	Ca5a	0.50
31	Q9DBG1	Sterol 26-hydroxylase, mitochondrial	Cyp27a1	0.53
32	Q8R164	Valacyclovir hydrolase	Bphl	0.60
33	Q99LC5	Electron transfer flavoprotein subunit alpha, mitochondria	Etfa	0.63
34	Q9CQS4	Solute carrier family 25 member 46	Slc25a46	0.63
35	P41216	Long-chain-fatty-acid--CoA ligase 1	Acsl1	0.63
36	Q99N15	17beta-hydroxysteroid dehydrogenase type 10/short chain L-3-hydroxyacyl-CoA dehydrogenase	Hsd17b10	0.67
37	P06795	Multidrug resistance protein 1B	Abcb1b	0.67
38	Q64521	Glycerol-3-phosphate dehydrogenase, mitochondrial	Gpd2	0.67
39	Q8BW75	Amine oxidase [flavin-containing] B	Maob	0.67
40	Q03265	ATP synthase subunit alpha, mitochondrial	Atp5a1	0.67
41	Q6P3A8	2-oxoisovalerate dehydrogenase subunit beta, mitochondrial	Bckdhb	0.67
42	P50544	Very long-chain specific acyl-CoA dehydrogenase, mitochondrial	Acadvl	0.68
43	Q9DCW4	Electron transfer flavoprotein subunit beta	Etfb	0.69
44	P00405	Cytochrome c oxidase subunit 2	Mtco2	0.70
45	Q8BMS1	Trifunctional enzyme subunit alpha, mitochondrial	Hadha	0.71
46	Q8VCW8	Acyl-CoA synthetase family member 2, mitochondrial	Acsf2	0.71
47	P52196	Thiosulfate sulfurtransferase	Tst	0.75
48	Q9CZS1	Aldehyde dehydrogenase X, mitochondrial	Aldh1b1	0.75
49	O88696	ATP-dependent Clp protease proteolytic subunit, mitochondrial	Clpp	0.75
50	Q61425	Hydroxyacyl-coenzyme A dehydrogenase, mitochondrial (HCDH)	Hadh	0.75
51	Q99MR8	Methylcrotonoyl-CoA carboxylase subunit alpha, mitochondrial	Mccc1	0.75
52	Q60931	Voltage-dependent anion-selective channel protein 3	Vdac3	0.75
53	P61922	4-aminobutyrate aminotransferase, mitochondrial	Abat	0.75
54	Q922Q1	Mitochondrial amidoxime reducing component 2 (mARC2)	Mosc2	0.78
55	Q9Z2I0	LETM1 and EF-hand domain-containing protein 1, mitochondrial	Letm1	0.80
56	P12787	Cytochrome c oxidase subunit 5A, mitochondrial	Cox5a	0.83
57	Q9DCY0	Glycine N-acyltransferase-like protein Keg1	Keg1	0.83
58	Q9QXX4	Calcium-binding mitochondrial carrier protein Aralar2 (Citrin)	Slc25a13	0.84
59	P11725	Ornithine carbamoyltransferase, mitochondrial	Otc	0.85
60	P51660	Peroxisomal multifunctional enzyme type 2	Hsd17b4	0.86
61	Q8BH95	Enoyl-CoA hydratase, mitochondrial	Echs1	0.87
62	P11352	Glutathione peroxidase 1	Gpx1	0.88
63	Q6PB66	Leucine-rich PPR motif-containing protein, mitochondrial	Lrpprc	0.88
64	P19783	Cytochrome c oxidase subunit 4 isoform 1, mitochondrial	Cox4i1	0.90
65	Q9D881	Cytochrome c oxidase subunit 5B, mitochondrial	Cox5b	0.90
66	P26443	Glutamate dehydrogenase 1, mitochondrial	Glud1	0.91
67	H7BWY3	Alanine--glyoxylate aminotransferase 2, mitochondrial	Agxt2	0.91
68	P38647	Stress-70 protein, mitochondrial (75 kDa glucose-regulated protein) (GRP-75)	Hspa9	0.92
69	P54869	Hydroxymethylglutaryl-CoA synthase, mitochondrial	Hmgcs2	0.92

70	Q922U2	Keratin, type II cytoskeletal 5	Krt5	0.95
71	Q9DBT9	Dimethylglycine dehydrogenase, mitochondrial	Dmgdh	0.97

Suppl. Table 9. Mitochondrial proteins associated with OPA1 in steady state

A/A	ACCESSION NUMBER	PROTEIN NAME	GENE	PEARSON
1	E0CXD1	Dynamin-like 120 kDa protein, mitochondrial	Opa1	1
2	P24270	Catalase	Cat	0.960
3	P47791	Glutathione reductase, mitochondrial	Gsr	0.947
4	E9PZP7	Malic enzyme	Me3	0.943
5	Q8CC88	von Willebrand factor A domain-containing protein 8	Vwa8	0.931
6	Q8BUY5	Complex I assembly factor TIMMDC1, mitochondrial	Timmdc1	0.921
7	J3QMG3	Voltage-dependent anion-selective channel protein 3	Vdac3	0.918
8	Q9D6Y7	Mitochondrial peptide methionine sulfoxide reductase	Msra	0.916
9	Q9QYA2	Mitochondrial import receptor subunit TOM40 homolog	Tomm40	0.911
10	Q9CPQ3	Mitochondrial import receptor subunit TOM22 homolog	Tomm22	0.911
11	O35459	Delta(3,5)-Delta(2,4)-dienoyl-CoA isomerase, mitochondrial	Ech1	0.907
12	Q9JIK9	28S ribosomal protein S34, mitochondrial	Mrps34	0.904
13	B8JJA9	Cytochrome c oxidase subunit 7C, mitochondrial	Cox7c	0.904
14	P56379	6.8 kDa mitochondrial proteolipid	Mp68	0.903
15	Q9CPY7	Cytosol aminopeptidase	Lap3	0.902
16	P55096	ATP-binding cassette sub-family D member 3	Abcd3	0.893
17	Q61733	28S ribosomal protein S31, mitochondrial	Mrps31	0.885
18	P53395	Lipoamide acyltransferase component of branched-chain alpha-keto acid dehydrogenase complex, mitochondrial	Dbt	0.879
19	P05201	Aspartate aminotransferase, cytoplasmic	Got1	0.876
20	Q3TL44	NLR family member X1	Nlrx1	0.875
21	E9Q8F4	NAD(P) transhydrogenase, mitochondrial	Nnt	0.874
22	P51660	Peroxisomal multifunctional enzyme type 2	Hsd17b4	0.871
23	D3Z6B9	Mitochondrial 10-formyltetrahydrofolate dehydrogenase	Aldh1l2	0.870
24	Q9QZH6	Evolutionarily conserved signaling intermediate in Toll pathway, mitochondrial	Ecsit	0.853
25	Q9CZP5	Mitochondrial chaperone BCS1	Bcs1l	0.850
26	P15532	Nucleoside diphosphate kinase A	Nme1	0.847
27	Q3U3G8	Serine hydrolase-like protein	Serhl	0.847
28	Q9EQ20	Methylmalonate-semialdehyde dehydrogenase [acylating], mitochondrial	Aldh6a1	0.841
29	A2ALN0	ATP-binding cassette sub-family D member 1	Abcd1	0.838
30	G3UVV4	Hexokinase-1	Hk1	0.836
31	Q9CQE3	28S ribosomal protein S17, mitochondrial	Mrps17	0.835
32	Q60714	Long-chain fatty acid transport protein 1	Slc27a1	0.835
33	Q9JKL4	NADH dehydrogenase [ubiquinone]1 alpha subcomplex assembly factor 3	Ndufaf3	0.831
34	Q60930	Voltage-dependent anion-selective channel protein 2	Vdac2	0.826

35	Q8CGK3	Lon protease homolog, mitochondrial	Lonp1	0.823
36	Q91VA7	Isocitrate dehydrogenase [NAD]subunit, mitochondrial	Idh3b	0.816
37	D3YTQ5	Acyl-CoA dehydrogenase family member 11	Acad11	0.815
38	P63038	60 kDa heat shock protein, mitochondrial	Hspd1	0.815
39	Q9Z2I0	LETM1 and EF-hand domain-containing protein 1, mitochondrial	Letm1	0.807
40	Q8BK72	28S ribosomal protein S27, mitochondrial	Mrps27	0.794
41	P61922	4-aminobutyrate aminotransferase, mitochondrial	Abat	0.794
42	F8WGD9	1-acyl-sn-glycerol-3-phosphate acyltransferase epsilon	Agpat5	0.790
43	O08715	A-kinase anchor protein 1, mitochondrial	Akap1	0.790
44	E9QM21	Bcl-2 homologous antagonist/killer	Bak1	0.790
45	P35564	Calnexin	Canx	0.790
46	E9Q3U7	Cytochrome c oxidase assembly protein COX16 homolog, mitochondrial	Cox16	0.790
47	P61804	Dolichyl-diphosphooligosaccharide--protein glycosyltransferase subunit DAD1	Dad1	0.790
48	O54734	Dolichyl-diphosphooligosaccharide--protein glycosyltransferase 48 kDa subunit	Ddost	0.790
49	Q3U7R1	Extended synaptotagmin-1	Esyt1	0.790
50	Q9CR59	Growth arrest and DNA damage-inducible proteins-interacting protein 1	Gadd45gip1	0.790
51	D3YX27	Serine protease HTRA2, mitochondrial	Htra2	0.790
52	E0CYL3	Calcium uniporter protein, mitochondrial	Mcu	0.790
53	Q99N84	28S ribosomal protein S18b, mitochondrial	Mrps18b	0.790
54	Q80ZS3	28S ribosomal protein S26, mitochondrial	Mrps26	0.790
55	Q791T5	Mitochondrial carrier homolog 1	Mtch1	0.790
56	Q9D0F9	Phosphoglucomutase-1	Pgm2	0.790
57	P61014	Cardiac phospholamban	Pln	0.790
58	Q922Q4	Pyrroline-5-carboxylate reductase 2	Pycr2	0.790
59	Q3U186	Probable arginine--tRNA ligase, mitochondrial	Rars2	0.790
60	Q9D938	Transmembrane protein 160	Tmem160	0.790
61	B1AXP6	Mitochondrial import receptor subunit TOM5 homolog	Tomm5	0.790
62	Q9CZW5	Mitochondrial import receptor subunit TOM70	Tomm70a	0.790
63	P68373	Tubulin alpha-1C chain	Tuba1c	0.790
64	O88967	ATP-dependent zinc metalloprotease YME1L1	Yme1l1	0.790
65	P97449	Aminopeptidase N	Anpep	0.790
66	A2AQ17	Complex I intermediate-associated protein 30, mitochondrial	Ndufaf1	0.790
67	O08807	Peroxiredoxin-4	Prdx4	0.790
68	Q9D1H6	NADH dehydrogenase [ubiquinone]1 alpha subcomplex assembly factor 4	Ndufaf4	0.784
69	O55028	[3-methyl-2-oxobutanoate dehydrogenase [lipoamide]]kinase, mitochondrial	Bckdk	0.783
70	D3Z2K2	28S ribosomal protein S14, mitochondrial	Mrps14	0.780
71	F2Z471	Voltage-dependent anion-selective channel protein 1	Vdac1	0.772
72	Q9CQV5	28S ribosomal protein S24, mitochondrial	Mrps24	0.768
73	Q9CXW2	28S ribosomal protein S22, mitochondrial	Mrps22	0.742

74	P11679	Keratin, type II cytoskeletal 8	Krt8	0.731
75	Q64516	Glycerol kinase	Gk	0.721
76	Q9D5T0	ATPase family AAA domain-containing protein 1	Atad1	0.716
77	Q3URS9	Coiled-coil domain-containing protein 51	Ccdc51	0.710
78	Q14C51	Pentatricopeptide repeat domain-containing protein 3, mitochondrial	Ptcd3	0.710
79	P08228	Superoxide dismutase [Cu-Zn]	Sod1	0.698
80	Q8BMS1	Trifunctional enzyme subunit alpha, mitochondrial	Hadha	0.692
81	G3UXK7	Cytochrome c-type heme lyase	Hccs	0.688
82	Q9DCM2	Glutathione S-transferase kappa 1	Gstk1	0.686
83	P52480	Pyruvate kinase PKM	Pkm	0.681
84	G3UZJ4	Peroxiredoxin-5, mitochondrial	Prdx5	0.678
85	H3BKI6	ATPase family AAA domain-containing protein 3	Atad3a	0.677
86	Q99N87	28S ribosomal protein S5, mitochondrial	Mrps5	0.671
87	Q8BJZ4	28S ribosomal protein S35, mitochondrial	Mrps35	0.670
88	Q9DCX2	ATP synthase subunit d, mitochondrial	Atp5h	0.639
89	P03930	ATP synthase protein 8	mt-Atp8	0.635
90	Q9D6R2	Isocitrate dehydrogenase [NAD]subunit alpha, mitochondrial	Idh3a	0.631
91	Q8JZN7	Mitochondrial Rho GTPase 2	Rhot2	0.628
92	P70404	Isocitrate dehydrogenase [NAD]subunit gamma 1, mitochondrial	Idh3g	0.622
93	Q99JY0	Trifunctional enzyme subunit beta, mitochondrial	Hadhb	0.621
94	Q8C3X2	Coiled-coil domain-containing protein 90B, mitochondrial	Ccdc90b	0.620
95	Q91VC9	Growth hormone-inducible transmembrane protein	Ghitm	0.592
96	D3Z7C8	Branched-chain-amino-acid aminotransferase	Bcat2	0.576
97	Q9MD68	Cytochrome c oxidase subunit 1	mt-Co1	0.553
98	Q9CXD6	Mitochondrial calcium uniporter regulator 1	Mcur1	0.532
99	Q505D7	Optic atrophy 3 protein homolog	Opa3	0.532
100	P56382	ATP synthase subunit epsilon, mitochondrial	Atp5e	0.531
101	Q9WVJ3	Carboxypeptidase Q	Cpq	0.519
102	Q1XH17	Tripartite motif-containing protein 72	Trim72	0.517
103	D3YVW0	Metaxin-1	Mtx1	0.516
104	Q8VCF0	Mitochondrial antiviral-signaling protein	Mavs	0.512
105	Q99J39	Malonyl-CoA decarboxylase, mitochondrial	Mlycd	0.510
106	F6ZKZ3	Sulfide:quinone oxidoreductase, mitochondrial	Sqrdl	0.498
107	Q9CR76	Transmembrane protein 186	Tmem186	0.495
108	Q8VD26	Transmembrane protein 143	Tmem143	0.484
109	D3YXS8	Mitochondrial import receptor subunit TOM40B	Tomm40l	0.483
110	Q8JZN5	Acyl-CoA dehydrogenase family member 9, mitochondrial	Acad9	0.481
111	E9Q7L0	Protein Ogdhl	Ogdhl	0.477
112	J3KMM5	Calcium-transporting ATPase	Atp2a2	0.472
113	B0QZS8	Mitochondrial import inner membrane translocase subunit Tim22	Timm22	0.471
114	Q9CPQ8	ATP synthase subunit g, mitochondrial	Atp5l	0.461
115	P97450	ATP synthase-coupling factor 6, mitochondrial	Atp5j	0.458

116	P85094	Isochorismatase domain-containing protein 2A, mitochondrial	Isoc2a	0.450
117	Q9QWL7	Keratin, type I cytoskeletal 17	Krt17	0.413
118	Q9CRB9	MICOS complex subunit Mic19	Chchd3	0.412
119	P99028	Cytochrome b-c1 complex subunit 6, mitochondrial	Uqcrh	0.408
120	P17182	Alpha-enolase	Eno1	0.403
121	Q8BMF4	Dihydrolipoyllysine-residue acetyltransferase component of pyruvate dehydrogenase complex, mitochondrial	Dlat	0.400
122	D3Z7S4	ATP synthase subunit delta, mitochondrial	Atp5d	0.398
123	P38647	Stress-70 protein, mitochondrial	Hspa9	0.395
124	Q9D7N3	28S ribosomal protein S9, mitochondrial	Mrps9	0.390
125	Q01768	Nucleoside diphosphate kinase B	Nme2	0.383
126	A2ACG7	Dolichyl-diphosphooligosaccharide--protein glycosyltransferase subunit 2	Rpn2	0.382
127	E9Q8B3	DnaJ homolog subfamily C member 11	Dnajc11	0.378
128	Q9CPX7	28S ribosomal protein S16, mitochondrial	Mrps16	0.371
129	D6RGL7	ATP synthase F(0) complex subunit B1, mitochondrial	Atp5f1	0.370
130	P43023	Cytochrome c oxidase subunit 6A2, mitochondrial	Cox6a2	0.366
131	P10126	Elongation factor 1-alpha 1	Eef1a1	0.366
132	Q8CGP5	Histone H2A type 1-F	Hist1h2af	0.366
133	Q6NXH9	Keratin, type II cytoskeletal 73	Krt73	0.366
134	P00405	Cytochrome c oxidase subunit 2	mt-Co2	0.366
135	Q9WV85	Nucleoside diphosphate kinase 3	Nme3	0.366
136	Q01853	Transitional endoplasmic reticulum ATPase	Vcp	0.366
137	Q9D0L4	Uncharacterized aarF domain-containing protein kinase 1	Adck1	0.365
138	E9Q5B5	Hexokinase-2	Hk2	0.363
139	Q6PB66	Leucine-rich PPR motif-containing protein, mitochondrial	Lrpprc	0.348
140	Q922U2	Keratin, type II cytoskeletal 5	Krt5	0.328
141	P51174	Long-chain specific acyl-CoA dehydrogenase, mitochondrial	Acadl	0.321
142	Q9CPU4	Microsomal glutathione S-transferase 3	Mgst3	0.315
143	P61027	Ras-related protein Rab-10	Rab10	0.307
144	Q99KD6	Cox7a2l protein	Cox7a2l	0.304
145	E9Q800	MICOS complex subunit Mic60	Immt	0.304
146	Q61781	Keratin, type I cytoskeletal 14	Krt14	0.304
147	Q9ESW4	Acylglycerol kinase, mitochondrial	Agk	0.301
148	F8WHP8	ATP synthase subunit f, mitochondrial	Atp5j2	0.299
149	Q9CZS1	Aldehyde dehydrogenase X, mitochondrial	Aldh1b1	0.297
150	G3UYR8	Alpha-aminoadipic semialdehyde dehydrogenase	Aldh7a1	0.296
151	D3YYN7	Sodium/potassium-transporting ATPase subunit alpha-2	Atp1a2	0.296
152	D3ZFQ8	Cytochrome c-1 (Predicted), isoform CRA_c	Cyc1	0.296
153	E9PWN2	Isoleucine--tRNA ligase, mitochondrial	Iars2	0.296
154	Q9CRB8	Mitochondrial fission process protein 1	Mtfp1	0.296
155	P35487	Pyruvate dehydrogenase E1 component subunit alpha, testis-specific form, mitochondrial	Pdha2	0.296
156	E9Q933	Transmembrane protein 11, mitochondrial	Tmem11	0.296
157	Q3ULD5	Methylcrotonoyl-CoA carboxylase beta chain, mitochondrial	Mccc2	0.291

158	P48771	Cytochrome c oxidase subunit 7A2, mitochondrial	Cox7a2	0.287
159	P56392	Cytochrome c oxidase subunit 7A1, mitochondrial	Cox7a1	0.286
160	Q9D312	Keratin, type I cytoskeletal 20	Krt20	0.280
161	D3Z7V3	Sarcolemmal membrane-associated protein	Slmap	0.275
162	P04919	Band 3 anion transport protein	Slc4a1	0.272
163	Q61102	ATP-binding cassette sub-family B member 7, mitochondrial	Abcb7	0.272
164	P26443	Glutamate dehydrogenase 1, mitochondrial	Glud1	0.268
165	Q9JHW2	Omega-amidase NIT2	Nit2	0.265
166	P97742	Carnitine O-palmitoyltransferase 1, liver isoform	Cpt1a	0.264
167	Q9CQX2	Cytochrome b5 type B	Cyb5b	0.264
168	O35972	39S ribosomal protein L23, mitochondrial	Mrpl23	0.259
169	Q3TTY5	Keratin, type II cytoskeletal 2 epidermal	Krt2	0.256
170	P07310	Creatine kinase M-type	Ckm	0.255
171	P08113	Endoplasmin	Hsp90b1	0.247
172	Q60597	2-oxoglutarate dehydrogenase, mitochondrial	Ogdh	0.243
173	Q9QXX4	Calcium-binding mitochondrial carrier protein Aralar2	Slc25a13	0.229
174	A2AKU9	ATP synthase subunit gamma	Atp5c1	0.216
175	P47738	Aldehyde dehydrogenase, mitochondrial	Aldh2	0.214
176	Q921S7	39S ribosomal protein L37, mitochondrial	Mrpl37	0.212
177	Q78IK2	Up-regulated during skeletal muscle growth protein 5	Usmg5	0.206
178	Q8BWF0	Succinate-semialdehyde dehydrogenase, mitochondrial	Aldh5a1	0.203
179	P58059	28S ribosomal protein S21, mitochondrial	Mrps21	0.202
180	Q9CXT8	Mitochondrial-processing peptidase subunit beta	Pmpcb	0.202
181	Q9CQB4	Cytochrome b-c1 complex subunit 7	Uqcrb	0.196
182	Q3UER8	Fibrinogen gamma chain	Fgg	0.195
183	P50544	Very long-chain specific acyl-CoA dehydrogenase, mitochondrial	Acadvl	0.189
184	D6RJ70	Kynurenine--oxoglutarate transaminase 3	Ccbl2	0.187
185	A2A513	Keratin, type I cytoskeletal 10	Krt10	0.180
186	P59017	Bcl-2-like protein 13	Bcl2l13	0.174
187	B1AX78	Hydroxysteroid dehydrogenase-like protein 2	Hsdl2	0.171
188	B1ASZ3	Glycerol kinase	Gyk	0.162
189	Q8BH59	Calcium-binding mitochondrial carrier protein Aralar1	Slc25a12	0.159
190	A2AFW6	Mitochondrial carrier homolog 2	Mtch2	0.154
191	Q8CI78	Required for meiotic nuclear division protein 1 homolog	Rmnd1	0.149
192	Q99MR8	Methylcrotonoyl-CoA carboxylase subunit alpha, mitochondrial	Mccc1	0.144
193	Q76LV0	Glutathione peroxidase	Gpx4	0.141
194	P14094	Sodium/potassium-transporting ATPase subunit beta-1	Atp1b1	0.140
195	Q8BWM0	Prostaglandin E synthase 2	Ptges2	0.137
196	P12787	Cytochrome c oxidase subunit 5A, mitochondrial	Cox5a	0.132
197	Q9R0H0	Peroxisomal acyl-coenzyme A oxidase 1	Acox1	0.132
198	Q9CXJ4	ATP-binding cassette sub-family B member 8, mitochondrial	Abcb8	0.131
199	G3X9M0	28S ribosomal protein S29, mitochondrial	Dap3	0.129
200	P00158	Cytochrome b	mt-Cytb	0.126
201	Q9DB15	39S ribosomal protein L12, mitochondrial	Mrpl12	0.125

202	Q9CPQ1	Cytochrome c oxidase subunit 6C	Cox6c	0.117
203	P04104	Keratin, type II cytoskeletal 1	Krt1	0.116
204	M0QWX2	Cytochrome c oxidase subunit 4 isoform 1, mitochondrial	Cox4i1	0.112
205	Q62425	Cytochrome c oxidase subunit NDUFA4	Ndufa4	0.111
206	Q9D881	Protein Gm11273	Cox5b	0.110
207	E9Q4M4	MICOS complex subunit Mic25	Chchd6	0.107
208	Q8K0E8	Fibrinogen beta chain	Fgb	0.107
209	Q9WU65	Glycerol kinase 2	Gk2	0.107
210	E0CXB1	Proteasome subunit alpha type-6	Psma6	0.107
211	F8WHN1	39S ribosomal protein L15, mitochondrial	Mrpl15	0.105
212	Q9JI39	ATP-binding cassette sub-family B member 10, mitochondrial	Abcb10	0.101
213	Q9CZN7	Serine hydroxymethyltransferase	Shmt2	0.101

Suppl. Table 10. Mitochondrial Proteins associated with OPA1 that decrease after apoptotic stimulation

A/A	ACCESSION NUMBER	PROTEIN NAME	GENE	Fold change
1	P61922	4-aminobutyrate aminotransferase, mitochondrial	Abat	0.00
2	Q61102	ATP-binding cassette sub-family B member 7, mitochondrial	Abcb7	0.88
3	Q9CXJ4	ATP-binding cassette sub-family B member 8, mitochondrial	Abcb8	0.99
4	A2ALN0	ATP-binding cassette sub-family D member 1	Abcd1	0.20
5	P55096	ATP-binding cassette sub-family D member 3	Abcd3	0.38
6	D3YTQ5	Acyl-CoA dehydrogenase family member 11	Acad11	0.33
7	Q8JZN5	Acyl-CoA dehydrogenase family member 9, mitochondrial	Acad9	0.63
8	P51174	Long-chain specific acyl-CoA dehydrogenase, mitochondrial	Acadl	0.85
9	P50544	Very long-chain specific acyl-CoA dehydrogenase, mitochondrial	Acadvl	0.91
10	Q9R0H0	Peroxisomal acyl-coenzyme A oxidase 1	Acox1	0.17
11	Q9D0L4	Uncharacterized aarF domain-containing protein kinase 1	Adck1	0.80
12	Q9ESW4	Acylglycerol kinase, mitochondrial	Agk	0.33
13	F8WGD9	1-acyl-sn-glycerol-3-phosphate acyltransferase epsilon	Agpat5	0.00
14	O08715	A-kinase anchor protein 1, mitochondrial	Akap1	0.00
15	Q9CZS1	Aldehyde dehydrogenase X, mitochondrial	Aldh1b1	0.56
16	D3Z6B9	Mitochondrial 10-formyltetrahydrofolate dehydrogenase	Aldh1l2	0.15
17	P47738	Aldehyde dehydrogenase, mitochondrial	Aldh2	0.64
18	Q8BWF0	Succinate-semialdehyde dehydrogenase, mitochondrial	Aldh5a1	0.60
19	Q9EQ20	Methylmalonate-semialdehyde dehydrogenase [acylating], mitochondrial	Aldh6a1	0.63
20	P97449	Aminopeptidase N	Anpep	0.00
21	Q9D5T0	ATPase family AAA domain-containing protein 1	Atad1	0.40
22	H3BKI6	ATPase family AAA domain-containing protein 3	Atad3a	0.81
23	P14094	Sodium/potassium-transporting ATPase subunit beta-1	Atp1b1	0.92
24	J3KMM5	Calcium-transporting ATPase	Atp2a2	0.89
25	A2AKU9	ATP synthase subunit gamma	Atp5c1	0.73
26	D3Z7S4	ATP synthase subunit delta, mitochondrial	Atp5d	0.82

27	P56382	ATP synthase subunit epsilon, mitochondrial	Atp5e	0.80
28	D6RGL7	ATP synthase F(0) complex subunit B1, mitochondrial	Atp5f1	0.38
29	Q9DCX2	ATP synthase subunit d, mitochondrial	Atp5h	0.56
30	P97450	ATP synthase-coupling factor 6, mitochondrial	Atp5j	0.80
31	F8WHP8	ATP synthase subunit f, mitochondrial	Atp5j2	0.62
32	Q9CPQ8	ATP synthase subunit g, mitochondrial	Atp5l	0.84
33	E9QM21	Bcl-2 homologous antagonist/killer	Bak1	0.00
34	D3Z7C8	Branched-chain-amino-acid aminotransferase	Bcat2	0.49
35	O55028	[3-methyl-2-oxobutanoate dehydrogenase [lipoamide]]kinase, mitochondrial	Bckdk	0.27
36	P59017	Bcl-2-like protein 13	Bcl2l13	0.58
37	Q9CZP5	Mitochondrial chaperone BCS1	Bcs1l	0.28
38	P35564	Calnexin	Canx	0.00
39	P24270	Catalase	Cat	0.34
40	D6RJ70	Kynurenine--oxoglutarate transaminase 3	Ccbl2	0.28
41	Q3URS9	Coiled-coil domain-containing protein 51	Ccdc51	0.40
42	Q8C3X2	Coiled-coil domain-containing protein 90B, mitochondrial	Ccdc90b	0.22
43	Q9CRB9	MICOS complex subunit Mic19	Chchd3	0.90
44	P07310	Creatine kinase M-type	Ckm	0.63
45	E9Q3U7	Cytochrome c oxidase assembly protein COX16 homolog, mitochondrial	Cox16	0.00
46	M0QWX2	Cytochrome c oxidase subunit 4 isoform 1, mitochondrial	Cox4i1	0.55
47	P12787	Cytochrome c oxidase subunit 5A, mitochondrial	Cox5a	0.43
48	Q9D881	Protein Gm11273	Cox5b	0.50
49	Q9CPQ1	Cytochrome c oxidase subunit 6C	Cox6c	0.40
50	P56392	Cytochrome c oxidase subunit 7A1, mitochondrial	Cox7a1	0.48
51	P48771	Cytochrome c oxidase subunit 7A2, mitochondrial	Cox7a2	0.83
52	Q99KD6	Cox7a2l protein	Cox7a2l	0.69
53	B8JJA9	Cytochrome c oxidase subunit 7C, mitochondrial	Cox7c	0.40
54	Q9WVJ3	Carboxypeptidase Q	Cpq	0.19
55	Q9CQX2	Cytochrome b5 type B	Cyb5b	0.33
56	Q9D0M3	Cytochrome c1, heme protein, mitochondrial	Cyc1	0.69
57	D3ZFQ8	Cytochrome c-1 (Predicted), isoform CRA_c	Cyc1	0.00
58	P61804	Dolichyl-diphosphooligosaccharide--protein glycosyltransferase subunit DAD1	Dad1	0.00
59	P53395	Lipoamide acyltransferase component of branched-chain alpha-keto acid dehydrogenase complex, mitochondrial	Dbt	0.45
60	O54734	Dolichyl-diphosphooligosaccharide--protein glycosyltransferase 48 kDa subunit	Ddost	0.00
61	Q8BMF4	Dihydrolipoyllysine-residue acetyltransferase component of pyruvate dehydrogenase complex, mitochondrial	Dlat	0.67
62	E9Q8B3	DnaJ homolog subfamily C member 11	Dnajc11	0.79
63	O35459	Delta(3,5)-Delta(2,4)-dienoyl-CoA isomerase, mitochondrial	Ech1	0.58
64	Q9QZH6	Evolutionarily conserved signaling intermediate in Toll pathway, mitochondrial	Ecsit	0.00
65	P17182	Alpha-enolase	Eno1	0.80

66	Q3U7R1	Extended synaptotagmin-1	Esyt1	0.50
67	Q9CR59	Growth arrest and DNA damage-inducible proteins-interacting protein 1	Gadd45gip1	0.00
68	Q91VC9	Growth hormone-inducible transmembrane protein	Ghitm	0.00
69	Q64516	Glycerol kinase	Gk	0.26
70	Q9WU65	Glycerol kinase 2	Gk2	0.00
71	P26443	Glutamate dehydrogenase 1, mitochondrial	Glud1	0.69
72	P05201	Aspartate aminotransferase, cytoplasmic	Got1	0.50
73	Q76LV0	Glutathione peroxidase	Gpx4	0.67
74	P47791	Glutathione reductase, mitochondrial	Gsr	0.67
75	Q9DCM2	Glutathione S-transferase kappa 1	Gstk1	0.30
76	Q8BMS1	Trifunctional enzyme subunit alpha, mitochondrial	Hadha	0.79
77	Q99JY0	Trifunctional enzyme subunit beta, mitochondrial	Hadhb	0.68
78	G3UXK7	Cytochrome c-type heme lyase	Hccs	0.80
79	Q8CGP5	Histone H2A type 1-F	Hist1h2af	0.00
80	G3UVV4	Hexokinase-1	Hk1	0.63
81	E9Q5B5	Hexokinase-2	Hk2	0.18
82	P51660	Peroxisomal multifunctional enzyme type 2	Hsd17b4	0.38
83	B1AX78	Hydroxysteroid dehydrogenase-like protein 2	Hsdl2	0.91
84	P08113	Endoplasmin	Hsp90b1	0.61
85	P38647	Stress-70 protein, mitochondrial	Hspa9	0.75
86	P63038	60 kDa heat shock protein, mitochondrial	Hspd1	0.69
87	E9PWN2	Isoleucine--tRNA ligase, mitochondrial	Iars2	0.00
88	Q9D6R2	Isocitrate dehydrogenase [NAD]subunit alpha, mitochondrial	Idh3a	0.96
89	Q91VA7	Isocitrate dehydrogenase [NAD]subunit, mitochondrial	Idh3b	0.57
90	P70404	Isocitrate dehydrogenase [NAD]subunit gamma 1, mitochondrial	Idh3g	0.78
91	E9Q800	MICOS complex subunit Mic60	Immt	0.86
92	P85094	Isochorismatase domain-containing protein 2A, mitochondrial	Isoc2a	0.87
93	P04104	Keratin, type II cytoskeletal 1	Krt1	0.78
94	A2A513	Keratin, type I cytoskeletal 10	Krt10	0.77
95	Q61781	Keratin, type I cytoskeletal 14	Krt14	0.57
96	Q9QWL7	Keratin, type I cytoskeletal 17	Krt17	0.53
97	Q3TTY5	Keratin, type II cytoskeletal 2 epidermal	Krt2	0.72
98	Q922U2	Keratin, type II cytoskeletal 5	Krt5	0.73
99	P11679	Keratin, type II cytoskeletal 8	Krt8	0.89
100	Q9CPY7	Cytosol aminopeptidase	Lap3	0.38
101	Q9Z2I0	LETM1 and EF-hand domain-containing protein 1, mitochondrial	Letm1	0.48
102	Q8CGK3	Lon protease homolog, mitochondrial	Lonp1	0.49
103	Q6PB66	Leucine-rich PPR motif-containing protein, mitochondrial	Lrpprc	0.60
104	Q8VCF0	Mitochondrial antiviral-signaling protein	Mavs	0.00
105	Q99MR8	Methylcrotonoyl-CoA carboxylase subunit alpha, mitochondrial	Mccc1	0.66
106	Q3ULD5	Methylcrotonoyl-CoA carboxylase beta chain, mitochondrial	Mccc2	0.44
107	Q9CXD6	Mitochondrial calcium uniporter regulator 1	Mcur1	0.43
108	E9PZP7	Malic enzyme	Me3	0.36
109	Q9CPU4	Microsomal glutathione S-transferase 3	Mgst3	0.90

110	Q99J39	Malonyl-CoA decarboxylase, mitochondrial	Mlycd	0.42
111	P56379	6.8 kDa mitochondrial proteolipid	Mp68	0.33
112	Q9DB15	39S ribosomal protein L12, mitochondrial	Mrpl12	0.00
113	F8WHN1	39S ribosomal protein L15, mitochondrial	Mrpl15	0.75
114	O35972	39S ribosomal protein L23, mitochondrial	Mrpl23	0.64
115	Q921S7	39S ribosomal protein L37, mitochondrial	Mrpl37	0.47
116	Q9CPX7	28S ribosomal protein S16, mitochondrial	Mrps16	0.75
117	Q99N84	28S ribosomal protein S18b, mitochondrial	Mrps18b	0.00
118	P58059	28S ribosomal protein S21, mitochondrial	Mrps21	0.50
119	Q9CXW2	28S ribosomal protein S22, mitochondrial	Mrps22	0.29
120	Q9CQV5	28S ribosomal protein S24, mitochondrial	Mrps24	0.33
121	Q80ZS3	28S ribosomal protein S26, mitochondrial	Mrps26	0.00
122	Q8BK72	28S ribosomal protein S27, mitochondrial	Mrps27	0.40
123	Q61733	28S ribosomal protein S31, mitochondrial	Mrps31	0.00
124	Q9JIK9	28S ribosomal protein S34, mitochondrial	Mrps34	0.36
125	Q99N87	28S ribosomal protein S5, mitochondrial	Mrps5	0.67
126	Q9D7N3	28S ribosomal protein S9, mitochondrial	Mrps9	0.70
127	Q9D6Y7	Mitochondrial peptide methionine sulfoxide reductase	Msra	0.64
128	P03930	ATP synthase protein 8	mt-Atp8	0.65
129	Q791T5	Mitochondrial carrier homolog 1	Mtch1	0.00
130	A2AFW6	Mitochondrial carrier homolog 2	Mtch2	0.86
131	Q9MD68	Cytochrome c oxidase subunit 1	mt-Co1	0.20
132	P00405	Cytochrome c oxidase subunit 2	mt-Co2	0.00
133	P00158	Cytochrome b	mt-Cytb	0.60
134	D3YVW0	Metaxin-1	Mtx1	0.65
135	Q62425	Cytochrome c oxidase subunit NDUFA4	Ndufa4	0.76
136	A2AQ17	Complex I intermediate-associated protein 30, mitochondrial	Ndufaf1	0.00
137	Q9JKL4	NADH dehydrogenase [ubiquinone]1 alpha subcomplex assembly factor 3	Ndufaf3	0.55
138	Q9D1H6	NADH dehydrogenase [ubiquinone]1 alpha subcomplex assembly factor 4	Ndufaf4	0.00
139	Q9JHW2	Omega-amidase NIT2	Nit2	0.63
140	Q3TL44	NLR family member X1	Nlrx1	0.36
141	P15532	Nucleoside diphosphate kinase A	Nme1	0.20
142	Q01768	Nucleoside diphosphate kinase B	Nme2	0.17
143	Q9WV85	Nucleoside diphosphate kinase 3	Nme3	0.00
144	E9Q8F4	NAD(P) transhydrogenase, mitochondrial	Nnt	0.51
145	Q60597	2-oxoglutarate dehydrogenase, mitochondrial	Ogdh	0.80
146	E9Q7L0	Protein Ogdhl	Ogdhl	0.53
147	E0CXD1	Dynamin-like 120 kDa protein, mitochondrial	Opa1	0.44
148	Q505D7	Optic atrophy 3 protein homolog	Opa3	0.94
149	P35487	Pyruvate dehydrogenase E1 component subunit alpha, testis-specific form, mitochondrial	Pdha2	0.00
150	Q9D0F9	Phosphoglucomutase-1	Pgm2	0.00
151	P52480	Pyruvate kinase PKM	Pkm	0.14
152	P61014	Cardiac phospholamban	Pln	0.00
153	Q9CXT8	Mitochondrial-processing peptidase subunit beta	Pmpcb	0.63

154	G3UZJ4	Peroxiredoxin-5, mitochondrial	Prdx5	0.53
155	Q14C51	Pentatricopeptide repeat domain-containing protein 3, mitochondrial	Ptcd3	0.93
156	Q8BWM0	Prostaglandin E synthase 2	Ptges2	0.86
157	Q922Q4	Pyrroline-5-carboxylate reductase 2	Pycr2	0.00
158	P61027	Ras-related protein Rab-10	Rab10	0.50
159	Q3U186	Probable arginine--tRNA ligase, mitochondrial	Rars2	0.00
160	Q8JZN7	Mitochondrial Rho GTPase 2	Rhot2	0.00
161	Q8CI78	Required for meiotic nuclear division protein 1 homolog	Rmnd1	0.53
162	A2ACG7	Dolichyl-diphosphooligosaccharide--protein glycosyltransferase subunit 2	Rpn2	0.00
163	Q3U3G8	Serine hydrolase-like protein	Serhl	0.33
164	D6RHN5	Serpin B13	Serpinb13	0.00
165	Q8BH59	Calcium-binding mitochondrial carrier protein Aralar1	Slc25a12	0.64
166	Q9QXX4	Calcium-binding mitochondrial carrier protein Aralar2	Slc25a13	0.71
167	Q60714	Long-chain fatty acid transport protein 1	Slc27a1	0.00
168	P04919	Band 3 anion transport protein	Slc4a1	0.68
169	P08228	Superoxide dismutase [Cu-Zn]	Sod1	0.40
170	F6ZKZ3	Sulfide:quinone oxidoreductase, mitochondrial	Sqrdl	0.43
171	B0QZS8	Mitochondrial import inner membrane translocase subunit Tim22	Timm22	0.60
172	Q8BUY5	Complex I assembly factor TIMMDC1, mitochondrial	Timmdc1	0.54
173	Q8VD26	Transmembrane protein 143	Tmem143	0.65
174	Q9D938	Transmembrane protein 160	Tmem160	0.00
175	Q9CR76	Transmembrane protein 186	Tmem186	0.50
176	Q9CPQ3	Mitochondrial import receptor subunit TOM22 homolog	Tomm22	0.52
177	Q9QYA2	Mitochondrial import receptor subunit TOM40 homolog	Tomm40	0.43
178	D3YXS8	Mitochondrial import receptor subunit TOM40B	Tomm40l	0.20
179	B1AXP6	Mitochondrial import receptor subunit TOM5 homolog	Tomm5	0.00
180	Q9CZW5	Mitochondrial import receptor subunit TOM70	Tomm70a	0.00
181	Q9CQB4	Cytochrome b-c1 complex subunit 7	Uqcrb	0.59
182	P99028	Cytochrome b-c1 complex subunit 6, mitochondrial	Uqcrh	0.43
183	Q78IK2	Up-regulated during skeletal muscle growth protein 5	Usmg5	0.59
184	Q01853	Transitional endoplasmic reticulum ATPase	Vcp	0.00
185	F2Z471	Voltage-dependent anion-selective channel protein 1	Vdac1	0.67
186	Q60930	Voltage-dependent anion-selective channel protein 2	Vdac2	0.66
187	J3QMG3	Voltage-dependent anion-selective channel protein 3	Vdac3	0.60
188	Q8CC88	von Willebrand factor A domain-containing protein 8	Vwa8	0.54
189	O88967	ATP-dependent zinc metalloprotease YME1L1	Yme1l1	0.00

Suppl. Table 11. Mitochondrial proteins associated with OPA1 that decrease upon apoptotic cristae remodeling			
A/A	**ACCESSION NUMBER**	**PROTEIN NAME**	**GENE**
1	P61922	4-aminobutyrate aminotransferase, mitochondrial	Abat
2	Q61102	ATP-binding cassette sub-family B member 7, mitochondrial	Abcb7
3	Q9CXJ4	ATP-binding cassette sub-family B member 8, mitochondrial	Abcb8
4	A2ALN0	ATP-binding cassette sub-family D member 1	Abcd1
5	P55096	ATP-binding cassette sub-family D member 3	Abcd3
6	D3YTQ5	Acyl-CoA dehydrogenase family member 11	Acad11
7	Q8JZN5	Acyl-CoA dehydrogenase family member 9, mitochondrial	Acad9
8	Q9D0L4	Uncharacterized aarF domain-containing protein kinase 1	Adck1
9	Q9ESW4	Acylglycerol kinase, mitochondrial	Agk
10	Q9CZS1	Aldehyde dehydrogenase X, mitochondrial	Aldh1b1
11	D3Z6B9	Mitochondrial 10-formyltetrahydrofolate dehydrogenase	Aldh1l2
12	P47738	Aldehyde dehydrogenase, mitochondrial	Aldh2
13	Q8BWF0	Succinate-semialdehyde dehydrogenase, mitochondrial	Aldh5a1
14	Q9EQ20	Methylmalonate-semialdehyde dehydrogenase [acylating], mitochondrial	Aldh6a1
15	Q9D5T0	ATPase family AAA domain-containing protein 1	Atad1
16	A2AKU9	ATP synthase subunit gamma	Atp5c1
17	D6RGL7	ATP synthase F(0) complex subunit B1, mitochondrial	Atp5f1
18	Q9DCX2	ATP synthase subunit d, mitochondrial	Atp5h
19	F8WHP8	ATP synthase subunit f, mitochondrial	Atp5j2
20	Q9CPQ8	ATP synthase subunit g, mitochondrial	Atp5l
21	D3Z7C8	Branched-chain-amino-acid aminotransferase	Bcat2
22	O55028	[3-methyl-2-oxobutanoate dehydrogenase [lipoamide]]kinase, mitochondrial	Bckdk
23	P59017	Bcl-2-like protein 13	Bcl2l13
24	Q9CZP5	Mitochondrial chaperone BCS1	Bcs1l
25	P24270	Catalase	Cat
26	Q3URS9	Coiled-coil domain-containing protein 51	Ccdc51
27	Q8C3X2	Coiled-coil domain-containing protein 90B, mitochondrial	Ccdc90b
28	M0QWX2	Cytochrome c oxidase subunit 4 isoform 1, mitochondrial	Cox4i1
29	P12787	Cytochrome c oxidase subunit 5A, mitochondrial	Cox5a
30	Q9D881	Protein Gm11273	Cox5b
31	Q9CPQ1	Cytochrome c oxidase subunit 6C	Cox6c
32	P56392	Cytochrome c oxidase subunit 7A1, mitochondrial	Cox7a1
33	B8JJA9	Cytochrome c oxidase subunit 7C, mitochondrial	Cox7c
34	Q9WVJ3	Carboxypeptidase Q	Cpq
35	Q9CQX2	Cytochrome b5 type B	Cyb5b
36	D3ZFQ8	Cytochrome c-1 (Predicted), isoform CRA_c	Cyc1
37	Q9D0M3	Cytochrome c1, heme protein, mitochondrial	Cyc1
38	P53395	Lipoamide acyltransferase component of branched-chain alpha-keto acid dehydrogenase complex, mitochondrial	Dbt

39	O54734	Dolichyl-diphosphooligosaccharide--protein glycosyltransferase 48 kDa subunit	Ddost
40	O35459	Delta(3,5)-Delta(2,4)-dienoyl-CoA isomerase, mitochondrial	Ech1
41	Q9QZH6	Evolutionarily conserved signaling intermediate in Toll pathway, mitochondrial	Ecsit
42	Q64516	Glycerol kinase	Gk
43	Q9WU65	Glycerol kinase 2	Gk2
44	P26443	Glutamate dehydrogenase 1, mitochondrial	Glud1
45	P05201	Aspartate aminotransferase, cytoplasmic	Got1
46	Q76LV0	Glutathione peroxidase	Gpx4
47	P47791	Glutathione reductase, mitochondrial	Gsr
48	Q8BMS1	Trifunctional enzyme subunit alpha, mitochondrial	Hadha
49	Q99JY0	Trifunctional enzyme subunit beta, mitochondrial	Hadhb
50	G3UXK7	Cytochrome c-type heme lyase	Hccs
51	G3UVV4	Hexokinase-1	Hk1
52	E9Q5B5	Hexokinase-2	Hk2
53	P51660	Peroxisomal multifunctional enzyme type 2	Hsd17b4
54	P38647	Stress-70 protein, mitochondrial	Hspa9
55	P63038	60 kDa heat shock protein, mitochondrial	Hspd1
56	Q91VA7	Isocitrate dehydrogenase [NAD]subunit, mitochondrial	Idh3b
57	E9Q800	MICOS complex subunit Mic60	Immt
58	P04104	Keratin, type II cytoskeletal 1	Krt1
59	A2A513	Keratin, type I cytoskeletal 10	Krt10
60	Q61781	Keratin, type I cytoskeletal 14	Krt14
61	Q9QWL7	Keratin, type I cytoskeletal 17	Krt17
62	Q3TTY5	Keratin, type II cytoskeletal 2 epidermal	Krt2
63	Q922U2	Keratin, type II cytoskeletal 5	Krt5
64	P11679	Keratin, type II cytoskeletal 8	Krt8
65	Q9CPY7	Cytosol aminopeptidase	Lap3
66	Q9Z2I0	LETM1 and EF-hand domain-containing protein 1, mitochondrial	Letm1
67	Q8CGK3	Lon protease homolog, mitochondrial	Lonp1
68	Q6PB66	Leucine-rich PPR motif-containing protein, mitochondrial	Lrpprc
69	Q8VCF0	Mitochondrial antiviral-signaling protein	Mavs
70	Q99MR8	Methylcrotonoyl-CoA carboxylase subunit alpha, mitochondrial	Mccc1
71	Q3ULD5	Methylcrotonoyl-CoA carboxylase beta chain, mitochondrial	Mccc2
72	Q9CXD6	Mitochondrial calcium uniporter regulator 1	Mcur1
73	E9PZP7	Malic enzyme	Me3
74	Q9CPU4	Microsomal glutathione S-transferase 3	Mgst3
75	Q99J39	Malonyl-CoA decarboxylase, mitochondrial	Mlycd
76	P56379	6.8 kDa mitochondrial proteolipid	Mp68
77	Q9DB15	39S ribosomal protein L12, mitochondrial	Mrpl12
78	O35972	39S ribosomal protein L23, mitochondrial	Mrpl23
79	Q9CXW2	28S ribosomal protein S22, mitochondrial	Mrps22
80	Q8BK72	28S ribosomal protein S27, mitochondrial	Mrps27
81	Q9JIK9	28S ribosomal protein S34, mitochondrial	Mrps34
82	Q9D6Y7	Mitochondrial peptide methionine sulfoxide reductase	Msra

83	P03930	ATP synthase protein 8	mt-Atp8
84	A2AFW6	Mitochondrial carrier homolog 2	Mtch2
85	Q9MD68	Cytochrome c oxidase subunit 1	mt-Co1
86	P00405	Cytochrome c oxidase subunit 2	mt-Co2
87	P00158	Cytochrome b	mt-Cytb
88	D3YVW0	Metaxin-1	Mtx1
89	Q62425	Cytochrome c oxidase subunit NDUFA4	Ndufa4
90	Q9JKL4	NADH dehydrogenase [ubiquinone]1 alpha subcomplex assembly factor 3	Ndufaf3
91	Q9D1H6	NADH dehydrogenase [ubiquinone]1 alpha subcomplex assembly factor 4	Ndufaf4
92	Q9JHW2	Omega-amidase NIT2	Nit2
93	Q3TL44	NLR family member X1	Nlrx1
94	P15532	Nucleoside diphosphate kinase A	Nme1
95	Q01768	Nucleoside diphosphate kinase B	Nme2
96	Q9WV85	Nucleoside diphosphate kinase 3	Nme3
97	E9Q8F4	NAD(P) transhydrogenase, mitochondrial	Nnt
98	Q60597	2-oxoglutarate dehydrogenase, mitochondrial	Ogdh
99	E0CXD1	Dynamin-like 120 kDa protein, mitochondrial	Opa1
100	P52480	Pyruvate kinase PKM	Pkm
101	Q9CXT8	Mitochondrial-processing peptidase subunit beta	Pmpcb
102	G3UZJ4	Peroxiredoxin-5, mitochondrial	Prdx5
103	Q8BWM0	Prostaglandin E synthase 2	Ptges2
104	P61027	Ras-related protein Rab-10	Rab10
105	Q3U186	Probable arginine--tRNA ligase, mitochondrial	Rars2
106	Q8JZN7	Mitochondrial Rho GTPase 2	Rhot2
107	Q8CI78	Required for meiotic nuclear division protein 1 homolog	Rmnd1
108	Q3U3G8	Serine hydrolase-like protein	Serhl
109	Q8BH59	Calcium-binding mitochondrial carrier protein Aralar1	Slc25a12
110	Q9QXX4	Calcium-binding mitochondrial carrier protein Aralar2	Slc25a13
111	Q60714	Long-chain fatty acid transport protein 1	Slc27a1
112	P04919	Band 3 anion transport protein	Slc4a1
113	P08228	Superoxide dismutase [Cu-Zn]	Sod1
114	F6ZKZ3	Sulfide:quinone oxidoreductase, mitochondrial	Sqrdl
115	B0QZS8	Mitochondrial import inner membrane translocase subunit Tim22	Timm22
116	Q8BUY5	Complex I assembly factor TIMMDC1, mitochondrial	Timmdc1
117	Q8VD26	Transmembrane protein 143	Tmem143
118	Q9CPQ3	Mitochondrial import receptor subunit TOM22 homolog	Tomm22
119	Q9QYA2	Mitochondrial import receptor subunit TOM40 homolog	Tomm40
120	D3YXS8	Mitochondrial import receptor subunit TOM40B	Tomm40l
121	Q9CZW5	Mitochondrial import receptor subunit TOM70	Tomm70a
122	Q9CQB4	Cytochrome b-c1 complex subunit 7	Uqcrb
123	P99028	Cytochrome b-c1 complex subunit 6, mitochondrial	Uqcrh
124	Q78IK2	Up-regulated during skeletal muscle growth protein 5	Usmg5
125	F2Z471	Voltage-dependent anion-selective channel protein 1	Vdac1
126	Q60930	Voltage-dependent anion-selective channel protein 2	Vdac2
127	J3QMG3	Voltage-dependent anion-selective channel protein 3	Vdac3

128	Q8CC88	von Willebrand factor A domain-containing protein 8	Vwa8

Suppl. Table 12. All the mitochondrial proteins that decrease after cBID^{wt}

A/A	Spot	Accession Number	Protein Name	Gene	Fold change
1	A1-2	E9Q7L0	Protein Ogdhl	Ogdhl	1.304
2	A1-2	P00507	Aspartate aminotransferase, mitochondrial	Got2	1.296
3	A3-4	P31000	Vimentin	Vim	2.426
4	A3-4	Q8VDD5	Myosin-9	Myh9	2.225
5	A3-4	Q3TCU5	Tapasin	Tapbp	1.755
6	A3-4	Q99KI0	Aconitate hydratase, mitochondrial	Aco2	1.750
7	A3-4	P48771	Cytochrome c oxidase subunit 7A2, mitochondrial	Cox7a2	1.667
8	A3-4	Q8BMS1	Trifunctional enzyme subunit alpha, mitochondrial	Hadha	1.662
9	A3-4	Q9CQL5	39S ribosomal protein L18, mitochondrial	Mrpl18	1.554
10	A3-4	P27773	Protein disulfide-isomerase A3	Pdia3	1.504
11	A3-4	Q8BGH2	Sorting and assembly machinery component 50 homolog	Samm50	1.491
12	A3-4	P49432	Pyruvate dehydrogenase E1 component subunit beta, mitochondrial	Pdhb	1.398
13	A3-4	P08249	Malate dehydrogenase, mitochondrial	Mdh2	1.355
14	A3-4	D3ZPP9	Similar to RIKEN cDNA 1110007C09 (Predicted), isoform CRA_a	BinCARD	1.337
15	A3-4	Q7TT47	Paraplegin	Spg7	1.316
16	A3-4	P19783	Cytochrome c oxidase subunit 4 isoform 1, mitochondrial	Cox4i1	1.295
17	A3-4	O55143	Sarcoplasmic/endoplasmic reticulum calcium ATPase 2	Atp2a2	1.229
18	A3-4	Q61833	Ribophorin	Rpn2	1.221
19	A3-4	P08461	Dihydrolipoyllysine-residue acetyltransferase component of pyruvate dehydrogenase complex, mitochondrial	Dlat	1.210
20	A5-6	Q80X68	Citrate synthase	Cs	2.479
21	A5-6	Q63965	Sideroflexin-1	Sfxn1	1.921
22	A5-6	A9UMV9	RCG37550, isoform CRA_a	Ndufa7	1.913
23	A5-6	P15178	Aspartate--tRNA ligase, cytoplasmic	Dars	1.757
24	A5-6	P68033	Actin, alpha cardiac muscle 1	Actc1	1.727
25	A5-6	Q8BGH2	Sorting and assembly machinery component 50 homolog	Samm50	1.510
26	A5-6	Q9Z1P6	NADH dehydrogenase [ubiquinone]1 alpha subcomplex subunit 7	Ndufa7	1.473
27	A5-6	P70565	Plakoglobin	Jup	1.470
28	A5-6	F1LW77	RAB33B, member of RAS oncogene family (Predicted), isoform CRA_b	Rab33b	1.421

29	A5-6	Q8C2Z6	Putative uncharacterized protein	Chchd6	1.388
30	A5-6	Q9D8L3	Translocon-associated protein subunit delta	Ssr4	1.369
31	A5-6	Q5BK63	NADH dehydrogenase [ubiquinone]1 alpha subcomplex subunit 9, mitochondrial	Ndufa9	1.356
32	A5-6	Q8BMR3	Dolichyl-diphosphooligosaccharide--protein glycosyltransferase subunit 1	Rpn1	1.328
33	A5-6	Q8C454	Putative uncharacterized protein	Mtx2	1.308
34	A5-6	Q7TP78	Protein Ndufa8	Ndufa8	1.308
35	A5-6	Q3UJW1	Putative uncharacterized protein	Aldh2	1.266
36	A5-6	Q9CPP6	NADH dehydrogenase [ubiquinone]1 alpha subcomplex subunit 5	Ndufa5	1.262
37	A5-6	O55143	Sarcoplasmic/endoplasmic reticulum calcium ATPase 2	Atp2a2	1.248
38	A5-6	P27773	Protein disulfide-isomerase A3	Pdia3	1.246
39	A5-6	Q8BFR5	Elongation factor Tu, mitochondrial	Tufm	1.235
40	A5-6	Q61833	Ribophorin	Rpn2	1.204
41	A7	Q99KI0	Aconitate hydratase, mitochondrial	Aco2	2.558
42	A7	Q6P3V9	Ribosomal protein L4	Rpl4	2.549
43	A7	Q80X68	Citrate synthase	Cs	2.406
44	A7	Q62261	Spectrin beta chain, non-erythrocytic 1	Sptbn1	2.048
45	A7	P27773	Protein disulfide-isomerase A3	Pdia3	2.027
46	A7	Q6PHC1	Eno1 protein	Eno1	2.023
47	A7	Q8BMS1	Trifunctional enzyme subunit alpha, mitochondrial	Hadha	1.819
48	A7	Q7TP78	Protein Ndufa8	Ndufa8	1.764
49	A7	Q60587	Trifunctional enzyme subunit beta, mitochondrial	Hadhb	1.650
50	A7	E9PVS5	MICOS complex subunit Mic60	Mic60	1.380
51	A7	B1ASE2	ATP synthase subunit d, mitochondrial	Atp5h	1.392
52	A7	P19234	NADH dehydrogenase [ubiquinone]flavoprotein 2, mitochondrial	Ndufv2	1.323
53	A7	Q8BFR5	Elongation factor Tu, mitochondrial	Tufm	1.299
54	A7	Q02253	Methylmalonate-semialdehyde dehydrogenase [acylating], mitochondrial	Aldh6a1	1.284
55	A7	P63038	60 kDa heat shock protein, mitochondrial	Hspd1	1.280
56	A7	D3Z0L4	MICOS complex subunit Mic19	Chchd3	1.272
57	A7	Q03265	ATP synthase subunit alpha, mitochondrial	Atp5a1	1.267
58	A7	Q3UZQ3	Elongation factor 1-alpha	Eef1a1	1.264
59	A7	F1LXA0	Protein LOC100910710	Ndufa12	1.254
60	A7	A9UMV9	RCG37550, isoform CRA_a	Ndufa7	1.252
61	A7	P00507	Aspartate aminotransferase, mitochondrial	Got2	1.231
62	A7	Q3U9G2	Putative uncharacterized protein	Hspa5	1.230

Suppl. Table 13. All the proteins that decrease during apoptotic cristae remodeling				
A/A	**Spot**	**Accession Number**	**Protein Name**	**Gene**
1	A1-2	P00507	Aspartate aminotransferase, mitochondrial	Got2
2	A1-2	E9Q7L0	Protein Ogdhl	Ogdhl
3	A3-4	Q99KI0	Aconitate hydratase, mitochondrial	Aco2
4	A3-4	O55143	Sarcoplasmic/endoplasmic reticulum calcium ATPase 2	Atp2a2
5	A3-4	P56480	ATP synthase subunit beta, mitochondrial	Atp5b
6	A3-4	P19783	Cytochrome c oxidase subunit 4 isoform 1, mitochondrial	Cox4i1
7	A3-4	P48771	Cytochrome c oxidase subunit 7A2, mitochondrial	Cox7a2
8	A3-4	P08461	Dihydrolipoyllysine-residue acetyltransferase component of pyruvate dehydrogenase complex, mitochondrial	Dlat
9	A3-4	Q8BMS1	Trifunctional enzyme subunit alpha, mitochondrial	Hadha
10	A3-4	E9Q800	MICOS complex subunit Mic60	Immt
11	A3-4	P08249	Malate dehydrogenase, mitochondrial	Mdh2
12	A3-4	Q9CQL5	39S ribosomal protein L18, mitochondrial	Mrpl18
13	A3-4	Q8VDD5	Myosin-9	Myh9
14	A3-4	P49432	Pyruvate dehydrogenase E1 component subunit beta, mitochondrial	Pdhb
15	A3-4	P27773	Protein disulfide-isomerase A3	Pdia3
16	A3-4	D3ZPP9	Similar to RIKEN cDNA 1110007C09 (Predicted), isoform CRA_a	BinCARD
17	A3-4	Q61833	Ribophorin	Rpn2
18	A3-4	Q7TT47	Paraplegin	Spg7
19	A3-4	Q3TCU5	Tapasin	Tapbp
20	A3-4	P31000	Vimentin	Vim
21	A5-6	P68033	Actin, alpha cardiac muscle 1	Actc1
22	A5-6	Q3UJW1	Putative uncharacterized protein	Aldh2
23	A5-6	Q8C2Z6	Putative uncharacterized protein	Chchd6
24	A5-6	Q80X68	Citrate synthase	Cs
25	A5-6	P15178	Aspartate--tRNA ligase, cytoplasmic	Dars
26	A5-6	P70565	Plakoglobin	Jup
27	A5-6	Q8C454	Putative uncharacterized protein	Mtx2
28	A5-6	Q9CPP6	NADH dehydrogenase [ubiquinone]1 alpha subcomplex subunit 5	Ndufa5
29	A5-6	Q9Z1P6	NADH dehydrogenase [ubiquinone]1 alpha subcomplex subunit 7	Ndufa7
30	A5-6	Q7TP78	Protein Ndufa8	Ndufa8
31	A5-6	Q5BK63	NADH dehydrogenase [ubiquinone]1 alpha subcomplex subunit 9, mitochondrial	Ndufa9
32	A5-6	P27773	Protein disulfide-isomerase A3	Pdia3
33	A5-6	F1LW77	RAB33B, member of RAS oncogene family (Predicted), isoform CRA_b	Rab33b
34	A5-6	Q8BMR3	Dolichyl-diphosphooligosaccharide--protein glycosyltransferase subunit 1	Rpn1
35	A5-6	Q61833	Ribophorin	Rpn2

36	A5-6	Q63965	Sideroflexin-1	Sfxn1
37	A5-6	Q9D8L3	Translocon-associated protein subunit delta	Ssr4
38	A5-6	Q8BFR5	Elongation factor Tu, mitochondrial	Tufm
39	A7	Q99KI0	Aconitate hydratase, mitochondrial	Aco2
40	A7	Q02253	Methylmalonate-semialdehyde dehydrogenase [acylating], mitochondrial	Aldh6a1
41	A7	Q03265	ATP synthase subunit alpha, mitochondrial	Atp5a1
42	A7	B1ASE2	ATP synthase subunit d, mitochondrial	Atp5h
43	A7	Q8BMK4	Cytoskeleton-associated protein 4	Ckap4
44	A7	Q80X68	Citrate synthase	Cs
45	A7	Q3UZQ3	Elongation factor 1-alpha	Eef1a1
46	A7	Q6PHC1	Eno1 protein	Eno1
47	A7	P00507	Aspartate aminotransferase, mitochondrial	Got2
48	A7	Q3U9G2	Putative uncharacterized protein	Hspa5
49	A7	P63038	60 kDa heat shock protein, mitochondrial	Hspd1
50	A7	E9PVS5	MICOS complex subunit Mic60	Immt
51	A7	F1LXA0	Protein LOC100910710	Ndufa12
52	A7	A9UMV9	RCG37550, isoform CRA_a	Ndufa7
53	A7	Q7TP78	Protein Ndufa8	Ndufa8
54	A7	Q5BK63	NADH dehydrogenase [ubiquinone]1 alpha subcomplex subunit 9, mitochondrial	Ndufa9
55	A7	P19234	NADH dehydrogenase [ubiquinone]flavoprotein 2, mitochondrial	Ndufv2
56	A7	P27773	Protein disulfide-isomerase A3	Pdia3
57	A7	Q6P3V9	Ribosomal protein L4	Rpl4
58	A7	Q8BMR3	Dolichyl-diphosphooligosaccharide--protein glycosyltransferase subunit 1	Rpn1
59	A7	Q62261	Spectrin beta chain, non-erythrocytic 1	Sptbn1
60	A7	Q8BFR5	Elongation factor Tu, mitochondrial	Tufm

2.2. Mammalian mitochondrial cristae biogenesis is regulated by Mitofilin (Mic60)-OPA1 complexes that are eliminated during apoptosis

Mammalian mitochondrial cristae biogenesis is regulated by Mitofilin (Mic60)-OPA1 complexes that are eliminated during apoptosis

Christina Glytsou[1], Enrique Calvo[2], Irene Anastasia[1], Sara Cogliati[1,2], Andrea Raimondi[3], Norihito Shintani[4], Marta Loureiro[2], Jesùs Vazquez[2], Luca Pellegrini[5], Jose Antonio Enriquez[2], and Luca Scorrano[1, 6*], Maria Eugenia Soriano[1*]

[1] Department of Biology, University of Padova, Padova, Italy

[2] Centro Nacional de Investigaciones Cardiovasculares Carlos III, Madrid, Spain

[3] San Raffaele Scientific Institute, Imaging Research Center, Milano, Italy

[4] Advanced Pharmaco-science, Graduate School of Pharmaceutical Sciences, Osaka University, Osaka, Japan

[5] Department of Molecular Biology, Medical Biochemistry and Pathology, Université Laval, Quebec, Canada

[6] Dulbecco-Telethon Institute, Venetian Institute of Molecular Medicine, Padova, Italy

Address correspondence to Luca Scorrano: luca.scorrano@unipd.it and Maria Eugenia Soriano: mariaeugenia.soriano@unipd.it

ABSTRACT

Optic atrophy 1 (OPA1) and the core MICOS complex member, Mic60, are inner mitochondrial membrane proteins both involved in shaping mitochondrial cristae; however, it is unclear whether they cooperate or they operate in independent functional pathways. Here using proteomics, biochemical analysis and electron microscopy we show that OPA1 and Mic60 interact, composing high molecular weight complexes, which are essential for the cristae junction formation and are targeted early upon apoptotic cristae remodeling. Similarly, another MICOS component, Mic19, shares common complexes, suggesting a novel role of mammalian MICOS on cristae shape modulation during programmed cell death. Nevertheless, unlike OPA1, Mic60 does not regulate the width of cristae lumen or cristae junction mouth in physiological or apoptotic conditions. Overall, our data uncover the interplay between OPA1 and MICOS complex for the formation of cristae junctions and dissociate the mechanisms of cristae junction biogenesis from the control of cristae lumen width.

INTRODUCTION

Mitochondria regulate the energy status of the cell while coordinating a variety of other key cellular processes, like differentiation, intermediary metabolism, calcium homeostasis, and cell death (Kasahara et al., 2013). Such multiplicity of functions is possible because of the unique ultrastructural complexity of the organelle, organized in five sub-compartments: the outer membrane (OMM), the intermembrane space (IMS), the inner boundary membrane, the cristae, and the matrix; this organization allows the distribution of biochemical processes via the sub-compartmentalization of the proteins that attain and regulate them. For instance, the cristae are responsible for mitochondrial respiration because they host the oxidative phosphorylation components and create a microenvironment that, ultimately, allows their assembly in respiration-competent complexes and super-complexes (Acin-Perez et al., 2008; Acin-Perez and Enriquez, 2014). Therefore, cristae number and integrity dictate the bioenergetic capacity of the organelle, a concept emerged in the late '60s through the pioneering work of Charles Hackenbrock (Hackenbrock, 1966) and that has been recently validated in vivo using mouse genetic models (Cogliati et al., 2013; Varanita et al., 2015) .

Until recently, the cristae have been considered as a single ultrastructural component of the mitochondrion. However, functional and tomography electron microscopy studies have revealed a higher degree of structural complexity of this sub-compartment, whose function pivots on two key elements: the lumen and the cristae junction (Mannella, 2006; Mannella et al., 2013). The lumen is the space inside the invagination of the crista. Here, a critical functional element is the distance between the opposing faces of the IMM, the cristae lumen width (CLW), which controls RCS assembly and, in turn, mitochondrial respiration: the narrower the CLW, the higher the efficiency of oxidative phosphorylation

(Cogliati et al., 2013). The cristae junction (CJ) is the site at the top of the crista that separates its lumen from the IMS; in tomographic 3D reconstructions the CJ opens to the IMS in a 20-30 nm mouth that regulates the flow of metabolites (Mannella et al., 1994; Scorrano et al., 2002). During apoptosis the size of this CJ mouth increases, allowing the mobilization and passage of cytochrome c (cyt c) from the lumen to the IMS (Frezza et al., 2006; Scorrano et al., 2002). To date, it remains unclear whether changes in CLW and CJ mouth are coupled or independent events; however, their biogenesis and remodeling appear to share some common molecular mechanisms because both processes are regulated by the dynamin GTPase OPA1.

The mammalian OPA1 protein regulates steady-state cristae shape and apoptotic remodeling. Loss of OPA1 increases CLW, thereby decreasing mitochondrial respiration and sensitizing cells to intrinsic pro-apoptotic stimuli; instead, mild OPA1 overexpression decreases CL-width and delays CJ bore widening and cytochrome c release during apoptosis. OPA1 forms complexes of several hundreds kilo-Daltons that are eliminated during apoptosis, a finding that correlates with CLW and CJ bore remodeling during this process. In addition to OPA1, the mammalian mitochondrial protein Mic60 has also been shown to control cristae biogenesis. Mic60 is a key component of a large protein complex named MICOS (Mitochondrial contact site and cristae organizing system), which regulates CJ biogenesis from yeast to mammals. Neither OPA1 nor its yeast homolog, Mgm1p, is part of the MICOS complex. Therefore, it remains unsolved whether OPA1 and Mic60 participate in two distinct CJ biogenesis pathways or, instead, if they coordinate different steps of a single process that eludes our understanding.

The MICOS complex has been extensively characterized in yeast, where it exists as two independent MICOS sub-complexes: Mic27/Mic10/Mic12 and Mic60/Mic19. These two

sub-complexes independently localize to CJ and are connected via Mic19, which regulates sub-complex distribution. In mammals, the existence of these two-subcomplexes remains unexplored, but a homolog of Mic12 has not been found yet. Further, whereas genetic deletion of Mic10 in yeast causes the cristae to become stacked lamellar structures, similar to thylakoids in chloroplasts, silencing of its homolog in mammalian cells yields mitochondria with normal cristae (Li et al., 2015). These observations suggest that during vertebrate evolution the composition and regulation of the MICOS complex has changed, possibly to accommodate its recruitment into the process that widens the CJ mouth during apoptosis. Consistent with this possibility, silencing of Mic19 or Mic60, but not of Mic10, sensitizes cells to stimuli that trigger intrinsic apoptosis, a cellular program that, having emerged approx. 500 million years ago, is absent in yeast.

Here we used a combination of proteomics, electron tomography and functional analyses to unravel the crosstalk between OPA1 and the core MICOS complex component Mic60 in cristae biogenesis and remodeling. Our data indicate that mammalian Mic60 interacts with OPA1 to form high molecular weight complexes that are required to form CJs and that are eliminated during cristae remodeling to facilitate cytochrome c release during apoptosis. Our results identify a crosstalk between the core cristae biogenesis regulators and characterize the role of Mic60 during apoptotic cristae remodeling.

RESULTS

Yeast and Mammalian Mic60 are divergent orthologue proteins

It is well established that CJ remodeling during apoptosis regulates cyt c release, a notion that implies the recruitment of CJ proteins like OPA1 in this process at the onset of vertebrate evolution, when cyt c became a key activator of programmed cell death. However, the contribution of the core cristae biogenesis complex MICOS in cristae remodeling remains unresolved. In order to address this question, we first investigated whether the structure of yeast Mic60 and that of its vertebrate orthologue were conserved. A bioinformatics analysis indicated that the putative transmembrane helix (TMH) of yeast and mammalian Mic60 are divergent (Figure 1A). Per se, this finding is not unexpected because TMHs are typically poorly conserved; however, it is at odd with the fact that whereas the TMH of yeast Mic60 can form a highly structured hydrophobic α–helix, that of mammalian Mic60 is predicted to be poorly structured and hydrophobic, mostly because it contains two clusters of glycine residues. Furthermore, the TMH of Mic60 is strictly conserved from fish to man, a fact that supports the relevance of the differences between yeast and mammals Mic60 (Supplemental Figure 1A). This indicates that, in vertebrates only, the TMH is subjected to structural constraints that cannot be linked only to its membrane-anchoring function.

Evidence indicating that yeast and mammalian Mic60 are structurally unrelated proteins can also be inferred by the lack in the yeast protein of sequences that are conversely strictly conserved in all the vertebrate ones. These sequences span the middle domain of Mic60 and do not display any obvious homology with any other protein encoded by the mouse and human genome (Figure 1A and Supplemental Figure 1B), suggesting a strong purifying selection during vertebrate evolution. In unconstrained sequences evolving

neutrally, very few, if any, invariant residues would be expected to survive the 500 million years of evolution separating vertebrate orders, indicating that the conservation of the middle Mic60 domain was likely driven by functional constraints. In conclusion, whereas the C-terminal domain is conserved in all eukaryotic orthologues of Mic60 (Munoz-Gomez et al., 2015), a novel TMH and N-terminal domain emerged at the outset of vertebrate evolution (Supplemental Figures 1A and 1B), possibly to recruit Mic60 in a novel pathway or to confer to this CJ protein new partners and mechanisms of regulation, calling for an analysis of mammalian Mic60 function.

Mammalian Mic60 forms complexes that are eliminated during BID-induced cristae remodeling

Yeast and mammalian Mic60 form high molecular weight complexes (HMWC) (Guarani et al., 2015), but whether and how they change during metabolic, physiologic, or pathological processes remains unknown. Prompted by our bioinformatics analysis indicating a potential role for mammalian Mic60 in a higher eukaryotic process such as apoptosis, we decided to address if mammalian Mic60 HMWC change during apoptotic cristae remodeling when OPA1 containing HMWC are disassembled. Blue Native Gel Electrophoresis (BNGE) confirmed that Mic60 forms HMWC of 600-1000 kDa in purified mouse heart and liver mitochondria (Figure 1B). We next asked if these Mic60-containing complexes changed during apoptotic-cristae remodeling. To this end, protein complexes separated by BNGE from mouse heart mitochondria treated with recombinant BH3-only BCL-2 family member apoptosis activator cleaved BID (cBID) or with its cristae remodeling incompetent mutant $cBID^{KKAA}$ (Cogliati et al., 2013) were processed for mass spectrometry (MS) analysis. The color contour plot representation of the number of unique Mic60 and

Mic19 peptides identified by this semi-quantitative proteomic analysis in the different HMWC isolated from normal and apoptotic mitochondria showed that cBID, but not the cristae remodeling incompetent cBID^{KKAA} mutant greatly reduced the amount of Mic60 across the HMWC analyzed (Figure 1C). A quantitative proteomic analysis of mitochondrial complexes isolated from mouse adult fibroblasts (MAFs) after SILAC labeling (Supplemental Figure 2) confirmed that cBID, but not cBID^{KKAA}, caused a significant loss of a comprehensive set of Mic60 peptides in most of the Mic60-containing complexes (Figures 1D).

Since mammalian Mic60 interacts with Mic19 to regulate CJ biogenesis, we also asked whether Mic19 assembled and responded to apoptosis like Mic60. In BNGE Mic19 indeed formed HMWC migrating like the Mic60-containing ones (Figure 1B) and similarly targeted during cristae remodeling (Figures 1C and 1E). In conclusion, Mic60 and Mic19, two critical components of the mammalian MICOS, assemble into HMWC that are disrupted during apoptotic cristae remodeling.

Mic60 and OPA1 are part of the same complexes targeted during cristae remodeling

The discovery that Mic60 forms complexes that, like those of OPA1, are eliminated during cristae remodeling prompted us to investigate whether the two proteins interact and/or are part of the same complexes. To this end, we compared by BNGE and crosslinking analysis the migration pattern of Mic60- and OPA1-containing complexes. Interestingly, Mic60 and OPA1 were retrieved in HMWC with similar electrophoretic mobility and targeted during cBID induced cristae remodeling (Figure 2A and 2D). Then we turned to 3-dimension BN-BN-SDS-PAGE that allows the identification of proteins in detergent-resistant complexes (Figure 2B); immunoblotting of the 3rd dimension SDS gel

electrophoresis (SDS-GE) indicated that Mic60 was retrieved in the ~720 kDa OPA1 containing complex targeted during cristae remodeling (Cogliati et al., 2013) (Figure 2C). Indeed, a fraction of Mic60 co-immunoprecipitated with OPA1 (Figure 2E), further substantiating their interaction.

Given the physical interaction between Mic60 and OPA1, we next questioned whether both proteins are indispensable for Mic60/OPA1 complexes assembly. For this purpose, we turned to a genetic analysis to address the impact of *Opa1* acute ablation on Mic60-containing complexes. Upon adenoviral delivery of CRE recombinase to *Opa1*$^{flx/flx}$ mouse adult fibroblasts (MAFs) loss of *Opa1* largely abolished the HMW Mic60 complexes (Figure 2F, 2H and Supplementary Figure 3A); similarly, silencing of Mic60 lowered the amount of OPA1 HMWC (Figure 2G, 2I and Supplementary Figure 3B), indicating that the expression of both proteins is required for the formation of the Mic60/OPA1 complexes. In conclusion, a fraction of Mic60 exists in complex with OPA1 and the two proteins cooperatively form complexes eliminated during cristae remodeling.

Mic60 cooperates with OPA1 to regulate cristae biogenesis

The genetic and physical interaction between Mic60 and OPA1 prompted us to ask whether they regulate together cristae biogenesis and morphology. To this end, first we compared by electron microscopy (EM) the density of the cristae and of the CJ in Mic60-silenced cells, in *Opa1*-ablated cells, and in cells where we simultaneously silenced Mic60 and ablated Opa1 (Figures 3A-3B). Mic60 silencing or *Opa1* deletion reduced by 25% the number of cristae, and by 27% the number of CJ per cristae and 20% the number of CJ per mitochondrion (Figure 3C-3E); simultaneous silencing/deletion of these proteins does not have an additive effect on these parameters (Figure 3C-3E), suggesting that Mic60 and

OPA1 act on the same pathway and calling for an epistatic analysis. The results were further supported by quantification of the number of CJ per crista in 3D-reconstructed electron tomograms (Figures 6A and 6B).

When we silenced Mic60 in *Opa1*^{tg} MAFs, which mildly overexpress OPA1 (Figure 4A), cristae number and CJ density decreased, regardless of the higher level of expression of OPA1 (Figures 4B-4E). However, overexpression of Mic60 increases cristae and CJ density in cells expressing OPA1 but not in *Opa1*-ablated MAFs (Figure 5A-5D). We conclude that cristae biogenesis hinges on a mechanism that involves the formation of OPA1/Mic60 complexes (Figure 2).

Mic60 does not specify the width of the cristae lumen and of the cristae junction mouth

To investigate how Mic60 silencing reduces CJ density, we addressed whether Mic60 specifies the width of the cristae lumen and of the mouth of the CJ. To this goal, we returned to the *Opa1*$^{flx/flx}$ MAFs in which we silenced Mic60 in the presence or absence of OPA1 expression and measured these two parameters of the cristae.

Data showed that in the presence of normal levels of OPA1 expression, Mic60 silencing has a modest impact on CLW, increasing by 12% the distance between the opposite sides of the IMM that form the crista (Figure 3F). Silencing Mic60 in cells with higher level of OPA1 expression (*Opa1*^{tg} MAFs) does not increase CLW (Figure 4F); consistent with this observation, Mic60 overexpression per se also has no effect on CLW (Figure 5F). Taken together these findings indicate that Mic60 does not have a direct function on specifying the CLW, and that this parameter is uncoupled from the mechanism regulating the number of cristae and of the CJ.

To study the effect of Mic60 on the width of the CJ mouth, we used electron tomography combined with 3D reconstruction in the same set of cells used above. Data show that, compared to control cells, acute *Opa1* ablation increases the width of the CJ mouth by 30% (37.74 ± 1.57 nm vs. 51.82 ± 2.20 nm (Figure 6A, 6C). Instead, Mic60 silencing does not affect it (37.74 ± 1.57 nm vs. 38.48 ± 1.61 nm; Figure 6C), a finding confirmed by experiments showing that Mic60 silencing does not mobilize cyt c (Figure 7C). Consistent with these observations, we also found that Mic60 silencing and acute ablation of *Opa1*, together, do not exacerbate the phenotype caused by *Opa1* deletion alone (Figures 6A, 6C and 6E). Thus, under steady-state conditions Mic60 does not have a role in specifying the size of the CJ bore, a parameter that, instead, appears to be determined by an Opa1-mediated mechanism that is uncoupled from CJ biogenesis. This model is supported also by data showing that Mic60 is not the rate limiting factor that controls the opening of the CJ bore during apoptosis (Figure 7A, 7B).

DISCUSSION

The cristae structure is a key parameter that affects the functional status of mitochondria, while it is subjected to dynamic changes in response to the cellular metabolic demands and apoptotic triggering efficiency (Hackenbrock, 1966; Mannella et al., 2001; Scorrano et al., 2002; Cogliati et al., 2013). The main regulators of cristae architecture known so far are the multimers of OPA1, MICOS complex and the dimers of ATP-synthase.

An open question is whether these machineries are coordinated and whether the same mechanisms regulate cristae biogenesis and CLW. Loss of Opa1 impacts on both of these structural parameters of the organelle. In this study we show that silencing of Mic60 impacts on cristae biogenesis but not CLW; also, that Mic60 is a new master regulator of cristae biogenesis, and that this process requires the co-expression of Mic60 and OPA1 for the formation of HMW Mic60/OPA1-containing complexes. By implication, these findings support a model where the two events impinge on distinct mechanisms and that they can be uncoupled; here, an intriguing possibility would be that OPA1 cooperates with dimers of the ATPase to regulate CLW, and with Mic60 to regulate cristae biogenesis.

Mic60 silencing sensitizes cells to intrinsic pro-apoptotic stimuli (John et al., 2005). Our data show that this effect is unlikely due to the fact that such stimuli leads to increased CJ bore size because in Mic60-silenced MAFs stimulated with tBID, cyt c is mobilized like in mock-silenced control cells. Thus, such increased vulnerability to apoptosis could be explained by the fact that loss of Mic60 expression blunts CJ biogenesis and reduces mitochondrial respiratory capacity.

Our data show that Mic19 and Mic60 form HMWC that, on BN-PAGE analysis, have the same electrophoretic pattern of migration. These complexes are eliminated during cBID-induced apoptosis like the Mic60/OPA1-containing complexes raising the possibility that

mammalian Mic19 might also regulate mitochondria biogenesis through the OPA1 pathway.

In conclusion, we dissected the mechanisms for CJ biogenesis and CLW regulation. Mic60/OPA1 complexes are indispensable for CJ biogenesis and are targeted during cBID-induced apoptosis.

EXPERIMENTAL PROCEDURES

Cell culture, Transfection and Molecular Biology

WT, *Opa1*$^{flx/flx}$ and *Opa1*^{tg} SV40 transformed mouse adult fibroblast (MAFs) were generated from WT, *Opa1*$^{flx/flx}$ and *Opa1*^{tg} mice respectively as previously described (Cogliati et al., 2013). Cell lines were maintained in Dulbecco's Modified Eagle Medium (DMEM, Invitrogen) supplemented with 10% FBS (Invitrogen), 2 mM Glutamine, 50 U/ml Penicillin, 50 µg/ml Streptomycin, 50 µg/ml Uridine, and 0.1 mM non-essential aminoacids (Invitrogen). When indicated, glucose was substituted with 0.9 mg/ml galactose (Sigma).

Acute OPA1 ablation in *Opa1*$^{flx/flx}$ MAFs was obtained by infection with adenovirus expressing cytomegalovirus (CMV)-Cre-GFP (Ad-CRE-GFP: 200 pfu/cell). CMV-GFP (Ad-GFP) expressing adenoviruses was used as control (Vector Biolabs). Experiments were performed 48 hr after infection.

pcDNA6.2-hMic60-V5 vector (human, transcript variant 1 DNA NM_006839.1, subcloned by gateway technology from pCMV6-AC donor plasmid to pDEST-V5) was used for Mic60 overexpression. Lipofectamine was used as transfection reagent following manufacturer's instructions.

For RNAi experiments, Oligofectamine was used as transfecting reagent and the sequence of the siRNA for Mic60 used was the following: 5'- GAACAAAUGGACAGCUUUA-3'. Silencer Negative Control siRNA (Ambion, Life technologies) was used as negative control.

Recombinant Protein Expression

p7/p15 recombinant BID (wild type and mutant) was produced, purified and cleaved with caspase-8 as previously described (Frezza et al., 2006).

Mitochondrial isolation and in vitro assays

Mitochondria from Mouse Adult Fibroblasts (MAFs) and mouse liver and heart tissues were isolated by standard differential centrifugation as previously described (Frezza et al., 2007; Fernandez-Vizarra et al., 2010).

Mitochondrial treatment with cBID and cBID^{KKAA} at the concentration indicated in the Figure legends were performed in Experimental Buffer (EB) (1 mg/ml) containing 150 mM KCl, 10 mM Tris Mops, 10 µM EGTA-Tris, 1 mM Pi, with 5 mM glutamate/ 2.5 mM malate as respiration substrate, pH 7.4, 25°C.

BN-PAGE and 3D BN-BN-SDS gel electrophoresis (BN-BN-SDS-PAGE)

Blue-Native PAGE (BN-PAGE) analysis was done from samples prepared as indicated here. Isolated mitochondria from liver (250 µg), heart (250 µg) or MAFs (150 µg) previously treated or not as indicated in the figure legends, were resuspended in 50 µl Native solubilization buffer (NB) containing Native Page buffer 4X (Invitrogen), 1.25% digitonin and 1:100 protease inhibitor cocktail (PIC, SIGMA). After 10 min on ice the samples were centrifuged at maximal speed in a table bench centrifuge at 4°C. Supernatants were transferred into a new tube and 2 µl of 5% Coomassie G-250 (Invitrogen) was added before being loaded onto a precast NativePAGE 3-12% Bis-Tris Gel (Invitrogen) for biochemical experiments. Electrophoresis was performed in the presence of cathode (dark blue cathode: 45 min; light blue cathode: 90 min) and anode buffers prepared

following Invitrogen manufacturing instructions. When indicated, protein complexes were blotted onto a PVDF membrane and probed for the indicated antibodies.

Second BN-PAGE was performed by excising and casting the lane obtained from the first BN-PAGE on a single-well native gel (NuPAGE Novex 4-12% Bis-Tris ZOOM gel, Invitrogen). In the cathode buffers used 0.02% n-Dodecyl-D-maltoside (DDM, SIGMA) was added. Electrophoresis was performed at 125 V for 1 hr 30 min using dark cathode buffer and at 150 V, overnight using with light cathode buffer. During 2D BN-BN-PAGE, complexes resistant to detergent are aligned in a diagonal easily identified by Coomassie contained into the running samples.

The third dimension SDS-PAGE was performed after excising the diagonal and incubating it with reducing solutions RSa for 10 min, RSb for 7 min and RSc for 12 min, in order to facilitate the complexes dissociation during the 3D SDS (RSa=1x LDS sample buffer (Invitrogen), 4% β-mercaptoethanol, RSb=1x LDS sample buffer (Invitrogen), 1% N N-dimethylacrylamide (DMA, SIGMA) and RSc=1x LDS sample buffer (Invitrogen), 20% ethanol and 0.1% β-mercaptoethanol). After the treatment, the diagonal was loaded onto a gel (NuPAGE Novex 4-12% Bis-Tris ZOOM gel, Invitrogen) and run under denaturating conditions to separate the individual proteins that were then transferred onto polyvinylidene fluoride (PVDF) membranes and stained with the indicated antibodies.

BN-PAGE based semi-quantitative proteomic analysis

Mitochondrial proteins from two mouse hearts were solubilized as described above. Blue Native Electrophoresis (BN-PAGE) was used to separate the native membrane complexes in a homemade gradient gel from 4% to 13% acrylamide, 20 x 20 cm, for control samples and for samples treated with cBID or $cBID^{KKAA}$ (1 mg of protein per sample). The

electrophoresis was performed as described for the 1st dimension BN-PAGE. Subsequently, gels were stained using GelCode Blue Stain Reagent (Thermo Scientific). Each lane was divided and excised in 26 bands covering the whole electrophoretic run. Gel pieces were then digested with modified porcine trypsin (Promega) at a final ratio 1:20 (trypsin-protein). Digestion proceeded overnight at 37ºC in 100 mM ammonium bicarbonate, pH 8.8. The resulting tryptic peptide mixtures were subjected to nano-liquid chromatography coupled to mass spectrometry (LC-MS) for protein identification. Peptides were injected onto a C-18 reversed phase (RP) nano-column (75 µm I.D. and 50 cm, Acclaim PepMap100, Thermo Scientific) and analyzed in a continuous acetonitrile gradient consisting of 0-30% B in 240 min, 50-90% B in 3 min (B=90% acetonitrile, 0.5% acetic acid). A flow rate of ca. 200 nL/min was used to elute peptides from the RP nano-column to an emitter nanospray needle for real time ionization and peptide fragmentation on an Orbitrap Fusion mass spectrometer (Thermo Fisher, San José, CA, USA). For protein identification, tandem mass spectra were extracted and charge state deconvoluted by Proteome Discoverer 1.4.0.288 (Thermo Fisher Scientific). All MS/MS samples were analyzed using SEQUESTTM (Thermo Fisher Scientific).

SILAC labelling and quantitative proteomic analysis

Mouse adult fibroblasts (MAFs) were grown separately in DMEM medium containing 4.5 g/L glucose, 2 mM glutamine, 10% fetal bovine serum (FBS), 50 U/ml Penicillin, 50 mg/ml Streptomycin, 50 mg/ml Uridine and Phenol Red supplemented with either *light* L-Lysine and L-Arginine or *heavy* [U-$^{13}C_6$]-L-Lysine HCl and [U-$^{13}C_6$]-L-Arginine (100 mg/L of each amino acid) (SILAC Protein Identification and Quantification Media Kit, Invitrogen). After 6 doublings cell subpopulations, *light* and *heavy*, were harvested and mitochondria were

isolated separately. In experiment “a” *light* mitochondria were treated with 20 pmol/mg cBID for 30 min in EB, and *heavy* mitochondria were untreated. After centrifugation at 10000 *x g*, 10 min, 4°C, the pellets from both samples were mixed and resuspended together in NB indicated above. In experiment “b”, *light* mitochondria were untreated while *heavy* mitochondria were treated with 20 pmol/mg $cBID^{KKAA}$ for 30 min, 25°C. After centrifugation the samples were mixed and processed as in experiment “a” before proceeding with the BN-PAGE. Protein complexes (500 µg) from experiments “a” and “b” were loaded in parallel lanes and complexes were separated by BN-PAGE electrophoresis. Three lanes from experiment “a” and “b” were stained with Coomassie and bands between 600 and 1000 kDa were excised with a scalpel and digested with trypsin. Digestion proceeded overnight at 37ºC in 100 mM ammonium bicarbonate, pH 8.8. The resulting tryptic peptide mixtures were subjected to nano-liquid chromatography coupled to mass spectrometry (LC-MS) for protein identification. Peptides were injected onto a C-18 reversed phase (RP) nano-column (75 mm I.D. and 50 cm, Acclaim PepMap100, Thermo Scientific) and analyzed in a continuous acetonitrile gradient consisting of 0-30% B in 240 min, 50-90% B in 3 min (B=90% acetonitrile, 0.5% acetic acid). A flow rate of ca. 200 nL/min was used to elute peptides from the RP nano-column to an emitter nanospray needle for real time ionization and peptide fragmentation on a Q Exactive mass spectrometer (Thermo Fisher, San José, CA, USA). For protein identification, tandem mass spectra were extracted and charge state deconvoluted by Proteome Discoverer 1.4.0.288 (Thermo Fisher Scientific). All MS/MS samples were analyzed using SEQUESTTM (Thermo Fisher Scientific). Change in protein abundance in the studied complexes was considered when log (light/heavy) was > 1.2 or < -1.2 after treatment.

Biochemistry

Chemical crosslinking was performed by incubating mitochondria (0.5 mg/ml) with 10 mM (bismaleimidohexane) (BMH, PIERCE) in EB after the indicated treatments under the indicated experimental conditions. After 30 min the reaction was quenched with β-mercaptoethanol and mitochondria were spun at 12000 rpm, 10 min, 4°C. Then, the pellet was solubilized in laemmli buffer 2X and boiled to proceed with protein separation by in a 3-8% Tris-Acetate SDS-PAGE.

Protein levels of Mic60, OPA1, Fb, Mic19, Grp75 or actin were studied after lysis of mitochondria or cells with Ripa buffer in presence of proteases inhibitors, 30 min, 4°C. After centrifugation at maximal speed for 30 min, protein concentration was determined with Bradford reagent (Bio-Rad). The proteins were separated under denaturing conditions in 3–8% Tris-Acetate (NuPage, Invitrogen) or 7.5% Tris-Glycine (BioRad) gels, transferred onto PVDF membranes (Millipore) and probed using anti-Mic60 polyclonal (1:1000, Proteintech), anti-OPA1 monoclonal (1:1000, BD PharMingen), anti-Fp (Flavoprotein subunit of succinate dehydrogenase, complex-II) monoclonal (1:1000, Abcam), anti-Grp75 polyclonal (1:2000, Santa Cruz), anti-Mic19 polyclonal (1:1000, Proteintech), actin (1:15000, Millipore) antibodies. Isotype matched secondary antibodies were conjugated to horseradish peroxidase and chemiluminescence was detected with ECL (Amersham) using either traditional methods with films (Amersham) or Image Quant LAS 4000 (GE Healthcare Life Sciences).

Transmission Electron Microscopy, Tomographic Reconstruction, and Mitochondrial Morphometry

Scramble and Mic60-silenced cells were fixed and processed after 48 hr from transfection. In the case of cells infected with Ad-EV or Ad-CRE, and cells infected with retrovirus expressing tBID, cells were sorted after 24 hr to select GFP positive cells that were seeded and fixed for electron microscopy imaging after 48 hr from infection. For overexpression experiments the cells were co-transfected with mtRFP and pDEST-Mic60-V5, and after 24 hr cells were sorted, and RFP positive cells were seeded in 12 wells plates. After 48 hr from the transfection cells were fixed for electron microscopy imaging.

Cells were fixed for 1 hr at 25°C with glutaraldehyde at a final concentration of 1.25% (V/V), post-fixed in 1% OsO_4, 1.5% $K_4Fe(CN)_6$ in 0.1 M sodium cacodylate pH 7.4, stained with 0.5% uranyl acetate, dehydrated in ethanol and embedded in Embed 812.

For electron tomography, 200-250 nm thick sections were collected on formvar-coated copper slot grids and gold fiducials (10 nm) were applied on both surfaces of the grids. The samples were imaged in a 200 kV Tecnai G2 20 electron microscope (FEI, Eindhoven, The Netherlands) at magnification of 25k or 29k resulting in a pixel size of 0.92 nm and 0.77 nm respectively. Tilted images (+65/-65 according to a Saxton scheme with a starting angle of 1.5°) were acquired using Xplorer 3D (FEI, Eindhoven, The Netherlands) with an Eagle 2k × 2k CCD camera (FEI, Eindhoven, The Netherlands). Tilted series alignment and tomography reconstruction was done with IMOD (Mastronarde, 1997) and segmentation and 3D rendering were done with the Reconstruction software (Fiala, 2005). Measurements were made by using the software ImageJ and for quantification the z scale was stretched with a factor of 1.6 to correct for resin shrinkage (Mastronarde, 1997)

Quantitative analysis of the cristae width was performed in electron microscopy images with magnification x59000 and by using the Image J software. A number of 3-6 cristae per mitochondrion were measured from cells infected with Ad-EV and transfected with pcDNA6.2 empty vector (n=233), pcDNA6.2-hMic60-V5 (n=228), scramble siRNA (n=256), Mic60 siRNA (n=261), and from cells infected with ad-CRE and transfected with pcDNA6.2 empty vector (n=169), pcDNA6.2-hMic60-V5 (n=195), scramble siRNA (n=172), Mic60 siRNA (n=146)

Quantitative analysis of cristae and cristae junction number per mitochondrion were done by using x46000 or x 59000 magnification EM images, in blind by two different operators. The sample size is indicated in the figure legend.

Evolution analysis

Multiple sequence alignment was performed using ClustalW.

Acin-Perez,R. and Enriquez,J.A. (2014). The function of the respiratory supercomplexes: the plasticity model. Biochim. Biophys. Acta *1837*, 444-450.

Acin-Perez,R., Fernandez-Silva,P., Peleato,M.L., Perez-Martos,A., and Enriquez,J.A. (2008). Respiratory active mitochondrial supercomplexes. Mol. Cell *32*, 529-539.

Cogliati,S., Frezza,C., Soriano,M.E., Varanita,T., Quintana-Cabrera,R., Corrado,M., Cipolat,S., Costa,V., Casarin,A., Gomes,L.C., Perales-Clemente,E., Salviati,L., Fernandez-Silva,P., Enriquez,J.A., and Scorrano,L. (2013). Mitochondrial cristae shape determines respiratory chain supercomplexes assembly and respiratory efficiency. Cell *155*, 160-171.

Fernandez-Vizarra,E., Ferrin,G., Perez-Martos,A., Fernandez-Silva,P., Zeviani,M., and Enriquez,J.A. (2010). Isolation of mitochondria for biogenetical studies: An update. Mitochondrion. *10*, 253-262.

Fiala,J.C. (2005). Reconstruct: a free editor for serial section microscopy. J. Microsc. *218*, 52-61.

Frezza,C., Cipolat,S., Martins,d.B., Micaroni,M., Beznoussenko,G.V., Rudka,T., Bartoli,D., Polishuck,R.S., Danial,N.N., De Strooper,B., and Scorrano,L. (2006). OPA1 Controls Apoptotic Cristae Remodeling Independently from Mitochondrial Fusion. Cell *126*, 177-189.

Frezza,C., Cipolat,S., and Scorrano,L. (2007). Organelle isolation: functional mitochondria from mouse liver, muscle and cultured fibroblasts. Nat. Protoc. *2*, 287-295.

Guarani,V., McNeill,E.M., Paulo,J.A., Huttlin,E.L., Frohlich,F., Gygi,S.P., Van,V.D., and Harper,J.W. (2015). QIL1 is a novel mitochondrial protein required for MICOS complex stability and cristae morphology. Elife. *4*.

Hackenbrock,C.R. (1966). Ultrastructural bases for metabolically linked mechanical activity in mitochondria. I. Reversible ultrastructural changes with change in metabolic steady state in isolated liver mitochondria. J. Cell Biol. *30*, 269-297.

John,G.B., Shang,Y., Li,L., Renken,C., Mannella,C.A., Selker,J.M., Rangell,L., Bennett,M.J., and Zha,J. (2005). The mitochondrial inner membrane protein mitofilin controls cristae morphology. Mol. Biol. Cell *16*, 1543-1554.

Kasahara,A., Cipolat,S., Chen,Y., Dorn,G.W., and Scorrano,L. (2013). Mitochondrial fusion directs cardiomyocyte differentiation via calcineurin and Notch signaling. Science *342*, 734-737.

Li,H., Ruan,Y., Zhang,K., Jian,F., Hu,C., Miao,L., Gong,L., Sun,L., Zhang,X., Chen,S., Chen,H., Liu,D., and Song,Z. (2015). Mic60/Mitofilin determines MICOS assembly essential for mitochondrial dynamics and mtDNA nucleoid organization. Cell Death. Differ.

Mannella,C.A. (2006). Structure and dynamics of the mitochondrial inner membrane cristae. Biochim Biophys Acta *1763*, 542-548.

Mannella,C.A., Lederer,W.J., and Jafri,M.S. (2013). The connection between inner membrane topology and mitochondrial function. J. Mol. Cell Cardiol. *62*, 51-57.

Mannella,C.A., Marko,M., Penczek,P., Barnard,D., and Frank,J. (1994). The internal compartmentation of rat-liver mitochondria: tomographic study using the high-voltage transmission electron microscope. Microsc Res Tech *27*, 278-283.

Mannella,C.A., Pfeiffer,D.R., Bradshaw,P.C., Moraru,I.I., Slepchenko,B., Loew,L.M., Hsieh,C.E., Buttle,K., and Marko,M. (2001). Topology of the mitochondrial inner membrane: dynamics and bioenergetic implications. IUBMB. Life *52*, 93-100.

Mastronarde,D.N. (1997). Dual-axis tomography: an approach with alignment methods that preserve resolution. J. Struct. Biol. *120*, 343-352.

Munoz-Gomez,S.A., Slamovits,C.H., Dacks,J.B., Baier,K.A., Spencer,K.D., and Wideman,J.G. (2015). Ancient homology of the mitochondrial contact site and cristae organizing system points to an endosymbiotic origin of mitochondrial cristae. Curr. Biol. *25*, 1489-1495.

Scorrano,L., Ashiya,M., Buttle,K., Weiler,S., Oakes,S.A., Mannella,C.A., and Korsmeyer,S.J. (2002). A distinct pathway remodels mitochondrial cristae and mobilizes cytochrome c during apoptosis. Dev. Cell *2*, 55-67.

Varanita,T., Soriano,M.E., Romanello,V., Zaglia,T., Quintana-Cabrera,R., Semenzato,M., Menabç,R., Costa,V., Civiletto,G., Pesce,P., Viscomi,C., Zeviani,M., Di Lisa,F., Mongillo,M., Sandri,M., and Scorrano,L. (2015). The Opa1-Dependent Mitochondrial Cristae Remodeling Pathway Controls Atrophic, Apoptotic, and Ischemic Tissue Damage. Cell Metabolism *21*.

FIGURE LEGENDS

Figure 1. Mic60-complexes distribution is altered during cBID-induced cristae remodeling

A. Amino acid sequence alignment of the transmembrane helix of yeast and human Mic60, depicting the extent of conservation. Identical amino acids are marked with asterisk (*); strongly similar amino acids are marked with colons (:); weekly similar amino acids are marked with (.); non conserved amino acids are not marked ( ). The coiled-coil domains are highlighted.

B. BN-PAGE analysis of complexes extracted from mouse liver or heart mitochondria (125 µg each), transferred onto PVDF membrane and probed with anti-Mic60 or anti-Mic19 antibodies.

C. Coomassie staining after BN-PAGE (left panel) of complexes (500 µg) extracted from mouse heart mitochondria, untreated (control) or after 20 min of treatment with cBID or $cBID^{KKAA}$ (30 pmol x mg^{-1} protein) in Experimental buffer (EB). Gel bands were cut following the pattern and size indicated with black vertical lines in the Coomassie panel that were then analyzed by mass spectrometry. Color-contour plots show the number of peptides from Mic60 (middle panel) or Mic19 (right panel) identified by mass spectrometry along the BN-PAGE from high (top) to low (bottom) molecular weight. The color code represents the peptides' abundance in each complex either for Mic60 or Mic19 (color scale legend on the right of each panel).

D**.** Coomassie stained BN-PAGE (left panel) and heat map of samples from SILAC experiments "*a*" and "*b*" (right panel). Heat map shows the changes in intensity (number of peptides) of Mic60 peptides (#1-4) after the indicated treatments normalized to the

respective internal control. Color code defines a decrease (green) or increase (red) in peptides intensity of treated vs. control sample.

E. Heat map representation of quantitative changes in Mic19 peptides (#1-3) after the indicated treatment vs. the control. Color code defines a decrease (green) or increase (red) in peptides intensity of treated versus control sample. Three different samples were included in the analysis.

Figure 2. Mic60-OPA1 complexes are targeted by cBID

A. BN-PAGE of protein complexes (125 µg) extracted from mouse liver mitochondria (250 µg), untreated or after 30 min treatment with wild type cBID or $cBID^{KKAA}$. The gels were blotted onto PVDF membranes before probing with the indicated antibodies. Anti-Fp was used as protein loading control.

B. Schematic representation of three dimensional BN-BN-SDS-PAGE analysis of membrane complexes isolated from mouse liver mitochondria. DIG: digitonin, DDM: n-Dodecyl-D-maltoside.

C. Western blotting of third dimensional SDS PAGE using anti-OPA1 or anti-Mic60 antibodies.

D. Chemical crosslinking with BMH of isolated mitochondria from *Opa1*$^{flx/flx}$ MAFs untreated or treated for 15 min with cBID (20 pmol x mg^{-1}) in EB. Where indicated 5 mM BMH was added. Equal amounts of proteins (25 µg) were separated in Tris-Acetate 3-8% PAGE and transferred onto PVDF membrane before immune-detection with the indicated antibodies.

E. *Mic60 and OPA1 co-immunoprecipitate.* Mitochondrial lysates (125 µg) obtained from mouse embryonic fibroblasts were immuno-precipitated with anti-OPA1 antibody and

bound proteins were separated electrophoretically, blotted and immuno-detected with ant-OPA1 and anti-Mic60 antibodies. The *Input* lane contains 25 μg of the initial mitochondrial lysate and the unspecific immune-reactivity between lysate and beads is contained in the *IP-IgG* lane.

F. BN-PAGE analysis of protein complexes extracted from *Opa1*$^{flx/flx}$ MAFs mitochondria (150 μg) after 48 hr of infection with adenoviruses expressing the indicated insert (Ad-EV, empty vector; Ad-CRE, Cre recombinase). Protein complexes were blotted onto PVDF membrane and immuno-detected with the indicated antibodies. The same samples were run in parallel in the same gel and stained with Coomassie to compare protein loading (left panel).

G. BN-PAGE analysis of protein complexes extracted from *Opa1*$^{flx/flx}$ MAFs mitochondria (150 μg) after 48 hr from transfection with scramble (scr) or Mic60 siRNA oligos. Protein complexes were immuno-detected after blotting with the indicated antibodies. Anti-Fp was used as protein loading control.

H. Chemical crosslinking with 5 mM BMH of isolated mitochondria from *Opa1*$^{flx/flx}$ MAFs after 48 hr of infection with adenoviruses expressing the indicated insert (EV, empty vector; CRE, Cre recombinase). Equal amounts (25 μg) of proteins were separated in Tris-Acetate 3-8% PAGE and transferred onto PVDF membrane before immuno-detection with anti-Mic60 antibody.

I. Chemical crosslinking with 5 mM BMH of isolated mitochondria from *Opa1*$^{flx/flx}$ MAFs after 48 hr of transfection with scramble (scr) or Mic60 siRNA oligos. Equal amounts (25 μg) of proteins were separated by SDS-PAGE and transferred onto PVDF membrane before immuno-detection with anti-OPA1 antibody.

Figure 3. Mic60 silencing reduces cristae and CJ density

A. Mic60 and OPA1 protein levels in *Opa1*$^{flx/flx}$ MAFs transfected with scramble (scr) or Mic60 siRNA and after 16 hr infection with the indicated adenoviruses (Ad-EV-GFP or Ad-CRE-GFP). After 32 hr of infection, cells were lysed and equal amounts of proteins (25 µg) were loaded onto an SDS-PAGE, transferred to PVDF membrane and probed with the indicated antibodies. Fp protein served as protein loading control. Changes in protein expression were quantified by densitometry analysis by normalizing to Fp protein levels. Infection efficiency with the indicated adenoviruses was around 80% after counting GFP-positive cells respect to the total with a Laser Spinning Disk Confocal Andromeda (data not shown).

B. Electron micrographs of mitochondria from *Opa1*$^{flx/flx}$ MAFs in the experimental conditions described in Figure 3A. Cells were sorted for GFP-positive cells, fixed and processed for EM analysis. Scale bars represent 200 nm.

C. Quantification of cristae number per mitochondrion in 70 randomly selected mitochondria from each indicated experimental condition. Data represent the mean ± SEM of four independent experiments. Paired sample t-test *** $p<0.001$.

D. Quantification of CJ number per crista in 143 randomly selected cristae from each indicated experimental condition. Data represent the mean ± SEM of four independent experiments. Paired sample t-test *** $p<0.001$.

E. Quantification of CJ number per mitochondrion in 70 randomly selected mitochondria from each experimental condition. Data represent average ± SEM of four independent experiments. Paired sample t-test *** $p<0.001$.

F. Morphometric analysis of cristae lumen width, CLW, in 60 randomly selected mitochondria from each experimental condition. Data represent average ± SEM of four

independent experiments (n=120-170 cristae in each condition). Paired sample t-test *** p<0.001.

Figure 4. OPA1 overexpression protects from cristae widening but not from loss of cristae and CJ density during Mic60 silencing

A. OPA1 and Mic60 protein levels in wt and *Opa1^{tg}* MAFs. Protein samples (25 µg) were separated in a Tris-Acetate 3-8% PAGE, blotted onto a PVDF membrane and probed with the indicated antibodies. Actin was used as protein loading control. The same procedure was followed to detect protein expression levels in wt and *Opa1^{tg}* MAFs 48 hr post-transfection with scramble (scr) or Mic60 siRNA oligos. Changes in protein expression were quantified by densitometry analysis and normalized to actin protein levels.

B. Electron micrographs of mitochondria. WT and *Opa1^{tg}* MAFs were transfected with scramble (scr) or Mic60 siRNA oligos and after 48 hr they were fixed to be processed for electron microscopy. The scale bars represent 200 nm.

C. Quantification of cristae number per mitochondrion in 40 randomly selected mitochondria in the indicated experimental condition. Data represent average ± SEM of three independent experiments. Paired sample t-test *** p<0.001.

D. Quantification of CJ number per crista in 40 randomly selected cristae in the indicated experimental condition. Data represent average ± SEM of four independent experiments. Paired sample t-test *p<0.05.

E. Quantification of CJ number per mitochondrion in 40 randomly selected mitochondria in the indicated experimental condition. Data represent average ± SEM of four independent experiments. Paired sample t-test *** p<0.001.

F. Morphometric analysis of cristae lumen width in 40 randomly selected mitochondria in each experimental condition. Data represent average ± SEM of three independent experiments. Paired sample t-test *** p<0.001.

Figure 5. Mic60 overexpression increases the number of cristae and CJ only in presence of OPA1

A. Electron micrographs of mitochondria from *Opa1*$^{flx/flx}$ MAFs infected with the indicated adenoviruses (Ad-EV-GFP or Ad-CRE-GFP). 16 hr post-infection cells were co-transfected with mt-RFP and Mic60-V5 or empty vector (EV). Then, cells were sorted for RFP –positive cells 24 hr post-transfection and seeded in new plates. After 16 hr, cells were fixed to be processed for EM analysis. Scale bars represent 500 nm or 2 µm, as indicated. Infection efficiency with the indicated adenoviruses was around 80% after counting GFP-positive cells respect to the total with a Laser Spinning Disk Confocal Andromeda.

B. Quantification of cristae number per mitochondrion in 30 randomly selected mitochondria from each experimental condition. Data represent average ± SEM of three independent experiments. Paired sample t-test *p<0.05.

C. Quantification of CJ number per crista of 143 randomly selected cristae from each experimental condition. Data represent average ± SEM of three independent experiments. Paired sample t-test *** p<0.001; ** p<0.01.

D. Quantification CJ number per mitochondrion in 30 randomly selected mitochondria from each experimental condition. Data represent average ± SEM of three independent experiments. Paired sample t-test *** p<0.001; *p<0.05.

E. Morphometric analysis CLW in 30 randomly selected mitochondria from each experimental condition. Data represent average ± SEM of three independent experiments. Paired sample t-test *** p<0.001; ** p<0.01.

Figure 6. Mic60 does not regulate CJ mouth width in steady state

A. Rotations of surface-rendered views of tomographic reconstructions of mitochondria from *Opa1*$^{flx/flx}$ MAFs in the indicated experimental conditions treated and processed as indicated in Figure 3A-B. Inner membrane is depicted in orange and cristae compartment in cyan. Outer membrane has been peeled out to highlight CJ.

B. Quantification of CJ number per cristae in the indicated experimental conditions described in (A). Data represent average ± SEM of three independent experiments (4 to 9 different tomograms for each experimental condition). Paired sample t-test *** p<0.001.

C.-D. Quantification of CJ mouth width in the indicated experimental conditions described in (A). Data represent average ± SEM of three independent experiments (4 to 9 different tomograms for each experimental condition). Paired sample t-test *** p<0.001; ** p<0.01.

Figure 7. Mic60 has no effect in widening the CJ mouth and cytochrome c release during apoptosis

A. Electron micrographs (left panel) and rotations of surface-rendered views of tomographic reconstructions (right panel) of mitochondria from *Opa1*$^{flx/flx}$ MAFs infected with the retrovirus pMIG-tBid and transfected with the indicated siRNAs. For EM the scale

bars represent 200 nm. In tomographs inner membrane is depicted in orange and cristae compartment in cyan. Outer membrane has been peeled out to highlight CJ.

B. Quantification of CJ mouth width in the indicated experimental conditions. Data represent average ± SEM of three independent experiments. Paired sample t-test *** $p<0.001$; ** $p<0.01$.

C. Ascorbate/TMPD-driven respiration ratio of mitochondria isolated from *Opa1*$^{flx/flx}$ MAFs transfected with scramble (scr) or Mic60 siRNA oligos. As positive control of cytochrome c mobilization, mitochondria were treated with recombinant cBID (10 pmol x mg^{-1} protein). Data represent average ± SEM of three independent experiments.

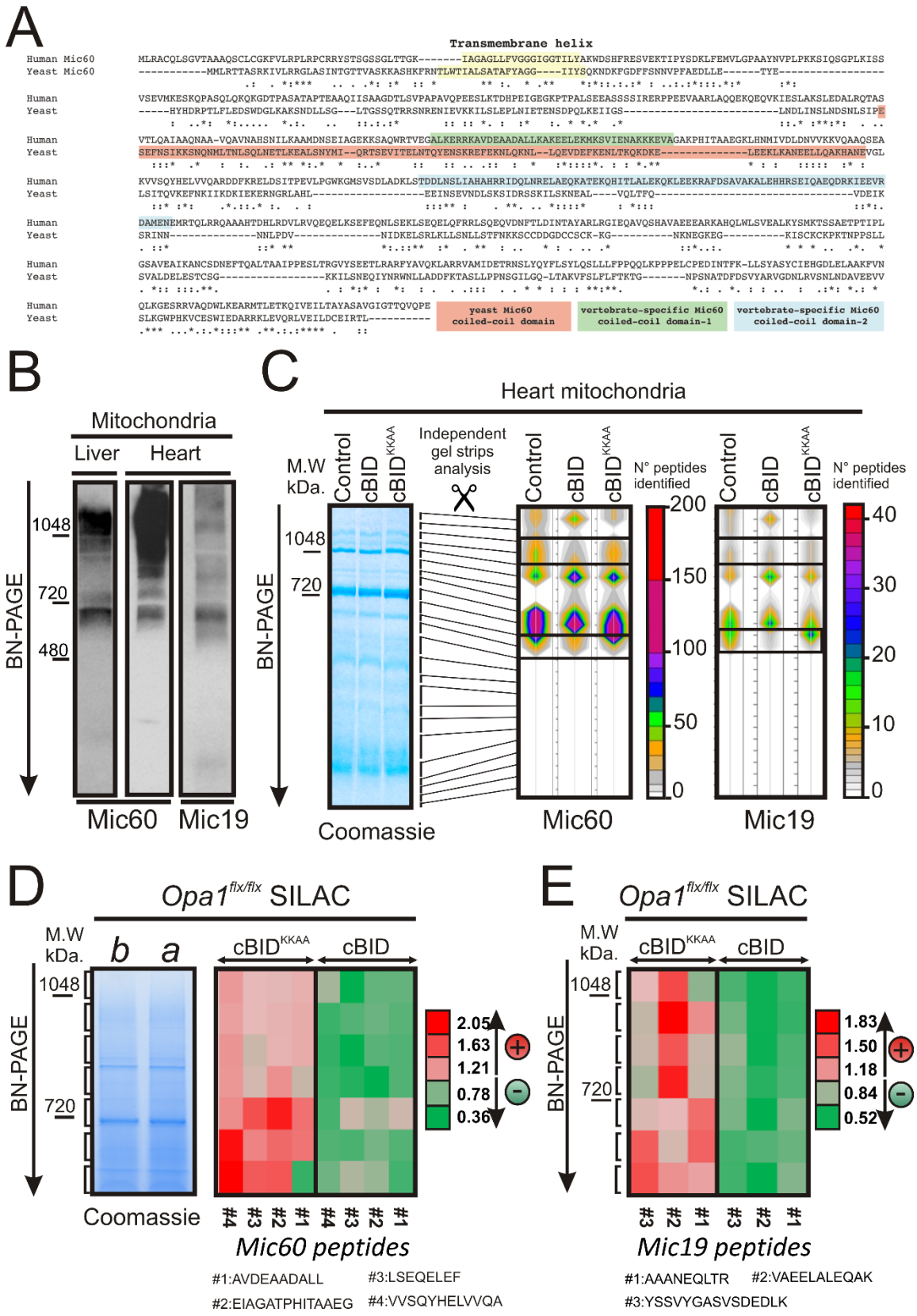
A
Transmembrane helix
Human Mic60
Yeast Mic60
Human
Yeast
yeast Mic60 coiled-coil domain
vertebrate-specific Mic60 coiled-coil domain-1
vertebrate-specific Mic60 coiled-coil domain-2
B
Mitochondria
Liver
Heart
BN-PAGE
1048
720
480
Mic60
Mic19
C
Heart mitochondria
M.W kDa.
Control
cBID
cBID^KKAA
Independent gel strips analysis
N° peptides identified
Coomassie
Mic60
Mic19
D
Opa1^flx/flx SILAC
b
a
Coomassie
Mic60 peptides
#1:AVDEAADALL
#2:EIAGATPHITAAEG
#3:LSEQELEF
#4:VVSQYHELVVQA
E
Opa1^flx/flx SILAC
Mic19 peptides
#1:AAANEQLTR
#2:VAEELALEQAK
#3:YSSVYGASVSDEDLK

Figure 1

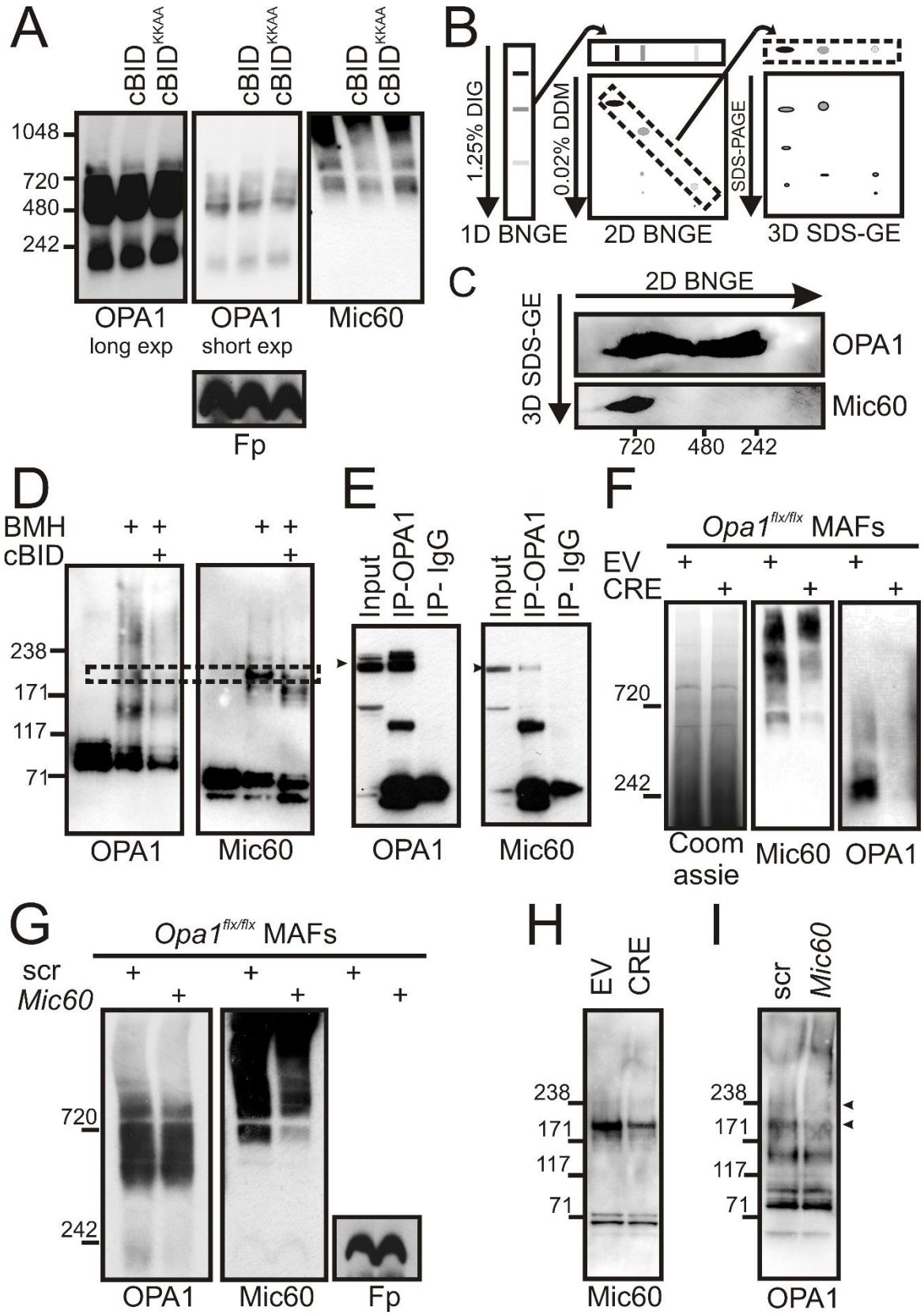
A
cBID
cBID^KKAA
1048
720
480
242
OPA1
long exp
OPA1
short exp
Mic60
Fp
B
1.25% DIG
0.02% DDM
SDS-PAGE
1D BNGE
2D BNGE
3D SDS-GE
C
2D BNGE
3D SDS-GE
OPA1
Mic60
720
480
242
D
BMH
cBID
238
171
117
71
OPA1
Mic60
E
Input
IP-OPA1
IP- IgG
OPA1
Mic60
F
Opa1^flx/flx MAFs
EV
CRE
720
242
Coom assie
Mic60
OPA1
G
Opa1^flx/flx MAFs
scr
Mic60
720
242
OPA1
Mic60
Fp
H
EV
CRE
238
171
117
71
Mic60
I
scr
Mic60
238
171
117
71
OPA1

Figure 2

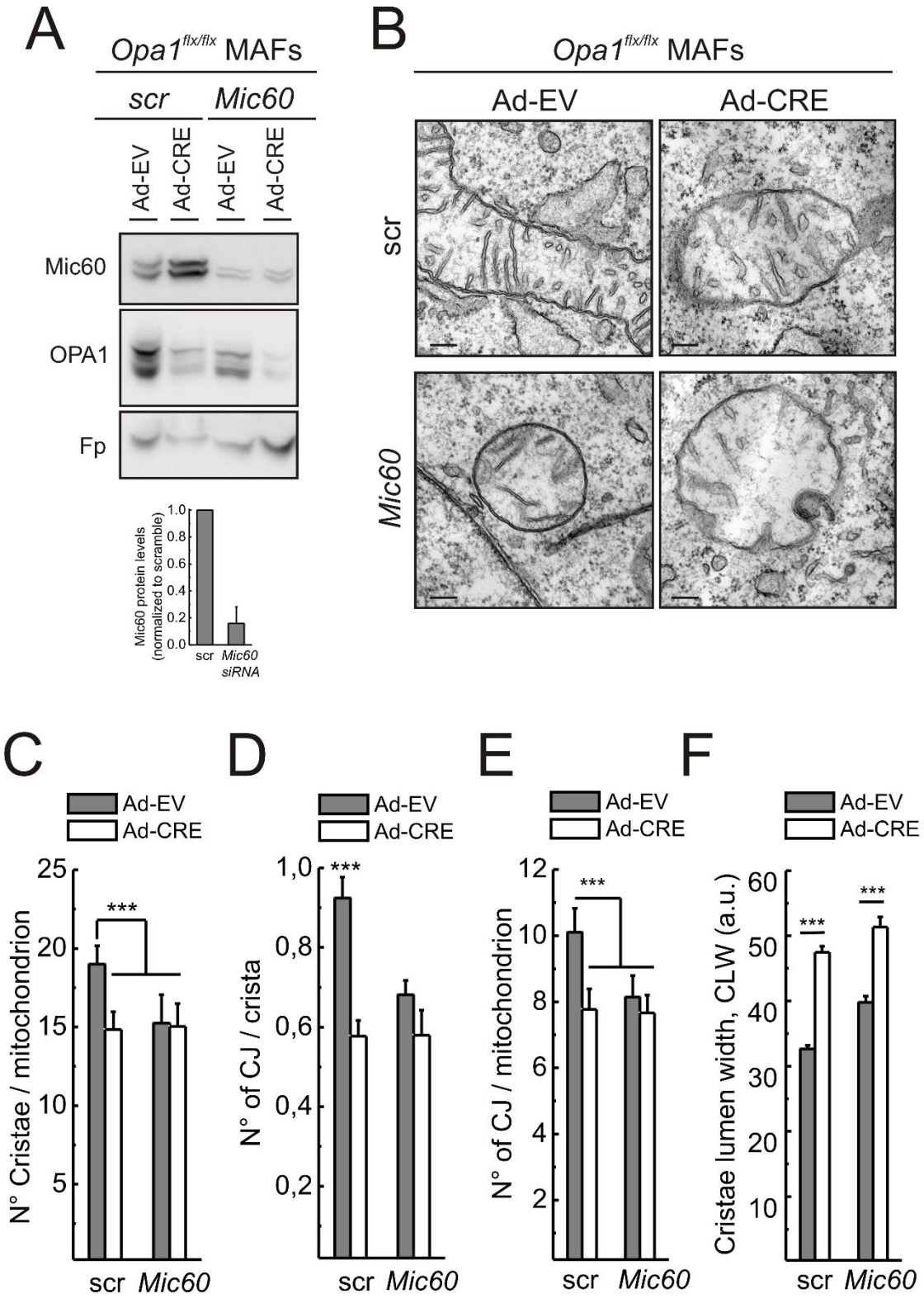
A
Opa1flx/flx MAFs
scr
Mic60
Ad-EV
Ad-CRE
Ad-EV
Ad-CRE
Mic60
OPA1
Fp
Mic60 protein levels (normalized to scramble)
1.0
0.8
0.6
0.4
0.2
0.0
scr
Mic60 siRNA
B
Opa1flx/flx MAFs
Ad-EV
Ad-CRE
scr
Mic60
C
Ad-EV
Ad-CRE
N° Cristae / mitochondrion
25
20
15
10
5
***
scr
Mic60
D
Ad-EV
Ad-CRE
N° of CJ / crista
1,0
0,8
0,6
0,4
0,2
***
scr
Mic60
E
Ad-EV
Ad-CRE
N° of CJ / mitochondrion
12
10
8
6
4
2
***
scr
Mic60
F
Ad-EV
Ad-CRE
Cristae lumen width, CLW (a.u.)
60
50
40
30
20
10
***
***
scr
Mic60

Figure 3

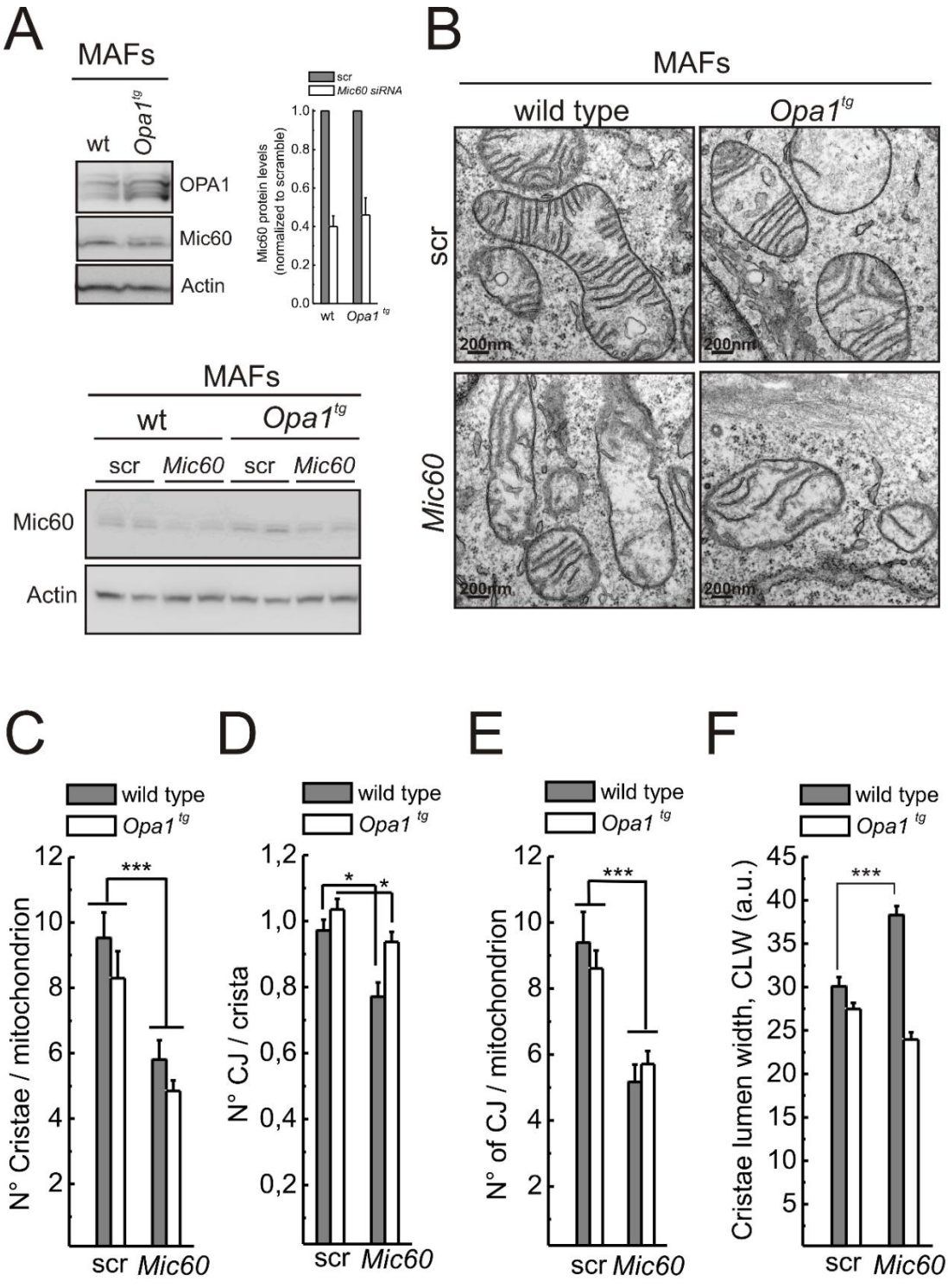
A
MAFs
wt
Opa1tg
OPA1
Mic60
Actin
scr
Mic60 siRNA
Mic60 protein levels (normalized to scramble)
1.0
0.8
0.6
0.4
0.2
0.0
wt
Opa1 tg
MAFs
wt
Opa1tg
scr
Mic60
scr
Mic60
Mic60
Actin
B
MAFs
wild type
Opa1tg
scr
Mic60
200nm
200nm
200nm
200nm
C
wild type
Opa1 tg
N° Cristae / mitochondrion
12
10
8
6
4
2
***
scr
Mic60
D
wild type
Opa1 tg
N° CJ / crista
1,2
1,0
0,8
0,6
0,4
0,2
*
*
scr
Mic60
E
wild type
Opa1 tg
N° of CJ / mitochondrion
12
10
8
6
4
2
***
scr
Mic60
F
wild type
Opa1 tg
Cristae lumen width, CLW (a.u.)
45
40
35
30
25
20
15
10
5
***
scr
Mic60

Figure 4

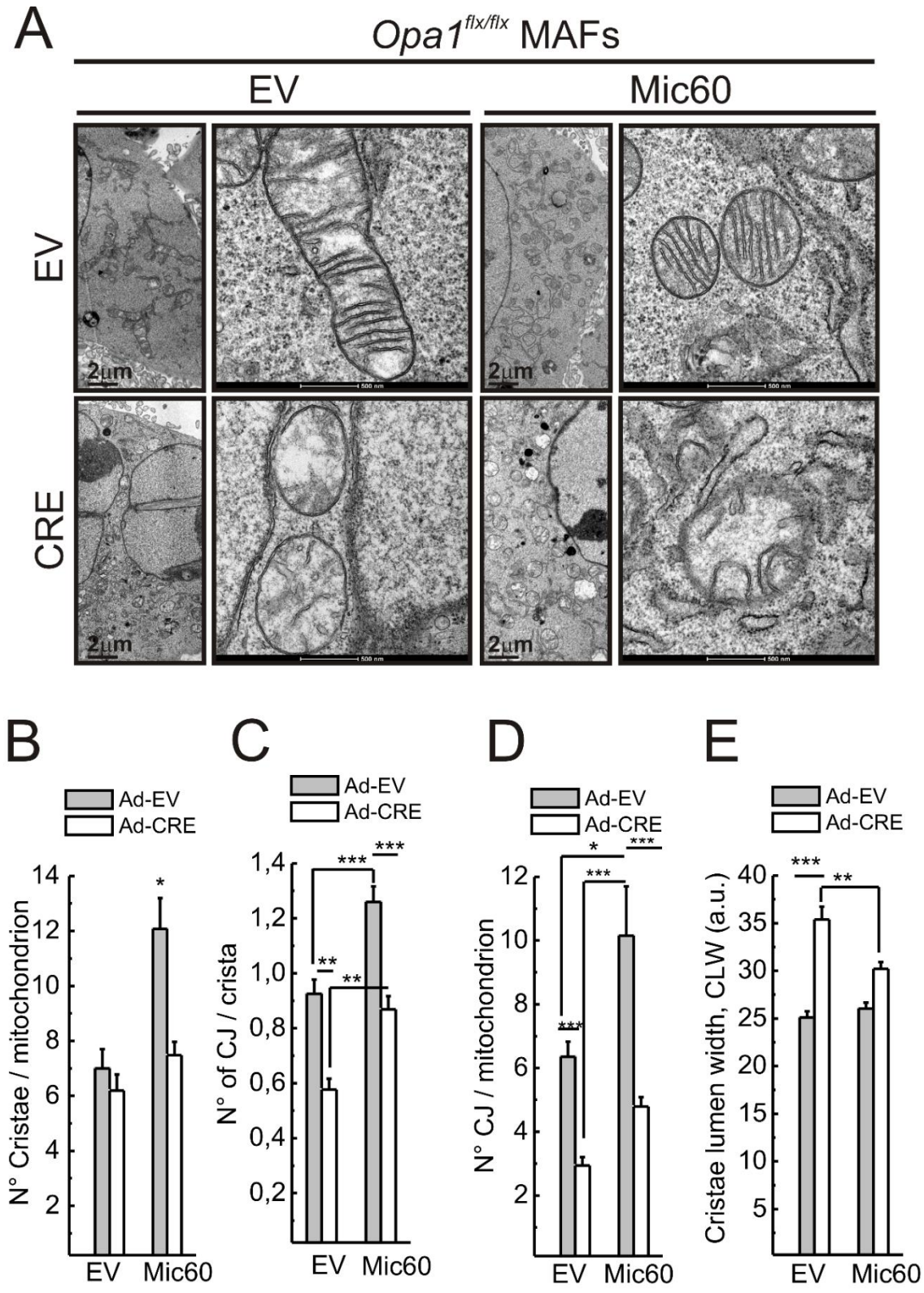
A
Opa1flx/flx MAFs
EV
Mic60
EV
CRE
2µm
B
Ad-EV
Ad-CRE
N° Cristae / mitochondrion
EV
Mic60
C
N° of CJ / crista
D
N° CJ / mitochondrion
E
Cristae lumen width, CLW (a.u.)

Figure 5

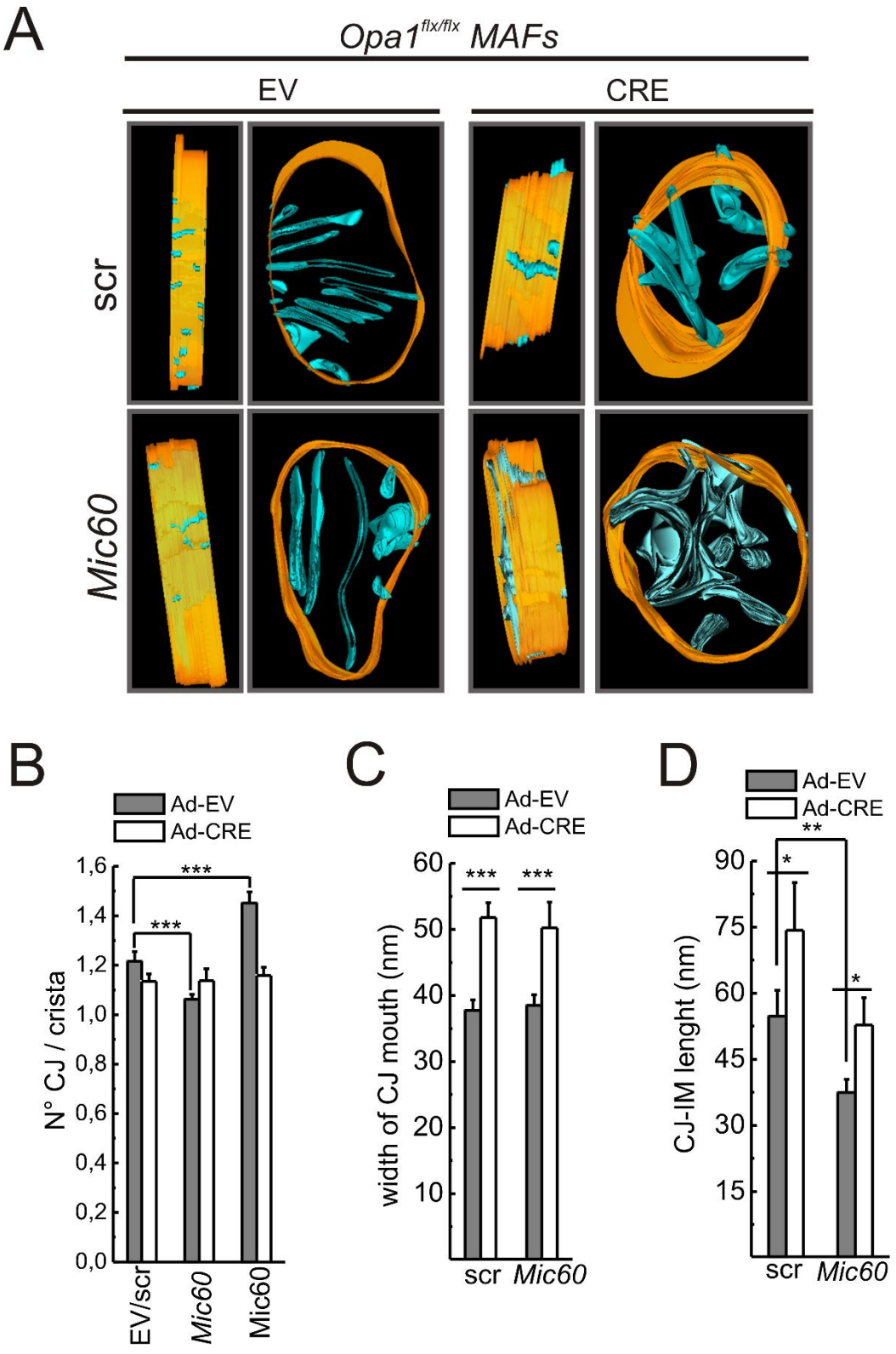
A
Opa1flx/flx MAFs
EV
CRE
scr
Mic60
B
Ad-EV
Ad-CRE
N° CJ / crista
1,6
1,4
1,2
1,0
0,8
0,6
0,4
0,2
0,0
***
***
EV/scr
Mic60
Mic60
C
Ad-EV
Ad-CRE
width of CJ mouth (nm)
60
50
40
30
20
10
***
***
scr
Mic60
D
Ad-EV
Ad-CRE
CJ-IM lenght (nm)
90
75
60
45
30
15
**
*
*
scr
Mic60

Figure 6

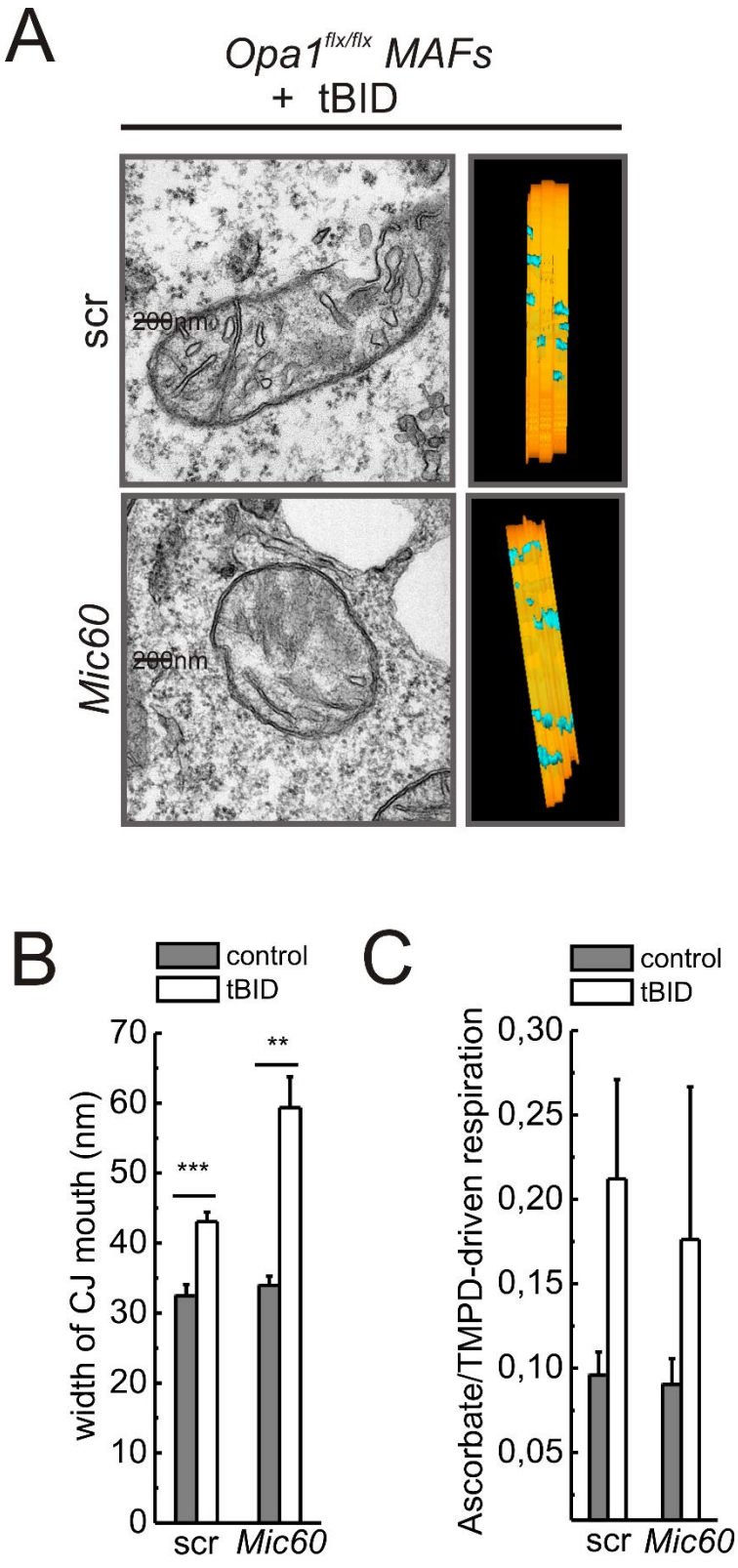
A
Opa1flx/flx MAFs
+ tBID
scr
Mic60
200nm
200nm
B
control
tBID
width of CJ mouth (nm)
70
60
50
40
30
20
10
0
***
**
scr
Mic60
C
control
tBID
Ascorbate/TMPD-driven respiration
0,30
0,25
0,20
0,15
0,10
0,05
scr
Mic60

Figure 7

Mammalian mitochondria cristae biogenesis is regulated by Mitofilin (Mic60)-OPA1 complexes that are eliminated during apoptosis

Christina Glytsou[1], Enrique Calvo[2], Irene Anastasia[1], Sara Cogliati[1,2], Andrea Raimondi[3], Norihito Shintani[4], Marta Loureiro[2], Jesùs Vazquez[2], Luca Pellegrini[5], Jose Antonio Enriquez[2], and Luca Scorrano[1, 6*], Maria Eugenia Soriano[1*]

Supplemental online material

Supplementary experimental procedures

Virus production and infection

The retroviral expression vector MSCV-IRES-GFP containing truncated BID (pMIG-tBid) was used to generate amphotropic retrovirus expressing tBID as described previously (Cogliati et al., 2013). 24 hr post infection the GFP-positive cells were sorted and after 48 hr they were fixed and processed for EM he efficiency of transduction was around 80-90% estimated by counting GFP positive cells with an epifluorescence microscope. Experiments were performed 48 hr after infection.

In Vitro Mitochondrial Assays

Ascorbate/TMPD-driven respiration was determined as previously described by Scorrano and coworkers (Scorrano et al., 2002).

Supplemental figure legends

Supplemental Figure 1.

A. Multiple amino acid sequence alignment of the predicted Mic60 transmembrane helix of vertebrates (upper panel) and mammals (lower panel), depicting the extent of conservation. Identical amino acids are marked with asterisk (*); strongly similar amino acids are marked with colons (:); weekly similar amino acids are marked with (.); non conserved amino acids are not marked ( ). The coiled-coil domains are highlighted. Conserved clusters of glycine residues are underlined in red.

B. Organization and alignment of the predicted protein domains of Mic60 homologues from yeast to human.

Supplemental Figure 2. Schematic representation of SILAC experiment workflow. Experiment *"a"* contains complexes extracted from control and cBID treated mitochondria isolated from mouse adult fibroblasts (MAFs) grown in a medium containing *heavy* or *light* amino acids respectively. Experiment *"b"* contained complexes extracted from control (*light*) and $cBID^{KKAA}$ treated (*heavy*) mitochondria. After BN-PAGE, Coomassie stained bands from 500 to 1048 kDa were excised and analyzed by qualitative and quantitative mass spectrometry.

Supplemental Figure 3.

A.B. Equal amounts of proteins (40 µg) from $Opa1^{flx/flx}$ MAFs infected with the indicated adenovirus (Ad-EV or Ad-CRE) were separated in Tris-Acetate 3-8% PAGE and

immunoblotted with the indicated antibodies. Fp protein was used as protein loading control.

C. Mic60 protein levels of cellular lysates from *Opa1*$^{flx/flx}$ MAFs 48 hr post-transfection with scramble (scr) or Mic60 siRNA oligos. siRNA #1, #2 and #3 represent three different siRNA oligos.

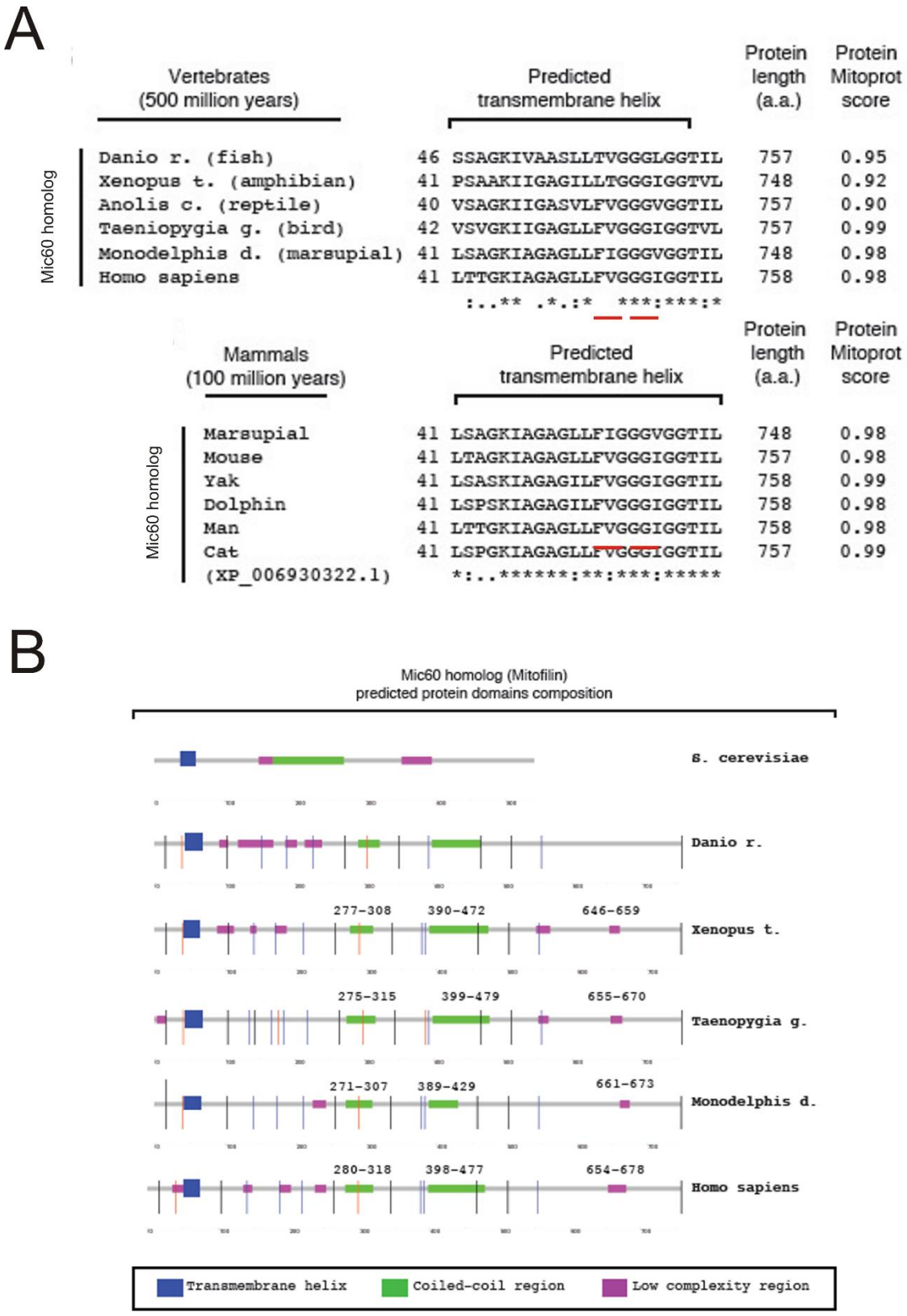

Suppl. Figure 1

Suppl. Figure 2

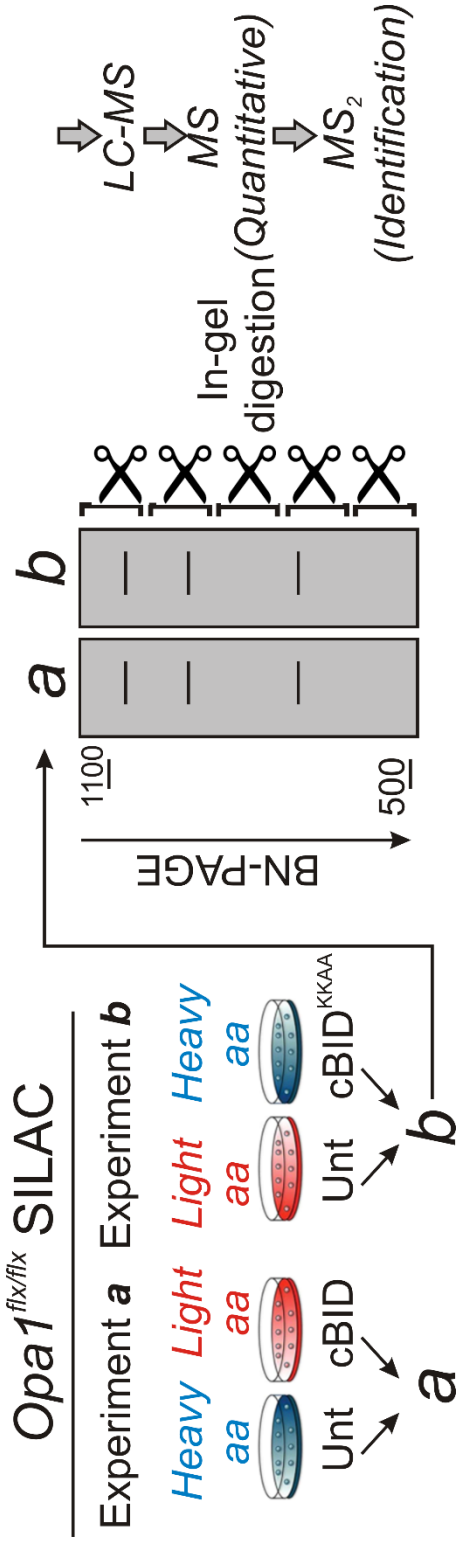

A

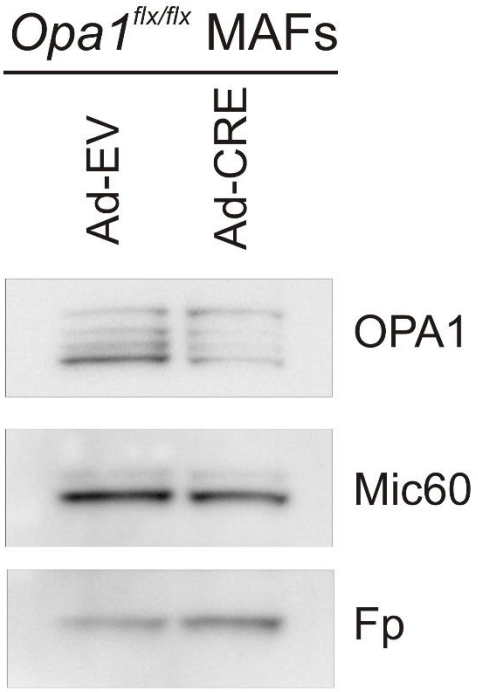

B

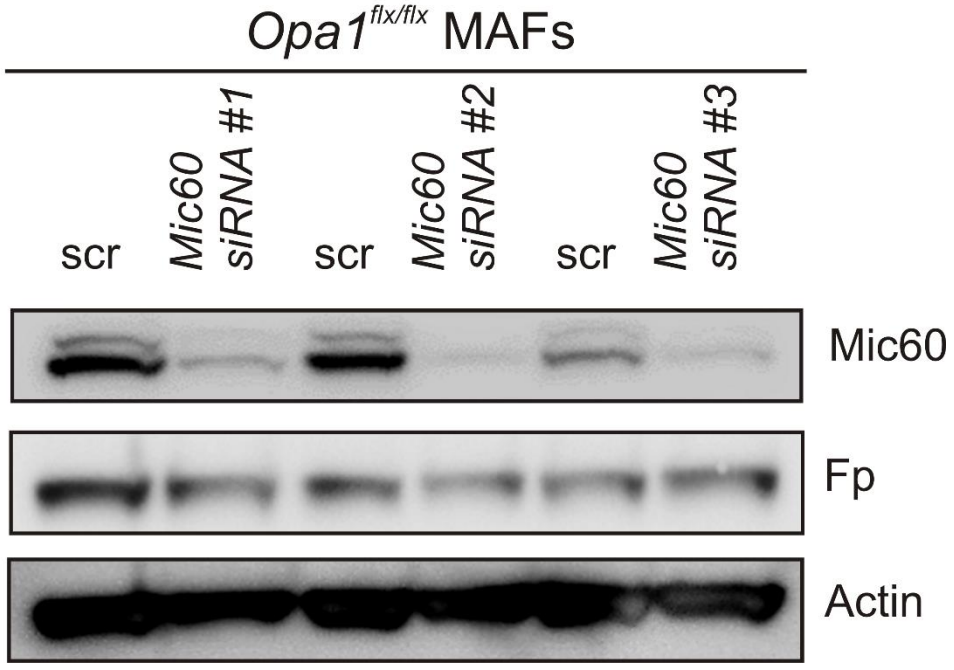

Suppl. Figure 3

2.3. Nitric Oxide-Associated 1 (NOA1) is part of the OPA1-containing complexes targeted during cell death

Nitric Oxide-Associated 1 (NOA1) is part of the OPA1-containing complexes targeted during cell death

Christina Glytsou[1], Marta Medaglia[1], Nicolo Ilaqua[1], Enrique Calvo[2], Jesùs Vazquez[2], Jose Antonio Enriquez[2], Luca Scorrano[1,3*] and Maria Eugenia Soriano[1*]

[1] Department of Biology, University of Padova, Padova, Italy

[2] Centro Nacional de Investigaciones Cardiovasculares Carlos III, Madrid, Spain

[3] Dulbecco-Telethon Institute, Venetian Institute of Molecular Medicine, Padova, Italy

Address correspondence to Luca Scorrano: luca.scorrano@unipd.it and Maria Eugenia Soriano: mariaeugenia.soriano@unipd.it

Abstract

Apoptotic cristae remodeling is controlled by heteromeric complexes containing Optic Atrophy 1 (OPA1) and disrupted by apoptotic stimuli. Composition of these complexes and the role of the OPA1 partners in controlling cristae shape are unclear. Here we identify nitric oxide-associated 1 (NOA1) as a member of OPA1-containing complexes targeted during apoptosis and cooperating with OPA1 in cristae shape regulation. Complexomic analysis retrieved NOA1 in heart mitochondria OPA1 containing complexes disrupted upon cristae remodeling. The OPA1-NOA1 interaction was confirmed biochemically and genetically. NOA1 genetic ablation causes mitochondrial fragmentation and cristae disorganization, corrected by NOA1 re-introduction as well as by OPA1 overexpression, supporting the OPA1 and NOA1 crosstalk in cristae shape morphogenesis. Functionally, NOA1 ablation phenocopies the effect of OPA1 deletion on respiratory complexes assembly, oxidative phosphorylation, apoptosis and mitochondria-dependent cell growth. Thus NOA1 cooperates with OPA1 in the regulation of mitochondrial function and ultrastructure during life and death of the cell.

Introduction

Mitochondria are key organelles for energy production, intermediate metabolism, calcium signaling, developmental control and last but not least programmed cell death (Dimmer and Scorrano, 2006). Their multiplicity of functions is reflected by their extremely complex structure, compartmentalization and dynamic organization. Mitochondria possess the outer mitochondrial membrane (OMM), that separates them from the cytosol, and the inner mitochondrial membrane (IMM) that encloses the matrix and constitutes the site of oxidative phosphorylation. The IMM can be further subdivided into two different compartments, the inner boundary membrane (IBM) and the cristae, a network of tubules and lamellae connected to the IBM by narrow tubular structures called cristae junctions. Dynamic changes in shape contribute to specific mitochondrial functions, such as apoptosis amplification (Vogel et al., 2006; Scorrano et al., 2002). "Cristae remodeling" indeed describes a set of morphological alterations that occur early after apoptotic stimulation and favor the mobilization of the cristae-endowed cytochrome c to the intermembrane space and eventually to the cytosol, thereby maximizing the efficiency of the intrinsic apoptotic pathway (Scorrano et al., 2002).

Optic Atrophy 1 (OPA1) is a mitochondrial shaping protein which controls cristae shape and remodeling by forming high molecular weight (HMW) complexes in the cristae to maintain them tight under physiological conditions. Upon apoptotic stimuli, OPA1-containing HMW complexes are disrupted with concomitant enlargement of the cristae junctions and cytochrome c release (Frezza et al., 2006; Cogliati et al., 2013). Little is known on the formation of these HMW, except that both the membrane anchored and the soluble forms of OPA1 are needed (Cipolat et al., 2006; Frezza et al., 2006). We therefore performed comprehensive proteomic analyses of native liver, fibroblast and

heart mitochondrial complexes identifying multiple OPA1 interactors that are targeted during apoptosis (Soriano & Glytsou et al., in preparation).

Among the OPA1 partners we identified a mitochondrial GTPase christened Nitric Oxide-Associated 1 (NOA1), a highly conserved protein across bacteria and eukaryotes. NOA1 belongs to the circularly permutated GTPase family (Sudhamsu et al., 2008), but its exact molecular action in eukaryotes is still obscure. Its bacterial orthologue, YqeH, along with other members of its protein superfamily are required for proper ribosome biogenesis and assembly (Loh et al., 2007; Uicker et al., 2007; Anand et al., 2009). In eukaryotes, NOA1 contains a classical mitochondrial targeting sequence (MTS) (Zemojtel et al., 2006), but also a classical bipartite nuclear localization signal (Al-Furoukh et al., 2014). In yeast, the NOA1 orthologue YOR205C (alternative names: mitochondrial GTPase MTG3, AIM40, GEP3, FMP38) is important for the correct assembly of the small mitoribosomal subunit, efficient respiration, and mtDNA stability (Paul et al., 2012). Two genetic interactome studies in yeast identified it as a genetic interactor of prohibitins, essential scaffolds that modulate mitochondrial cristae organization (Osman et al., 2009b). Yeast strains lacking YOR205C display decreased cardiolipin and PE levels (Hoppins et al., 2011; Osman et al., 2009a), and *Noa1* deletion in mice results in lethality at midgestation. Functional studies in mammalian cells suggested that NOA1 is required for mitochondrial protein synthesis, ATP production and apoptosis. However, the mechanism by which NOA1 impacts on mitochondrial functions is still undefined.

Here we unravel the physical and functional interaction between OPA1 and NOA1. Our data indicate that NOA1, like OPA1, is essential for mitochondrial structure, function and mitochondria-dependent cell growth.

Results

NOA1 and OPA1 are retrieved in the same HMW complexes targeted during apoptosis

Three dimensional BlueNative (BN)-BN-SDS PAGE followed by LC/MS analysis in normal and apoptotic mouse liver mitochondria revealed a list of candidate proteins that quantitatively change in OPA1-containing complexes during apoptosis (Soriano et al., in preparation). Among the identified proteins whose levels are significantly reduced in apoptosis, our attention was caught by a protein christened nitric oxide associated 1 (NOA1). BN-PAGE of digitonin solubilized mitochondrial complexes (Fig. 1A) followed by trypsinization, liquid chromatography (LC) and mass spectrometry (MS) allowed us to localize OPA1 and NOA1 in the same complexes in mouse heart, brain and a cell line, FC57 (Fig. 1B). Thus, targeted MS/LC analysis provided further evidence that NOA1 and OPA1 are found in two common macromolecular assemblies, which correspond to the spots 13-15 (approximate molecular weight 700-500kD) and 19-24 (approximate molecular weight 380-240kD). These MS data prompted us to verify biochemically whether OPA1 and NOA1 share the same complexes. First, we confirmed that overexpressed V5-tagged NOA1 and OPA1 could be crosslinked in a complex that is disrupted upon cristae remodeling induction by recombinant caspase-8 cleaved BID (cBID) (Frezza et al., 2006) (Fig. 1C, arrows). Second, V5-tagged NOA1 expressed in mouse embryonic fibroblasts (MEFs) could pull-down OPA1 (Fig. 1D). Third, endogenous OPA1 and NOA1 could be immunoprecipitated (Fig. 1E). Thus OPA1 and NOA1 are retrieved in the same complexes and physically interact.

mNOA1 resides predominately in the mitochondrial intermembrane space

Given the dual targeting sequences present in mammalian NOA1, we wished to verify if

and where it resided in mitochondria. Confocal imaging indicated that endogenous Noa1 co-localized with the mitochondrial marker Tim23 in HeLa cells (Bergmann's co-localization 78.1%, SEM 0.02, Supplementary Fig. S1A), without being detected into the nucleus in steady state conditions. Carbonate extraction in purified mouse liver mitochondria showed that mNOA1 is a peripherally associated membrane protein (Supplementary Fig. S1B). In order to examine NOA1 submitochondrial localization, we performed Proteinase K (PK) accessibility assay. The pattern of NOA1 was superimposable to that of OPA1 (Supplementary Fig. S1C), indicating that they share their localization in the IMS. Overall, NOA1 is a mitochondrial protein peripherally associated to the IMM facing the IMS.

NOA1 and OPA1 genetically interact

We next aimed to shed more light on the genetic relationship between the two proteins. To this end, we capitalized on *Noa1*$^{-/-}$ MEFs (Kolanczyk et al., 2011). Immunoblotting confirmed that NOA1 was absent in *Noa1*$^{-/-}$ MEFs. When we probed the same lysates for OPA1, we surprisingly observed an increase of OPA1 levels. This upregulation was specific, because OPA1 levels turned back to normal when NOA1 was reintroduced (Fig. 1F). The OPA1 upregulation was due to an increase in its transcript levels as indicated by quantitative real-time PCR (Fig. 1G). Reciprocally, NOA1 was absent in *Opa1*$^{-/-}$ MEFs, and its levels turned back to normal upon OPA1 re-introduction (Fig. 1H). Taken together, these data indicate that OPA1 and NOA1 interact also genetically.

NOA1 deficiency alters mitochondrial shape and ultrastructure

Since NOA1 and OPA1 physically and genetically interact, we next analyzed whether

changes in NOA1 levels altered mitochondrial morphology and ultrastructure. 3D-reconstructions of z-stacks of confocal images of wt and *Noa1*$^{-/-}$ MEFs expressing mitochondrial targeted dsRED (mtRFP) showed that mitochondria of *Noa1*$^{-/-}$ MEFs were 50% shorter than their wild type counterparts (Fig. 2A,B).

Mitochondrial fragmentation was accompanied by ultrastructural derangements with concentric cristae structures, as indicated by electron microscopy (EM) (Fig. 2C). *Noa1*$^{-/-}$ mitochondria were characterized by increased cristae width lumen (maximal cristae width) and fewer cristae junctions (Fig. 2D,E), suggesting that NOA1 participates like OPA1 in cristae junction biogenesis and organization. Additional morphometric analysis confirmed that mitochondria lacking NOA1 were smaller (Fig. 2F), and that cristae surface to mitochondrial area ratio was increased (Fig. 1G). These phenotypes were specific, because they were corrected by NOA1 reintroduction in *Noa1*$^{-/-}$ MEFs (Fig. 1H, I). Interestingly, overexpression of OPA1 in cells lacking NOA1 corrected the aberrant mitochondrial ultrastructure at a similar extent as upon NOA1 re-introduction (Fig. 1H and 1I), further supporting the hypothesis of an OPA1-NOA1 functional interplay in the control of cristae shape. To verify whether these defects were a consequence of chronic *Noa1* ablation, we turned to acute NOA1 silencing in HeLa cells. Efficient reduction of NOA1 transcript and protein levels by siRNA (Fig. S2B,C) resulted in similar cristae shape aberrations (Fig. S2A), with a reduction in the number of cristae per mitochondrion and an increase in maximal cristae width (Fig. S2D, E).

To test the consequence of NOA1 overexpression on the mitochondrial shape, MEFs were transfected with a plasmid expressing GFP-tagged NOA1 and GFP positive cells were sorted cytofluorimetrically and processed to be analyzed by EM. Mitochondria appeared elongated in cells overexpressing NOA1, as also confirmed by morphometric analysis

(Figure S2F,G). Collectively, these data indicate that NOA1 participates in the regulation of mitochondrial morphology, ultrastructure and cristae junction biogenesis.

NOA1 is essential for OXPHOS subunits stability and mitochondrial dependent cell survival and growth

Given the mitochondrial structure defects, we hypothesized that NOA1 ablation affects also mitochondrial functions. Indeed, Seahorse analysis showed impaired mitochondrial respiration in *Noa1*$^{-/-}$ MEFs (Fig. 3A). Due to the fact that OPA1 is a core regulator of cristae shape, a factor that controls the assembly of respiratory supercomplexes and therefore OXPHOS efficiency (Cogliati et al., 2013), we hypothesized that likewise, its partner NOA1 might affect respirasomes formation. Blue native PAGE of *Noa1*$^{-/-}$ mitochondrial extracts revealed a defect in the assembly even of individual respiratory complexes (Fig. 3B), potentially explaining the OXPHOS dysfunction. To understand whether the observed respiratory defect was a consequence of mtDNA loss, we measured by qPCR the *Sdha* (nuclear encoded) and *Mtco2* (mtDNA encoded) ratio that was unaltered in *Noa1*$^{-/-}$ cells (Fig. 3C), suggesting that mtDNA levels were not affected by loss of Noa1. Alternatively, the respiratory defects might be a consequence of abnormal mitochondrial translation. While the protein levels of several OXPHOS subunits were decreased in NOA1 deficient cells, this reduction was not restricted to mtDNA encoded proteins (like MTCO1 of CIV and ND4 of CI), but also to nuclear encoded OXPHOS subunits (NDUFB8 of CI) (Fig. 3D). These results suggest a general instability of OXPHOS proteins, probably due to the inability of respiratory chain complexes to properly assemble, as a consequence of altered cristae shape.

To understand whether the observed ultrastructural and bioenergetics defects had any

functional consequence, we measured growth of *Noa1*$^{-/-}$ cells in galactose-containing medium to force cells to rely on mitochondrial OXPHOS to generate ATP. *Noa1*$^{-/-}$ cells not only grew slower in galactose-containing medium (Fig. 4A), but they also underwent apoptosis, as indicated by flow cytometry analysis (Fig. 4B). Furthermore, *Noa1*$^{-/-}$ MEFs were more sensitive to H_2O_2 induced apoptosis (Fig. 4C) and NOA1 levels decreased, probably as a consequence of NOA1 cleavage (as indicated by the appearance of a novel lower MW immunoreactive band) in mitochondria treated with the apoptotic stimulus cBID (Fig. 4D). Thus, NOA1 is essential for mitochondrial function, impacting on mitochondria-dependent cell growth and viability.

Discussion

Cristae biogenesis, maintenance and dynamics are mainly mediated by protein complexes. One of the major regulators is OPA1, which resides in the IMM forming complexes (Frezza et al., 2006) along with multiple interactors, among which is NOA1 (Soriano et al., in preparation). Here we describe that NOA1 and OPA1 interact physically and functionally.

NOA1 peripherally associated membrane protein residing inside mitochondria. Worth noting, we did not observe any nuclear localization, which was reported previously (Al-Furoukh et al., 2014). Although NOA1 was previously localized in the mitochondrial matrix (Tang et al., 2009), our experiments of protease accessibility place it instead in the IMS, where it interacts with both soluble and transmembrane forms of OPA1.

The HMW complexes, in which OPA1 and NOA1 are retrieved, are targeted during apoptosis. Upon apoptosis induction in isolated mitochondria, NOA1 is possibly proteolytically cleaved, which could be a potential mechanism for the dissociation of OPA1/NOA1 complexes early during cell death stimulation. Similar to OPA1 ablation (Frezza et al., 2006), NOA1 loss sensitizes cells to programmed cell death induced by H_2O_2, indicating that it acts as an anti-apoptotic protein. Taken together, we suggest that OPA1 and NOA1 share common complexes whose integrity is lost early during cell death, providing probably a protective mechanism against apoptotic cristae remodeling under physiological conditions.

Not only the two proteins coexist in the same HMW complexes, but they also interact genetically and physically. Noteworthy, OPA1 is upregulated in *Noa1*$^{-/-}$ MEFs, possibly to serve as a compensatory response, whereas NOA1 is absent in *Opa1*$^{-/-}$ cells, indicating that the latter is essential for NOA1 stability.

Electron and confocal microscopy morphometric analysis allowed us to demonstrate that

NOA1 plays a key role in mitochondrial morphology and ultrastructure maintenance. Even though the phenotypes between *Opa1*$^{-/-}$ and *Noa1*$^{-/-}$ MEFs are not identical, mitochondria of both genotypes are fragmented and their cristae architecture is severely altered. Similar structural defects were observed also upon acute Noa1 ablation, excluding that the cristae alterations are a consequence of chronic Noa1 depletion. Interestingly, the ultrastructural defects of NOA1 deficient mitochondria can be corrected by the overexpression of OPA1 further supporting a model in which that the two proteins are functionally linked.

Since cristae shape regulates the efficiency of mitochondrial respiration (Cogliati et al., 2013), our prediction was that the *Noa1*$^{-/-}$ abnormal cristae structure resulted in impaired oxidative phosphorylation. Indeed, previous (Kolanczyk et al., 2011; Heidler et al., 2011) and our own results confirmed that when NOA1 is lacking mitochondrial respiration is defective. However, this was not caused by a reduction in mtDNA copy number (Kolanczyk et al., 2011), as it is conversely the case for cells chronically lacking mitochondrial fusion proteins (Chen et al., 2010). NOA1 orthologues in bacteria and yeast are required for proper mitoribosome biogenesis and assembly (Loh et al., 2007; Uicker et al., 2007; Anand et al., 2009) and mitochondrial translation defects are caused by mammalian NOA1 ablation (Kolanczyk et al., 2011), possibly explaining the respiration defect observed in *Noa1*$^{-/-}$ cells. We also found that levels of various OXPHOS subunits are remarkably decreased in *Noa1*$^{-/-}$ cells, but this reduction was global and not restricted to mtDNA encoded proteins. Our results suggest that the impaired respiration is a consequence of the instability of OXPHOS proteins and not of defective mitochondrial protein-synthesis. Interestingly, Blue Native PAGE revealed that respiratory complexes failed to be properly assembled in *Noa1*$^{-/-}$ MEFs, in line with previously published studies (Kolanczyk et al., 2011; Heidler et al., 2011) and with the changes observed upon genetic and apoptotic cristae

shape alterations (Cogliati et al., 2013). We therefore propose that OXPHOS subunits degradation in *Noa1*$^{-/-}$ cells results from the inability of respiratory chain complexes to properly assemble (Acin-Perez et al., 2008). Given that the GTPase domain of mammalian NOA1 contains a 100-aa insert absent from the bacterial homologue of NOA1 (YeqH), we could possibly suggest a diversity or multiplicity in its function along evolution. Collectively, we propose that mammalian NOA1 functions as a regulator of cristae shape, which is essential for the appropriate respiratory complexes formation and, thus, the efficient bioenergetic activity of mitochondria.

While upon NOA1 loss mitochondria fragment, NOA1 overexpression causes mitochondrial elongation, suggesting that NOA1 directly or indirectly contributes to organelle fusion and that NOA1 is a functional partner of OPA1 not only in cristae structure maintenance, but also in its profusion role. Further biochemical studies are required to test this hypothesis.

Intriguingly, high-throughput screens in yeast and mammals revealed NOA1 as a potential genetic or physical interactor of prohibitins, respectively. Considering that prohibitins control mitochondrial ultrastructure via regulating OPA1 processing, it would be interesting for the future to unveil the precise relationship between NOA1, OPA1 and prohibitins in the course of cristae shape maintenance.

To sum up, mammalian NOA1 cooperates with OPA1 in the regulation of the mitochondrial morphology, cristae shape and cristae remodeling, by participating in the formation of common macromolecular assemblies. NOA1, like its interactor OPA1, is essential for cristae integrity, which influences OXPHOS complexes assembly, efficiency and, subsequently, mitochondria-dependent cell viability, but it additionally participates in programmed cell death execution.

Experimental procedures

Cell culture, cell growth experiments and transfections

Noa1$^{+/+}$ and *Noa1*$^{-/-}$ mouse embryonic fibroblasts were maintained in Dulbecco's Modified Eagle Medium (DMEM, Invitrogen) supplemented with 10% fetal bovine serum (FBS, Invitrogen), 50 U/ml Penicillin, 50 µg/ml Streptomycin, 0.1 mM non-essential amino acids (0.89 g/l L-alanine, 1.32 g/l L-asparagine, 1.33 g/l L-aspartic acid, 1.47 g/l L-glutamic acid, 0.75 g/l glycine, 1.15 g/l L-proline, 1.05 g/l L-serine, Invitrogen), 50 µg/ml L-uridine, 1 mM sodium pyruvate, 10% Amniomax C-100 supplement (Invitrogen). When indicated, glucose was substituted with 0.9 mg/ml galactose (Sigma).

The medium (DMEM) for HeLa was supplemented with 10% of fetal bovine serum (FBS), 50 U/ml Penicillin, 50 µg/ml Streptomycin, 0.1 mM non-essential amino acids and 2 mM glutamine.

Opa1$^{+/+}$, *Opa1*$^{-/-}$, *Opa1*$^{-/-}$::OPA1 mouse embryonic fibroblasts (MEFs) and *Opa1*$^{flx/flx}$ mouse adult fibroblasts (MAFs) were cultured as previously described (Cogliati et al., 2013). All the cell lines were cultured at 37°C in a 5% CO_2 atmosphere.

Plasmid transfections were performed using Lipofectamine2000 following manufacturer's instructions (Invitrogen).

For cell growth, equal numbers of cells were seeded in 12-well plates. Viable cells were counted daily for 3 days using a hemocytometer as determined by Trypan Blue exclusion and normalized to the initial number of cells.

Mitochondria Isolation

Mitochondria from mouse liver and cell lines were isolated by standard differential centrifugation as previously described (Frezza et al., 2007). Mouse heart and brain mitochondria were purified as described in (Fernandez-Vizarra et al., 2010).

Molecular biology

pcDNA3.2-hNOA1-V5 and pcDNA47-hNOA1-GFP were generated by subcloning the plasmid pDONR221-hNOA1 (DNASU) into the corresponding vectors (Invitrogen) using the Gateway cloning system. Constructs were confirmed by sequencing. pMSCV-OPA1 and mitochondrial targeted red fluorescent protein (mtRFP), which corresponds to pDsRed2-Mito, were previously described (Cipolat et al., 2004).

Biochemistry

Cell lysis was performed with RIPA buffer (150 mM NaCl, 1% Nonidet P-40, 0.25% deoxycholate, 1 mM EDTA, 50 mM Tris, pH 7.4) in the presence of complete protease-inhibitor mixture (Sigma). Protein concentration was measured by Bradford protein assay (Biorad). Proteins (20-30 μg) were separated by 4–12% Tris-MOPS SDS–PAGE or 3%–8% Tris-acetate polyacrylamide gels (NuPage, Invitrogen), transferred onto PVDF membranes (Millipore) and probed using the following antibodies: mouse monoclonal anti-OPA1 (1:1000 BD Biosciences), rabbit polyclonal anti-C4orf14 (1:500 Proteintech), rabbit polyclonal anti-GRP75 (1:2000 Santa Cruz Biotechnology), rabbit polyclonal anti-VDAC (1:1000 Abcam), mouse monoclonal anti-V5 (1:1000 Invitrogen), mouse monoclonal anti-SDHA (1:5000 Abcam), rabbit polyclonal anti-TOM20 (1:1000 Santa Cruz Biotechnology), rabbit polyclonal anti-GAPDH (1:1000 Sigma), rabbit polyclonal anti-ND4 (1:500 Santa

Cruz Biotechnology), mouse monoclonal anti-NDUFB8 (1:1000 Abcam), mouse monoclonal anti-MTCO1 (1:1000 Abcam), mouse monoclonal anti-cytochrome c (1:1000 BD Pharmigen), mouse monoclonal anti-ATP5a (1:4000 Abcam) and mouse monoclonal anti-actin clone C4 (1:10000 Millipore). Isotype matched, horseradish peroxidase-conjugated secondary antibodies (GE Healthcare Life Sciences) were used followed by detection of chemiluminescence using the ECL western blotting substrate (Life Technologies) and ImageQuant LAS 4000 (GE Healthcare Life Sciences).

For protein crosslinking, mitochondria (0.5 mg/ml) purified from MAFs were treated, when indicated, with 50 pmol cBID per mg in experimental buffer (E.B., 150 mM KCl, 10 mM Tris-Mops pH 7.4, 10 µM EGTA-Tris, 1 mM Pi and 5/2.5 mM Glutamate/Malate) for 30 min at room temperature agitating. The reaction was quenched with a centrifugation at 10000 x g. Subsequently, mitochondria were resolved in 10 mM bismaleimidohexane (BMH, PIERCE) in E.B., incubated with the crosslinker for 1 hr at 25°C, spun and dissolved in SDS-PAGE loading buffer (NuPage, Invitrogen). Mitochondrial proteins (20 µg) were separated on 7% Tris-acetate polyacrylamide gels (NuPage, Invitrogen) and western blotting was performed as described before.

Immunoprecipitation

For immunoprecipitations, MEFs transfected with pcDNA3.2-hNOA1-V5 were lysed in PBS 0.1% Triton-X 100 supplemented with a protease inhibitor cocktail (PIC, Sigma-Aldrich). Equal amounts of lysates (150 µg) were diluted 1:5 in PBS with PIC and pre-cleared with 10 µl of Dynabeads (Magnetic beads, ThermoFisher). Dynabeads were blocked with PBS 1% BSA, 10% FBS for 5 min and then incubated with the indicated antibody (1:50, 30 min, 25°C). Then, pre-cleared extracts were precipitated in the Dynabeads-antibody complex

for 1 hr at 25°C. Precipitates were washed extensively three times in lysis buffer and bound complexes were eluted with 2× SDS-PAGE sample buffer (NuPAGE, Invitrogen), boiled and analyzed by immunoblotting. As a negative control lysates were incubated with plain Dynabeads in the absence of any antibody.

Blue Native PAGE for respiratory supercomplexes

5 x 10^6 cells were spun down, washed and resuspended in 400 µl of 4% digitonin in PBS with the addition of protease inhibitor cocktail (PIC, SIGMA) and incubated on ice for 10min. The samples were centrifuged at 10000 x g for 10 min at 4°C, washed with cold PBS and centrifuged again. The pellet was suspended in 100 µl of native buffer (Native sample buffer (Invitrogen), 1% Dodecyl D Maltoside (DDM, SIGMA) and PIC (SIGMA), incubated 5 min on ice and centrifuged at 22000 x g for 30 min at 4°C to extract the soluble complexes. 10 µl of Native PAGE Sample additive G250 5% (Invitrogen) were added into the supernatant. Equal volumes were loaded onto a 3-12% Native Bis-Tris gel (Invitrogen).

Recombinant Protein Expression

p7/p15 recombinant BID was produced, purified and cleaved with caspase-8 as previously described (Frezza et al., 2006).

Quantitative RT-PCR

Total RNA from cultured fibroblasts was extracted using RNeasy Mini Kit (Qiagen) and treated with DNAase I (Sigma) for 15 min at room temperature. mRNA was retrotranscribed using Superscript III RT–PCR Kit and oligo-$(dT)_{20}$ primers (Invitrogen). Real-time quantitative PCR was performed on a 7900 Genetic Analyzer (Applied

Biosystems) using GoTaq Green Master Mix (Promega). Reaction conditions were standard (95°C 15 s, 60°C 30 s; 40 cycles). Oligonucleotides used in the reactions were the following: 5′-TGACAAACTTAAGGAGGCTGTG-3′ and 5′- CATTGTGCTGAATAACCCTCAA-3′ for mouse Opa1, 5′-GTCTCCTGCGACTTCAAC-3′ and 5′-TCATTGTCATACCAGGAAATGAGC-3′ for mouse *Gapdh*, 5′-TGTGATTGAAAACATCTACCTTCCA-3′ and 5′-TTTAAGCTTGATATCCACTGTGGTGT-3′ for human *OPA1*, 5′-ATGTCGTAGGAAGAGTTGGA-3′ and 5′- GTCAAAGGCAAGTGAATCAG-3′ for human *NOA1*, 5′-AACAGCGACACCCACTCCTC-3′ and 5′- CATACCAGGAAATGAGCTTGACAA-3′ for human *GAPDH*. All the results were normalized to GAPDH mRNA expression.

Live Imaging

To visualize mitochondrial network, 10^5 cells were seeded onto 25 mm coverslips and transfected with mtRFP. 24 hr post-transfection, the coverslips were covered with Hank's Balanced Salt Solution (HBSS) supplemented with 10 mM Hepes and fluorescence signals were analyzed using IMIC Andromeda system (Fondis Electronic) equipped with ORCA-03G Camera (Hamamatsu), a × 60 oil objective (UPLAN × 60 oil, 1.35NA, Olympus), 488 and 561 nm lasers for excitation and FF01-446/523/600/677 (Semrock) as emission filter. Stacks of 10 images separated by 0.5 µm along the z axis were acquired a × 60 objective (oil; CFI Plan APO 1.4 NA) and 561 nm (50 mW) excitation (Santo-Domingo et al., 2013). 3D reconstruction and volume rendering were performed using a plug-in of ImageJ 1.44o software (National Institutes of Health). Mitochondrial length was quantified with Image J tool 'Freehand line selection' by measuring the average mitochondrial major axis length of 10 mitochondria per cell in 20 cells per sample.

Transmission electron microscopy and mitochondrial morphometry

Cells were fixed with freshly prepared glutaraldehyde at a final concentration of 1.25% (V/V) in 0.1 M Sodium cacodylate trihydrate pH 7.2 for 1 hr at 37ºC and washed in 0.1 M Sodium cacodylate trihydrate. Embedding and staining were performed as described in (Scorrano et al., 2002). When indicated, cell sorting was performed before fixation. MEFs were transfected with pcDNA47-hNOA1-GFP or pcDNA47-GFP and the next day harvested and sorted using flow cytometry with FACS Canto (BD Biosciences). The cells expressing GFP were cultured into dishes and fixed after 16 hr. For electron microscopy visualization, thin sections were imaged on a Tecnai-12 electron microscope (Philips-FEI) at the EM Facility of University of Padova. For morphometric analysis, mitochondrial parameters were measured using Image J (National Institutes of Health).

Seahorse analysis

Oxygen consumption rate (OCR, pmol/min) was determined using XF24 Extracellular Flux Analyzer and the XF cell mito stress test kit (Seahorse Biosciences). 9000 wt MEFs or 36000 *Noa1*$^{-/-}$ MEFs per well were seeded in an XF24 cell culture microplate and, after 24 hr, the normal medium was exchanged with the Cellular Assay Solution (8.3 g/L DMEM, 5 g/L Glucose, 0.58 g/L Glutamine, 1 mM Sodium Pyruvate, 0.015 g/L Phenol Red, pH 7.2). The assay consisted of oxygen consumption measurements during time starting with the basal conditions and followed by sequential injections of Oligomycin 1.3 µM, FCCP 0.4 µM and Rotenone 1.0 µM/Antimycin 1.2 µM. Three measurements were performed after each compound injection. The analysis was performed simultaneously in the same plate for the control and *Noa1*$^{-/-}$ cells.

Measurement of mitochondrial DNA copy number

Total cellular DNA was isolated from 5 x 10^6 MEFs using DNeasy Blood & Tissue Kit (Qiagen) and was amplified by real time PCR using GoTaq Green Master Mix (Promega) following manufacturer's indications. Reaction conditions were (95°C 15 s, 60°C 60 s; 40 cycles). The oligodeoxynucleotides used were specific for the mtDNA encoded gene mt-Co2 (3'- CTACAAGACGCCACAT-5' and 3'- GAGGGGGAGAGCAAT-5') and the nuclear encoded gene Sdha (3'-TACTACAGCCCCAAGTCT-5' and 3'- TGGACCCATCTTCTATGC-5'). The mtDNA copy number per cell was calculated using Sdha amplification as a reference for nuclear DNA content.

Cell viability assay

For cell death analysis, 1,5x10^4 MEFs of the indicated genotype were seeded in 12-well-plates. After 24 hr the medium was changed for fresh glucose- or galactose-containing medium. Cells were harvested at the indicated time points and stained with annexin-V FITC and propidium iodide (eBiosciences). Cell viability was measured by flow cytometry (FACSCalibur, BD Biosciences) as the percentage of annexin-V and PI negative events.

Acknowledgments

We thank Mateusz Kolanczyk for kindly providing us with *Noa1*$^{+/+}$ and *Noa1*$^{-/-}$ MEFs.

Acin-Perez,R., Fernandez-Silva,P., Peleato,M.L., Perez-Martos,A., and Enriquez,J.A. (2008). Respiratory active mitochondrial supercomplexes. Mol. Cell *32*, 529-539.

Al-Furoukh,N., Kardon,J.R., Kruger,M., Szibor,M., Baker,T.A., and Braun,T. (2014). NOA1, a novel ClpXP substrate, takes an unexpected nuclear detour prior to mitochondrial import. PLoS. One. *9*, e103141.

Anand,B., Surana,P., Bhogaraju,S., Pahari,S., and Prakash,B. (2009). Circularly permuted GTPase YqeH binds 30S ribosomal subunit: Implications for its role in ribosome assembly. Biochem. Biophys. Res. Commun. *386*, 602-606.

Chen,H., Vermulst,M., Wang,Y.E., Chomyn,A., Prolla,T.A., McCaffery,J.M., and Chan,D.C. (2010). Mitochondrial fusion is required for mtDNA stability in skeletal muscle and tolerance of mtDNA mutations. Cell *141*, 280-289.

Cipolat,S., Martins de Brito O., Dal Zilio B., and Scorrano,L. (2004). OPA1 requires mitofusin 1 to promote mitochondrial fusion. Proc. Natl. Acad. Sci. U. S. A *101*, 15927-15932.

Cipolat,S., Rudka,T., Hartmann,D., Costa,V., Serneels,L., Craessaerts,K., Metzger,K., Frezza,C., Annaert,W., D'Adamio,L., Derks,C., Dejaegere,T., Pellegrini,L., D'Hooge,R., Scorrano,L., and De Strooper,B. (2006). Mitochondrial Rhomboid PARL Regulates Cytochrome c Release during Apoptosis via OPA1-Dependent Cristae Remodeling. Cell *126*, 163-175.

Cogliati,S., Frezza,C., Soriano,M.E., Varanita,T., Quintana-Cabrera,R., Corrado,M., Cipolat,S., Costa,V., Casarin,A., Gomes,L.C., Perales-Clemente,E., Salviati,L., Fernandez-Silva,P., Enriquez,J.A., and Scorrano,L. (2013). Mitochondrial cristae shape determines respiratory chain supercomplexes assembly and respiratory efficiency. Cell *155*, 160-171.

Dimmer,K.S. and Scorrano,L. (2006). (De)constructing mitochondria: what for? Physiology. (Bethesda.) *21*, 233-241.

Fernandez-Vizarra,E., Ferrin,G., Perez-Martos,A., Fernandez-Silva,P., Zeviani,M., and Enriquez,J.A. (2010). Isolation of mitochondria for biogenetical studies: An update. Mitochondrion. *10*, 253-262.

Frezza,C., Cipolat,S., Martins,d.B., Micaroni,M., Beznoussenko,G.V., Rudka,T., Bartoli,D., Polishuck,R.S., Danial,N.N., De Strooper,B., and Scorrano,L. (2006). OPA1 Controls Apoptotic Cristae Remodeling Independently from Mitochondrial Fusion. Cell *126*, 177-189.

Frezza,C., Cipolat,S., and Scorrano,L. (2007). Organelle isolation: functional mitochondria from mouse liver, muscle and cultured fibroblasts. Nat. Protoc. *2*, 287-295.

Heidler,J., Al-Furoukh,N., Kukat,C., Salwig,I., Ingelmann,M.E., Seibel,P., Kruger,M., Holtz,J., Wittig,I., Braun,T., and Szibor,M. (2011). Nitric oxide-associated protein 1 (NOA1) is necessary for oxygen-dependent regulation of mitochondrial respiratory complexes. J. Biol. Chem. *286*, 32086-32093.

Hoppins,S., Collins,S.R., Cassidy-Stone,A., Hummel,E., Devay,R.M., Lackner,L.L., Westermann,B., Schuldiner,M., Weissman,J.S., and Nunnari,J. (2011). A mitochondrial-focused genetic interaction map reveals a scaffold-like complex required for inner membrane organization in mitochondria. J. Cell Biol. *195*, 323-340.

Kolanczyk,M., Pech,M., Zemojtel,T., Yamamoto,H., Mikula,I., Calvaruso,M.A., van den Brand,M.l., Richter,R., Fischer,B., Ritz,A., Kossler,N., Thurisch,B., Spoerle,R., Smeitink,J., Kornak,U., Chan,D., Vingron,M., Martasek,P., Lightowlers,R.N., Nijtmans,L., Schuelke,M., Nierhaus,K.H., and Mundlos,S. (2011). NOA1 is an essential GTPase required for mitochondrial protein synthesis. Molecular Biology of the Cell *22*, 1-11.

Loh,P.C., Morimoto,T., Matsuo,Y., Oshima,T., and Ogasawara,N. (2007). The GTP-binding protein YqeH participates in biogenesis of the 30S ribosome subunit in Bacillus subtilis. Genes Genet. Syst. *82*, 281-289.

Osman,C., Haag,M., Potting,C., Rodenfels,J., Dip,P.V., Wieland,F.T., Brugger,B., Westermann,B., and Langer,T. (2009a). The genetic interactome of prohibitins: coordinated control of cardiolipin and phosphatidylethanolamine by conserved regulators in mitochondria. J. Cell Biol. *184*, 583-596.

Osman,C., Merkwirth,C., and Langer,T. (2009b). Prohibitins and the functional compartmentalization of mitochondrial membranes. J. Cell Sci. *122*, 3823-3830.

Paul,M.F., Alushin,G.M., Barros,M.H., Rak,M., and Tzagoloff,A. (2012). The putative GTPase encoded by MTG3 functions in a novel pathway for regulating assembly of the small subunit of yeast mitochondrial ribosomes. J. Biol. Chem. *287*, 24346-24355.

Rizk,A., Paul,G., Incardona,P., Bugarski,M., Mansouri,M., Niemann,A., Ziegler,U., Berger,P., and Sbalzarini,I.F. (2014). Segmentation and quantification of subcellular structures in fluorescence microscopy images using Squassh. Nat. Protoc. *9*, 586-596.

Santo-Domingo,J., Giacomello,M., Poburko,D., Scorrano,L., and Demaurex,N. (2013). OPA1 promotes pH flashes that spread between contiguous mitochondria without matrix protein exchange. EMBO J. *32*, 1927-1940.

Scorrano,L., Ashiya,M., Buttle,K., Weiler,S., Oakes,S.A., Mannella,C.A., and Korsmeyer,S.J. (2002). A distinct pathway remodels mitochondrial cristae and mobilizes cytochrome c during apoptosis. Dev. Cell *2*, 55-67.

Sudhamsu,J., Lee,G.I., Klessig,D.F., and Crane,B.R. (2008). The structure of YqeH. An AtNOS1/AtNOA1 ortholog that couples GTP hydrolysis to molecular recognition. J. Biol. Chem. *283*, 32968-32976.

Tang,T., Zheng,B., Chen,S.H., Murphy,A.N., Kudlicka,K., Zhou,H., and Farquhar,M.G. (2009). hNOA1 interacts with complex I and DAP3 and regulates mitochondrial respiration and apoptosis. J. Biol. Chem. *284*, 5414-5424.

Uicker,W.C., Schaefer,L., Koenigsknecht,M., and Britton,R.A. (2007). The essential GTPase YqeH is required for proper ribosome assembly in Bacillus subtilis. J. Bacteriol. *189*, 2926-2929.

Vogel,F., Bornhovd,C., Neupert,W., and Reichert,A.S. (2006). Dynamic subcompartmentalization of the mitochondrial inner membrane. J. Cell Biol. *175*, 237-247.

Zemojtel,T., Kolanczyk,M., Kossler,N., Stricker,S., Lurz,R., Mikula,I., Duchniewicz,M., Schuelke,M., Ghafourifar,P., Martasek,P., Vingron,M., and Mundlos,S. (2006). Mammalian mitochondrial nitric oxide synthase: characterization of a novel candidate. FEBS Lett. *580*, 455-462.

Figure legends

Figure 1. NOA1 and OPA1 interact physically and genetically

A. Coomassie staining after Blue Native PAGE of digitonin solubilized mitochondrial extracts. The picture shows the approximate molecular weight of each of the thirty different spots in which Blue Native gel lane was cut, in order to be subjected to LC/MS analysis, as shown in the figure 1B.

B. Graph depicting OPA1 and NOA1 peptides identified along the Blue Native gel lane by liquid chromatography and mass spectrometry in mitochondria from mouse brain, heart and a cell line (FC57).

C. Mitochondrial crosslinking. MAFs were transfected with pcDNA3.2-hNOA1-V5. After 24 hr mitochondria were isolated, when indicated, treated with 50 pmol/mg of cBID for 30 min at room temperature, spun and crosslinked with 10 mM BMH for 1 hr at 25°C. Equal amounts of proteins (20 μg) were separated by SDS-PAGE and immunoblotted using anti-V5 and anti-OPA1 antibodies. Arrows denote the complexes.

D. NOA1-V5 was immunoprecipitated from MEFs transfected with pcDNA3.2-hNOA1-V5 and analyzed by SDS-PAGE/immunoblotting as indicated. For input 15 μg of cell lysates were loaded. Cell lysates incubated with beads without antibody served as a negative control.

E. OPA1 was immunoprecipitated from MEFs transfected with pcDNA3.2-hNOA1-V5 and analyzed by SDS-PAGE/immunoblotting as indicated. For input 15 μg of cell lysates were loaded. Cell lysates incubated with beads without antibody served as a negative control.

F. Equal amounts (30 μg) of the whole lysates from *Noa1*$^{+/+}$ and *Noa1*$^{-/-}$ MEFs transfected with the plasmids pcDNA3.2-hNOA1-V5 (NOA1-V5) or empty vector (EV), when indicated, were separated by SDS PAGE and immunoblotted using anti-OPA1 and anti-actin.

G. qPCR analysis of mOPA1 transcript levels of *Noa1*$^{-/-}$ MEFs, normalized to GAPDH and to wt MEFs. Data represent mean ± SEM of three independent experiments.

H. Equal amounts (30 μg) of the whole lysates from *Opa1*$^{+/+}$, *Opa1*$^{-/-}$ and *Opa1*$^{-/-}$::OPA1 MEFs transfected with the indicated plasmids were separated by SDS PAGE and immunoblotted using anti-NOA1 and anti-GAPDH.

Figure 2. NOA1 deficiency alters mitochondrial morphology and ultrastructure

A. Representative confocal images of MEFs of the indicated genotype transfected with mtRFP.

B. Quantification of the average mitochondrial length. Data represent mean ± SEM of three independent experiments (10 mitochondria per cell, 20 cells per sample).

C. Electron microscopy analysis of *Noa1*$^{+/+}$ and *Noa1*$^{-/-}$ MEFs. The scale bar represents 500 nm.

D. Quantification of the number of cristae per mitochondrion in *Noa1*$^{+/+}$ and *Noa1*$^{-/-}$ MEFs. Data represent mean ± SDV of 20 randomly selected mitochondria.

E. Morphometric analysis of the maximal cristae width. Data represent mean ± SDV of 300 cristae.

F. Quantification of mitochondrial perimeter in *Noa1*$^{+/+}$ and *Noa1*$^{-/-}$ MEFs. Data represent mean ± SEM of three independent experiments (25 mitochondria per experiment).

G. Morphometric analysis of the ratio cristae surface area to mitochondrial surface area. Data represent mean ± SDV of 25 randomly selected mitochondria.

H. Electron microscopy analysis of *Noa1*$^{-/-}$ MEFs transfected, where indicated, with empty vector (EV), pcDNA3.2-hNOA1-V5 (NOA1) or pMSCV-OPA1 (OPA1). The scale bar represents 500 nm.

I. Morphometric analysis of the cristae width. Data represent mean ± SDV of 514 cristae.

Figure 3. NOA1 loss leads to a global reduction of mitochondrial respiratory chain complexes subunits

A. Oxygen consumption rate is measured by Seahorse XF Cell Mito Stress Test Kit in basal conditions and after the addition of oligomycin 1.3 μM (A), FCCP 0.4 μM (B) and rotenone 1 μM/antimycin 1.2 μM (C). The blue horizontal line connotes the basal respiration of wt cells.

B. BN PAGE analysis of OXPHOS proteins in mitochondria from wt and *Noa1*$^{-/-}$ MEFs. Equal amounts (150 μg) of solubilized membrane complexes were separated in native conditions, transferred onto PVDF membranes and probed with the indicated antibodies.

C. mtDNA copy number quantification. Total DNA was isolated from the indicated cell lines. mtDNA and ncDNA was amplified by RT-PCR using specific primers. The mtDNA copy number was normalized to the mtDNA copy number of the correspondent WT cell line. Data are average ± SEM of two independent experiments.

D. Equal amounts (30 μg) of mitochondrial proteins were separated by SDS PAGE, transferred onto PVDF membranes and probed with the indicated antibodies against various OXPHOS subunits.

Figure 4. NOA1 is required for mitochondrial dependent cell growth and viability

A. *Growth curve.* Cells of the indicated genotype were cultured in DMEM supplemented with the indicated monosaccharide. Viable cells were counted using Trypan blue exclusion and compared to the seeding cell number. Data represent the mean ± SEM of three independent experiments.

B. *Cell viability.* Cells of the indicated genotype were cultured in DMEM supplemented with the indicated monosaccharide. Viable cells were determined cytofluorimetrically as the percentage of Annexin-V negative cells. Data represent the mean ± SEM of three independent experiments.

C. Purified mouse liver mitochondria (0.5 mg/ml) were incubated in experimental buffer and treated for the indicated time with 20 pmol/mg of cBID at 25°C. Proteins (20 μg) were separated with SDS-PAGE and immunoblotted with the indicated antibodies.

D. *Noa1*$^{+/+}$ and *Noa1*$^{-/-}$ MEFs were treated with 1 mM H_2O_2 for the indicated times and viability was determined cytofluorimetrically as the percentage of Annexin-V and Propidium Iodide negative cells. Data represent mean ± SEM of two independent experiments.

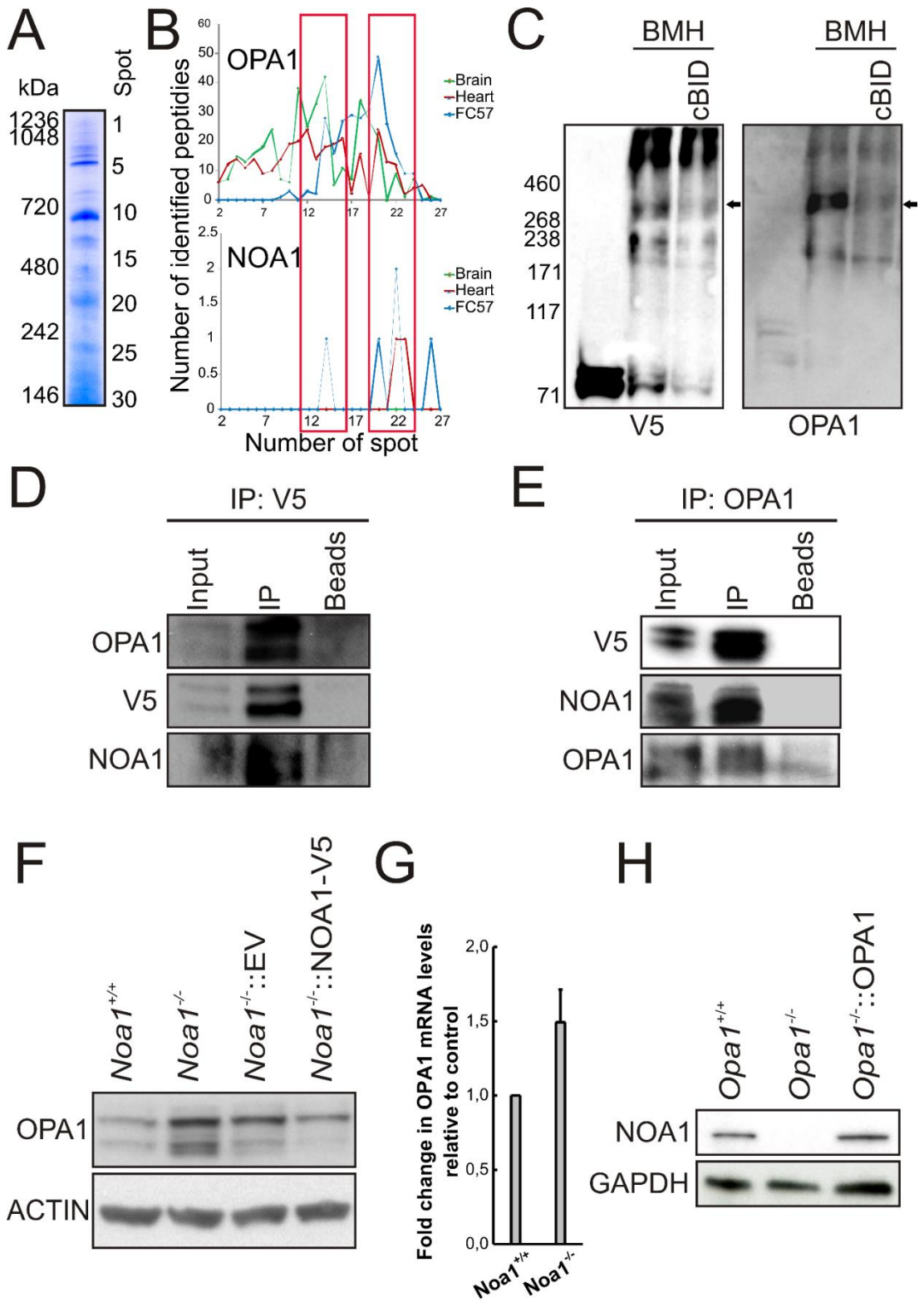
A
kDa
Spot
1236
1048
720
480
242
146
1
5
10
15
20
25
30
B
OPA1
NOA1
Brain
Heart
FC57
Number of identified peptides
Number of spot
C
BMH
cBID
460
268
238
171
117
71
V5
OPA1
D
IP: V5
Input
IP
Beads
OPA1
V5
NOA1
E
IP: OPA1
Input
IP
Beads
V5
NOA1
OPA1
F
Noa1+/+
Noa1-/-
Noa1-/-::EV
Noa1-/-::NOA1-V5
OPA1
ACTIN
G
Fold change in OPA1 mRNA levels relative to control
2,0
1,5
1,0
0,5
0,0
Noa1+/+
Noa1-/-
H
Opa1+/+
Opa1-/-
Opa1-/-::OPA1
NOA1
GAPDH

Figure 1

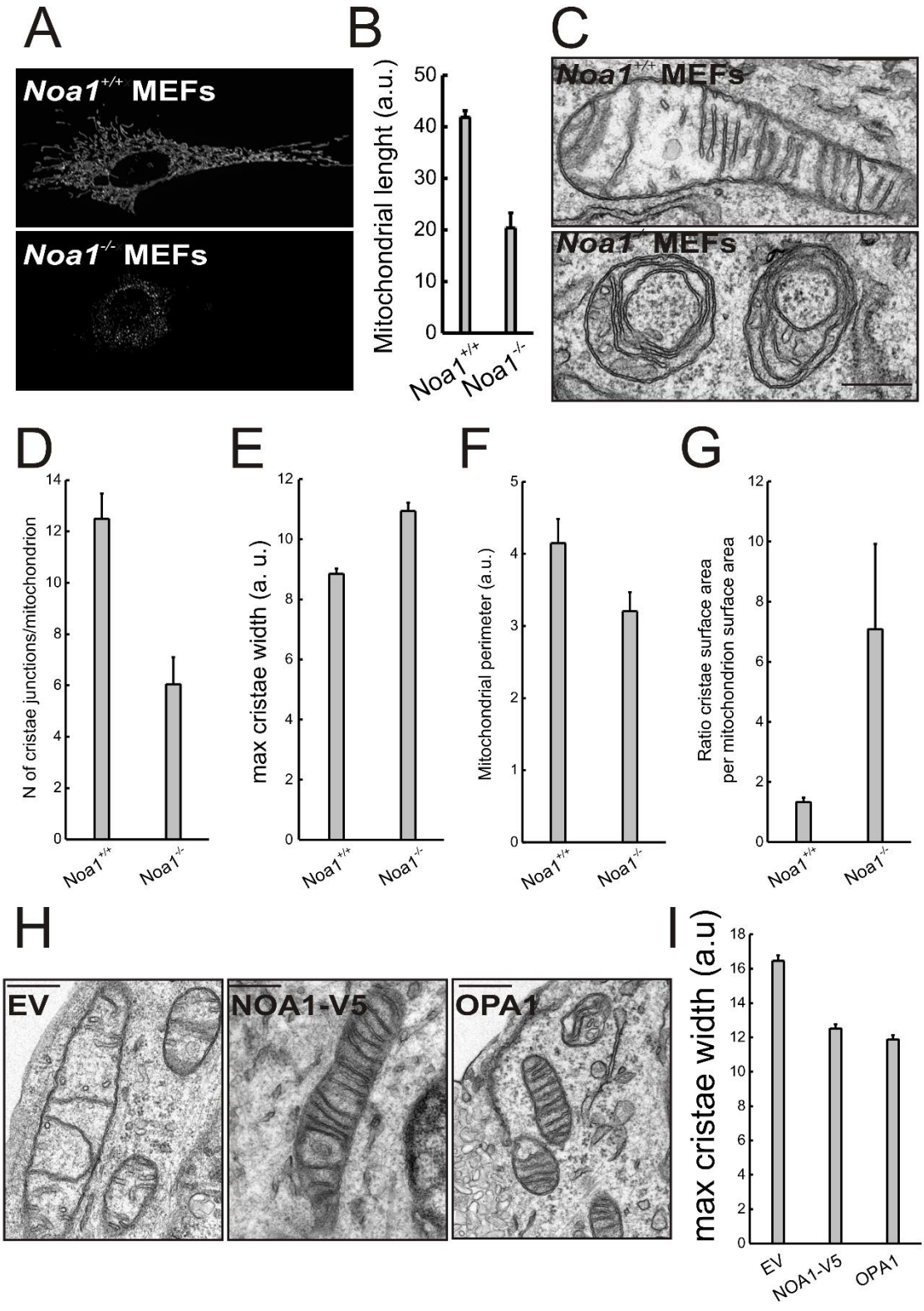
A
Noa1+/+ MEFs
Noa1-/- MEFs
B
Mitochondrial lenght (a.u.)
50
40
30
20
10
0
Noa1+/+
Noa1-/-
C
Noa1+/+ MEFs
Noa1-/- MEFs
D
N of cristae junctions/mitochondrion
14
12
10
8
6
4
2
0
Noa1+/+
Noa1-/-
E
max cristae width (a. u.)
12
10
8
6
4
2
0
Noa1+/+
Noa1-/-
F
Mitochondrial perimeter (a.u.)
5
4
3
2
1
0
Noa1+/+
Noa1-/-
G
Ratio cristae surface area per mitochondrion surface area
12
10
8
6
4
2
0
Noa1+/+
Noa1-/-
H
EV
NOA1-V5
OPA1
I
max cristae width (a.u)
18
16
14
12
10
8
6
4
2
0
EV
NOA1-V5
OPA1

Figure 2

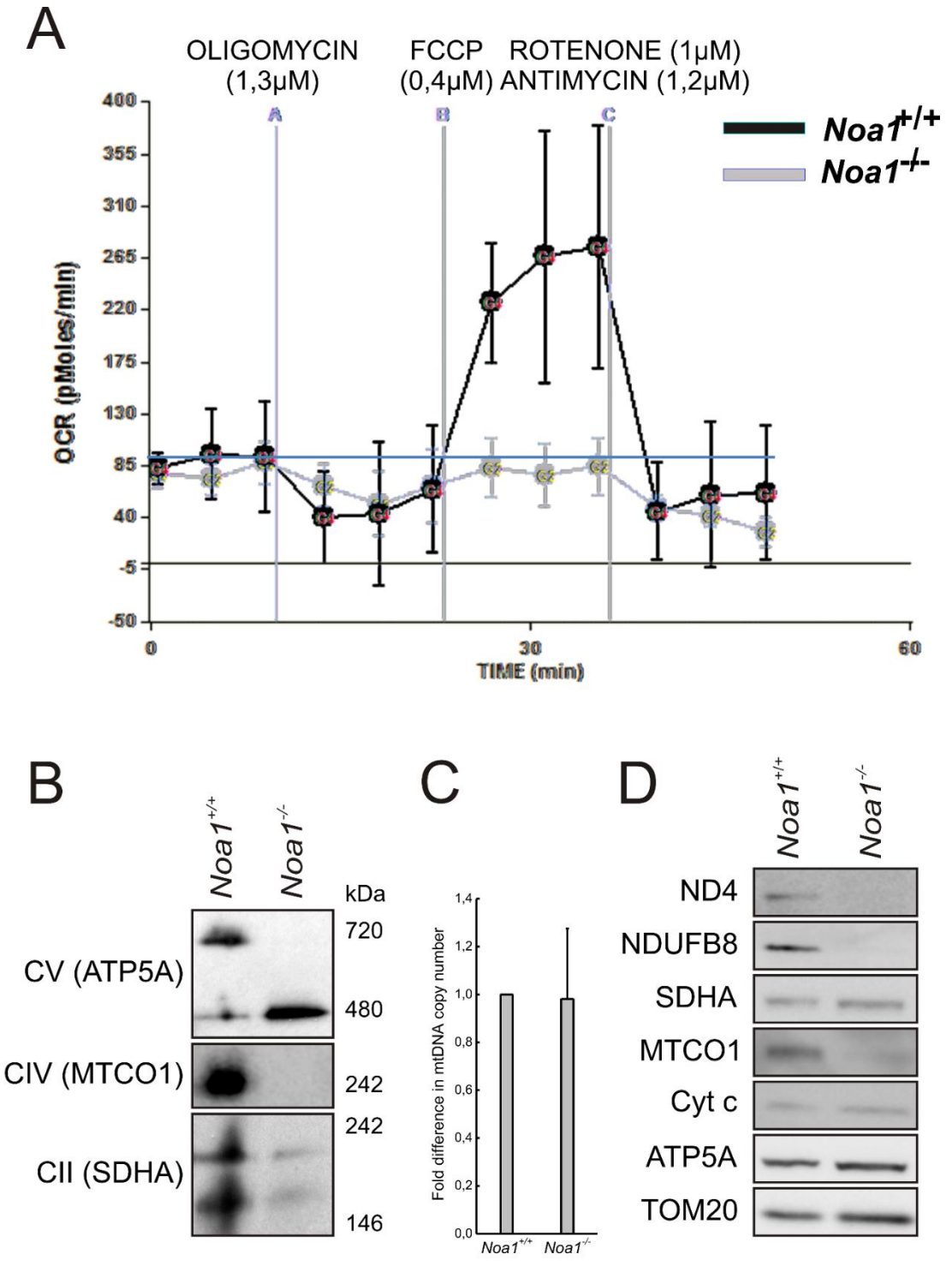
A
OLIGOMYCIN (1,3µM)
FCCP (0,4µM)
ROTENONE (1µM) ANTIMYCIN (1,2µM)
A
B
C
Noa1+/+
Noa1-/-
OCR (pMoles/min)
400
355
310
265
220
175
130
85
40
-5
-50
0
30
60
TIME (min)
B
Noa1+/+
Noa1-/-
kDa
CV (ATP5A)
CIV (MTCO1)
CII (SDHA)
720
480
242
242
146
C
Fold difference in mtDNA copy number
1,4
1,2
1,0
0,8
0,6
0,4
0,2
0,0
Noa1+/+
Noa1-/-
D
Noa1+/+
Noa1-/-
ND4
NDUFB8
SDHA
MTCO1
Cyt c
ATP5A
TOM20

Figure 3

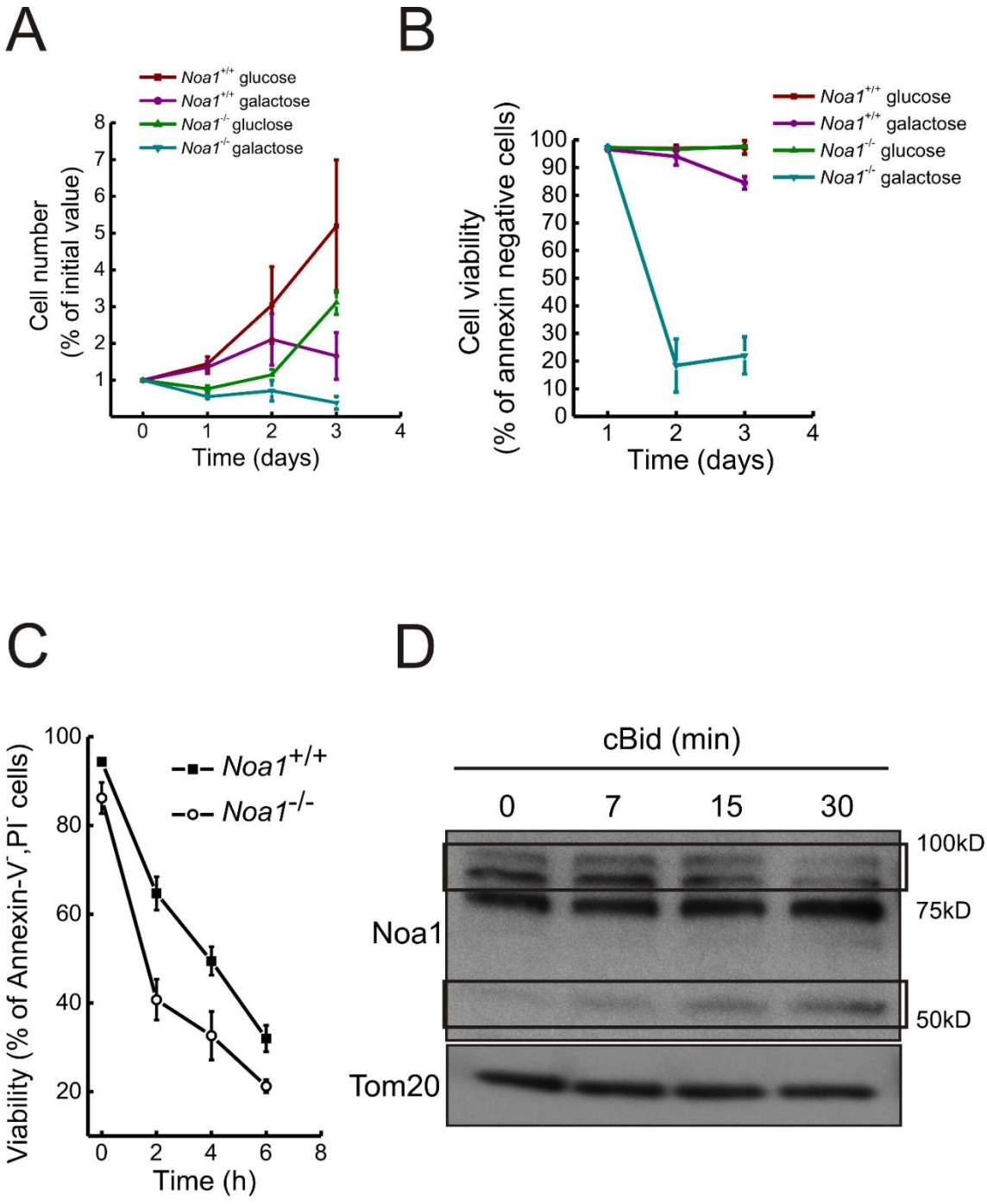
A
B
C
D
Noa1+/+ glucose
Noa1+/+ galactose
Noa1-/- gluclose
Noa1-/- galactose
Cell number (% of initial value)
Time (days)
Cell viability (% of annexin negative cells)
Noa1-/- glucose
Noa1-/- galactose
Viability (% of Annexin-V-,PI- cells)
Time (h)
cBid (min)
0
7
15
30
100kD
75kD
50kD
Noa1
Tom20

Figure 4

Nitric Oxide-Associated 1 (NOA1) is part of the OPA1-containing complexes targeted during cell death

Christina Glytsou[1], Marta Medaglia[1], Nicolo Ilaqua[1], Enrique Calvo[2], Jesùs Vazquez[2], Jose Antonio Enriquez[2], Luca Scorrano[1,3*] and Maria Eugenia Soriano[1*]

Supplemental online material

Supplementary experimental procedures

RNA Interference (RNAi)

RNAi experiments were performed using 200 nM of the sihNOA1 (5'-GGUCAUACGUUACUCCAGA-3')dTdT and Oligofectamine (Invitrogen) following manufacturer's instruction. HeLa cells transfected with scrambled siRNA were used as control. The cells were analyzed 72 hr after transfection.

Proteinase K accessibility assay

Purified mouse liver mitochondria (0.5 mg/ml) diluted in isolation buffer (I.B., 0.2 M sucrose, 0.1 mM EGTA-Tris, 10 mM Tris/MOPS, pH 7.4) were treated with Proteinase K (PK, 5 µg/mg) for 15 min at 4°C. Where indicated, hypotonic rupture of the OMM was achieved by diluting the mitochondrial suspension 1:40 in 2 mM or 20 mM HEPES/KOH pH 7.4; Triton X-100 was added where indicated at a final concentration of 0.3% (v/v). The PK reaction was quenched with 1 mM PMSF for 5 min at 4°C and the samples were spun at 4°C, 12000 x g for 10 min. The pellets were resuspended in SDS-PAGE loading buffer (NuPAGE, Invitrogen) and 30 µg of protein were separated by SDS–PAGE and immunoblotted using the indicated antibodies.

Carbonate extraction

Carbonate extraction was performed in purified mouse liver mitochondria (0.5 mg/ml) by incubation in 0.1 M Na_2CO_3 pH 11.2 for 30 min, 4°C. Soluble and membrane fractions were separated by centrifugation at 24000 x g for 1 h, 4°C. The supernatant was precipitated with 10% TCA, 20 min, 4°C, centrifuged at 18000 x g, 30 min, 4°C and the pellet was

washed with cold acetone. Equal amounts (10 μg) of proteins from total, pellet or supernatant were separated by SDS PAGE and immunoblotted using the indicated antibodies.

Analysis of cell death

Cells of the indicative genotype were treated with 1 mM H_2O_2. At the indicated time points, cells were harvested and stained with Annexin-V FITC (eBiosciences). Cell viability was measured by flow cytometry (FACSCalibur, BD Biosciences) as the percentage of Annexin-V-negative events.

Immunofluorescence

HeLa cells grown on glass coverslips were fixed with freshly prepared, ice-cold 3.7% formaldehyde in PBS for 30 min, followed by permeabilization with 0.1% Triton X-100 in PBS for 10 min. Next, the coverslips were washed with PBS, incubated with blocking buffer (10% FBS + 1% BSA in PBS) for 20min and, then, with primary antibodies for 2 hr at room temperature. We used antibodies against NOA1 (1:50, Proteintech) and TIM23 (1:50, BD Biosciences) diluted in the blocking buffer. The cells were then washed with PBS and incubated with the appropriate secondary antibodies labeled with Alexa Fluor 488 (1:300, for the antibody against NOA1) or Alexa Fluor 568 (1:1000, for the antibody against TIM23) (ThermoFisher) for 1 hour at room temperature. The coverslips were mounted with one drop of Prolong gold antifade reagent (Life Technologies). Fluorescence signals were analyzed under a Nikon Eclipse TE300 inverted microscope equipped with a PerkinElmer Ultraview LCI confocal system. Confocal images of TRIC and FITC fluorescence were acquired along the z-axis, deconvolved and 3D reconstructed using the appropriate

plugins of ImageJ (National Institutes of Health). Co-localization analysis was performed in 3D projections using “Squass” (segmentation and quantification of subcellular shapes) software (Rizk et al., 2014) which was implemented into ImageJ.

Supplemental figure legends

Figure S1. NOA1 resides in the inner mitochondrial compartments

A. Representative confocal images of HeLa cells stained for Tim23 and Noa1. Endogenous Noa1 co-localizes with the mitochondrial marker Tim23 (Bergmann's colocalization 78.1%, SEM 0.02).

B. *Carbonate extraction*. Purified mouse liver mitochondria (0.5 mg/ml) were incubated in 0.1 M Na_2CO_3 pH 11.2 for 30 min, 4°C. Soluble and membrane fractions were separated by centrifugation. Equal amounts (10µg) of proteins from total (T), pellet (P) or supernatant (S) were separated by SDS–PAGE and immunoblotted using the indicated antibodies.

C. *Proteinase K accessibility assay.* Purified mouse liver mitochondria (0.5 mg/ml) incubated in isolation buffer (I.B., 0.2 M sucrose, 10 mM Tris/MOPS, 0.1 mM EGTA-Tris, pH 7.4) were treated as indicated in the figure and 30 µg of protein were separated by SDS–PAGE and immunoblotted using the indicated antibodies. PK, proteinase K; SW, swelling.

Figure S2. Acute Noa1 ablation or overexpression affect mitochondrial ultrastructure

A. Representative electron micrographs of HeLa transfected with siRNA targeting hNOA1 (sihNOA1) or a negative siRNA (scramble). The scale bar represents 500 nm.

B. qPCR analysis of hNOA1 transcript levels in HeLa transfected with sihNOA1, depicting the efficiency of silencing. The data were normalized to GAPDH and to WT MEFs and represent the mean ± SEM of three independent experiments.

C. Western blotting in whole cell lysates from HeLa transfected with scramble or sihNOA1.

D. Morphometric analysis of the maximal cristae width. Data represent the average ± SEM of two independent experiments (320 cristae per experiment).

E. Quantitative analysis of the number of cristae per mitochondrion. Data represent mean ± SEM of three independent experiments (at least 40 mitochondria per experiment).

F. Representative electron micrographs of MEFs transfected with the indicated plasmids, sorted in FACS for GFP positive, re-cultured and subsequently fixed. The scale bar represents 1 μm.

G. Morphometric analysis of the mitochondrial perimeter. Data represent mean ± SDV of 63 randomly selected mitochondria.

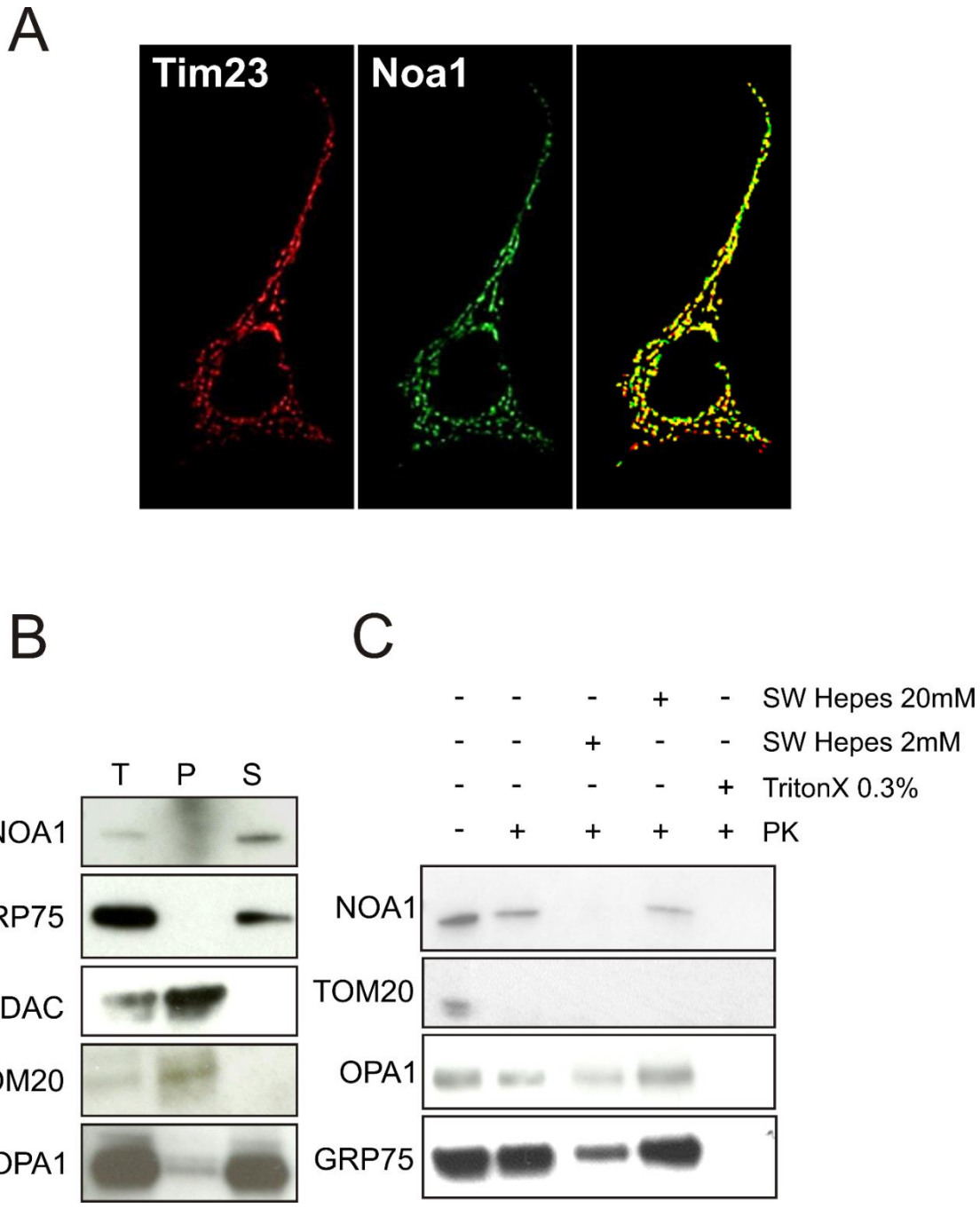

Suppl. Figure S1

Suppl. Figure S2

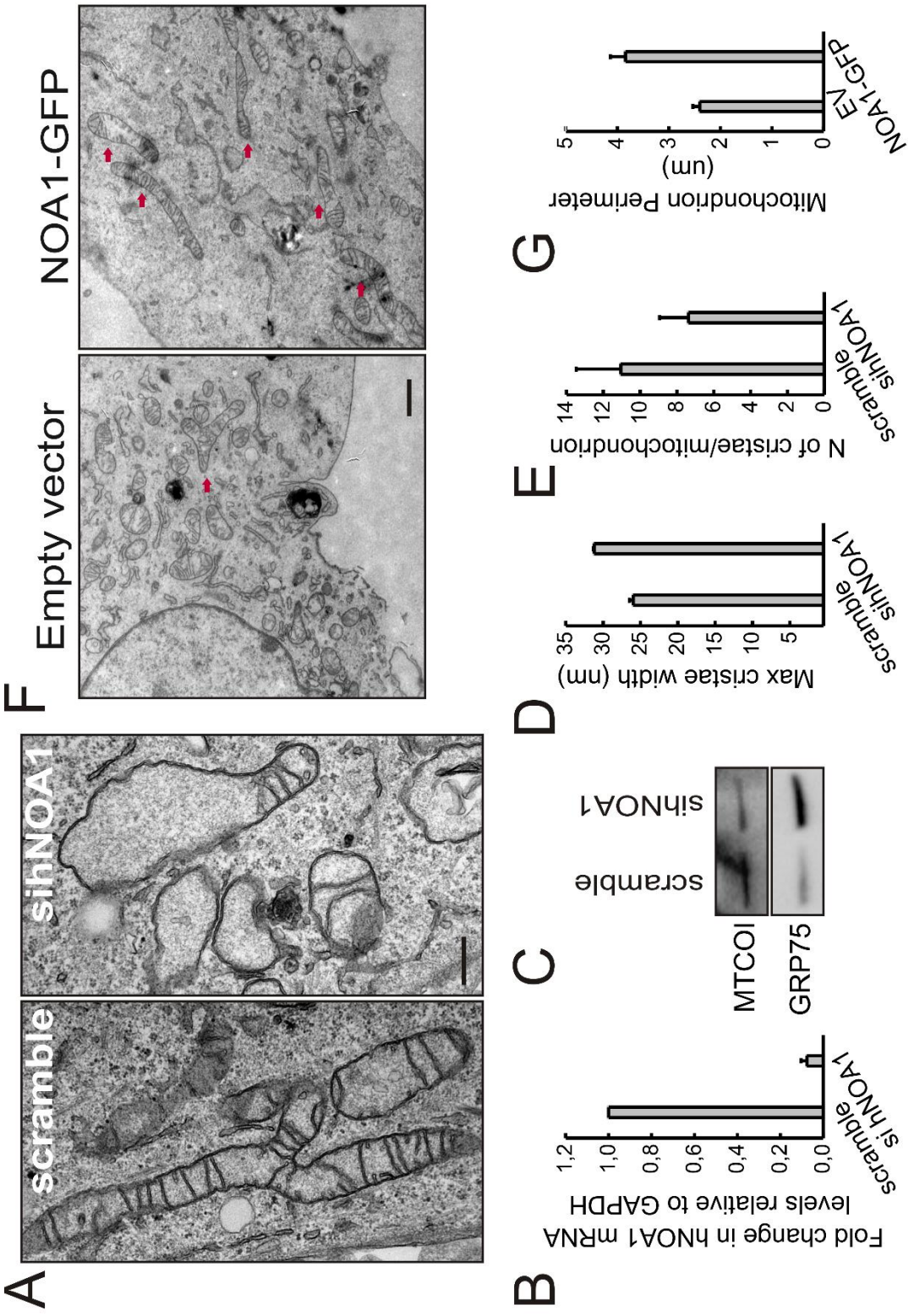

Chapter III

General discussion

3. Discussion

Mitochondrial cristae are the sites of oxidative phosphorylation, since they host all the complexes implicated in respiration. The shape of cristae alters dynamically in response to the metabolic demands of the cell in order to enhance OXPHOS efficiency (Hackenbrock, 1966; Mannella et al., 2001; Hackenbrock et al., 1980; Cogliati et al., 2013). Additionally, mitochondrial ultrastructure is subjected to remodeling early during apoptosis facilitating the mobilization of cytochrome c; thus amplifying the intrinsic cell death program (Scorrano et al., 2002). The main regulators of cristae architecture known so far are the MICOS complex, the dimers of ATP-synthase and the multimers of OPA1. Whether and how these machineries are coordinated is still unexplored.

OPA1 is a pleiotropic protein, that regulates cristae shape and remodeling independently of its profusion role (Frezza et al., 2006; Griparic et al., 2004). OPA1 is organized in high molecular weight complexes residing in the cristae junctions, while they are eliminated after stimulation by the caspase 8-cleaved pro-apoptotic BID (cBID). Using high-throughput approaches based on blue native PAGE, we demonstrated that OPA1 associates with multiple proteins to form these macromolecular assemblies. Our experimental design allowed us to distinguish the candidate OPA1 interactors that leave OPA1 complexes during apoptotic cristae remodeling; hence suggesting that these proteins likely participate in the control of cristae rearrangements.

Among the identified OPA1 interactors, our attention was firstly caught by the two major components of MICOS complex, Mic60 and Mic19. Biochemical experiments confirmed that OPA1, Mic60 and Mic19 share common complexes that are targeted during

apoptosis. Further investigation based on electron microscopy and genetics uncovered a cooperation between OPA1 and Mic60 for cristae biogenesis regulation. Nevertheless, Mic60 is not implicated in the definition of cristae junction diameter, like OPA1. Thus, it is conceivable that Mic60 plays a role in apoptosis not by directly widening cristae junctions, but indirectly, likely via regulating mitochondrial respiratory capacity. Overall, we propose that OPA1 multimers and MICOS are associated physically and functionally, while they execute additional distinct functions.

Furthermore, we focused on another candidate OPA1 co-player, NOA1, whose precise function is still undefined. Similarly, performing biochemical analysis, we validated the physical and genetic interaction between OPA1 and NOA1. Electron microscopy unveiled an interplay between the two proteins in the regulation of cristae shape. We showed that NOA1 is required for the effective mitochondrial respiration, as well as apoptosis and mitochondria-dependent cell viability and growth. Consequently, our research identified NOA1 as a novel partner of OPA1 in mitochondrial ultrastructure and function during life and death of the cell.

Given the fact that NOA1 overexpression leads to mitochondria elongation, we can hypothesize that NOA1 is a functional partner of OPA1 not only in cristae structure maintenance, but probably also in its profusion role. Considering that, to date, OPA1 is the only identified protein that can fuse the inner mitochondrial membrane, the discovery of a novel IMM fusogenic polypeptide seems intriguing. We are currently trying to establish an *in vitro* fusion assay, in order to examine the possibility that recombinant NOA1 is capable to fuse liposomes or whether it acts through OPA1 pathway.

In addition, our proteomic approaches detected core and loosely associated members of the ATP-synthase to be part of the OPA1-containing complexes, while they were found to

be dissociated from them upon cBID-induced cristae remodeling. Elaborate studies have indicated that the dimerization of ATP-synthase drives the positive curvature of the cristae tip; thus complex V is a main regulator of cristae shape (Davies et al., 2012). The notion that OPA1 collaborates with ATP-synthase dimers to control the whole cristae shape in a coordinated manner arises our interest and calls for biochemical investigation.

Overall, our studies on the composition and distribution of OPA1-containing complexes in steady state and cristae remodeling could shed light on the pathogenesis of Autosomal Dominant Optic Atrophy (ADOA), a pathology where OPA1 is mutated (Alexander et al., 2000). Additionally, the anti-apoptotic function of OPA1 serves as a fundamental protective mechanism in denervation-induced muscular atrophy, ischemic heart and brain damage, as well as hepatocellular apoptosis (Varanita et al., 2015). Consequently, knowledge deriving from my thesis can contribute to the specificity of potential therapies targeting OPA1-dependent cristae remodeling in atrophic, apoptotic, and ischemic tissue damage. On the other hand, targeting OPA1 anti-apoptotic action by inhibiting its GTPase activity might contribute to anti-cancer therapies via sensitizing transformed cells to programmed cell death. Similarly, understanding the interactions of OPA1 can add to the specificity of its inhibition and, as a result, to the efficacy of the treatment.

In general, my Thesis provided hints on the interactions of the cristae shaping IMM protein, OPA1, in life and death of the cell.

4. Reference List

Abrams,A.J., Hufnagel,R.B., Rebelo,A., Zanna,C., Patel,N., Gonzalez,M.A., Campeanu,I.J., Griffin,L.B., Groenewald,S., Strickland,A.V., Tao,F., Speziani,F., Abreu,L., Schule,R., Caporali,L., La,M.C., Maresca,A., Liguori,R., Lodi,R., Ahmed,Z.M., Sund,K.L., Wang,X., Krueger,L.A., Peng,Y., Prada,C.E., Prows,C.A., Schorry,E.K., Antonellis,A., Zimmerman,H.H., Abdul-Rahman,O.A., Yang,Y., Downes,S.M., Prince,J., Fontanesi,F., Barrientos,A., Nemeth,A.H., Carelli,V., Huang,T., Zuchner,S., and Dallman,J.E. (2015). Mutations in SLC25A46, encoding a UGO1-like protein, cause an optic atrophy spectrum disorder. Nat. Genet. *47*, 926-932.

Acin-Perez,R., Fernandez-Silva,P., Peleato,M.L., Perez-Martos,A., and Enriquez,J.A. (2008). Respiratory active mitochondrial supercomplexes. Mol. Cell *32*, 529-539.

Adams,J.M. and Cory,S. (2001). Life-or-death decisions by the Bcl-2 protein family. Trends. Biochem. Sci. *26*, 61-66.

Adams,J.M. and Cory,S. (2007). The Bcl-2 apoptotic switch in cancer development and therapy. Oncogene *26*, 1324-1337.

Akepati,V.R., Muller,E.C., Otto,A., Strauss,H.M., Portwich,M., and Alexander,C. (2008). Characterization of OPA1 isoforms isolated from mouse tissues. J. Neurochem. *106*, 372-383.

Al-Furoukh,N., Kardon,J.R., Kruger,M., Szibor,M., Baker,T.A., and Braun,T. (2014). NOA1, a novel ClpXP substrate, takes an unexpected nuclear detour prior to mitochondrial import. PLoS. One. *9*, e103141.

Alavi,M.V., Bette,S., Schimpf,S., Schuettauf,F., Schraermeyer,U., Wehrl,H.F., Ruttiger,L., Beck,S.C., Tonagel,F., Pichler,B.J., Knipper,M., Peters,T., Laufs,J., and Wissinger,B. (2007). A splice site mutation in the murine Opa1 gene features pathology of autosomal dominant optic atrophy. Brain *130*, 1029-1042.

Alexander,C., Votruba,M., Pesch,U.E., Thiselton,D.L., Mayer,S., Moore,A., Rodriguez,M., Kellner,U., Leo-Kottler,B., Auburger,G., Bhattacharya,S.S., and Wissinger,B. (2000). OPA1, encoding a dynamin-related GTPase, is mutated in autosomal dominant optic atrophy linked to chromosome 3q28. Nat. Genet. *26*, 211-215.

Alirol,E., James,D., Huber,D., Marchetto,A., Vergani,L., Martinou,J.C., and Scorrano,L. (2006). The mitochondrial fission protein hFis1 requires the endoplasmic reticulum gateway to induce apoptosis. Mol. Biol. Cell *17*, 4593-4605.

Alkhaja,A.K., Jans,D.C., Nikolov,M., Vukotic,M., Lytovchenko,O., Ludewig,F., Schliebs,W., Riedel,D., Urlaub,H., Jakobs,S., and Deckers,M. (2012). MINOS1 is a conserved component of mitofilin complexes and required for mitochondrial function and cristae organization. Mol. Biol. Cell *23*, 247-257.

Allen,R.D., Schroeder,C.C., and Fok,A.K. (1989). An investigation of mitochondrial inner membranes by rapid-freeze deep-etch techniques. J. Cell Biol. *108*, 2233-2240.

Amutha,B., Gordon,D.M., Gu,Y., and Pain,D. (2004). A novel role of Mgm1p, a dynamin-related GTPase, in ATP synthase assembly and cristae formation/maintenance. Biochem J *381*, 19-23.

An,H.J., Cho,G., Lee,J.O., Paik,S.G., Kim,Y.S., and Lee,H. (2013). Higd-1a interacts with Opa1 and is required for the morphological and functional integrity of mitochondria. Proc. Natl. Acad. Sci. U. S. A *110*, 13014-13019.

Anand,B., Surana,P., Bhogaraju,S., Pahari,S., and Prakash,B. (2009). Circularly permuted GTPase YqeH binds 30S ribosomal subunit: Implications for its role in ribosome assembly. Biochem. Biophys. Res. Commun. *386*, 602-606.

Anand,B., Surana,P., and Prakash,B. (2010). Deciphering the catalytic machinery in 30S ribosome assembly GTPase YqeH. PLoS. One. *5*, e9944.

Anand,R., Wai,T., Baker,M.J., Kladt,N., Schauss,A.C., Rugarli,E., and Langer,T. (2014). The i-AAA protease YME1L and OMA1 cleave OPA1 to balance mitochondrial fusion and fission. J Cell Biol *204*, 919-929.

Anton,F., Fres,J.M., Schauss,A., Pinson,B., Praefcke,G.J., Langer,T., and Escobar-Henriques,M. (2011). Ugo1 and Mdm30 act sequentially during Fzo1-mediated mitochondrial outer membrane fusion. J. Cell Sci. *124*, 1126-1135.

Artal-Sanz,M., Tsang,W.Y., Willems,E.M., Grivell,L.A., Lemire,B.D., van der Spek,H., and Nijtmans,L.G. (2003). The mitochondrial prohibitin complex is essential for embryonic viability and germline function in Caenorhabditis elegans. J. Biol. Chem. *278*, 32091-32099.

Baburamani,A.A., Hurling,C., Stolp,H., Sobotka,K., Gressens,P., Hagberg,H., and Thornton,C. (2015). Mitochondrial Optic Atrophy (OPA) 1 Processing Is Altered in Response to Neonatal Hypoxic-Ischemic Brain Injury. Int. J. Mol. Sci. *16*, 22509-22526.

Bach,D., Pich,S., Soriano,F.X., Vega,N., Baumgartner,B., Oriola,J., Daugaard,J.R., Lloberas,J., Camps,M., Zierath,J.R., Rabasa-Lhoret,R., Wallberg-Henriksson,H., Laville,M., Palacin,M., Vidal,H., Rivera,F., Brand,M., and Zorzano,A. (2003). Mitofusin-2 determines mitochondrial network architecture and mitochondrial metabolism. A novel regulatory mechanism altered in obesity. J. Biol. Chem. *278*, 17190-17197.

Back,J.W., Sanz,M.A., De,J.L., De Koning,L.J., Nijtmans,L.G., De Koster,C.G., Grivell,L.A., Van Der Spek,H., and Muijsers,A.O. (2002). A structure for the yeast prohibitin complex: Structure prediction and evidence from chemical crosslinking and mass spectrometry. Protein Sci. *11*, 2471-2478.

Ban,T., Heymann,J.A., Song,Z., Hinshaw,J.E., and Chan,D.C. (2010). OPA1 disease alleles causing dominant optic atrophy have defects in cardiolipin-stimulated GTP hydrolysis and membrane tubulation. Hum. Mol. Genet. *19*, 2113-2122.

Banerjee,S. and Chinthapalli,B. (2014). A proteomic screen with Drosophila Opa1-like identifies Hsc70-5/Mortalin as a regulator of mitochondrial morphology and cellular homeostasis. Int. J. Biochem. Cell Biol. *54*, 36-48.

Barat,M., Rickwood,D., Dufresne,C., and Mounolou,J.C. (1985). Characterization of DNA-protein complexes from the mitochondria of Xenopus laevis oocytes. Exp. Cell Res. *157*, 207-217.

Barneo-Munoz,M., Juarez,P., Civera-Tregon,A., Yndriago,L., Pla-Martin,D., Zenker,J., Cuevas-Martin,C., Estela,A., Sanchez-Arago,M., Forteza-Vila,J., Cuezva,J.M., Chrast,R., and Palau,F. (2015). Lack of GDAP1 induces neuronal calcium and mitochondrial defects in a knockout mouse model of charcot-marie-tooth neuropathy. PLoS. Genet. *11*, e1005115.

Baseler,W.A., Dabkowski,E.R., Williamson,C.L., Croston,T.L., Thapa,D., Powell,M.J., Razunguzwa,T.T., and Hollander,J.M. (2011). Proteomic alterations of distinct mitochondrial subpopulations in the type 1 diabetic heart: contribution of protein import dysfunction. Am. J. Physiol Regul. Integr. Comp Physiol *300*, R186-R200.

Baxter,R.V., Ben,O.K., Rochelle,J.M., Stajich,J.E., Hulette,C., Dew-Knight,S., Hentati,F., Ben,H.M., Bel,S., Stenger,J.E., Gilbert,J.R., Pericak-Vance,M.A., and Vance,J.M. (2002). Ganglioside-induced differentiation-associated protein-1 is mutant in Charcot-Marie-Tooth disease type 4A/8q21. Nat. Genet. *30*, 21-22.

Belenguer,P. and Pellegrini,L. (2013). The dynamin GTPase OPA1: more than mitochondria? Biochim. Biophys. Acta *1833*, 176-183.

Benard,G., Bellance,N., James,D., Parrone,P., Fernandez,H., Letellier,T., and Rossignol,R. (2007). Mitochondrial bioenergetics and structural network organization. J. Cell. Sci. *120*, 838-848.

Bereiter-Hahn,J. and Voth,M. (1994). Dynamics of mitochondria in living cells: shape changes, dislocations, fusion, and fission of mitochondria. Microsc. Res. Tech. *27*, 198-219.

Bernardi,P. and Azzone,G.F. (1981). Cytochrome c as an electron shuttle between the outer and inner mitochondrial membranes. J. Biol. Chem. *256*, 7187-7192.

Bogenhagen,D.F., Rousseau,D., and Burke,S. (2008). The layered structure of human mitochondrial DNA nucleoids. J. Biol. Chem. *283*, 3665-3675.

Boissan,M., Montagnac,G., Shen,Q., Griparic,L., Guitton,J.+., Romao,M., Sauvonnet,N., Lagache,T., Lascu,I., Raposo,G., Desbourdes,C.+., Schlattner,U., Lacombe,M.L., Polo,S., van der Bliek,A.M., Roux,A.l., and Chavrier,P. (2014). Nucleoside diphosphate kinases fuel dynamin superfamily proteins with GTP for membrane remodeling. Science *344*, 1510-1515.

Bornhovd,C., Vogel,F., Neupert,W., and Reichert,A.S. (2006). Mitochondrial membrane potential is dependent on the oligomeric state of F1F0-ATP synthase supracomplexes. J. Biol. Chem. *281*, 13990-13998.

Braschi,E., Zunino,R., and McBride,H.M. (2009). MAPL is a new mitochondrial SUMO E3 ligase that regulates mitochondrial fission. EMBO. Rep. *10*, 748-754.

Brighton,C.T. and Hunt,R.M. (1974). Mitochondrial calcium and its role in calcification. Histochemical localization of calcium in electron micrographs of the epiphyseal growth plate with K-pyroantimonate. Clin. Orthop. Relat Res. 406-416.

Browman,D.T., Hoegg,M.B., and Robbins,S.M. (2007). The SPFH domain-containing proteins: more than lipid raft markers. Trends Cell Biol. *17*, 394-402.

Bui,H.T., Karren,M.A., Bhar,D., and Shaw,J.M. (2012). A novel motif in the yeast mitochondrial dynamin Dnm1 is essential for adaptor binding and membrane recruitment. J. Cell Biol. *199*, 613-622.

Cain,K., Bratton,S.B., and Cohen,G.M. (2002). The Apaf-1 apoptosome: a large caspase-activating complex. Biochimie *84*, 203-214.

Campanella,M., Casswell,E., Chong,S., Farah,Z., Wieckowski,M.R., Abramov,A.Y., Tinker,A., and Duchen,M.R. (2008). Regulation of mitochondrial structure and function by the F1Fo-ATPase inhibitor protein, IF1. Cell Metab *8*, 13-25.

Carelli,V., Musumeci,O., Caporali,L., Zanna,C., La,M.C., Del,D., V, Porcelli,A.M., Rugolo,M., Valentino,M.L., Iommarini,L., Maresca,A., Barboni,P., Carbonelli,M., Trombetta,C., Valente,E.M., Patergnani,S., Giorgi,C., Pinton,P., Rizzo,G., Tonon,C., Lodi,R., Avoni,P., Liguori,R., Baruzzi,A., Toscano,A., and Zeviani,M. (2015). Syndromic parkinsonism and dementia associated with OPA1 missense mutations. Ann. Neurol. *78*, 21-38.

Cereghetti,G.M., Stangherlin,A., Martins de,B.O., Chang,C.R., Blackstone,C., Bernardi,P., and Scorrano,L. (2008). Dephosphorylation by calcineurin regulates translocation of Drp1 to mitochondria. Proc. Natl. Acad. Sci. U. S. A *105*, 15803-15808.

Chan,E.Y. and McQuibban,G.A. (2012). Phosphatidylserine decarboxylase 1 (Psd1) promotes mitochondrial fusion by regulating the biophysical properties of the mitochondrial membrane and alternative topogenesis of mitochondrial genome maintenance protein 1 (Mgm1). J. Biol. Chem. *287*, 40131-40139.

Chang,C.R. and Blackstone,C. (2007). Cyclic AMP-dependent protein kinase phosphorylation of Drp1 regulates its GTPase activity and mitochondrial morphology. J. Biol Chem. *282*, 21583-21587.

Chang,C.R., Manlandro,C.M., Arnoult,D., Stadler,J., Posey,A.E., Hill,R.B., and Blackstone,C. (2010). A lethal de novo mutation in the middle domain of the dynamin-related GTPase Drp1 impairs higher order assembly and mitochondrial division. J Biol. Chem. *285*, 32494-32503.

Chen,H., Chomyn,A., and Chan,D.C. (2005). Disruption of fusion results in mitochondrial heterogeneity and dysfunction. J. Biol. Chem. *280*, 26185-26192.

Chen,H., Detmer,S.A., Ewald,A.J., Griffin,E.E., Fraser,S.E., and Chan,D.C. (2003). Mitofusins Mfn1 and Mfn2 coordinately regulate mitochondrial fusion and are essential for embryonic development. J. Cell Biol. *160*, 189-200.

Chen,H., McCaffery,J.M., and Chan,D.C. (2007). Mitochondrial fusion protects against neurodegeneration in the cerebellum. Cell. *130*, 548-562.

Chen,H., Vermulst,M., Wang,Y.E., Chomyn,A., Prolla,T.A., McCaffery,J.M., and Chan,D.C. (2010). Mitochondrial fusion is required for mtDNA stability in skeletal muscle and tolerance of mtDNA mutations. Cell *141*, 280-289.

Chiang,Y.Y., Chen,S.L., Hsiao,Y.T., Huang,C.H., Lin,T.Y., Chiang,I.P., Hsu,W.H., and Chow,K.C. (2009). Nuclear expression of dynamin-related protein 1 in lung adenocarcinomas. Mod. Pathol. *22*, 1139-1150.

Cho,D.H., Nakamura,T., Fang,J., Cieplak,P., Godzik,A., Gu,Z., and Lipton,S.A. (2009). S-nitrosylation of Drp1 mediates beta-amyloid-related mitochondrial fission and neuronal injury. Science. *324*, 102-105.

Christie,D.A., Lemke,C.D., Elias,I.M., Chau,L.A., Kirchhof,M.G., Li,B., Ball,E.H., Dunn,S.D., Hatch,G.M., and Madrenas,J. (2011). Stomatin-like protein 2 binds cardiolipin and regulates mitochondrial biogenesis and function. Mol. Cell Biol. *31*, 3845-3856.

Cipolat,S., Martins de Brito O., Dal Zilio B., and Scorrano,L. (2004). OPA1 requires mitofusin 1 to promote mitochondrial fusion. Proc. Natl. Acad. Sci. U. S. A *101*, 15927-15932.

Cipolat,S., Rudka,T., Hartmann,D., Costa,V., Serneels,L., Craessaerts,K., Metzger,K., Frezza,C., Annaert,W., D'Adamio,L., Derks,C., Dejaegere,T., Pellegrini,L., D'Hooge,R., Scorrano,L., and De Strooper,B. (2006). Mitochondrial Rhomboid PARL Regulates Cytochrome c Release during Apoptosis via OPA1-Dependent Cristae Remodeling. Cell *126*, 163-175.

Civiletto,G., Varanita,T., Cerutti,R., Gorletta,T., Barbaro,S., Marchet,S., Lamperti,C., Viscomi,C., Scorrano,L., and Zeviani,M. (2015). Opa1 overexpression ameliorates the clinical phenotype of two mitochondrial disease mouse models. Cell Metabolism.

Cogliati,S., Frezza,C., Soriano,M.E., Varanita,T., Quintana-Cabrera,R., Corrado,M., Cipolat,S., Costa,V., Casarin,A., Gomes,L.C., Perales-Clemente,E., Salviati,L., Fernandez-Silva,P., Enriquez,J.A., and Scorrano,L. (2013). Mitochondrial cristae shape determines respiratory chain supercomplexes assembly and respiratory efficiency. Cell *155*, 160-171.

Costa,V., Giacomello,M., Hudec,R., Lopreiato,R., Ermak,G., Lim,D., Malorni,W., Davies,K.J., Carafoli,E., and Scorrano,L. (2010). Mitochondrial fission and cristae disruption increase the response of cell models of Huntington's disease to apoptotic stimuli. EMBO Mol Med *2*, 490-503.

Cuesta,A., Pedrola,L., Sevilla,T., Garcia-Planells,J., Chumillas,M.J., Mayordomo,F., LeGuern,E., Marin,I., Vilchez,J.J., and Palau,F. (2002). The gene encoding ganglioside-induced differentiation-associated protein 1 is mutated in axonal Charcot-Marie-Tooth type 4A disease. Nat. Genet. *30*, 22-25.

Czarnecka,A.M., Campanella,C., Zummo,G., and Cappello,F. (2006). Mitochondrial chaperones in cancer: from molecular biology to clinical diagnostics. Cancer Biol. Ther. *5*, 714-720.

Da,C.S., Parone,P.A., Gonzalo,P., Bienvenut,W.V., Tondera,D., Jourdain,A., Quadroni,M., and Martinou,J.C. (2008). SLP-2 interacts with prohibitins in the mitochondrial inner membrane and contributes to their stability. Biochim. Biophys. Acta *1783*, 904-911.

Danial,N.N. and Korsmeyer,S.J. (2004). Cell death: critical control points. Cell *116*, 205-219.

Darshi,M., Mendiola,V.L., Mackey,M.R., Murphy,A.N., Koller,A., Perkins,G.A., Ellisman,M.H., and Taylor,S.S. (2011). ChChd3, an inner mitochondrial membrane protein, is essential for maintaining crista integrity and mitochondrial function. J Biol Chem. *286*, 2918-2932.

Daum,B., Walter,A., Horst,A., Osiewacz,H.D., and Kuhlbrandt,W. (2013). Age-dependent dissociation of ATP synthase dimers and loss of inner-membrane cristae in mitochondria. Proc. Natl. Acad. Sci. U. S. A *110*, 15301-15306.

Davies,K.M., Anselmi,C., Wittig,I., Faraldo-Gomez,J.D., and Kuhlbrandt,W. (2012). Structure of the yeast F1Fo-ATP synthase dimer and its role in shaping the mitochondrial cristae. Proc. Natl. Acad. Sci. U. S. A *109*, 13602-13607.

Davies,K.M., Strauss,M., Daum,B., Kief,J.H., Osiewacz,H.D., Rycovska,A., Zickermann,V., and Kuhlbrandt,W. (2011). Macromolecular organization of ATP synthase and complex I in whole mitochondria. Proc. Natl. Acad. Sci. U. S. A *108*, 14121-14126.

Davies,V.J., Hollins,A.J., Piechota,M.J., Yip,W., Davies,J.R., White,K.E., Nicols,P.P., Boulton,M.E., and Votruba,M. (2007). Opa1 deficiency in a mouse model of autosomal dominant optic atrophy impairs mitochondrial morphology, optic nerve structure and visual function. Hum. Mol. Genet. *16*, 1307-1318.

de Brito,O.M. and Scorrano,L. (2008a). Mitofusin 2 tethers endoplasmic reticulum to mitochondria. Nature. *456*, 605-610.

de Brito,O.M. and Scorrano,L. (2008b). Mitofusin 2: a mitochondria-shaping protein with signaling roles beyond fusion. Antioxid. Redox. Signal. *10*, 621-633.

Delettre,C., Griffoin,J.M., Kaplan,J., Dollfus,H., Lorenz,B., Faivre,L., Lenaers,G., Belenguer,P., and Hamel,C.P. (2001). Mutation spectrum and splicing variants in the OPA1 gene. Hum. Genet. *109*, 584-591.

Delettre,C., Lenaers,G., Griffoin,J.M., Gigarel,N., Lorenzo,C., Belenguer,P., Pelloquin,L., Grosgeorge,J., Turc-Carel,C., Perret,E., Astarie-Dequeker,C., Lasquellec,L., Arnaud,B., Ducommun,B., Kaplan,J., and Hamel,C.P. (2000). Nuclear gene OPA1, encoding a mitochondrial dynamin-related protein, is mutated in dominant optic atrophy. Nat. Genet. *26*, 207-210.

Delivani,P., Adrain,C., Taylor,R.C., Duriez,P.J., and Martin,S.J. (2006). Role for CED-9 and Egl-1 as regulators of mitochondrial fission and fusion dynamics. Mol Cell *21*, 761-773.

Demongeot,J., Glade,N., Hansen,O., and Moreira,A. (2007). An open issue: the inner mitochondrial membrane (IMM) as a free boundary problem. Biochimie *89*, 1049-1057.

Deng,Y. and Almsherqi,Z.A. (2015). Evolution of cubic membranes as antioxidant defence system. Interface Focus. *5*, 20150012.

Deng,Y., Kohlwein,S.D., and Mannella,C.A. (2002). Fasting induces cyanide-resistant respiration and oxidative stress in the amoeba Chaos carolinensis: implications for the cubic structural transition in mitochondrial membranes. Protoplasma *219*, 160-167.

Deng,Y., Marko,M., Buttle,K.F., Leith,A., Mieczkowski,M., and Mannella,C.A. (1999). Cubic membrane structure in amoeba (Chaos carolinensis) mitochondria determined by electron microscopic tomography. J. Struct. Biol. *127*, 231-239.

DeVay,R.M., Dominguez-Ramirez,L., Lackner,L.L., Hoppins,S., Stahlberg,H., and Nunnari,J. (2009). Coassembly of Mgm1 isoforms requires cardiolipin and mediates mitochondrial inner membrane fusion. J. Cell Biol. *186*, 793-803.

Dewson,G., Kratina,T., Sim,H.W., Puthalakath,H., Adams,J.M., Colman,P.M., and Kluck,R.M. (2008). To trigger apoptosis, Bak exposes its BH3 domain and homodimerizes via BH3:groove interactions. Mol. Cell *30*, 369-380.

Dimmer,K.S., Navoni,F., Casarin,A., Trevisson,E., Endele,S., Winterpacht,A., Salviati,L., and Scorrano,L. (2008). LETM1, deleted in Wolf Hirschhorn syndrome is required for normal mitochondrial morphology and cellular viability. Hum Mol Genet *17*, 201-214.

Dimmer,K.S. and Scorrano,L. (2006). (De)constructing mitochondria: what for? Physiology. (Bethesda.) *21*, 233-241.

Du,C., Fang,M., Li,Y., Li,L., and Wang,X. (2000). Smac, a mitochondrial protein that promotes cytochrome c-dependent caspase activation by eliminating IAP inhibition. Cell *102*, 33-42.

Duvezin-Caubet,S., Koppen,M., Wagener,J., Zick,M., Israel,L., Bernacchia,A., Jagasia,R., Rugarli,E.I., Imhof,A., Neupert,W., Langer,T., and Reichert,A.S. (2007). OPA1 processing reconstituted in yeast depends on the subunit composition of the m-AAA protease in mitochondria. Mol. Biol. Cell *18*, 3582-3590.

Dyck,J.R., Barr,A.J., Barr,R.L., Kolattukudy,P.E., and Lopaschuk,G.D. (1998). Characterization of cardiac malonyl-CoA decarboxylase and its putative role in regulating fatty acid oxidation. Am. J. Physiol. *275*, H2122-H2129.

Dyck,J.R., Berthiaume,L.G., Thomas,P.D., Kantor,P.F., Barr,A.J., Barr,R., Singh,D., Hopkins,T.A., Voilley,N., Prentki,M., and Lopaschuk,G.D. (2000). Characterization of rat liver malonyl-CoA decarboxylase and the study of its role in regulating fatty acid metabolism. Biochem. J. *350 Pt 2599-608*, -608.

Ehses,S., Raschke,I., Mancuso,G., Bernacchia,A., Geimer,S., Tondera,D., Martinou,J.C., Westermann,B., Rugarli,E.I., and Langer,T. (2009). Regulation of OPA1 processing and mitochondrial fusion by m-AAA protease isoenzymes and OMA1. J Cell Biol *187*, 1023-1036.

Ellis,C.E., Murphy,E.J., Mitchell,D.C., Golovko,M.Y., Scaglia,F., Barcelo-Coblijn,G.C., and Nussbaum,R.L. (2005). Mitochondrial lipid abnormality and electron transport chain impairment in mice lacking alpha-synuclein. Mol. Cell Biol. *25*, 10190-10201.

Esposti,M.D., Erler,J.T., Hickman,J.A., and Dive,C. (2001). Bid, a widely expressed proapoptotic protein of the Bcl-2 family, displays lipid transfer activity. Mol. Cell Biol. *21*, 7268-7276.

Eura,Y., Ishihara,N., Oka,T., and Mihara,K. (2006). Identification of a novel protein that regulates mitochondrial fusion by modulating mitofusin (Mfn) protein function. J. Cell Sci. *119*, 4913-4925.

Fernandez-Silva,P., Enriquez,J.A., and Montoya,J. (2003). Replication and transcription of mammalian mitochondrial DNA. Exp. Physiol. *88*, 41-56.

Ferre,M., Amati-Bonneau,P., Tourmen,Y., Malthiery,Y., and Reynier,P. (2005). eOPA1: an online database for OPA1 mutations. Hum. Mutat. *25*, 423-428.

Ferreira-da-Silva,A., Valacca,C., Rios,E., Populo,H., Soares,P., Sobrinho-Simoes,M., Scorrano,L., Maximo,V., and Campello,S. (2015). Mitochondrial dynamics protein Drp1 is overexpressed in oncocytic thyroid tumors and regulates cancer cell migration. PLoS. One. *10*, e0122308.

Ferrer,P.E., Frederick,P., Gulbis,J.M., Dewson,G., and Kluck,R.M. (2012). Translocation of a Bak C-terminus mutant from cytosol to mitochondria to mediate cytochrome C release: implications for Bak and Bax apoptotic function. PLoS. One. *7*, e31510.

Frank,S., Gaume,B., Bergmann-Leitner,E.S., Leitner,W.W., Robert,E.G., Catez,F., Smith,C.L., and Youle,R.J. (2001). The role of dynamin-related protein 1, a mediator of mitochondrial fission, in apoptosis. Dev. Cell *1*, 515-525.

Frey,T.G. and Mannella,C.A. (2000). The internal structure of mitochondria. Trends Biochem. Sci. *25*, 319-324.

Frezza,C., Cipolat,S., Martins,d.B., Micaroni,M., Beznoussenko,G.V., Rudka,T., Bartoli,D., Polishuck,R.S., Danial,N.N., De Strooper,B., and Scorrano,L. (2006). OPA1 Controls Apoptotic Cristae Remodeling Independently from Mitochondrial Fusion. Cell *126*, 177-189.

Friedman,J.R., Mourier,A., Yamada,J., McCaffery,J.M., and Nunnari,J. (2015a). MICOS coordinates with respiratory complexes and lipids to establish mitochondrial inner membrane architecture. Elife. *4*.

Friedman,J.R., Mourier,A., Yamada,J., McCaffery,J.M., and Nunnari,J. (2015b). MICOS coordinates with respiratory complexes and lipids to establish mitochondrial inner membrane architecture. Elife. *4*.

Friedman,J.R., Lackner,L.L., West,M., DiBenedetto,J.R., Nunnari,J., and Voeltz,G.K. (2011). ER Tubules Mark Sites of Mitochondrial Division. Science *334*, 358-362.

Fritz,S., Rapaport,D., Klanner,E., Neupert,W., and Westermann,B. (2001). Connection of the mitochondrial outer and inner membranes by Fzo1 is critical for organellar fusion. J. Cell Biol. *152*.

Fry,M. and Green,D.E. (1981). Cardiolipin requirement for electron transfer in complex I and III of the mitochondrial respiratory chain. J. Biol. Chem. *256*, 1874-1880.

Gad,H., Ringstad,N., Low,P., Kjaerulff,O., Gustafsson,J., Wenk,M., Di,P.G., Nemoto,Y., Crun,J., Ellisman,M.H., De,C.P., Shupliakov,O., and Brodin,L. (2000). Fission and uncoating of synaptic clathrin-coated vesicles are perturbed by disruption of interactions with the SH3 domain of endophilin. Neuron *27*, 301-312.

Garrido,C., Galluzzi,L., Brunet,M., Puig,P.E., Didelot,C., and Kroemer,G. (2006). Mechanisms of cytochrome c release from mitochondria. Cell Death. Differ. *13*, 1423-1433.

Gavathiotis,E., Reyna,D.E., Davis,M.L., Bird,G.H., and Walensky,L.D. (2010). BH3-triggered structural reorganization drives the activation of proapoptotic BAX. Mol. Cell *40*, 481-492.

Gawlowski,T., Suarez,J., Scott,B., Torres-Gonzalez,M., Wang,H., Schwappacher,R., Han,X., Yates,J.R., Hoshijima,M., and Dillmann,W. (2012). Modulation of Dynamin-related Protein 1 (DRP1) Function by Increased O-linked-+¦-N-acetylglucosamine Modification (O-GlcNAc) in Cardiac Myocytes. J. Biol. Chem. *287*, 30024-30034.

Genova,M.L. and Lenaz,G. (2014). Functional role of mitochondrial respiratory supercomplexes. Biochim. Biophys. Acta *1837*, 427-443.

Germain,M., Mathai,J.P., McBride,H.M., and Shore,G.C. (2005). Endoplasmic reticulum BIK initiates DRP1-regulated remodelling of mitochondrial cristae during apoptosis. EMBO J. *24*, 1546-1556.

Gilkerson,R., Bravo,L., Garcia,I., Gaytan,N., Herrera,A., Maldonado,A., and Quintanilla,B. (2013). The mitochondrial nucleoid: integrating mitochondrial DNA into cellular homeostasis. Cold Spring Harb. Perspect. Biol. *5*, a011080.

Gilkerson,R.W., Selker,J.M., and Capaldi,R.A. (2003). The cristal membrane of mitochondria is the principal site of oxidative phosphorylation. FEBS Lett. *546*, 355-358.

Girard,M., Lariviere,R., Parfitt,D.A., Deane,E.C., Gaudet,R., Nossova,N., Blondeau,F., Prenosil,G., Vermeulen,E.G., Duchen,M.R., Richter,A., Shoubridge,E.A., Gehring,K., McKinney,R.A., Brais,B., Chapple,J.P., and McPherson,P.S. (2012). Mitochondrial dysfunction and Purkinje cell loss in autosomal recessive spastic ataxia of Charlevoix-Saguenay (ARSACS). Proc. Natl. Acad. Sci. U. S. A *109*, 1661-1666.

Goldstein,J.C., Waterhouse,N.J., Juin,P., Evan,G.I., and Green,D.R. (2000). The coordinate release of cytochrome c during apoptosis is rapid, complete and kinetically invariant. Nat. Cell Biol. *2*, 156-162.

Gomes,L.C., Di,B.G., and Scorrano,L. (2011). During autophagy mitochondria elongate, are spared from degradation and sustain cell viability. Nat. Cell Biol. *13*, 589-598.

Gonzalvez,F., Pariselli,F., Dupaigne,P., Budihardjo,I., Lutter,M., Antonsson,B., Diolez,P., Manon,S., Martinou,J.C., Goubern,M., Wang,X., Bernard,S., and Petit,P.X. (2005). tBid interaction with cardiolipin primarily orchestrates mitochondrial dysfunctions and subsequently activates Bax and Bak. Cell Death Differ *12*, 614-626.

Gonzalvez,F., Schug,Z.T., Houtkooper,R.H., MacKenzie,E.D., Brooks,D.G., Wanders,R.J., Petit,P.X., Vaz,F.M., and Gottlieb,E. (2008). Cardiolipin provides an essential activating platform for caspase-8 on mitochondria. J. Cell Biol. *183*, 681-696.

Griparic,L., Kanazawa,T., and van der Bliek,A.M. (2007). Regulation of the mitochondrial dynamin-like protein Opa1 by proteolytic cleavage. J. Cell Biol *178*, 757-764.

Griparic,L., van der Wel,N.N., Orozco,I.J., Peters,P.J., and van der Bliek,A.M. (2004). Loss of the intermembrane space protein Mgm1/OPA1 induces swelling and localized constrictions along the lengths of mitochondria. J. Biol. Chem. *279*, 18792-18798.

Gross,A., Yin,X.M., Wang,K., Wei,M.C., Jockel,J., Milliman,C., Erdjument,B.H., Tempst,P., and Korsmeyer,S.J. (1999). Caspase cleaved BID targets mitochondria and is required for cytochrome c release, while BCL-XL prevents this release but not tumor necrosis factor-R1/Fas death. J. Biol. Chem. *274*, 1156-1163.

Guan,K., Farh,L., Marshall,T.K., and Deschenes,R.J. (1993). Normal mitochondrial structure and genome maintenance in yeast requires the dynamin-like product of the MGM1 gene. Curr Genet *24*, 141-148.

Guarani,V., McNeill,E.M., Paulo,J.A., Huttlin,E.L., Frohlich,F., Gygi,S.P., Van,V.D., and Harper,J.W. (2015). QIL1 is a novel mitochondrial protein required for MICOS complex stability and cristae morphology. Elife. *4*.

Guo,F.Q., Okamoto,M., and Crawford,N.M. (2003). Identification of a plant nitric oxide synthase gene involved in hormonal signaling. Science *302*, 100-103.

Hackenbrock,C.R. (1966). Ultrastructural bases for metabolically linked mechanical activity in mitochondria. I. Reversible ultrastructural changes with change in metabolic steady state in isolated liver mitochondria. J. Cell Biol. *30*, 269-297.

Hackenbrock,C.R., Schneider,H., Lemasters,J.J., and Hochli,M. (1980). Relationships between bilayer lipid, motional freedom of oxidoreductase components, and electron transfer in the mitochondrial inner membrane. Adv. Exp. Med. Biol. *132*, 245-263.

Hajek,P., Chomyn,A., and Attardi,G. (2007). Identification of a novel mitochondrial complex containing mitofusin 2 and stomatin-like protein 2. J. Biol. Chem. *282*, 5670-5681.

Hales,K.G. and Fuller,M.T. (1997). Developmentally regulated mitochondrial fusion mediated by a conserved, novel, predicted GTPase. Cell *90*, 121-129.

Han,X., Yang,J., Yang,K., Zhao,Z., Abendschein,D.R., and Gross,R.W. (2007). Alterations in myocardial cardiolipin content and composition occur at the very earliest stages of diabetes: a shotgun lipidomics study. Biochemistry *46*, 6417-6428.

He,J., Cooper,H.M., Reyes,A., Di,R.M., Kazak,L., Wood,S.R., Mao,C.C., Fearnley,I.M., Walker,J.E., and Holt,I.J. (2012). Human C4orf14 interacts with the mitochondrial nucleoid and is involved in the biogenesis of the small mitochondrial ribosomal subunit. Nucleic Acids Res. *40*, 6097-6108.

Head,B., Griparic,L., Amiri,M., Gandre-Babbe,S., and van der Bliek,A.M. (2009). Inducible proteolytic inactivation of OPA1 mediated by the OMA1 protease in mammalian cells. J. Cell Biol. *187*, 959-966.

Heidler,J., Al-Furoukh,N., Kukat,C., Salwig,I., Ingelmann,M.E., Seibel,P., Kruger,M., Holtz,J., Wittig,I., Braun,T., and Szibor,M. (2011). Nitric oxide-associated protein 1 (NOA1) is necessary for oxygen-dependent regulation of mitochondrial respiratory complexes. J. Biol. Chem. *286*, 32086-32093.

Herlan,M., Vogel,F., Bornhovd,C., Neupert,W., and Reichert,A.S. (2003). Processing of Mgm1 by the rhomboid-type protease Pcp1 is required for maintenance of mitochondrial morphology and of mitochondrial DNA. J. Biol. Chem. *278*, 27781-27788.

Hermann,G.J., Thatcher,J.W., Mills,J.P., Hales,K.G., Fuller,M.T., Nunnari,J., and Shaw,J.M. (1998). Mitochondrial fusion in yeast requires the transmembrane GTPase Fzo1p. J. Cell Biol. *143*, 359-373.

Hockenbery,D., Nunez,G., Milliman,C., Schreiber,R.D., and Korsmeyer,S.J. (1990). Bcl-2 is an inner mitochondrial membrane protein that blocks programmed cell death. Nature *348*, 334-336.

Hoppins,S., Collins,S.R., Cassidy-Stone,A., Hummel,E., DeVay,R.M., Lackner,L.L., Westermann,B., Schuldiner,M., Weissman,J.S., and Nunnari,J. (2011a). A mitochondrial-focused genetic interaction map reveals a scaffold-like complex required for inner membrane organization in mitochondria. J Cell Biol *195*, 323-340.

Hoppins,S., Collins,S.R., Cassidy-Stone,A., Hummel,E., Devay,R.M., Lackner,L.L., Westermann,B., Schuldiner,M., Weissman,J.S., and Nunnari,J. (2011b). A mitochondrial-focused genetic interaction map reveals a scaffold-like complex required for inner membrane organization in mitochondria. J. Cell Biol. *195*, 323-340.

Hoppins,S., Edlich,F., Cleland,M.M., Banerjee,S., McCaffery,J.M., Youle,R.J., and Nunnari,J. (2011c). The soluble form of Bax regulates mitochondrial fusion via MFN2 homotypic complexes. Mol Cell *41*, 150-160.

Hsu,Y.T., Wolter,K.G., and Youle,R.J. (1997). Cytosol-to-membrane redistribution of Bax and Bcl-X(L) during apoptosis. Proc. Natl. Acad. Sci. U. S. A *94*, 3668-3672.

Huang,K.C., Mukhopadhyay,R., and Wingreen,N.S. (2006). A curvature-mediated mechanism for localization of lipids to bacterial poles. PLoS. Comput. Biol. *2*, e151.

Huang,P., Yu,T., and Yoon,Y. (2007). Mitochondrial clustering induced by overexpression of the mitochondrial fusion protein Mfn2 causes mitochondrial dysfunction and cell death. Eur. J. Cell Biol. *86*, 289-302.

Huang,S., Kerschbaum,H.H., Engel,E., and Hermann,A. (1997). Biochemical characterization and histochemical localization of nitric oxide synthase in the nervous system of the snail, Helix pomatia. J. Neurochem. *69*, 2516-2528.

Ingerman,E., Perkins,E.M., Marino,M., Mears,J.A., McCaffery,J.M., Hinshaw,J.E., and Nunnari,J. (2005). Dnm1 forms spirals that are structurally tailored to fit mitochondria. J Cell Biol *170*, 1021-1027.

Ishihara,N., Eura,Y., and Mihara,K. (2004). Mitofusin 1 and 2 play distinct roles in mitochondrial fusion reactions via GTPase activity. J. Cell Sci. *117*, 6535-6546.

Ishihara,N., Fujita,Y., Oka,T., and Mihara,K. (2006). Regulation of mitochondrial morphology through proteolytic cleavage of OPA1. EMBO J. *25*, 2966-2977.

Itoh,K., Tamura,Y., Iijima,M., and Sesaki,H. (2013). Effects of Fcj1-Mos1 and mitochondrial division on aggregation of mitochondrial DNA nucleoids and organelle morphology. Mol. Biol. Cell *24*, 1842-1851.

Jagasia,R., Grote,P., Westermann,B., and Conradt,B. (2005). DRP-1-mediated mitochondrial fragmentation during EGL-1-induced cell death in C. elegans. Nature *433*, 754-760.

Jahani-Asl,A. and Slack,R.S. (2007). The phosphorylation state of Drp1 determines cell fate. EMBO Rep. *8*, 912-913.

Jiang,X., Jiang,H., Shen,Z., and Wang,X. (2014). Activation of mitochondrial protease OMA1 by Bax and Bak promotes cytochrome c release during apoptosis. Proc. Natl. Acad. Sci. U. S. A *111*, 14782-14787.

John,G.B., Shang,Y., Li,L., Renken,C., Mannella,C.A., Selker,J.M., Rangell,L., Bennett,M.J., and Zha,J. (2005). The mitochondrial inner membrane protein mitofilin controls cristae morphology. Mol. Biol. Cell *16*, 1543-1554.

Jones,B.A. and Fangman,W.L. (1992). Mitochondrial DNA maintenance in yeast requires a protein containing a region related to the GTP-binding domain of dynamin. Genes. Dev. *6*, 380-389.

Joshi,A.S., Thompson,M.N., Fei,N., Huttemann,M., and Greenberg,M.L. (2012). Cardiolipin and mitochondrial phosphatidylethanolamine have overlapping functions in mitochondrial fusion in Saccharomyces cerevisiae. J. Biol. Chem. *287*, 17589-17597.

Jouaville,L.S., Ichas,F., Holmuhamedov,E.L., Camacho,P., and Lechleiter,J.D. (1995). Synchronization of calcium waves by mitochondrial substrates in Xenopus laevis oocytes. Nature *377*, 438-441.

Kamei,S., Chen-Kuo-Chang,M., Cazevieille,C., Lenaers,G., Olichon,A., Belenguer,P., Roussignol,G., Renard,N., Eybalin,M., Michelin,A., Delettre,C., Brabet,P., and Hamel,C.P. (2005). Expression of the Opa1 mitochondrial protein in retinal ganglion cells: its downregulation causes aggregation of the mitochondrial network. Invest Ophthalmol. Vis. Sci. *46*, 4288-4294.

Karbowski,M., Jeong,S.Y., and Youle,R.J. (2004). Endophilin B1 is required for the maintenance of mitochondrial morphology. J. Cell Biol. *166*, 1027-1039.

Karbowski,M., Lee,Y.J., Gaume,B., Jeong,S.Y., Frank,S., Nechushtan,A., Santel,A., Fuller,M., Smith,C.L., and Youle,R.J. (2002). Spatial and temporal association of Bax with mitochondrial fission sites, Drp1, and Mfn2 during apoptosis. J. Cell Biol. *159*, 931-938.

Karbowski,M., Neutzner,A., and Youle,R.J. (2007). The mitochondrial E3 ubiquitin ligase MARCH5 is required for Drp1 dependent mitochondrial division. J. Cell Biol *178*, 71-84.

Kasashima,K., Ohta,E., Kagawa,Y., and Endo,H. (2006). Mitochondrial functions and estrogen receptor-dependent nuclear translocation of pleiotropic human prohibitin 2. J. Biol. Chem. *281*, 36401-36410.

Kasashima,K., Sumitani,M., Satoh,M., and Endo,H. (2008). Human prohibitin 1 maintains the organization and stability of the mitochondrial nucleoids. Exp. Cell Res. *314*, 988-996.

Khalifat,N., Fournier,J.B., Angelova,M.I., and Puff,N. (2011). Lipid packing variations induced by pH in cardiolipin-containing bilayers: the driving force for the cristae-like shape instability. Biochim. Biophys. Acta *1808*, 2724-2733.

Khalifat,N., Puff,N., Bonneau,S., Fournier,J.B., and Angelova,M.I. (2008). Membrane deformation under local pH gradient: mimicking mitochondrial cristae dynamics. Biophys. J. *95*, 4924-4933.

Kijima,K., Numakura,C., Izumino,H., Umetsu,K., Nezu,A., Shiiki,T., Ogawa,M., Ishizaki,Y., Kitamura,T., Shozawa,Y., and Hayasaka,K. (2005). Mitochondrial GTPase mitofusin 2 mutation in Charcot-Marie-Tooth neuropathy type 2A. Hum. Genet. *116*, 23-27.

Kjer,P., Jensen,O.A., and Klinken,L. (1983). Histopathology of eye, optic nerve and brain in a case of dominant optic atrophy. Acta Ophthalmol. (Copenh) *61*, 300-312.

Kline,L.B. and Glaser,J.S. (1979). Dominant optic atrophy. The clinical profile. Arch. Ophthalmol. *97*, 1680-1686.

Kluck,R.M., Esposti,M.D., Perkins,G., Renken,C., Kuwana,T., Bossy-Wetzel,E., Goldberg,M., Allen,T., Barber,M.J., Green,D.R., and Newmeyer,D.D. (1999). The pro-apoptotic proteins, Bid and Bax, cause a limited permeabilization of the mitochondrial outer membrane that is enhanced by cytosol. J. Cell Biol. *147*, 809-822.

Knott,A.B. and Bossy-Wetzel,E. (2008). Impairing the mitochondrial fission and fusion balance: a new mechanism of neurodegeneration. Ann. N. Y. Acad. Sci. *1147*, 283-292.

Knott,A.B., Perkins,G., Schwarzenbacher,R., and Bossy-Wetzel,E. (2008). Mitochondrial fragmentation in neurodegeneration. Nat. Rev. Neurosci. *9*, 505-518.

Kolanczyk,M., Pech,M., Zemojtel,T., Yamamoto,H., Mikula,I., Calvaruso,M.A., van den Brand,M., Richter,R., Fischer,B., Ritz,A., Kossler,N., Thurisch,B., Spoerle,R., Smeitink,J., Kornak,U., Chan,D., Vingron,M., Martasek,P., Lightowlers,R.N., Nijtmans,L., Schuelke,M., Nierhaus,K.H., and Mundlos,S. (2011). NOA1 is an essential GTPase required for mitochondrial protein synthesis. Mol. Biol. Cell *22*, 1-11.

Kukat,C., Davies,K.M., Wurm,C.A., Spahr,H., Bonekamp,N.A., Kuhl,I., Joos,F., Polosa,P.L., Park,C.B., Posse,V., Falkenberg,M., Jakobs,S., Kuhlbrandt,W., and Larsson,N.G. (2015). Cross-strand binding of TFAM to a single mtDNA molecule forms the mitochondrial nucleoid. Proc. Natl. Acad. Sci. U. S. A *112*, 11288-11293.

Kukat,C., Wurm,C.A., Spahr,H., Falkenberg,M., Larsson,N.G., and Jakobs,S. (2011). Super-resolution microscopy reveals that mammalian mitochondrial nucleoids have a uniform size and frequently contain a single copy of mtDNA. Proc. Natl. Acad. Sci. U. S. A *108*, 13534-13539.

Kuwana,T., Mackey,M.R., Perkins,G., Ellisman,M.H., Latterich,M., Schneiter,R., Green,D.R., and Newmeyer,D.D. (2002). Bid, Bax, and lipids cooperate to form supramolecular openings in the outer mitochondrial membrane. Cell *111*, 331-342.

Landes,T., Emorine,L.J., Courilleau,D., Rojo,M., Belenguer,P., and rnaune-Pelloquin,L. (2010). The BH3-only Bnip3 binds to the dynamin Opa1 to promote mitochondrial fragmentation and apoptosis by distinct mechanisms. EMBO Rep. *11*, 459-465.

Lange,C., Nett,J.H., Trumpower,B.L., and Hunte,C. (2001). Specific roles of protein-phospholipid interactions in the yeast cytochrome bc1 complex structure. EMBO J. *20*, 6591-6600.

Lawson,V.H., Graham,B.V., and Flanigan,K.M. (2005). Clinical and electrophysiologic features of CMT2A with mutations in the mitofusin 2 gene. Neurology. *65*, 197-204.

Lee,J.H., Nguyen,K.H., Mishra,S., and Nyomba,B.L. (2010). Prohibitin is expressed in pancreatic beta-cells and protects against oxidative and proapoptotic effects of ethanol. FEBS J. *277*, 488-500.

Lee,Y.J., Jeong,S.Y., Karbowski,M., Smith,C.L., and Youle,R.J. (2004). Roles of the mammalian mitochondrial fission and fusion mediators Fis1, Drp1, and Opa1 in apoptosis. Mol. Biol. Cell *15*, 5001-5011.

Letai,A., Bassik,M.C., Walensky,L.D., Sorcinelli,M.D., Weiler,S., and Korsmeyer,S.J. (2002). Distinct BH3 domains either sensitize or activate mitochondrial apoptosis, serving as prototype cancer therapeutics. Cancer Cell *2*, 183-192.

Li,H., Ruan,Y., Zhang,K., Jian,F., Hu,C., Miao,L., Gong,L., Sun,L., Zhang,X., Chen,S., Chen,H., Liu,D., and Song,Z. (2015). Mic60/Mitofilin determines MICOS assembly essential for mitochondrial dynamics and mtDNA nucleoid organization. Cell Death. Differ.

Li,L.Y., Luo,X., and Wang,X. (2001). Endonuclease G is an apoptotic DNase when released from mitochondria. Nature *412*, 95-99.

Lindsten,T., Ross,A.J., King,A., Zong,W.X., Rathmell,J.C., Shiels,H.A., Ulrich,E., Waymire,K.G., Mahar,P., Frauwirth,K., Chen,Y., Wei,M., Eng,V.M., Adelman,D.M., Simon,M.C., Ma,A., Golden,J.A., Evan,G.,

Korsmeyer,S.J., MacGregor,G.R., and Thompson,C.B. (2000). The combined functions of proapoptotic Bcl-2 family members bak and bax are essential for normal development of multiple tissues. Mol. Cell *6*, 1389-1399.

Lisak,D.A., Schacht,T., Enders,V., Habicht,J., Kiviluoto,S., Schneider,J., Henke,N., Bultynck,G., and Methner,A. (2015). The transmembrane Bax inhibitor motif (TMBIM) containing protein family: Tissue expression, intracellular localization and effects on the ER CA(2)(+)-filling state. Biochim. Biophys. Acta *1853*, 2104-2114.

Liu,X.S., Kim,C.N., Yang,J., Jemmerson,R., and Wang,X.D. (1996). Induction of apoptotic program in cell free extracts: requirement for dATP and cytochrome c. Cell *86*, 147-157.

Lodi,R., Tonon,C., Valentino,M.L., Iotti,S., Clementi,V., Malucelli,E., Barboni,P., Longanesi,L., Schimpf,S., Wissinger,B., Baruzzi,A., Barbiroli,B., and Carelli,V. (2004). Deficit of in vivo mitochondrial ATP production in OPA1-related dominant optic atrophy. Ann. Neurol. *56*, 719-723.

Loh,P.C., Morimoto,T., Matsuo,Y., Oshima,T., and Ogasawara,N. (2007). The GTP-binding protein YqeH participates in biogenesis of the 30S ribosome subunit in Bacillus subtilis. Genes Genet. Syst. *82*, 281-289.

Luo,X., Budihardjo,I., Zou,H., Slaughter,C., and Wang,X. (1998). Bid, a Bcl2 interacting protein, mediates cytochrome c release from mitochondria in response to activation of cell surface death receptors. Cell *94*, 481-490.

Lutter,M., Fang,M., Luo,X., Nishijima,M., Xie,X., and Wang,X. (2000). Cardiolipin provides specificity for targeting of tBid to mitochondria. Nat. Cell Biol. *2*, 754-761.

Makino,A., Scott,B.T., and Dillmann,W.H. (2010). Mitochondrial fragmentation and superoxide anion production in coronary endothelial cells from a mouse model of type 1 diabetes. Diabetologia *53*, 1783-1794.

Makino,A., Suarez,J., Gawlowski,T., Han,W., Wang,H., Scott,B.T., and Dillmann,W.H. (2011). Regulation of mitochondrial morphology and function by O-GlcNAcylation in neonatal cardiac myocytes. Am. J. Physiol Regul. Integr. Comp Physiol *300*, R1296-R1302.

Mannella,C.A., Marko,M., Penczek,P., Barnard,D., and Frank,J. (1994). The internal compartmentation of rat-liver mitochondria: tomographic study using the high-voltage transmission electron microscope. Microsc Res Tech *27*, 278-283.

Mannella,C.A., Pfeiffer,D.R., Bradshaw,P.C., Moraru,I.I., Slepchenko,B., Loew,L.M., Hsieh,C.E., Buttle,K., and Marko,M. (2001). Topology of the mitochondrial inner membrane: dynamics and bioenergetic implications. IUBMB. Life *52*, 93-100.

Marchbank,N.J., Craig,J.E., Leek,J.P., Toohey,M., Churchill,A.J., Markham,A.F., Mackey,D.A., Toomes,C., and Inglehearn,C.F. (2002). Deletion of the OPA1 gene in a dominant optic atrophy family: evidence that haploinsufficiency is the cause of disease. J. Med. Genet. *39*, e47.

Margulis,L. (1971). The origin of plant and animal cells. Am. Sci. *59*, 230-235.

Martinou,J.C., Desagher,S., and Antonsson,B. (2000). Cytochrome c release from mitochondria: all or nothing. Nat. Cell Biol. *2*, E41-E43.

Martins,L.M., Morrison,A., Klupsch,K., Fedele,V., Moisoi,N., Teismann,P., Abuin,A., Grau,E., Geppert,M., Livi,G.P., Creasy,C.L., Martin,A., Hargreaves,I., Heales,S.J., Okada,H., Brandner,S., Schulz,J.B., Mak,T., and Downward,J. (2004). Neuroprotective role of the Reaper-related serine protease HtrA2/Omi revealed by targeted deletion in mice. Mol. Cell Biol. *24*, 9848-9862.

Marzo,I., Brenner,C., Zamzami,N., Jurgensmeier,J.M., Susin,S.A., Vieira,H.L., Prevost,M.C., Xie,Z., Matsuyama,S., Reed,J.C., and Kroemer,G. (1998). Bax and adenine nucleotide translocator cooperate in the mitochondrial control of apoptosis. Science *281*, 2027-2031.

Mayorov,V.I., Lowrey,A.J., Biousse,V., Newman,N.J., Cline,S.D., and Brown,M.D. (2008). Mitochondrial oxidative phosphorylation in autosomal dominant optic atrophy. BMC. Biochem. *9*, 22.

McKenzie,M., Lazarou,M., Thorburn,D.R., and Ryan,M.T. (2006). Mitochondrial respiratory chain supercomplexes are destabilized in Barth Syndrome patients. J. Mol. Biol. *361*, 462-469.

Meeusen,S., DeVay,R., Block,J., Cassidy-Stone,A., Wayson,S., McCaffery,J.M., and Nunnari,J. (2006). Mitochondrial inner-membrane fusion and crista maintenance requires the dynamin-related GTPase Mgm1. Cell *127*, 383-395.

Meisinger,C., Rissler,M., Chacinska,A., Szklarz,L.K., Milenkovic,D., Kozjak,V., Schonfisch,B., Lohaus,C., Meyer,H.E., Yaffe,M.P., Guiard,B., Wiedemann,N., and Pfanner,N. (2004). The mitochondrial morphology protein Mdm10 functions in assembly of the preprotein translocase of the outer membrane. Dev. Cell *7*, 61-71.

Merkwirth,C., Dargazanli,S., Tatsuta,T., Geimer,S., Lower,B., Wunderlich,F.T., von Kleist-Retzow,J.C., Waisman,A., Westermann,B., and Langer,T. (2008). Prohibitins control cell proliferation and apoptosis by regulating OPA1-dependent cristae morphogenesis in mitochondria. Genes Dev. *22*, 476-488.

Messerschmitt,M., Jakobs,S., Vogel,F., Fritz,S., Dimmer,K.S., Neupert,W., and Westermann,B. (2003). The inner membrane protein Mdm33 controls mitochondrial morphology in yeast. J. Cell Biol. *160*, 553-564.

Mishra,P. and Chan,D.C. (2014). Mitochondrial dynamics and inheritance during cell division, development and disease. Nat Rev Mol Cell Biol *15*, 634-646.

Mitchell,P. and Moyle,J. (1967). Chemiosmotic hypothesis of oxidative phosphorylation. Nature *213*, 137-139.

Mitsopoulos,P., Chang,Y.H., Wai,T., Konig,T., Dunn,S.D., Langer,T., and Madrenas,J. (2015). Stomatin-like protein 2 is required for in vivo mitochondrial respiratory chain supercomplex formation and optimal cell function. Mol. Cell Biol. *35*, 1838-1847.

Mootha,V.K., Wei,M.C., Buttle,K.F., Scorrano,L., Panoutsakopoulou,V., Mannella,C.A., and Korsmeyer,S.J. (2001). A reversible component of mitochondrial respiratory dysfunction in apoptosis can be rescued by exogenous cytochrome c. EMBO J. *20*, 661-671.

Moreau,M., Lee,G.I., Wang,Y., Crane,B.R., and Klessig,D.F. (2008). AtNOS/AtNOA1 is a functional Arabidopsis thaliana cGTPase and not a nitric-oxide synthase. J. Biol. Chem. *283*, 32957-32967.

Munoz-Gomez,S.A., Slamovits,C.H., Dacks,J.B., Baier,K.A., Spencer,K.D., and Wideman,J.G. (2015). Ancient homology of the mitochondrial contact site and cristae organizing system points to an endosymbiotic origin of mitochondrial cristae. Curr. Biol. *25*, 1489-1495.

Myung,J., Gulesserian,T., Fountoulakis,M., and Lubec,G. (2003). Deranged hypothetical proteins Rik protein, Nit protein 2 and mitochondrial inner membrane protein, Mitofilin, in fetal Down syndrome brain. Cell Mol. Biol. (Noisy. -le-grand) *49*, 739-746.

Nakamura,N., Kimura,Y., Tokuda,M., Honda,S., and Hirose,S. (2006). MARCH-V is a novel mitofusin 2- and Drp1-binding protein able to change mitochondrial morphology. EMBO. Rep. *7*, 1019-1022.

Neuspiel,M., Zunino,R., Gangaraju,S., Rippstein,P., and McBride,H.M. (2005). Activated Mfn2 signals mitochondrial fusion, interferes with Bax activation and reduces susceptibility to radical induced depolarization. J. Biol. Chem. *280*, 25060-25070.

Newmeyer,D.D. and Ferguson-Miller,S. (2003). Mitochondria: releasing power for life and unleashing the machineries of death. Cell *112*, 481-490.

Niemann,A., Ruegg,M., La,P., V, Schenone,A., and Suter,U. (2005). Ganglioside-induced differentiation associated protein 1 is a regulator of the mitochondrial network: new implications for Charcot-Marie-Tooth disease. J. Cell Biol. *170*, 1067-1078.

Nijtmans,L.G., Artal,S.M., Grivell,L.A., and Coates,P.J. (2002). The mitochondrial PHB complex: roles in mitochondrial respiratory complex assembly, ageing and degenerative disease. Cell Mol. Life Sci. *59*, 143-155.

Nijtmans,L.G., de,J.L., Artal,S.M., Coates,P.J., Berden,J.A., Back,J.W., Muijsers,A.O., van der Spek,H., and Grivell,L.A. (2000). Prohibitins act as a membrane-bound chaperone for the stabilization of mitochondrial proteins. EMBO J. *19*, 2444-2451.

Norton,M., Ng,A.C., Baird,S., Dumoulin,A., Shutt,T., Mah,N., Andrade-Navarro,M.A., McBride,H.M., and Screaton,R.A. (2014). ROMO1 is an essential redox-dependent regulator of mitochondrial dynamics. Sci. Signal. *7*, ra10.

Nouraini,S., Six,E., Matsuyama,S., Krajewski,S., and Reed,J.C. (2000). The putative pore-forming domain of Bax regulates mitochondrial localization and interaction with Bcl-X(L). Mol. Cell Biol. *20*, 1604-1615.

Oka,T., Sayano,T., Tamai,S., Yokota,S., Kato,H., Fujii,G., and Mihara,K. (2008). Identification of a novel protein MICS1 that is involved in maintenance of mitochondrial morphology and apoptotic release of cytochrome c. Mol. Biol. Cell *19*, 2597-2608.

Okamoto,K. and Shaw,J.M. (2005). Mitochondrial morphology and dynamics in yeast and multicellular eukaryotes. Annu. Rev. Genet. *39*, 503-536.

Olichon,A., Baricault,L., Gas,N., Guillou,E., Valette,A., Belenguer,P., and Lenaers,G. (2003). Loss of OPA1 perturbates the mitochondrial inner membrane structure and integrity, leading to cytochrome c release and apoptosis. J. Biol. Chem. *278*, 7743-7746.

Olichon,A., Emorine,L.J., Descoins,E., Pelloquin,L., Brichese,L., Gas,N., Guillou,E., Delettre,C., Valette,A., Hamel,C.P., Ducommun,B., Lenaers,G., and Belenguer,P. (2002). The human dynamin-related protein OPA1 is anchored to the mitochondrial inner membrane facing the inter-membrane space. FEBS Lett. *523*, 171-176.

Olichon,A., Landes,T., rnaune-Pelloquin,L., Emorine,L.J., Mils,V., Guichet,A., Delettre,C., Hamel,C., mati-Bonneau,P., Bonneau,D., Reynier,P., Lenaers,G., and Belenguer,P. (2007). Effects of OPA1 mutations on mitochondrial morphology and apoptosis: relevance to ADOA pathogenesis. J. Cell Physiol *211*, 423-430.

Omori,A., Ichinose,S., Kitajima,S., Shimotohno,K.W., Murashima,Y.L., Shimotohno,K., and Seto-Ohshima,A. (2002). Gerbils of a seizure-sensitive strain have a mitochondrial inner membrane protein with different isoelectric points from those of a seizure-resistant strain. Electrophoresis *23*, 4167-4174.

Ong,S.E. and Mann,M. (2007). Stable isotope labeling by amino acids in cell culture for quantitative proteomics. Methods Mol. Biol. *359*, 37-52.

Osman,C., Haag,M., Potting,C., Rodenfels,J., Dip,P.V., Wieland,F.T., Brugger,B., Westermann,B., and Langer,T. (2009). The genetic interactome of prohibitins: coordinated control of cardiolipin and phosphatidylethanolamine by conserved regulators in mitochondria. J. Cell Biol. *184*, 583-596.

Otera,H., Wang,C., Cleland,M.M., Setoguchi,K., Yokota,S., Youle,R.J., and Mihara,K. (2010). Mff is an essential factor for mitochondrial recruitment of Drp1 during mitochondrial fission in mammalian cells. J Cell Biol. *191*, 1141-1158.

Ott,M., Robertson,J.D., Gogvadze,V., Zhivotovsky,B., and Orrenius,S. (2002). Cytochrome c release from mitochondria proceeds by a two-step process. Proc. Natl. Acad. Sci. U. S. A *99*, 1259-1263.

Palade,G.E. (1952). The fine structure of mitochondria. Anat. Rec. *114*, 427-451.

Palmer,C.S., Osellame,L.D., Laine,D., Koutsopoulos,O.S., Frazier,A.E., and Ryan,M.T. (2011). MiD49 and MiD51, new components of the mitochondrial fission machinery. EMBO Rep. *12*, 565-573.

Parone,P.A., Da,C.S., Tondera,D., Mattenberger,Y., James,D.I., Maechler,P., Barja,F., and Martinou,J.C. (2008). Preventing mitochondrial fission impairs mitochondrial function and leads to loss of mitochondrial DNA. PLoS. One. *3*, e3257.

Patten,D.A., Wong,J., Khacho,M., Soubannier,V., Mailloux,R.J., Pilon-Larose,K., MacLaurin,J.G., Park,D.S., McBride,H.M., Trinkle-Mulcahy,L., Harper,M.E., Germain,M., and Slack,R.S. (2014a). OPA1-dependent cristae modulation is essential for cellular adaptation to metabolic demand. EMBO J *33*, 2676-2691.

Patten,D.A., Wong,J., Khacho,M., Soubannier,V., Mailloux,R.J., Pilon-Larose,K., MacLaurin,J.G., Park,D.S., McBride,H.M., Trinkle-Mulcahy,L., Harper,M.E., Germain,M., and Slack,R.S. (2014b). OPA1-dependent cristae modulation is essential for cellular adaptation to metabolic demand. EMBO J. *33*, 2676-2691.

Paul,M.F., Alushin,G.M., Barros,M.H., Rak,M., and Tzagoloff,A. (2012). The putative GTPase encoded by MTG3 functions in a novel pathway for regulating assembly of the small subunit of yeast mitochondrial ribosomes. J. Biol. Chem. *287*, 24346-24355.

Paumard,P., Vaillier,J., Coulary,B., Schaeffer,J., Soubannier,V., Mueller,D.M., Brethes,D., di Rago,J.P., and Velours,J. (2002). The ATP synthase is involved in generating mitochondrial cristae morphology. EMBO J. *21*, 221-230.

Pebay-Peyroula,E., Dahout-Gonzalez,C.Γ., Kahn,R., TrΓ©zΓ©guet,V.Γ., Lauquin,G.J.M., and Brandolin,G.Γ. (2003). Structure of mitochondrial ADP/ATP carrier in complex with carboxyatractyloside. Nature *426*, 39-44.

Pellegrini,L. and Scorrano,L. (2007). A cut short to death: Parl and Opa1 in the regulation of mitochondrial morphology and apoptosis. Cell Death. Differ.

Pesch,U.E., Leo-Kottler,B., Mayer,S., Jurklies,B., Kellner,U., Apfelstedt-Sylla,E., Zrenner,E., Alexander,C., and Wissinger,B. (2001). OPA1 mutations in patients with autosomal dominant optic atrophy and evidence for semi-dominant inheritance. Hum. Mol Genet. *10*, 1359-1368.

Pfanner,N., van der Laan,M., Amati,P., Capaldi,R.A., Caudy,A.A., Chacinska,A., Darshi,M., Deckers,M., Hoppins,S., Icho,T., Jakobs,S., Ji,J., Kozjak-Pavlovic,V., Meisinger,C., Odgren,P.R., Park,S.K., Rehling,P., Reichert,A.S., Sheikh,M.S., Taylor,S.S., Tsuchida,N., van der Bliek,A.M., van der Klei,I.J., Weissman,J.S., Westermann,B., Zha,J., Neupert,W., and Nunnari,J. (2014). Uniform nomenclature for the mitochondrial contact site and cristae organizing system. J Cell Biol *204*, 1083-1086.

Pfeiffer,D.R., Gudz,T.I., Novgorodov,S.A., and Erdahl,W.L. (1995). The peptide mastoparan is a potent facilitator of the mitochondrial permeability transition. J. Biol. Chem. *270*, 4923-4932.

Pfeiffer,K., Gohil,V., Stuart,R.A., Hunte,C., Brandt,U., Greenberg,M.L., and Schagger,H. (2003). Cardiolipin stabilizes respiratory chain supercomplexes. J. Biol. Chem. *278*, 52873-52880.

Pfohler,C., Preuss,K.D., Tilgen,W., Stark,A., Regitz,E., Fadle,N., and Pfreundschuh,M. (2007). Mitofilin and titin as target antigens in melanoma-associated retinopathy. Int. J. Cancer *120*, 788-795.

Pich,S., Bach,D., Briones,P., Liesa,M., Camps,M., Testar,X., Palacin,M., and Zorzano,A. (2005). The Charcot-Marie-Tooth type 2A gene product, Mfn2, up-regulates fuel oxidation through expression of OXPHOS system. Hum. Mol. Genet. *14*, 1405-1415.

Praefcke,G.J. and McMahon,H.T. (2004). The dynamin superfamily: universal membrane tubulation and fission molecules? Nat Rev Mol Cell Biol *5*, 133-147.

Rabl,R., Soubannier,V., Scholz,R., Vogel,F., Mendl,N., Vasiljev-Neumeyer,A., Korner,C., Jagasia,R., Keil,T., Baumeister,W., Cyrklaff,M., Neupert,W., and Reichert,A.S. (2009). Formation of cristae and crista junctions in mitochondria depends on antagonism between Fcj1 and Su e/g. J. Cell Biol. *185*, 1047-1063.

Ramachandran,R., Surka,M., Chappie,J.S., Fowler,D.M., Foss,T.R., Song,B.D., and Schmid,S.L. (2007). The dynamin middle domain is critical for tetramerization and higher-order self-assembly. EMBO J. *26*, 559-566.

Rapaport,D., Brunner,M., Neupert,W., and Westermann,B. (1998). Fzo1p is a mitochondrial outer membrane protein essential for the biogenesis of functional mitochondria in Saccharomyces cerevisiae. J. Biol. Chem. *273*, 20150-20155.

Rappold,P.M., Cui,M., Grima,J.C., Fan,R.Z., de Mesy-Bentley,K.L., Chen,L., Zhuang,X., Bowers,W.J., and Tieu,K. (2014). Drp1 inhibition attenuates neurotoxicity and dopamine release deficits in vivo. Nat. Commun. *5*, 5244.

Reimers,K., Choi,C.Y., Bucan,V., and Vogt,P.M. (2007). The growth-hormone inducible transmembrane protein (Ghitm) belongs to the Bax inhibitory protein-like family. Int. J. Biol. Sci. *3*, 471-476.

Richter-Dennerlein,R., Korwitz,A., Haag,M., Tatsuta,T., Dargazanli,S., Baker,M., Decker,T., Lamkemeyer,T., Rugarli,E.I., and Langer,T. (2014). DNAJC19, a mitochondrial cochaperone associated with cardiomyopathy, forms a complex with prohibitins to regulate cardiolipin remodeling. Cell Metab *20*, 158-171.

Rimessi,A., Giorgi,C., Pinton,P., and Rizzuto,R. (2008). The versatility of mitochondrial calcium signals: from stimulation of cell metabolism to induction of cell death. Biochim. Biophys. Acta *1777*, 808-816.

Rizzuto,R., Pinton,P., Ferrari,D., Chami,M., Szabadkai,G., Magalhaes,P.J., Di Virgilio,F., and Pozzan,T. (2003). Calcium and apoptosis: facts and hypotheses. Oncogene *22*, 8619-8627.

Robinson,N.C. (1993). Functional binding of cardiolipin to cytochrome c oxidase. J. Bioenerg. Biomembr. *25*, 153-163.

Rojo,M., Legros,F., Chateau,D., and Lombes,A. (2002). Membrane topology and mitochondrial targeting of mitofusins, ubiquitous mammalian homologs of the transmembrane GTPase Fzo. J. Cell Sci. *115*, 1663-1674.

Rossi,M.N., Carbone,M., Mostocotto,C., Mancone,C., Tripodi,M., Maione,R., and Amati,P. (2009). Mitochondrial localization of PARP-1 requires interaction with mitofilin and is involved in the maintenance of mitochondrial DNA integrity. J. Biol. Chem. *284*, 31616-31624.

Santel,A., Frank,S., Gaume,B., Herrler,M., Youle,R.J., and Fuller,M.T. (2003). Mitofusin-1 protein is a generally expressed mediator of mitochondrial fusion in mammalian cells. J. Cell Sci. *116*, 2763-2774.

Santel,A. and Fuller,M.T. (2001). Control of mitochondrial morphology by a human mitofusin. J. Cell Sci. *114*, 867-874.

Santos,D., Esteves,A.R., Silva,D.F., Januario,C., and Cardoso,S.M. (2015). The Impact of Mitochondrial Fusion and Fission Modulation in Sporadic Parkinson's Disease. Mol. Neurobiol. *52*, 573-586.

Satoh,M., Hamamoto,T., Seo,N., Kagawa,Y., and Endo,H. (2003). Differential sublocalization of the dynamin-related protein OPA1 isoforms in mitochondria. Biochem. Biophys. Res. Commun. *300*, 482-493.

Scaffidi,C., Fulda,S., Srinivasan,A., Friesen,C., Li,F., Tomaselli,K.J., Debatin,K.M., Krammer,P.H., and Peter,M.E. (1998). Two CD95 (APO-1/Fas) signaling pathways. EMBO J. *17*, 1675-1687.

Scaffidi,C., Schmitz,I., Zha,J., Korsmeyer,S.J., Krammer,P.H., and Peter,M.E. (1999). Differential modulation of apoptosis sensitivity in CD95 type I and type II cells. J. Biol. Chem. *274*, 22532-22538.

Schagger,H. and Pfeiffer,K. (2000). Supercomplexes in the respiratory chains of yeast and mammalian mitochondria. EMBO J. *19*, 1777-1783.

Schapira,A.H. (2006). Mitochondrial disease. Lancet. *368*, 70-82.

Schellenberg,B., Wang,P., Keeble,J.A., Rodriguez-Enriquez,R., Walker,S., Owens,T.W., Foster,F., Tanianis-Hughes,J., Brennan,K., Streuli,C.H., and Gilmore,A.P. (2013). Bax exists in a dynamic equilibrium between the cytosol and mitochondria to control apoptotic priming. Mol. Cell *49*, 959-971.

Schlame,M. and Ren,M. (2006). Barth syndrome, a human disorder of cardiolipin metabolism. FEBS Lett. *580*, 5450-5455.

Schmidt,A., Wolde,M., Thiele,C., Fest,W., Kratzin,H., Podtelejnikov,A.V., Witke,W., Huttner,W.B., and Soling,H.D. (1999). Endophilin I mediates synaptic vesicle formation by transfer of arachidonate to lysophosphatidic acid. Nature *401*, 133-141.

Scorrano,L., Ashiya,M., Buttle,K., Weiler,S., Oakes,S.A., Mannella,C.A., and Korsmeyer,S.J. (2002). A distinct pathway remodels mitochondrial cristae and mobilizes cytochrome c during apoptosis. Dev. Cell *2*, 55-67.

Scorrano,L., Oakes,S.A., Opferman,J.T., Cheng,E.H., Sorcinelli,M.D., Pozzan,T., and Korsmeyer,S.J. (2003). BAX and BAK regulation of endoplasmic reticulum Ca2+: a control point for apoptosis. Science *300*, 135-139.

Sesaki,H. and Jensen,R.E. (2001). UGO1 encodes an outer membrane protein required for mitochondrial fusion. J. Cell Biol. *152*, 1123-1134.

Sesaki,H. and Jensen,R.E. (2004). Ugo1p links the Fzo1p and Mgm1p GTPases for mitochondrial fusion. J Biol Chem. *279*, 28298-28303.

Sesaki,H., Southard,S.M., Yaffe,M.P., and Jensen,R.E. (2003). Mgm1p, a dynamin-related GTPase, is essential for fusion of the mitochondrial outer membrane. Mol. Biol. Cell *14*, 2342-2356.

Shepard,K.A. and Yaffe,M.P. (1999). The yeast dynamin-like protein, Mgm1p, functions on the mitochondrial outer membrane to mediate mitochondrial inheritance. J. Cell Biol. *144*, 711-720.

Shimizu,S., Narita,M., and Tsujimoto,Y. (1999). Bcl-2 family proteins regulate the release of apoptogenic cytochrome c by the mitochondrial channel VDAC. Nature *399*, 483-487.

Smirnova,E., Griparic,L., Shurland,D.L., and van der Bliek,A.M. (2001). Dynamin-related protein Drp1 is required for mitochondrial division in mammalian cells. Mol. Biol. Cell *12*, 2245-2256.

Song,W., Chen,J., Petrilli,A., Liot,G., Klinglmayr,E., Zhou,Y., Poquiz,P., Tjong,J., Pouladi,M.A., Hayden,M.R., Masliah,E., Ellisman,M., Rouiller,I., Schwarzenbacher,R., Bossy,B., Perkins,G., and Bossy-Wetzel,E. (2011). Mutant huntingtin binds the mitochondrial fission GTPase dynamin-related protein-1 and increases its enzymatic activity. Nat. Med. *17*, 377-382.

Song,Z., Chen,H., Fiket,M., Alexander,C., and Chan,D.C. (2007). OPA1 processing controls mitochondrial fusion and is regulated by mRNA splicing, membrane potential, and Yme1L. J. Cell Biol *178*, 749-755.

Song,Z., Ghochani,M., McCaffery,J.M., Frey,T.G., and Chan,D.C. (2009). Mitofusins and OPA1 mediate sequential steps in mitochondrial membrane fusion. Mol. Biol. Cell *20*, 3525-3532.

Sood,A., Jeyaraju,D.V., Prudent,J., Caron,A., Lemieux,P., McBride,H.M., Laplante,M., Toth,K., and Pellegrini,L. (2014). A Mitofusin-2-dependent inactivating cleavage of Opa1 links changes in mitochondria cristae and ER contacts in the postprandial liver. Proc. Natl. Acad. Sci. U. S. A *111*, 16017-16022.

SOTELO,J.R. and PORTER,K.R. (1959). An electron microscope study of the rat ovum. J. Biophys. Biochem. Cytol. *5*, 327-342.

Sparagna,G.C., Chicco,A.J., Murphy,R.C., Bristow,M.R., Johnson,C.A., Rees,M.L., Maxey,M.L., McCune,S.A., and Moore,R.L. (2007). Loss of cardiac tetralinoleoyl cardiolipin in human and experimental heart failure. J. Lipid Res. *48*, 1559-1570.

Spinazzi,M., Cazzola,S., Bortolozzi,M., Baracca,A., Loro,E., Casarin,A., Solaini,G., Sgarbi,G., Casalena,G., Cenacchi,G., Malena,A., Frezza,C., Carrara,F., Angelini,C., Scorrano,L., Salviati,L., and Vergani,L. (2008). A novel deletion in the GTPase domain of OPA1 causes defects in mitochondrial morphology and distribution, but not in function. Hum. Mol. Genet. *17*, 3291-3302.

Steglich,G., Neupert,W., and Langer,T. (1999). Prohibitins regulate membrane protein degradation by the m-AAA protease in mitochondria. Mol. Cell Biol. *19*, 3435-3442.

Stojanovski,D., Koutsopoulos,O.S., Okamoto,K., and Ryan,M.T. (2004). Levels of human Fis1 at the mitochondrial outer membrane regulate mitochondrial morphology. J. Cell Sci. *117*, 1201-1210.

Strauss,M., Hofhaus,G., Schroder,R.R., and Kuhlbrandt,W. (2008). Dimer ribbons of ATP synthase shape the inner mitochondrial membrane. EMBO J. *27*, 1154-1160.

Su,D.M., Zhang,Q., Wang,X., He,P., Zhu,Y.J., Zhao,J., Rennert,O.M., and Su,Y.A. (2009). Two types of human malignant melanoma cell lines revealed by expression patterns of mitochondrial and survival-apoptosis genes: implications for malignant melanoma therapy. Mol. Cancer Ther. *8*, 1292-1304.

Subburaj,Y., Cosentino,K., Axmann,M., Pedrueza-Villalmanzo,E., Hermann,E., Bleicken,S., Spatz,J., and Garcia-Saez,A.J. (2015). Bax monomers form dimer units in the membrane that further self-assemble into multiple oligomeric species. Nat. Commun. *6*, 8042.

Sudhamsu,J., Lee,G.I., Klessig,D.F., and Crane,B.R. (2008). The structure of YqeH. An AtNOS1/AtNOA1 ortholog that couples GTP hydrolysis to molecular recognition. J. Biol. Chem. *283*, 32968-32976.

Susin,S.A., Lorenzo,H.K., Zamzami,N., Marzo,I., Snow,B.E., Brothers,G.M., Mangion,J., Jacotot,E., Costantini,P., Loeffler,M., Larochette,N., Goodlett,D.R., Aebersold,R., Siderovski,D.P., Penninger,J.M., and Kroemer,G. (1999). Molecular characterization of mitochondrial apoptosis-inducing factor. Nature *397*, 441-446.

Suzuki,M., Jeong,S.Y., Karbowski,M., Youle,R.J., and Tjandra,N. (2003). The solution structure of human mitochondria fission protein Fis1 reveals a novel TPR-like helix bundle. J. Mol. Biol. *334*, 445-458.

Szklarczyk,R., Nooteboom,M., and Osiewacz,H.D. (2014). Control of mitochondrial integrity in ageing and disease. Philos. Trans. R. Soc. Lond B Biol. Sci. *369*, 20130439.

Taguchi,N., Ishihara,N., Jofuku,A., Oka,T., and Mihara,K. (2007). Mitotic phosphorylation of dynamin-related GTPase Drp1 participates in mitochondrial fission. J. Biol Chem. *282*, 11521-11529.

Tang,T., Zheng,B., Chen,S.H., Murphy,A.N., Kudlicka,K., Zhou,H., and Farquhar,M.G. (2009). hNOA1 interacts with complex I and DAP3 and regulates mitochondrial respiration and apoptosis. J. Biol. Chem. *284*, 5414-5424.

Tatsuta,T., Model,K., and Langer,T. (2005). Formation of membrane-bound ring complexes by prohibitins in mitochondria. Mol. Biol. Cell *16*, 248-259.

Tavernarakis,N., Driscoll,M., and Kyrpides,N.C. (1999). The SPFH domain: implicated in regulating targeted protein turnover in stomatins and other membrane-associated proteins. Trends Biochem. Sci. *24*, 425-427.

Todt,F., Cakir,Z., Reichenbach,F., Emschermann,F., Lauterwasser,J., Kaiser,A., Ichim,G., Tait,S.W., Frank,S., Langer,H.F., and Edlich,F. (2015). Differential retrotranslocation of mitochondrial Bax and Bak. EMBO J. *34*, 67-80.

Todt,F., Cakir,Z., Reichenbach,F., Youle,R.J., and Edlich,F. (2013). The C-terminal helix of Bcl-x(L) mediates Bax retrotranslocation from the mitochondria. Cell Death. Differ. *20*, 333-342.

Tondera,D., Grandemange,S., Jourdain,A., Karbowski,M., Mattenberger,Y., Herzig,S., Da Cruz,S., Clerc,P., Raschke,I., Merkwirth,C., Ehses,S., Krause,F., Chan,D.C., Alexander,C., Bauer,C., Youle,R., Langer,T., and Martinou,J.C. (2009). SLP-2 is required for stress-induced mitochondrial hyperfusion. EMBO. J. *28*, 1589-1600.

Twig,G., Elorza,A., Molina,A.J., Mohamed,H., Wikstrom,J.D., Walzer,G., Stiles,L., Haigh,S.E., Katz,S., Las,G., Alroy,J., Wu,M., Py,B.F., Yuan,J., Deeney,J.T., Corkey,B.E., and Shirihai,O.S. (2008). Fission and selective fusion govern mitochondrial segregation and elimination by autophagy. EMBO J. *27*, 433-446.

Tyurin,V.A., Tyurina,Y.Y., Osipov,A.N., Belikova,N.A., Basova,L.V., Kapralov,A.A., Bayir,H., and Kagan,V.E. (2007). Interactions of cardiolipin and lyso-cardiolipins with cytochrome c and tBid: conflict or assistance in apoptosis. Cell Death. Differ. *14*, 872-875.

Uicker,W.C., Schaefer,L., Koenigsknecht,M., and Britton,R.A. (2007). The essential GTPase YqeH is required for proper ribosome assembly in Bacillus subtilis. J. Bacteriol. *189*, 2926-2929.

Van Bergen,N.J., Crowston,J.G., Kearns,L.S., Staffieri,S.E., Hewitt,A.W., Cohn,A.C., Mackey,D.A., and Trounce,I.A. (2011). Mitochondrial oxidative phosphorylation compensation may preserve vision in patients with OPA1-linked autosomal dominant optic atrophy. PLoS. One. *6*, e21347.

van der Bliek,A.M., Shen,Q., and Kawajiri,S. (2013). Mechanisms of mitochondrial fission and fusion. Cold Spring Harb. Perspect. Biol. *5*.

van der Laan,M., Bohnert,M., Wiedemann,N., and Pfanner,N. (2012). Role of MINOS in mitochondrial membrane architecture and biogenesis. Trends Cell Biol *22*, 185-192.

Van Laar,V.S., Dukes,A.A., Cascio,M., and Hastings,T.G. (2008). Proteomic analysis of rat brain mitochondria following exposure to dopamine quinone: implications for Parkinson disease. Neurobiol. Dis. *29*, 477-489.

Varanita,T., Soriano,M.E., Romanello,V., Zaglia,T., Quintana-Cabrera,R., Semenzato,M., Menabç,R., Costa,V., Civiletto,G., Pesce,P., Viscomi,C., Zeviani,M., Di Lisa,F., Mongillo,M., Sandri,M., and Scorrano,L. (2015). The Opa1-Dependent Mitochondrial Cristae Remodeling Pathway Controls Atrophic, Apoptotic, and Ischemic Tissue Damage. Cell Metabolism *21*.

Verhagen,A.M., Ekert,P.G., Pakusch,M., Silke,J., Connolly,L.M., Reid,G.E., Moritz,R.L., Simpson,R.J., and Vaux,D.L. (2000). Identification of DIABLO, a mammalian protein that promotes apoptosis by binding to and antagonizing IAP proteins. Cell *102*, 43-53.

Verhagen,A.M., Silke,J., Ekert,P.G., Pakusch,M., Kaufmann,H., Connolly,L.M., Day,C.L., Tikoo,A., Burke,R., Wrobel,C., Moritz,R.L., Simpson,R.J., and Vaux,D.L. (2002). HtrA2 promotes cell death through its serine protease activity and its ability to antagonize inhibitor of apoptosis proteins. J. Biol. Chem. *277*, 445-454.

Vogel,F., Bornhovd,C., Neupert,W., and Reichert,A.S. (2006). Dynamic subcompartmentalization of the mitochondrial inner membrane. J. Cell Biol. *175*, 237-247.

von der,M.K., Muller,J.M., Bohnert,M., Oeljeklaus,S., Kwiatkowska,P., Becker,T., Loniewska-Lwowska,A., Wiese,S., Rao,S., Milenkovic,D., Hutu,D.P., Zerbes,R.M., Schulze-Specking,A., Meyer,H.E., Martinou,J.C., Rospert,S., Rehling,P., Meisinger,C., Veenhuis,M., Warscheid,B., van der Klei,I.J., Pfanner,N., Chacinska,A., and van der Laan,M. (2011). Dual role of mitofilin in mitochondrial membrane organization and protein biogenesis. Dev. Cell *21*, 694-707.

Votruba,M., Moore,A.T., and Bhattacharya,S.S. (1998). Clinical features, molecular genetics, and pathophysiology of dominant optic atrophy. J. Med. Genet. *35*, 793-800.

Walensky,L.D. (2013). Direct BAKtivation. Nat. Struct. Mol. Biol. *20*, 536-538.

Walensky,L.D., Kung,A.L., Escher,I., Malia,T.J., Barbuto,S., Wright,R.D., Wagner,G., Verdine,G.L., and Korsmeyer,S.J. (2004). Activation of apoptosis in vivo by a hydrocarbon-stapled BH3 helix. Science *305*, 1466-1470.

Wang,H., Lim,P.J., Karbowski,M., and Monteiro,M.J. (2009). Effects of overexpression of huntingtin proteins on mitochondrial integrity. Hum. Mol. Genet. *18*, 737-752.

Wang,X. (2001). The expanding role of mitochondria in apoptosis. Genes Dev. *15*, 2922-2933.

Wang,X., Yan,M.H., Fujioka,H., Liu,J., Wilson-Delfosse,A., Chen,S.G., Perry,G., Casadesus,G., and Zhu,X. (2012). LRRK2 regulates mitochondrial dynamics and function through direct interaction with DLP1. Hum. Mol. Genet. *21*, 1931-1944.

Wasiak,S., Zunino,R., and McBride,H.M. (2007). Bax/Bak promote sumoylation of DRP1 and its stable association with mitochondria during apoptotic cell death. J. Cell Biol. *177*, 439-450.

Waterham,H.R., Koster,J., van Roermund,C.W., Mooyer,P.A., Wanders,R.J., and Leonard,J.V. (2007). A lethal defect of mitochondrial and peroxisomal fission. N. Engl. J. Med. *356*, 1736-1741.

Weber,T.A., Koob,S., Heide,H., Wittig,I., Head,B., van der Bliek,A., Brandt,U., Mittelbronn,M., and Reichert,A.S. (2013). APOOL is a cardiolipin-binding constituent of the Mitofilin/MINOS protein complex determining cristae morphology in mammalian mitochondria. PLoS. One. *8*, e63683.

Wei,M.C., Lindsten,T., Mootha,V.K., Weiler,S., Gross,A., Ashiya,M., Thompson,C.B., and Korsmeyer,S.J. (2000). tBID, a membrane-targeted death ligand, oligomerizes BAK to release cytochrome c. Genes Dev. *14*, 2060-2071.

Wei,M.C., Zong,W.X., Cheng,E.H., Lindsten,T., Panoutsakopoulou,V., Ross,A.J., Roth,K.A., MacGregor,G.R., Thompson,C.B., and Korsmeyer,S.J. (2001). Proapoptotic BAX and BAK: a requisite gateway to mitochondrial dysfunction and death. Science *292*, 727-730.

White,K.E., Davies,V.J., Hogan,V.E., Piechota,M.J., Nichols,P.P., Turnbull,D.M., and Votruba,M. (2009). OPA1 deficiency associated with increased autophagy in retinal ganglion cells in a murine model of dominant optic atrophy. Invest Ophthalmol. Vis. Sci. *50*, 2567-2571.

Willis,S.N., Fletcher,J.I., Kaufmann,T., van Delft,M.F., Chen,L., Czabotar,P.E., Ierino,H., Lee,E.F., Fairlie,W.D., Bouillet,P., Strasser,A., Kluck,R.M., Adams,J.M., and Huang,D.C. (2007). Apoptosis initiated when BH3 ligands engage multiple Bcl-2 homologs, not Bax or Bak. Science *315*, 856-859.

Wolter,K.G., Hsu,Y.T., Smith,C.L., Nechushtan,A., Xi,X.G., and Youle,R.J. (1997). Movement of Bax from the cytosol to mitochondria during apoptosis. J. Cell Biol. *139*, 1281-1292.

Wong,E.D., Wagner,J.A., Gorsich,S.W., McCaffery,J.M., Shaw,J.M., and Nunnari,J. (2000). The dynamin-related GTPase, Mgm1p, is an intermembrane space protein required for maintenance of fusion competent mitochondria. J. Cell Biol. *151*, 341-352.

Wong,E.D., Wagner,J.A., Scott,S.V., Okreglak,V., Holewinske,T.J., Cassidy-Stone,A., and Nunnari,J. (2003). The intramitochondrial dynamin-related GTPase, Mgm1p, is a component of a protein complex that mediates mitochondrial fusion. J. Cell Biol. *160*, 303-311.

Xiao,L., Xian,H., Lee,K.Y., Xiao,B., Wang,H., Yu,F., Shen,H.M., and Liou,Y.C. (2015). Death-associated Protein 3 Regulates Mitochondrial-encoded Protein Synthesis and Mitochondrial Dynamics. J. Biol. Chem. *290*, 24961-24974.

Xiao,X., Hu,Y., Quiros,P.M., Wei,Q., Lopez-Otin,C., and Dong,Z. (2014). OMA1 mediates OPA1 proteolysis and mitochondrial fragmentation in experimental models of ischemic kidney injury. Am. J. Physiol Renal Physiol *306*, F1318-F1326.

Xie,J., Marusich,M.F., Souda,P., Whitelegge,J., and Capaldi,R.A. (2007). The mitochondrial inner membrane protein mitofilin exists as a complex with SAM50, metaxins 1 and 2, coiled-coil-helix coiled-coil-helix domain-containing protein 3 and 6 and DnaJC11. FEBS Lett. *581*, 3545-3549.

Yamaguchi,R., Lartigue,L., Perkins,G., Scott,R.T., Dixit,A., Kushnareva,Y., Kuwana,T., Ellisman,M.H., and Newmeyer,D.D. (2008). Opa1-mediated cristae opening is Bax/Bak and BH3 dependent, required for apoptosis, and independent of Bak oligomerization. Mol. Cell *31*, 557-569.

Yang,R.F., Sun,L.H., Zhang,R., Zhang,Y., Luo,Y.X., Zheng,W., Zhang,Z.Q., Chen,H.Z., and Liu,D.P. (2015). Suppression of Mic60 compromises mitochondrial transcription and oxidative phosphorylation. Sci. Rep. *5*, 7990.

Yang,R.F., Zhao,G.W., Liang,S.T., Zhang,Y., Sun,L.H., Chen,H.Z., and Liu,D.P. (2012). Mitofilin regulates cytochrome c release during apoptosis by controlling mitochondrial cristae remodeling. Biochem. Biophys. Res. Commun. *428*, 93-98.

Yoneda,M., Miyatake,T., and Attardi,G. (1994). Complementation of mutant and wild-type human mitochondrial DNAs coexisting since the mutation event and lack of complementation of DNAs introduced separately into a cell within distinct organelles. Mol. Cell Biol. *14*, 2699-2712.

Yoon,Y., Krueger,E.W., Oswald,B.J., and McNiven,M.A. (2003). The mitochondrial protein hFis1 regulates mitochondrial fission in mammalian cells through an interaction with the dynamin-like protein DLP1. Mol. Cell Biol. *23*, 5409-5420.

Yoon,Y., Pitts,K.R., and McNiven,M.A. (2001). Mammalian dynamin-like protein DLP1 tubulates membranes. Mol Biol Cell *12*, 2894-2905.

Youle,R.J. and van der Bliek,A.M. (2012). Mitochondrial fission, fusion, and stress. Science *337*, 1062-1065.

Yuan,H., Gerencser,A.A., Liot,G., Lipton,S.A., Ellisman,M., Perkins,G.A., and Bossy-Wetzel,E. (2007). Mitochondrial fission is an upstream and required event for bax foci formation in response to nitric oxide in cortical neurons. Cell Death. Differ. *14*, 462-471.

Zanna,C., Ghelli,A., Porcelli,A.M., Karbowski,M., Youle,R.J., Schimpf,S., Wissinger,B., Pinti,M., Cossarizza,A., Vidoni,S., Valentino,M.L., Rugolo,M., and Carelli,V. (2008). OPA1 mutations associated with dominant optic atrophy impair oxidative phosphorylation and mitochondrial fusion. Brain *131*, 352-367.

Zemojtel,T., Frohlich,A., Palmieri,M.C., Kolanczyk,M., Mikula,I., Wyrwicz,L.S., Wanker,E.E., Mundlos,S., Vingron,M., Martasek,P., and Durner,J. (2006a). Plant nitric oxide synthase: a never-ending story? Trends Plant Sci. *11*, 524-525.

Zemojtel,T., Kolanczyk,M., Kossler,N., Stricker,S., Lurz,R., Mikula,I., Duchniewicz,M., Schuelke,M., Ghafourifar,P., Martasek,P., Vingron,M., and Mundlos,S. (2006b). Mammalian mitochondrial nitric oxide synthase: characterization of a novel candidate. FEBS Lett. *580*, 455-462.

Zerbes,R.M., Bohnert,M., Stroud,D.A., von der,M.K., Kram,A., Oeljeklaus,S., Warscheid,B., Becker,T., Wiedemann,N., Veenhuis,M., van der Klei,I.J., Pfanner,N., and van der Laan,M. (2012). Role of MINOS in mitochondrial membrane architecture: cristae morphology and outer membrane interactions differentially depend on mitofilin domains. J. Mol. Biol *422*, 183-191.

Zha,J., Weiler,S., Oh,K.J., Wei,M.C., and Korsmeyer,S.J. (2000). Posttranslational N-myristoylation of BID as a molecular switch for targeting mitochondria and apoptosis. Science *290*, 1761-1765.

Zhang,M., Mileykovskaya,E., and Dowhan,W. (2002). Gluing the respiratory chain together. Cardiolipin is required for supercomplex formation in the inner mitochondrial membrane. J. Biol. Chem. *277*, 43553-43556.

Zhao,J., Liu,T., Jin,S., Wang,X., Qu,M., Uhlen,P., Tomilin,N., Shupliakov,O., Lendahl,U., and Nister,M. (2011). Human MIEF1 recruits Drp1 to mitochondrial outer membranes and promotes mitochondrial fusion rather than fission. EMBO J. *30*, 2762-2778.

Zhao,J., Zhang,J., Yu,M., Xie,Y., Huang,Y., Wolff,D.W., Abel,P.W., and Tu,Y. (2013a). Mitochondrial dynamics regulates migration and invasion of breast cancer cells. Oncogene *32*, 4814-4824.

Zhao,X., Tian,C., Puszyk,W.M., Ogunwobi,O.O., Cao,M., Wang,T., Cabrera,R., Nelson,D.R., and Liu,C. (2013b). OPA1 downregulation is involved in sorafenib-induced apoptosis in hepatocellular carcinoma. Lab Invest *93*, 8-19.

Zuchner,S., Mersiyanova,I.V., Muglia,M., Bissar-Tadmouri,N., Rochelle,J., Dadali,E.L., Zappia,M., Nelis,E., Patitucci,A., Senderek,J., Parman,Y., Evgrafov,O., Jonghe,P.D., Takahashi,Y., Tsuji,S., Pericak-Vance,M.A., Quattrone,A., Battologlu,E., Polyakov,A.V., Timmerman,V., Schroder,J.M., and Vance,J.M. (2004). Mutations in the mitochondrial GTPase mitofusin 2 cause Charcot-Marie-Tooth neuropathy type 2A. Nat. Genet. *36*, 449-451.